Design, Synthesis and Evaluation of PHP Inhibitors

Zur Erlangung des akademischen Grades eines
Doktors der Naturwissenschaften
(Dr. rer. nat.)
von der Fakultät für Chemie
der Technischen Universität Dortmund
angenommene

Dissertation

von

Martijn Eerland, MSc

aus Woerden, Niederlande

Dekan:		Prof. Dr. Klaus Jurkschat
1.	Gutachter	Prof. Dr. Herbert Waldmann
2.	Gutachter	Assoc. Prof. Dr. Christian Hedberg

Tag der mündlichen Prüfung: 21 Oktober 2015

Die vorliegende Arbeit entstand im Zeitraum von August 2008 bis April 2013 unter Anleitung von Prof. Dr. Herbert Waldmann und Dr. Christian Hedberg am Max-Planck-Institut für molekulare Physiologie und der Fakultät Chemie der Technischen Universität Dortmund.

Dedicated to my Friends and Family

"But all things noble are as difficult as they are rare."

Baruch de Spinoza (1632-1677)

Taken from *Ethics* (1677)

Abstract/Zusammenfassung

Abstract

An organism can significantly increase its complexity through increasing its protein diversity. This can be achieved through applying post-translational modifications (PTMs) to proteins, altering its structure after synthesis. From all possible enzyme catalyzed modifications, phosphorylation is arguably the most important. O-phosphorylation, the addition of a phosphate on a serine, threonine or tyrosine amino acid residue, can cause a dramatic change in protein function. Nowadays, more and more research is devoted to the less well understood amino acid N-phosphorylation. However, the relative chemical instability of the P-N bond makes it difficult to study. In particular histidine phosphorylation is now receiving more attention due to its high abundance in nature in general. Recently, antibodies against phospho-histidine have been reported and these tools will boost research in this field, like it did for phospho-tyrosine. The enzymes involved in histidine phosphorylation, kinases and phosphatases, are also subject of research and besides the non-selective nucleoside-diphosphate kinases (NDPKs) a highly specific phospho-histidine phosphatase (PHP) has been identified. Unique in its class and expressed in high levels in many different cell types, this enzyme can be an alternative key in opening the door to the evaluation of the significance of N-phosphorylation in higher organisms.

In order to investigate PHP function, enzyme knockdown through siRNA has shown great potential already. Chemical knockdown will be a valuable additional tool to reversibly inhibit the enzyme in a cellular setup. A small molecule inhibitor will also be useful in the evaluation of PHP as a potential drug target. PHP catalyzes the phospho-histidine hydrolysis reaction through activation of a water molecule (see figure). An imidazole equipped with a sulfonamide was hypothesized to mimic the transition state of PHP catalyzed phospho-histidine hydrolysis. This structural feature was explored as both small molecule inhibitor and peptide PHP inhibitor. In order to incorporate the imidazole sulfonamide in a peptide, the strategic building block **7** was prepared and successfully converted into several peptides using solid phase peptide synthesis (SPPS). For evaluation of the prepared compounds, biochemical assays were developed to assay the PHP inhibitory activity. Three different assaying techniques were successfully applied to study PHP activity and inhibition. A continues coupled enzyme UV absorption assay and a fluorescence assay utilizing a modest phospho-tyrosine hydrolysis activity of PHP were developed and successfully deployed to evaluate the prepared peptides and small molecules. Several small molecule inhibitors were identified with IC_{50} values ranging from 3 to 11 µM. In peptide form the sulfonamide imidazole failed to show inhibitory activity, indicating a different binding mode from what was hypothesized.

The identified small molecules **53b**, **53f**, **60c** and **86** were further evaluated with a Microscale Thermophoresis based binding assay and the solubility and cell permeability were assayed. Finally, the compounds were evaluated in a patch clamp ion channel whole cell assay and in a scratch type migration assay. In both assays little effect was observed for most compounds except for compound **86**. At 100 µM concentration **86** showed a significant inhibition of ion channel activation. This effect is different from expected as PHP inhibition was reported to increase channel activity. In the scratch assay no effect was observed besides occurance of cell death at a higher concentration of **86**. This effect might be attributed to a carbonic anhydrase activity of the inhibitor compound.

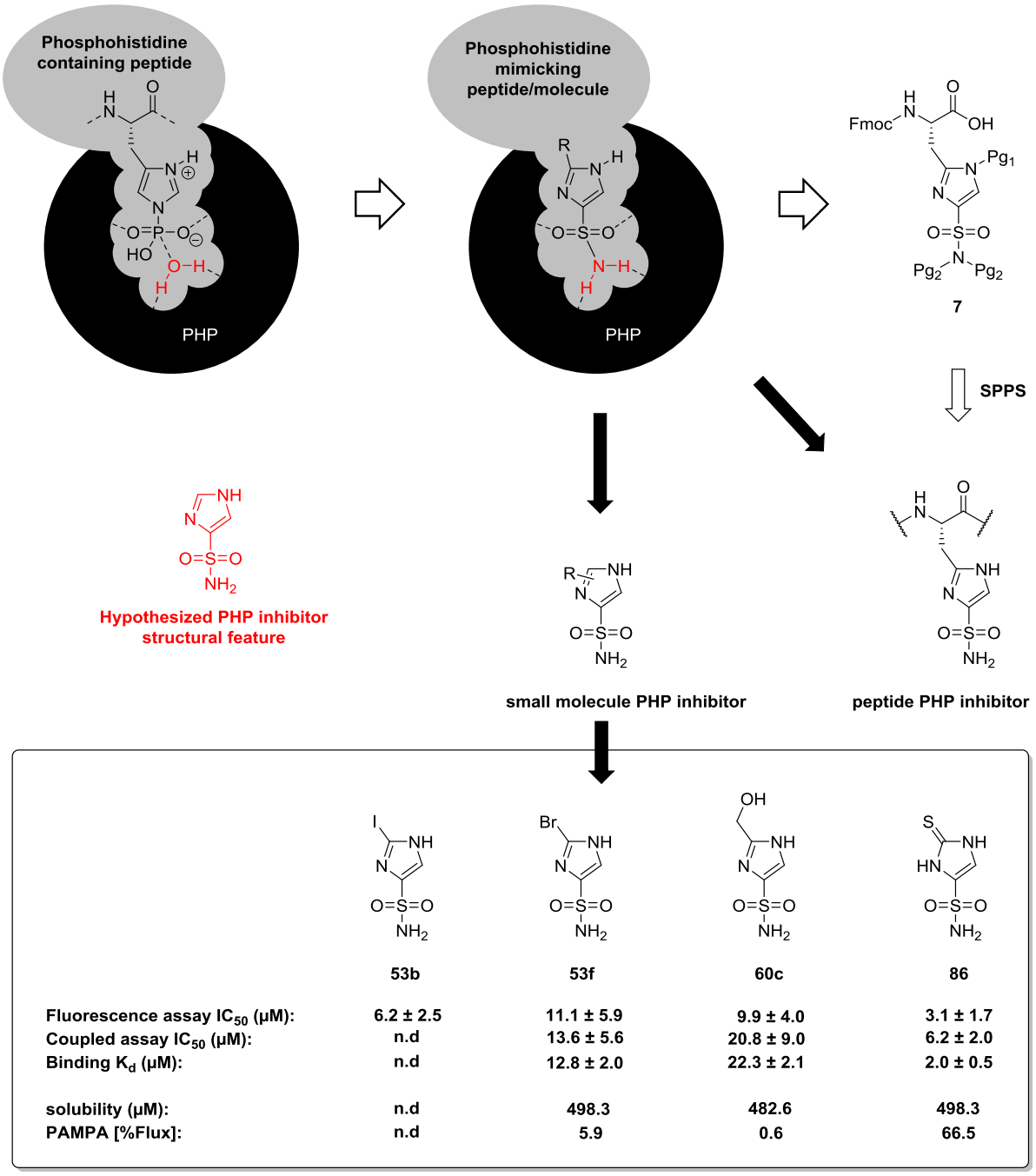

	53b	53f	60c	86
Fluorescence assay IC_{50} (µM):	6.2 ± 2.5	11.1 ± 5.9	9.9 ± 4.0	3.1 ± 1.7
Coupled assay IC_{50} (µM):	n.d	13.6 ± 5.6	20.8 ± 9.0	6.2 ± 2.0
Binding K_d (µM):	n.d	12.8 ± 2.0	22.3 ± 2.1	2.0 ± 0.5
solubility (µM):	n.d	498.3	482.6	498.3
PAMPA [%Flux]:	n.d	5.9	0.6	66.5

Besides investigating PHP, the developed building block **7** is also suitable for investigating other aspects of histidine phosphorylation. Building block **7**, and a phosphonate version developed earlier in our lab, was also incorporated into peptides derived from Histone H4. These peptides were designed to study the possible influence of histidine phosphorylation of epigenetic processed known to take place on the Histone H4. Lysine acetylation and methylation were studied on these peptides in order to see if a modification on an adjacent histidine, a known target for phosphorylation *in vivo*, would influence these processes. Unfortunately, no effect was found when comparing an N-phosphorylated target peptide to a non-phosphorylated version. Additionally, pull-down probes, based on Histone H4 were prepared in order to identify phospho-histidine interacting proteins. Also here, the peptides failed to identify novel proteins involved in histidine phosphorylation.

Zusammenfassung

Organismen können ihre Komplexität erheblich vergrößern, indem sie ihre Proteindiversität erhöhen. Dies kann zum Beispiel durch posttranslationale Modifikationen geschehen, die die Proteinstruktur nach der Synthese verändern. Von allen möglichen Modifikationen ist die Phosphorylierung die Wichtigste. O-Phosphorylierung an Serin-, Threonin- oder Tyrosinresten kann die Funktion eines Proteins erheblich verändern. Jedoch wird heutzutage mehr und mehr Aufwand betrieben auch die weit weniger erforschte N-Phosphorylierung von Proteinen zu verstehen. Dies wird allerdings durch die chemisch relativ instabile Natur der P-N-Bindung erschwert. Insbesondere die Histidinphosphorylierung steht dabei aufgrund ihrer Häufigkeit im Fokus. Kürzlich entwickelte Antikörper gegen diese Modifikation werden, ähnlich wie es vorher für Phoshotyrosin der Fall war, werden das Feld in Zukunft erheblich weiter bringen.
Auch die Enzyme der Histidinphosphorylierung, Kinasen und Phosphatasen, sind Gegenstand der aktuellen Forschung. Neben nicht-selektiven Nukleosid-Diphosphatkinasen (NDPKs) wurde eine hochspezifische Phosphohistidin-phosphatase (PHP) identitifiziert. Einzigartig in ihrer Klasse und hoch exprimiert in vielen verschiedenen Zelltypen, könnte dieses Enzym der Schlüssel zur Evaluierung der N-Phosphorylierung in höheren Organismen sein. Bisher wurde das Enzym durch siRNA vermittelte Knock-Down-Experimente erforscht. Ein chemischer, reversibler Knock-Down durch kleine Moleküle würde eine wertvolle Erweiterung dessen darstellen. Darüber hinaus können kleine Moleküle als Inhibitoren dazu dienen, PHP als potentielles Zielprotein in der Medikamentenentwicklung zu evaluieren.
PHP katalysiert die Hydrolyse von Phosphohistidin durch die Aktivierung eines Wassermoleküls (siehe Abbildung). Ein durch ein Sulfonamid modifiziertes Imidazol wurde als hypothetisches Pharmokphor und mögliches Übergangszustansmimetikum dieser Reaktion gewählt und sowohl als kleine Moleküle, als auch in Peptide inkorporiert und hinsichtlich potentieller PHP-Inhibition untersucht. Für die Synthese der Imidazol-Sulfonamidpeptide wurde der strategische Aminosäurebaustein 7 hergestellt und mittels SPPS erfolreich in Peptide eingebaut. Zur Untersuchung der PHP-Inhibition wurde ein biochemischer Assay entwickelt und letztendlich wurden drei Assaytechniken erfolgreich angewandt. Es wurde sowohl ein enzymgekoppelter UV-Absorptionsassay als auch ein fluoreszenzbasierter Assay entwickelt, die auf der schwachen Phosphotyrosin-Hydrolyseaktivität von PHP basieren. So konnten einige kleine Moleküle als PHP-Inhibitoren mit IC_{50}-Werten von 3 bis 11 µM identifiziert werden. Die getesteten Peptide zeigten keine Aktivität als PHP-Inhibitoren, was darauf schließen lässt, dass der ursprünglich vermutete Bindungsmodus nicht korrekt ist. Die kleinen Moleküle **53b**, **53f**, **60c** und **86** wurden hinsichtlich ihrer Bindung an PHP weiter mittels Microscale Thermophoresis untersucht. Zudem wurden ihre Löslichkeit und die Zellpermeabilität bestimmt. Letztlich kamen Patch Clamp Ionenkanalexperimente und Zellmigrationsassays hinzu. In beiden zeigten die Moleküle nur geringe Aktivität, mit Ausnahme von Verbindung **86**, welche bei einer Konzentration von 100µM eine signifikante Inhibierung der Ionenkanalaktivität zeigte. Dieser Effekt widerspricht den Erwartungen, da vorher bereits berichtet wurde, dass PHP-Inihibition die Ionenkanalaktivität erhöht. In den Zellmigrationsexperimenten zeigte die Verbindung keinen Effekt, mit Ausnahme von Toxizität in höheren Konzentrationen. Dieser Effekt könnte in Zusammenhang mit einer potentiellen Wirkung auf Carboanhydrasen erklärt werden.

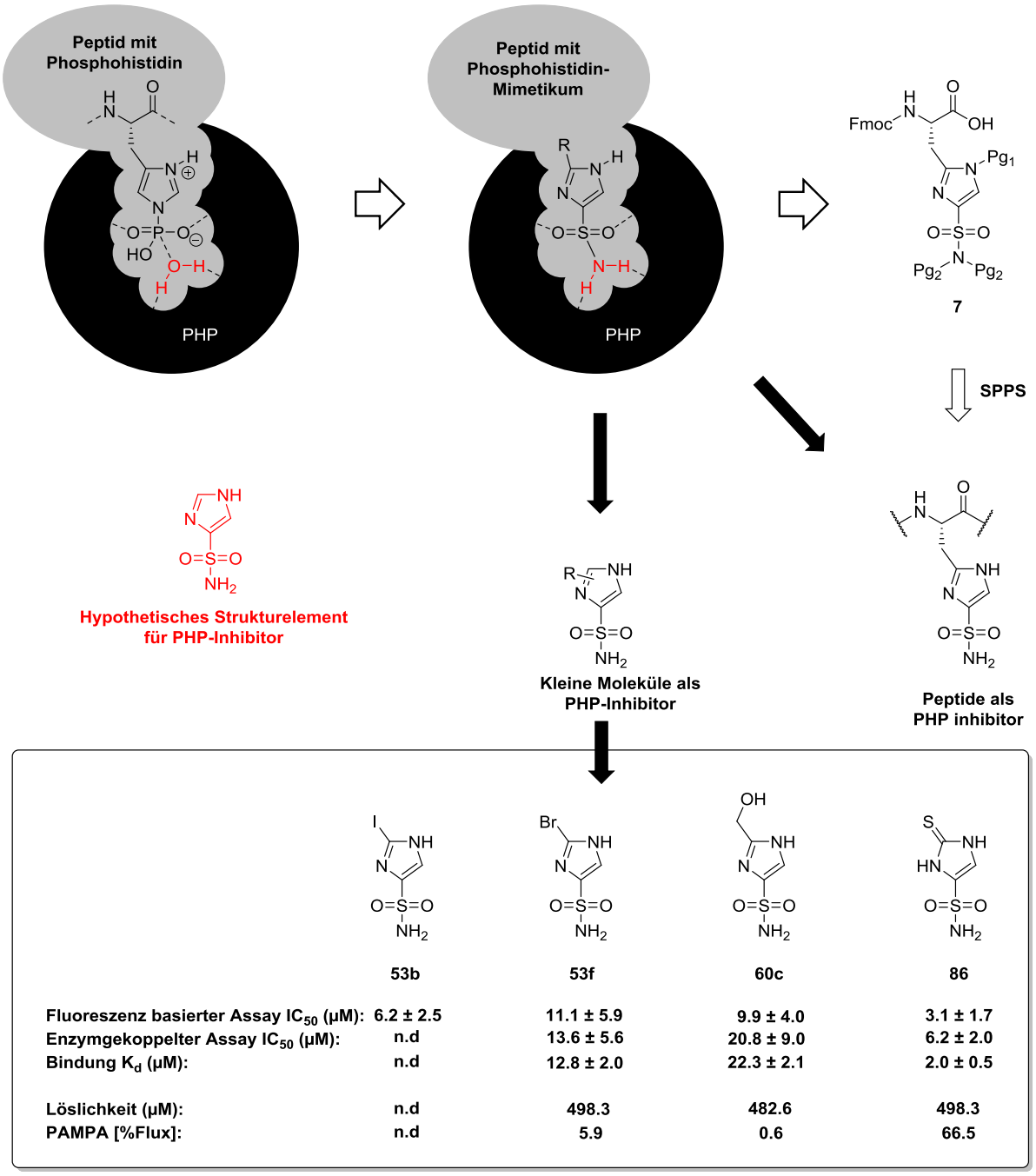

	53b	53f	60c	86
Fluoreszenz basierter Assay IC_{50} (µM):	6.2 ± 2.5	11.1 ± 5.9	9.9 ± 4.0	3.1 ± 1.7
Enzymgekoppelter Assay IC_{50} (µM):	n.d	13.6 ± 5.6	20.8 ± 9.0	6.2 ± 2.0
Bindung K_d (µM):	n.d	12.8 ± 2.0	22.3 ± 2.1	2.0 ± 0.5
Löslichkeit (µM):	n.d	498.3	482.6	498.3
PAMPA [%Flux]:	n.d	5.9	0.6	66.5

Neben der Erforschung von PHP kann der Aminosäurebaustein **7** auch dazu dienen andere Aspekte der Histidinphosphorylierung zu untersuchen. Baustein **7** und auch ein vorher in unserem Labor entwickelter Phosphonat-basierter Baustein wurden in Peptide, die von Histon H4 abgeleitet wurden eingebaut um den möglichen Einfluss von Histidinphosphorylierung auf epigenetische Prozesse zu erforschen. Dazu wurde der Effekt von Histidinmodifikationen in Nachbarschaft zu Lysinen auf deren Acetylierung und Methylierung untersucht, da diese in vivo bekannt dafür sind, phosphoryliert zu werden. Dabei zeigte sich jedoch kein Unterschied zwischen N-Phosphorylierten und nicht modifizierten Peptiden. Darüber hinaus wurden auch Sonden für *Pull Down*-Versuche hergestellt, die jedoch nicht zur Identifikation von neuen Proteinen, die in der Histidinphosphorylierung eine Rolle spielen, führten.

List of Abbreviations

AA	amino acid
Ac	acetyl
All	allyl
Alloc	allyloxycarbonyl
aq	aqueous
ATP	adenosine triphosphate
Bn	benzyl
Boc	tert-butoxycarbonyl
br	broad
Bu	butyl
Bz	benzoyl
°C	degrees Celcius (centigrade)
calc.	calculated
CAN	ceric ammonium nitrate
Cbz	benzyloxycarbonyl
CDI	carbonyldiimidazole
m-CPBA	meta-chloroperoxybenzoic acid
d (NMR)	doublet
DABCO	1,4-diazabicyclo[2.2.2]octane
dba	dibenzylidene acetone
DBU	1,8-diazabicyclo [5.4.0]undec-7-ene
dd (NMR)	doublet of doublets
DDQ	2,3-Dichloro-5,6-dicyano-1,4-benzoquinone
DCC	N,N-dicyclohexylcarbodiimide
DCM	dichloromethane
DIAD	diisopropyl azodicarboxylate
DIC	diisopropyl carbodiimide
DIPEA	diisopropylethylamine
DMAP	4-dimethylaminopyridine
DMB	2,4-dimethoxybenzyl
DMF	N,N-dimethylformamide
DMSO	dimethyl sulfoxide
dppf	1,1'-bis(diphenylphosphino)ferrocene
dt (NMR)	doublet of triplets
EDC	3-(ethyliminomethyleneamino)-N,N-dimethyl-propan-1-amine
Equiv	equivalents
ESI	electrospray ionization
Et	ethyl
et al.	et alia (and others)
Fmoc	9-fluorenylmethoxycarbonyl
h	hours
HATU	2-(1H-7-azabenzotriazol-1-yl)-1,1,3,3-tetramethyl uronium hexafluorophosphate
HBTU	O-benzotriazole-N,N,N’,N’-tetramethyl-uronium-hexafluoro-phosphate
HOAt	3-Hydroxytriazolo[4,5-b]pyridine
HOBt	N-hydroxybenzotriazole
HPLC	high performance liquid chromatography
HRMS	high resolution mass spectrometry
iPr	isopropyl

HMDS	bis(trimethylsilyl)amine
LCMS	high performance liquid chromatography mass spectrometry
m (NMR)	multiplet
Me	methyl
MeCN	acetonitrile
min	minutes
MM	Magic Mixture (TLC): MeOH 3, H_2O 2, AcOH 3, EtOAc 3
mp	melting point
MS	mass spectrometry
Ms	mesyl
m/z	mass to charge ratio
NDPK	nucleoside diphosphate kinases
NBS	N-bromosuccinimide
NMP	1-methyl-2-pyrrolidone
NMR	nuclear magnetic resonance
Ns	4-nitrobenzenesulfonyl
o	ortho
OSu	hydroxysuccinimide
p	phospho
p	para
Pbf	2,2,4,6,7-pentamethyldihydrobenzofuran-5-sulfonyl
Ph	phenyl
PHP	phosphohistidine phosphatase
ppm	parts per million
PTM	posttranslational modification
q	quartet
quant	quantitatively
Rf	retention factor
rt	room temperature
s	singlet (NMR)
sat.	saturated
S-Phos	2-dicyclohexylphosphino-2',6'-dimethoxybiphenyl
SPPS	solid phase peptide synthesis
t (NMR)	triplet
TBS	tert-butyldimethylsilyl
tBu	tert-butyl
Tf	trifluoromethanesulfonyl
TFA	trifluoroacetic acid
THF	tetrahydrofuran
TIPS	triisopropylsilane
TLC	thin layer chromatography
TMP	2,2,6,6-tetramethylpiperidine
TMS	trimethylsilyl
Trt	trityl (triphenylmethyl)
Ts	p-toluenesulfonyl
XantPhos	4,5-bis(diphenylphosphino)-9,9-dimethylxanthene
X-Phos	2-dicyclohexylphosphino-2’,4’,6’,-triisopropylbiphenyl

Amino acids

Ala	alanine (A)
Arg	arginine (R)
Asn	asparagine (N)
Asp	aspartate (D)
Cys	cysteine (C)
Gly	glycine (G)
Glu	glutamate (E)
Gln	glutamine (Q)
His	histidine (H)
Ile	Isoleucine (I)
Leu	leucine (L)
Lys	lysine (K)
Met	methionine (M)
Phe	phenylalanine (F)
Pro	proline (P)
Ser	serine (S)
Thr	threonine (T)
Trp	tryptophane (W)
Tyr	tyrosine (Y)
Val	valine (V)

Contents

Chapter 1: Introduction

1.1 Protein Phosphorylation

1.1.1 Post-Translational Modification

An important part of understanding the origin of life comes down to understanding the cell. All life on our planet and most likely in the universe, is based on this confined unit with a cell membrane that contains organic molecules, all having functions that are essential parts of the whole structure. Our deeper understanding started with unraveling the basics of genetics, the discovery of DNA, the relationship it has to proteins and finally mapping the entire genome. However, it is now clear that the relative small amount of genes (20,000 to 25,000) alone is by no means able to be responsible for the full complexity of higher order organisms like human beings.[1] In principle, there are two major mechanisms for expanding the coding capacity of the genes to generate a higher order of diversity in the proteome (see figure 1). The first route of diversification of proteins is at the transcriptional level, by mRNA manipulation. Splicing the primary RNA into different RNAs allows the organism to generate similar proteins that differ in function or localization.[2] Also, highly specific editing of RNA can be used to alter the RNA structure and therefore the protein outcome.[3] The second route to proteome expansion is post-translational modification (PTM) of the protein gene products. As the name implies, PTMs are covalent modifications, introduced by enzymes after the DNA has been transcribed into RNA and translated into proteins. These highly specific enzyme-catalyzed modifications can occur on the side chain residues or on the protein backbone. Proteome diversification by covalent modification does occur in prokaryotes but is much more frequent and diverse in the nucleated cells of eukaryotes. About 5% of the genome of higher order eukaryotes is dedicated to enzymes that perform more than 200 types of PTMs on the proteome.[4] The systematic investigation of the relationship between PTMs and functional changes is again a major undertaking, not unlike the *human genome project* in size and ambition.

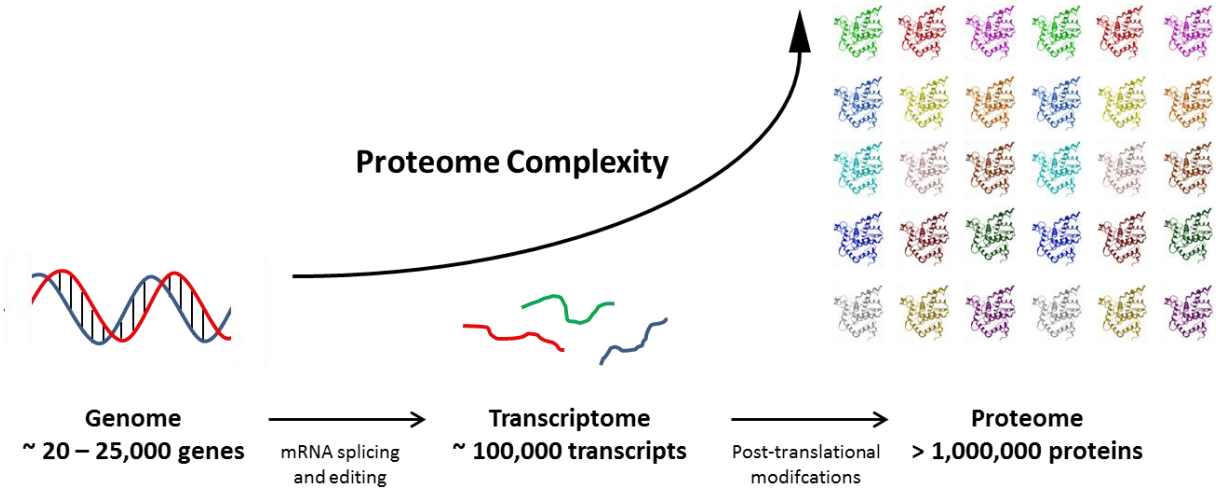

Figure 1: Increasing the proteomic diversity. The genome accounts for 20-25,000 genes however, the proteome is estimated to compass millions of proteins possessing a unique chemical identity. Manipulation of mRNA and the addition of post-translational modifications (PTMs) accounts for this added diversity. Figure adapted from www.piercenet.com.[5]

Besides hydrolytic cleavage of peptide backbones by proteases, all PTMs are enzyme-catalyzed covalent additions of a chemical group, usually an electrophilic fragment of a co-substrate, to a residue in a protein. The side chain that is modified is usually electron rich, thus acting as a nucleophile in the transfer.
The five most common types of PTMs are acylation, alkylation, glycosylation, oxidation and phosphorylation. Thoroughly studied examples are the acetylation (on Lys) or methylation (Lys, Arg) of histones, seen as an integral part of controlling selective gene transcription (epigenetics).[6] Myristoylation (*N*-terminal Gly) or palmitoylation (Cys) is a powerful modification to achieve membrane localization of proteins.[7] Glycosylation, in the form of asparagine-linked (N-linked) or serine/threonine/tyrosine-linked (O-linked) oligosaccharides forming important parts of major structural components of many cell surface and secreted proteins.[8] The sulfur containing amino acids cysteine and methionine are sensitive to oxidation.[9] The disulfide bonds that can occur between two cysteines often serve to stabilize protein structure in an intra-molecular fashion (e.g. insulin). And finally, there is protein phosphorylation, a well-known and studied modification of serine, threonine and tyrosine residues. Phosphorylation is arguable the most important of all PTMs and is for sure the most abundant. Introduction of the charged, di-anionic phosphate group on a neutral or positively charged amino acid induces a large change in the local protein microenvironment. Phosphorylation is often used as an on/off switch for enzyme activity, for instance in cellular signaling.

1.1.2 Phosphorylation, an important Post-Translational Modification

It is estimated that one-third of the proteins in the human proteome are substrates for phosphorylation at some point of their life time.[10] Generally, post-translational modifications can occur simultaneously at multiple sites within the same protein. Phosphorylation is no exception. For example, the Abelson (Abl) tyrosine kinase can be found phosphorylated at eleven different sites, (nine times tyrosine, one serine, one threonine) spread over the different catalytic and regulatory domains of the protein.[11] This results in a theoretical, 11! = 40420800 distinct isoforms possible for this particular protein alone. Potentially, every single added phosphorylation event can alter enzyme activity, localization and protein-protein interaction.
In the late 19th century it was already known that proteins exist in a phosphate bound state. Most examples of these ‘phospho-proteins’ were found in milk (caseins) and egg yolk (phosvitin) and were simply considered to be a biological method of providing phosphorus as a nutrient. Therefore, the existence of phospho-proteins was seen as a consequence of metabolic reactions, and nothing more, for almost a century after their discovery.[12] Regulation by protein phosphorylation was discovered by Edmund Fischer and Edwin Krebs who studied glycogen metabolism in the late 1950’s.[13] It was known that glycogen phosphorylase, the enzyme that degrades glycogen, exists in two forms, an active form (*phosphorylase a*) and an inactive form (*phosphorylase b*). Fischer and Krebs showed that the only difference is that *phosphorylase a* is phosphorylated on Ser^{14}, transforming it into the active enzyme. They received the Nobel Prize in 1992 for their pioneering studies. Since then, phosphorylation has been identified on many proteins, often on the same family of enzymes that facilitate phosphorylation (the kinases) or de-phosphorylation (the phosphatases) itself.

The reversibility of protein phosphorylation makes this type of PTM ideal for signal transduction, which allows cells to rapidly respond to extracellular stimuli. Signal transduction cascades are characterized by one or more membrane bound proteins that are physically stimulated, either through ligand binding or some other response (see figure 2). The signal is passed on to second messengers and signaling enzymes. In the case of phosphorylation, the signal is passed on to downstream kinases, which then phosphorylate and activate their downstream substrates, including additional kinases, until a specific response is achieved. Signal transduction cascades can be linear, in which kinase A activates kinase B, which activates kinase C and so forth. Signaling pathways that amplify the initial signal have also been discovered; kinase A activates multiple kinases, which in turn activate additional kinases. Consequently, a single molecule, such as an extracellular growth factor, can activate complex cellular programs such as proliferation.[14]

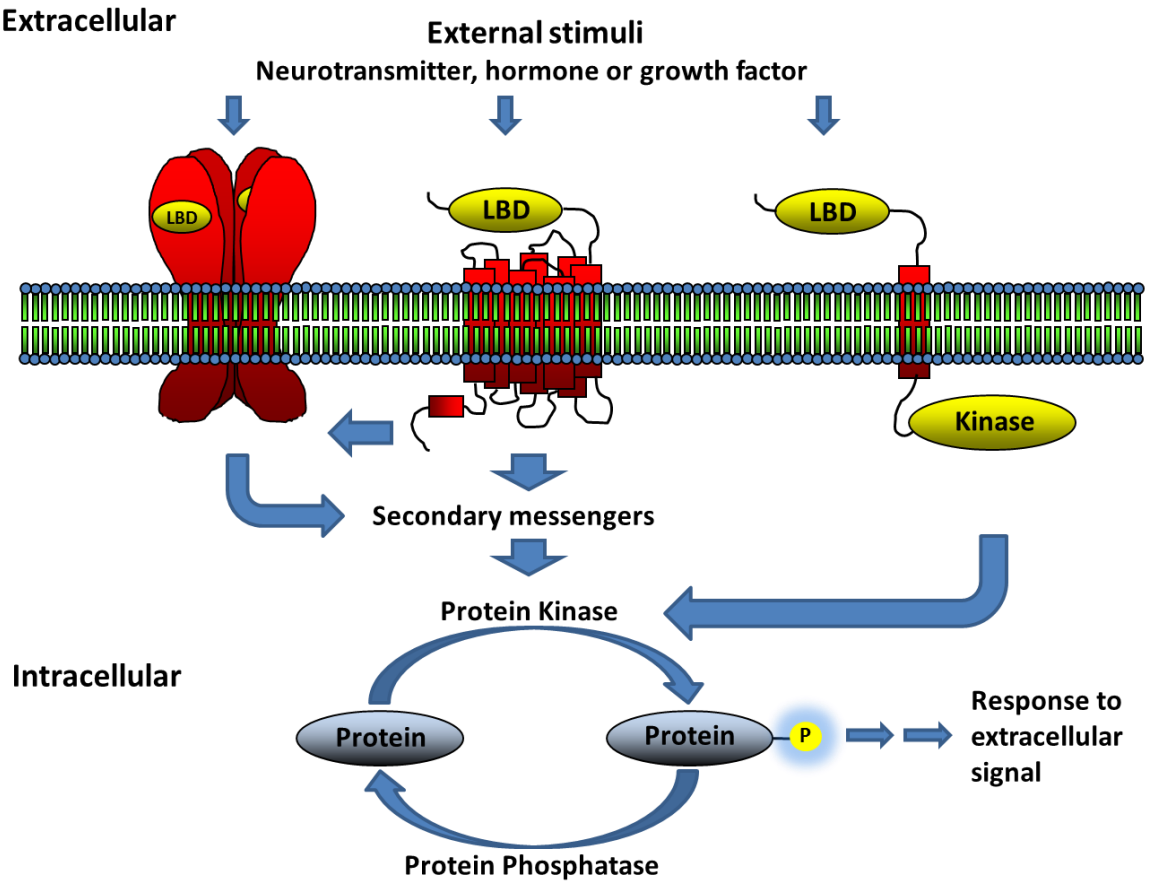

Figure 2: Cellular signaling and kinase activation through phosphorylation. Cellular signaling induced by binding of an external stimuli (like neurotransmitters, hormones or growth factors) to a ligand binding domain (LBD) of a membrane bound protein results in protein kinase activation through phosphorylation. Continuation of the signal is often a phosphorylation of one or more downstream kinases. Eventually, this signaling will result in a cellular response (e.g. protein expression, cell motility or cell division).

1.1.3 O-Phosphorylation, Kinases and Phosphatases

The enzymes responsible for protein phosphorylation (kinases) collectively form one of the largest classes of PTM enzymes.[15] This super-family of more than 500 protein kinases (PKs), referred to as the kinome, displays a large variety in its protein structure.[16] Ranging from small cytosolic enzymes to large membrane bound proteins with multiple domains. However, all share a highly conserved kinase activity domain. This conservation is due to the necessity of binding the co-substrate adenosine triphosphate (ATP) that is required as phosphate donor. This domain conservation has helped the identification of PKs in the genome. Kinases are classified according to the amino acid residue they phosphorylate. Greater than 98% of O-phosphorylation in eukaryotic cells occurs on serine and threonine residues by protein serine/threonine kinases (STKs). The remainder occurs on tyrosine residues by protein tyrosine kinases (TKs). A few PKs appear to phosphorylate tyrosine as well as serine/threonine residues and are classified as dual-specificity protein kinases (DSKs).[17] Finally, the lipid kinase PI3K possesses protein serine/threonine kinase activities, in addition to phosphorylating lipid phospho-inositides.[18]
As kinases often fulfill their role in tightly regulated signaling cascades, removal of the phosphate is of equal importance and justifies the presence of a large family of phosphatases. Protein phosphatases (PPs) are categorized by their selectivity for phospho-serine/phospho-threonine or phospho-tyrosine residues and are further categorized by sensitivity to endogenous inhibitors, requirements for cations, and *in vitro* substrate specificity. The major distinction is a protein serine/threonine phosphatase family (STPs) and a protein tyrosine phosphatase family (PTPs).[19] Additionally, a distinct family of dual-specificity protein phosphatases (DSPs) can be distinguished.[20] STPs mediate the hydrolysis of the P-O bond of the phosphorylated protein residue using a bimetallic (zinc, manganese or magnesium) center, while tyrosine phosphatases form a covalent thio-phosphoryl intermediate that facilitates release of the tyrosine residue. The approximately 150 PPs found in eukaryotes are responsible for the de-phosphorylation of proteins that are targeted by over 500 PKs. This makes it likely that most phosphatases have multiple substrates.
The use of phosphorylation/de-phosphorylation of a protein as a control mechanism has many advantages. It is fast; taking as little as a few seconds, it does not require new proteins to be made or degraded and is easily reversible. Disadvantages are there as well as aberrant regulation of phosphorylation can easily result in fatal diseases like cancer.[21] Certain kinases and phosphatases are highly specific, potentially targeting only a few proteins, while others are able to act broadly on many proteins. The targets of phosphorylation include most protein components of the cell, including enzymes, structural proteins, cell receptors, ion channels and signaling molecules. If a protein is controlled by its phosphorylation state, its activity will be directly dependent on the activity of the kinases and phosphatases that act on it. It is common for a phosphate group to be added or removed from a protein continuously, a cycle that allows a protein to switch rapidly from one state to another.
An important application of tyrosine phosphorylation, besides cell signaling, is facilitating interactions with proteins equipped with Src family homology domains (SH2 domains).[22] These domains have been shown to bind strongly to specific patterns in proteins including a phospho-tyrosine. This interaction allows direct localization/recruitment of a protein. This is an important element of the formation of protein clusters and the direction of enzyme activity.

1.1.4 Amino Acids targeted by Kinases

As stated earlier, several amino acid residues are known to be targets for phosphorylation (see figure 3). It is tempting to believe that it is mainly serine, threonine and tyrosine that are modified based on the large families of O-phosphorylation kinases and phosphatases identified and the overwhelming amount of research devoted to O-phosphorylation. However, the highly important two-component system in prokaryotes (see §1.2.1), with histidine and aspartate as substrates for phosphorylation, has been known for years. Initially, it was assumed that only O-phosphorylation is important for eukaryotes where N-phosphorylation is found exclusively in prokaryotes. Nowadays, more research effort is invested in the more exotic cases of N-phosphorylation in higher order species. Especially histidine phosphorylation seems interesting as it is estimated to be 10-100 fold more abundant in nature than phospho-tyrosine.[23] The Gibbs free energy of hydrolysis for O-phosphorylated amino acids is in the range of -6.5 to -9.5 kcal/mol. For a phospho-histidine this is significantly larger with values ranging from -12 to -14 kcal/mol.[24] This chemical instability is particularly evident at a pH lower than 7 where the half-life of a phospho-histidine species is in the order of seconds. This chemical instability makes histidine phosphorylation difficult to study and only recently phospho-histidine antibodies have been reported.[25] It was an antibody against phospho-tyrosine that boosted the research on tyrosine phosphorylation and a similar increase in publications on histidine phosphorylation is to be expected in upcoming years. Reports on phosphorylation and de-phosphorylation of arginine, lysine, cysteine and glutamate residues are even more limited.[26]

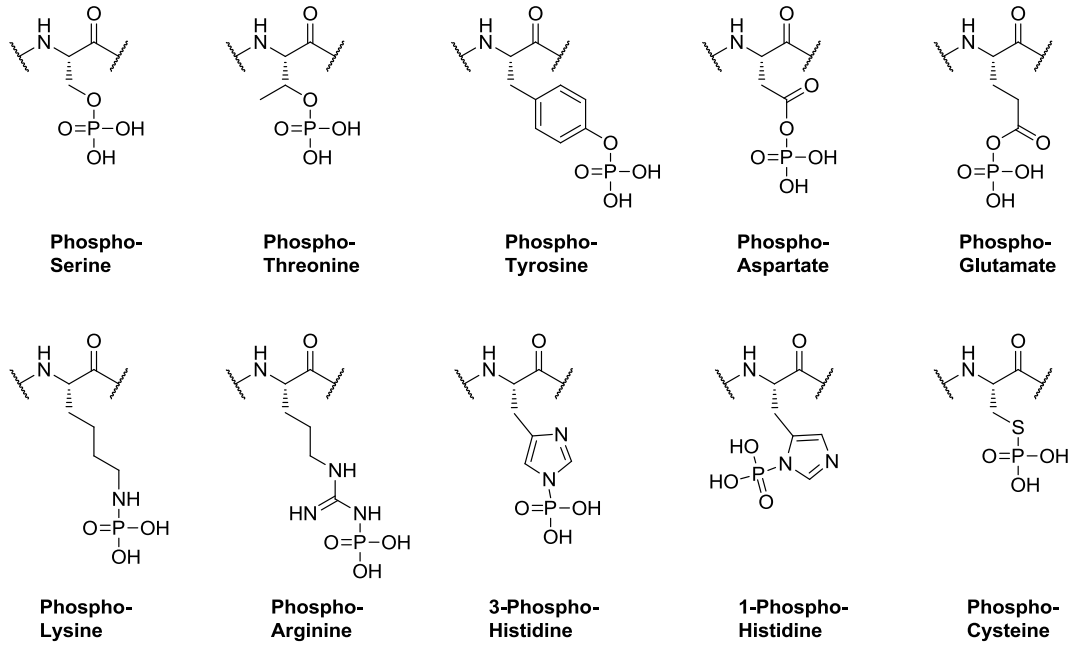

Figure 3: Chemical structures of phospho-amino acids. The structures of the well-known O-phosphorylated amino acids phospho-serine, phospho-threonine, phospho-tyrosine and the instable phospho-aspartate and phospho-glutamate are shown. Also given are the less well known and studies N-phosphorylated amino acids phospho-lysine, phospho-arginine and both phospho-histidine regio-isomers. Formation of phospho-cysteine is a reported but rare phenomenon.

1.2 Histidine Phosphorylation

1.2.1 The Two-component System in Prokaryotes

Intensive research performed the last twenty years has shown that bacteria use cleaver and quick signal transduction mechanisms to control specific gene expression. So-called two-component systems have been identified as the underlying mechanism. These signaling mechanisms allow the bacteria to respond to physical and chemical extracellular environmental changes by regulating osmolarity, nutrient uptake, redox potential, sporulation and the expression of virulence factors.[27] Histidine phosphorylation was found to be the key step in this process.
As an example, the bacteria *C. glutamicum* harbors 13 different two-component systems and one of them (MtrBA) is directly related to transcription regulation of target genes involved in the response to hyperosmotic stress (see figure 4). Two-component systems are in general a combination of a membrane bound sensor histidine kinase and a soluble response regulator protein located in the cytoplasm. A physical stimulus, related to a particular external stress factor, is sensed by the sensor kinase and transduced to an intracellular signal transduction cascade via auto-phosphorylation of a histidine on the sensor kinase. The activated phosphate is transferred to the response regulator (MtrA) and this activated transcription factor then interacts with specific binding sites near target genes on the DNA.[28]

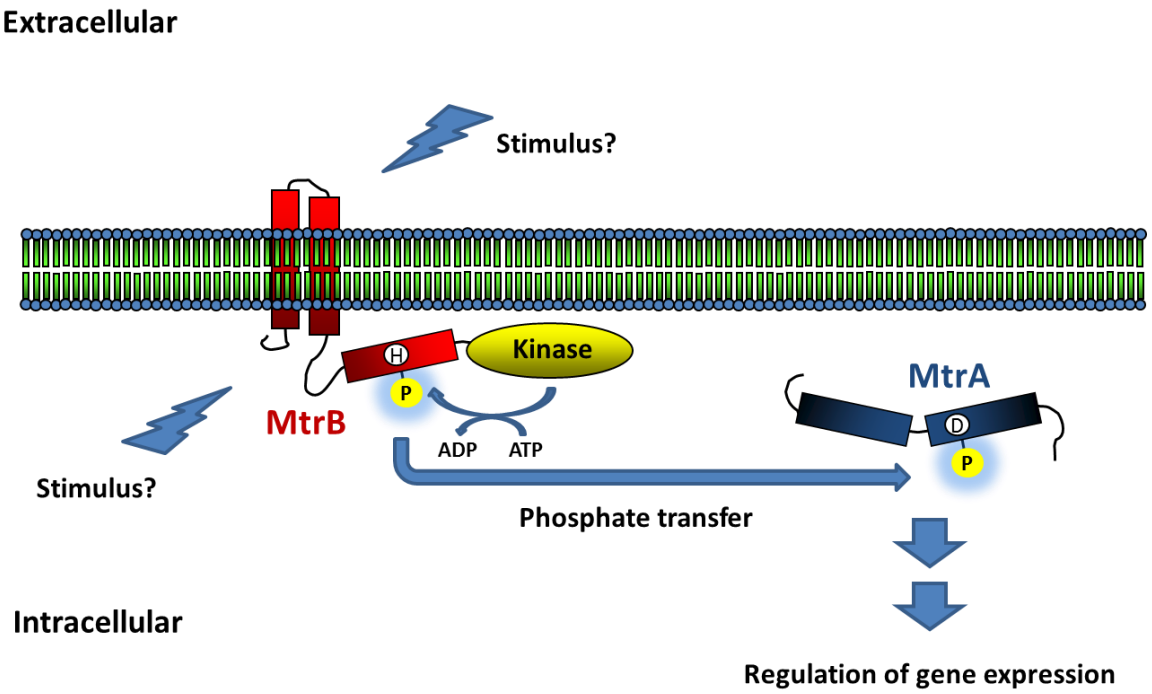

Figure 4: Representation of the two-component system MtrBA from *C. glutamicum*. Upon external stimuli the membrane bound histidine kinase MtrB auto-phosphorylates on a histidine (H). Interaction with the signaling molecule MtrA leads to phosphate transfer to MtrA on an aspartic acid (D) and consequent activation of this transcription factor. Figure adapted from www.kraemerlab.uni-koeln.de.[28]

The two-component system allows bacteria to take advantage of the chemically less stable nature of the N-P bond in the phosphorylated histidine. This quick phospho-transfer reaction speeds up signaling and allows for a quickly initiated response. Two-component signal transduction systems are used not only by bacteria, but also by other prokaryotes and higher plants. However, higher eukaryotes including mammals, use distinct signal transduction systems that incorporate O-phosphorylation as described in §1.1.2 and §1.1.3 rather than N-phosphorylation.

1.2.2 Histidine Phosphorylation in Eukaryotes

The overwhelming evidence found for histidine phosphorylation in bacteria (the two-component system) and the identification of O-phosphorylation as key in cell signaling in eukaryotes suggests a clear distinction; N-phosphorylation is used by prokaryotes and O-phosphorylation by eukaryotes. Nevertheless, homologs of the two-component system have been found in yeast, plant and fungi, and O-phosphorylation has also been found in prokaryotes.[29] The lack of tools to study histidine phosphorylation, especially in mammals, still hampers progress in this field.
In higher order eukaryotes phosphorylation of histidine on the β-subunit of trimeric G-proteins has been the focus for research. This phosphate can be transferred directly to the GDP attached to the α-subunit of the G-protein and activating it. A lot of effort has been invested in further elucidating this mechanism but the phospho-histidine intermediate appears to be very short-lived making it difficult to study.[30]
Histidine phosphorylation has also been shown to occur on the highly conserved histone H4 in various species.[31] There is much evidence on PTMs that are performed on the histones that control cellular processes like gene transcription, DNA repair, replication and recombination.[6] The two histidine residues on histone H4 that can be phosphorylated are in regions of the protein that form interactions with other histones in the nucleosome.[32] Here, histidine phosphorylation has the potential to disrupt the formation of nucleosome structure and influence DNA transcription directly. However, definite proof supporting this hypothesis has not been found yet.
ATP-citrate lyase (ACL) has been identified as a target of histidine phosphorylation.[33] In the cytosol, ACL cleaves citrate to form acetyl–coenzyme A (CoA) and oxaloacetate. Acetyl-CoA is used in the synthesis of acetylcholine, fatty acids, and cholesterol. Enzymatic removal of the histidine phosphate directly reduces its activity and slows down these metabolic pathways. An influence on acetylcholine synthesis suggests a role in the central nervous system (CNS). Indeed, an important role for ACL histidine phosphorylation has been found in the viability of neuronal cells.[34]
The intermediate conductance voltage-insensitive potassium channel KCa3.1 is the best example for understanding the potential of protein regulation by histidine phosphorylation. KCa3.1 has been shown to play a critical role in the stimulation of calcium influx in a number of cells.[35] Opening of the channel allows potassium to leave the cell and this facilitates influx of calcium from the endoplasmic reticulum (ER). His^{358}, which resides in the C terminus of the channel, is known to be phosphorylated in CD4 T cells. This initiates channel activation, and vice versa, de-phosphorylation leads to channel closing. T cell activation was shown to be directly influenced by the phosphorylation state of the KCa3.1 channel.
The kinases and phosphatases responsible for all these histidine phosphorylations appear to be much more rare in number that their O-phosphorylation counterparts.

1.2.3 The Kinases and Phosphatases involved in Histidine Phosphorylation

The before mentioned analytical difficulties to detect histidine phosphorylation has hindered research on the enzymes that are involved. Kinases and phosphatases involved in N-phosphorylation work mechanistically different from their O-phosphorylation counterparts and are therefore not easily found through sequence homology. Nevertheless, genomic sequencing has been successful in finding two-component like kinases in bacteria. Complete families of bacterial histidine kinases have been identified based on homology.[36] Dedicated histidine phosphatases however, seem to be rare in prokaryotes although not completely absent.[37] The kinases or the response regulator proteins of two component systems generally display aspartate phosphatase activity terminating the signal on their own.
Well studied and fully characterized histidine kinases and phosphatases in mammals have been limited to a single type of kinase and a single phosphatase. The Nucleoside Di-Phosphate Kinases (NDPKs) were originally seen as housekeeping kinases. They play a key role in nucleotide metabolism and catalyze the transfer of a phosphoryl group from a nucleoside triphosphate to a nucleoside diphosphate. Additionally, more functions for these kinases have been found in regulation of tumor metastasis, cell differentiation and cell motility.[30, 32] Of the nine different isoforms of NDPKs only two display intrinsic histidine phosphorylation activity. The NDPK-A and NDPK-B enzymes phosphorylate all target proteins mentioned in §1.2.2 *in vivo*, except for the histones in the cell nucleus. Here, the responsible kinases (Histone H4 histidine kinases or HHKs) have not been fully characterized.[30]
Several eukaryotic serine/threonine phosphatases have been shown to have moderate de-phosphorylation activity towards phospho-histidine. The histidine phosphorylation on histone H4 appears to be targeted by these phosphatases.[31] Also here, its relevance *in vivo* and to what extend it is an artifact remains unclear.
In 2002, a selective phosphatase was found and its primary structure fully sequenced. Until today this phospho-histidine phosphatase, or PHP (also known as PHP14 or PHPT1), remains the only fully evaluated enzyme that is truly dedicated to histidine phosphorylation in mammals. Its activity appears to be coupled to the NDPKs as it has the same realm of target proteins (see figure 5).

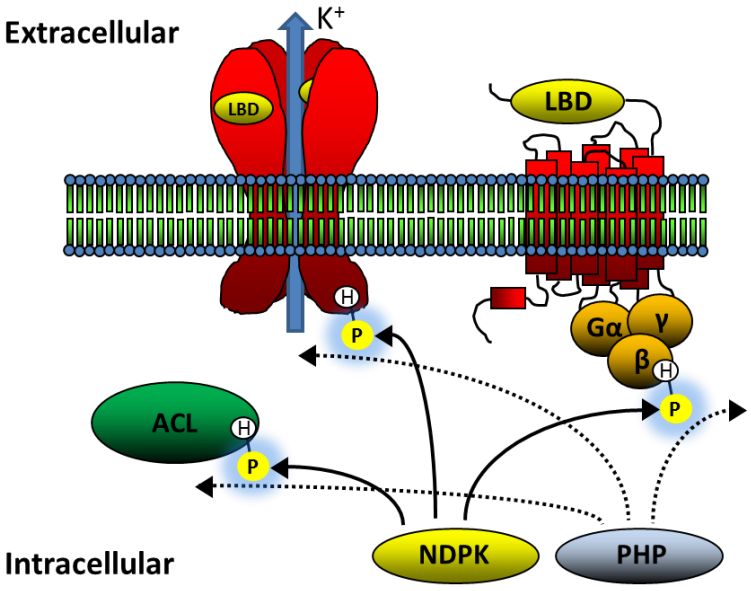

Figure 5: Histidine phosphorylation/ de-phosphorylation of KCa3.1, the β unit of G proteins and ACL by NDPK and PHP respectively. Activation of the intermediate conductance voltage-insensitive potassium channel KCa3.1 by a histidine kinase (NDPK-A or NDPK-B) leads to opening of the channel and release of potassium. This process can be terminated by PHP through removal of the phosphate. The same enzymes have also been shown to be responsible for the phosphorylation/ de-phosphorylation of ACL and the β-subunit of G proteins in vivo. Figure adapted from Klumpp et al. 2009.[38]

1.3 Phospho-histidine Phosphatase (PHP)

1.3.1 A mysterious enzyme

In 2002, two groups independently reported on a mammalian phosphatase selective for phospho-histidine. Klumpp and co-workers used the bacterial protein [^{32}P-His]cheA as bait in rabbit liver soluble extract.[39] Zetterqvist and co-workers used a synthetic phospho-histidine peptide to search for phosphatase activity in porcine liver cytosol extracts.[40] Isolation, purification and sequencing revealed a 14 kDa protein, eventually found in numerous organisms (see figure 6), but without homologues in bacteria and fungi. The enzyme showed no sensitivity for general phosphatase inhibitors like okadaic acid, microcystin, vanadate or genistein. This protein, clearly part of a novel class of enzymes, was named Phospho-Histidine Phosphatase (PHP). PHP has no structural resemblance to other phosphatases and its activity is not affected by EDTA, indicating catalytical independence from metals, like Zn, Mg or Ca. After ten years, PHP still remains enigmatic and stands out since no similar enzymes have been found. Its means of regulation remains to be clarified and its role in cell homeostasis is not even slightly clear. The expression levels (northern blot) in different tissues, high in brain and neuronal cells and elevated in heart and skeletal muscle, also do not give away much of its secrets. However, high expression levels in tissues where the epithelial cells have a short half-life was found, suggests an involvement in cell proliferation.[41]

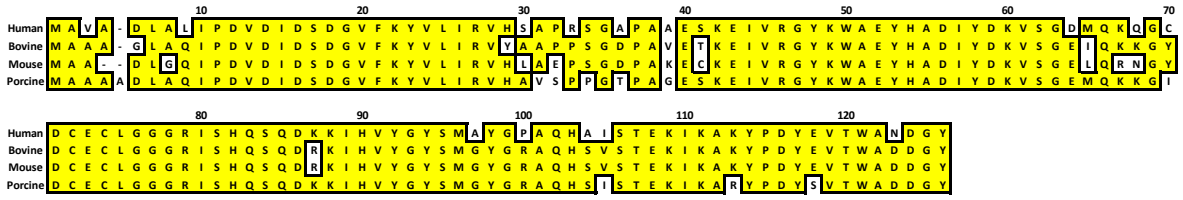

Figure 6: Alignment of human phospho-histidine phosphatase and interspecies homologous proteins. The amino acid sequence of human phospho-histidine phosphatase (PHP) compared with the homologous bovine, mouse and porcine sequences. Figure adapted from Ek et al. 2002.[40]

1.3.2 PHP in Healthy Tissues

PHP is found in virtually all vertebrates and tissue-types. Interestingly, it has been shown to be present in high quantity and activity in brain tissue and neurons.[33, 42] Already with its discovery by Klumpp and co-workers an important role for PHP in neuronal signaling was suggested. It was shown to be present in *C. elegance* exclusively in motor neurons along the ventral nerve cord.[39] Research in this line was continued and the effect of PHP overexpression and its interaction with ACL was studied in various neuronal cells.[42] A clear interaction was established between these two proteins and PHP was shown to de-phosphorylate ACL *in vivo* and by doing so reducing its activity. PHP can reduce neuronal cell viability through reducing the metabolic function of ACL and an increase in apoptosis was observed. It was suggested that excessive PHP activity can be linked to neurodegenerative diseases. A second study reporting the down-regulation of PHP with siRNA did not show an effect in human neuronal cell lines compared to untreated cells.[34]

PHP was also shown to have high expression levels in blood vessel walls.[41] Again, over-expression and down-regulation of PHP was used to study its function in cultured human umbilical-vein endothelial cells (HUVEC).[43] Over-expression led to reduced cell viability and increased levels of apoptosis. Down-regulation of PHP did not show an effect. The effect of over-expression is directly related to the enzyme's histidine phosphatase activity since over-expression of a catalytically non-active PHP mutant, H53A, showed no reduced cell viability.
In both studies siRNA was used for PHP down-regulation since there is no chemical inhibitor for PHP reported so far. An inhibitor could be used to more accurately study the effect of PHP and might even reveal PHP as a novel drug target in the treatment of neurodegenerative and cardiovascular disorders.

1.3.3 PHP in Cancerous Tissues

In 2003, the existence of an additional layer of N-phosphorylation on top of the O-phosphorylation in cell signaling was suggested.[44] This difficult-to-detect series of PTMs might be just as important in cell function and dysfunction as O-phosphorylation. Indeed, recently PHP has been linked to cancer.
In 2010, a study was published showing a relationship between PHP over-expression and metastasis of human lung cancer cell migration and invasion.[45] In human lung adenocarcinoma CL1-5 cells, high expression levels of PHP were found. This was correlated with lymph node metastasis in the tissues of human patients with lung cancer. The CL1-5 cell line normally shows high levels of invasive potential, but not after PHP gene silencing with siRNA. To further support the theory that PHP directly influences lung cancer metastasis, PHP was over-expressed in human non-small cell lung carcinoma cells (NCI H1299) and also here an increase in invasiveness and migration was observed. Comparing the CL1-5 cells with the siRNA PHP knockdown showed a remarkable difference in the expression pattern of an array of proteins that are described as cytoskeletal modulators. This suggests that PHP regulates cell migration/invasion via the cytoskeletal reorganization signaling pathway. This was further supported by comparing the siRNA PHP knockdown CL1-5 cells with CL1-0 cells. These CL1-0 cells are highly similar to CL1-5 but show poor metastatic properties. Knockdown of PHP expression from CL1-5 cells leads to an actin cytoskeletal rearrangement similar to that of the non-invasive CL1-0 cell line. How PHP activity influences cytoskeletal rearrangement is speculation but altering cytoplasmic calcium levels leads to cytoskeletal reorganization. PHP manipulation of G-proteins or KCa3.1 might very well be involved in this process.
In 2012, it was shown that level of PHP expression in hepatocellular carcinoma (HCC) tissues and cell lines are elevated compared to non-cancerous human liver tissue and cells.[46] HCC is an aggressive malignant tumor with high incidence and poor prognosis. A lentivirus-mediated delivery of siRNA targeting PHP was used to knockdown the enzyme. The results were more profound compare to the CL1-5 and NCI H1299 cells as both cell growth and proliferation were significantly inhibited.
These two studies are the first steps in mapping the role of PHP and its over-expression in cancerous tissues. There appears to be an important role for PHP in cell metastasis and a need for a chemical inhibitor to further elucidate PHP its role and function. It is even suggesting PHP as a possible drug target where small molecule inhibitors can be used as a novel chemotherapeutic.

1.3.4 The 3D Structure and Catalytical Mechanism of PHP

In 2005, Zetterqvist and co-workers, published a mutational study providing the first insights in PHP activity related to its structure.[47] In order to identify the active site, point mutations were introduced replacing conserved histidine and arginine residues for alanine. His^{53} and His^{102} were identified as being essential for catalytic activity as the mutations H53A and H102A lead to catalytically incompetent proteins. The mutations R45A and R78A decreased the activity by 89% and 50% respectively.
In 2006, a 1.9 Å resolution crystal structure was published (pdb code 2HW4, figure 7).[48] Here, the enzyme was described as: "a 125-amino acid human cytosolic protein that folds into a compact elbow-shaped molecule of a mixed α/β fold with novel topology". What was found by analyzing the surface of the protein around the essential His^{53} was a shallow pocket lined with AAs residues standing up from the protein surface (figure 7B). These residues show high conservation among the animal kingdom. Two distinct sets of conditions were used to crystallize the protein. A high concentration of sodium formate (pdb code 2HW4) or ammonium sulfate (pdb code 2NMM) was required to obtain diffracting crystals. The formate or sulfate anions were found well defined inside the active site of both structures (see figure 8A and 8B) and are kept in place by similar, but different, hydrogen bond networks. The phosphate-group from a phospho-histidine substrate is likely to bind in a similar fashion in order to facilitate PHP catalyzed hydrolysis.

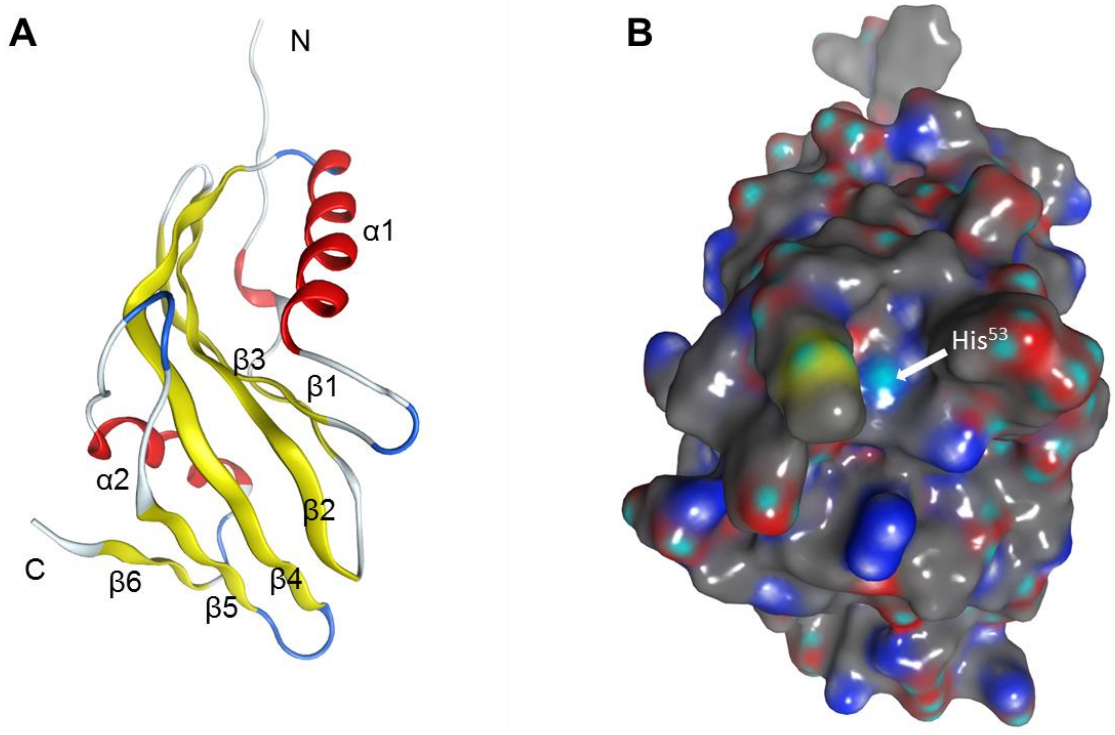

Figure 7: Crystal structure of PHP (pdb code 2HW4). A, Ribbon representation of PHP revealing 2 α-helices and 6 β-strands forming one folded β-sheet. **B,** Molecular surface representation with location of His^{53}. This residue is essential for catalytic activity, suggesting the catalytic site to be located in the shallow pocket above. The pocket is lined by several residues standing up from the protein surface. These residue show a high level of conservation among various species. Figure adapted from Busam et al. 2006.[48]

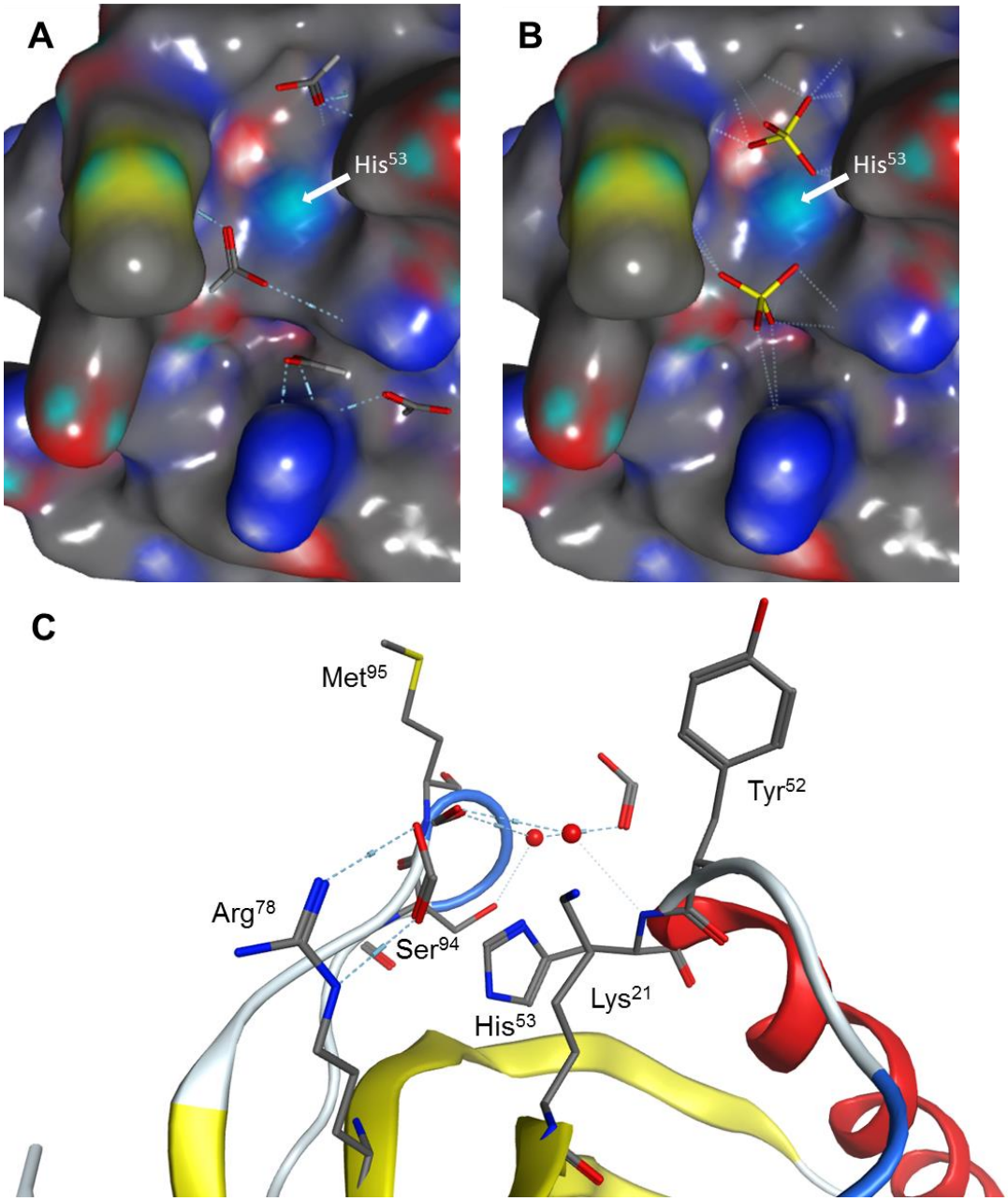

Figure 8: The proposed active site of PHP. A, A surface representation of the proposed active site with preserved formate ions (pdb code 2HW4). **B,** A surface representation of the proposed active site with preserved sulfate ions (pdb code 2NMM). **C,** A representation of the amino acids that line the active site and preserved water and formate ions. Figure adapted from Busam et al. 2006.[48]

The cavity is restricted by the upright standing residues Lys[21], Tyr[52], Arg[78], Ser[94] and Met[95] (see figure 8C). From these amino acids only Arg[78] was subjected to mutation in the forth-mentioned study. The R78A-mutant showed a reduced enzyme activity of 50% supporting the assignment of catalytic activity to this particular location. Lys[21] and Arg[78] were suggested to serve as substrate anchors. Interestingly, the crystal structure does not support the observation that H102A and R45A are detrimental for enzyme activity. Both residues are located far from the putative active site.

In 2009, a more detailed mutation study in combination with an NMR solution structure analysis was reported.[49] The active site was more accurately defined through NMR solution structure comparison of the free phosphate (P_i) bound versus non-bound version and a more extended point mutation study. Two possible catalytic sites, based on the NMR measurements were evaluated (see site I and site II in figure 9). Site I is in between the residues Tyr^{52}, His^{53} and Ala^{54} on one side and Ser^{94}, Met^{95}, Ala^{96}, Tyr^{97} and Gly^{98} on the other side. Site II can be found in between Lys^{21}, Arg^{78}, Ile^{79} and the residues Gly^{124} and Tyr^{125} on the flexible, in the X-ray structure non-visible, C-terminus. In both sites a conserved sulfate is present. Close examination of the P_i bound NMR solution structure shows a significantly larger influence on the residues from site I. This is further supported by point mutations of the majority of the amino acids forming the two sites. Indeed, H53A is completely inactive, but it has an enhancing effect on P_i binding. This suggests that the imidazole ring of His^{53} is not involved in substrate binding, but is essential for catalysis. The M95D and A96D mutations that were generated to introduce a negative charge at site I and the S94A mutation all show significant decreases in phosphate binding and catalytic activity. Ser^{94} is likely to form an H-bond with the phosphate, as is seen in crystal structure 2NMM, where the sulfate is coordinated with the serine OH. The mutations of site II residues, K21A and R78A show only poor effects on P_i binding or enzyme catalysis. Even a double mutant of these amino acids is still catalytically active. This clearly shows that these residues do not serve as substrate anchors as proposed before. Altogether, there is strong evidence for PHP exerting its catalytical activity at site I. Close analysis of chemical shifts in the P_i-bound NMR solution structure suggest a tight coordination of the substrate phosphate by multiple H-bonds between the protein backbone N-H of His^{53}, Ala^{54} and Ala^{96}. As mentioned before, Ser^{94} is likely to contribute and forming a complex hydrogen bond network very similar to the one observed in 2NMM for a sulfate anion.

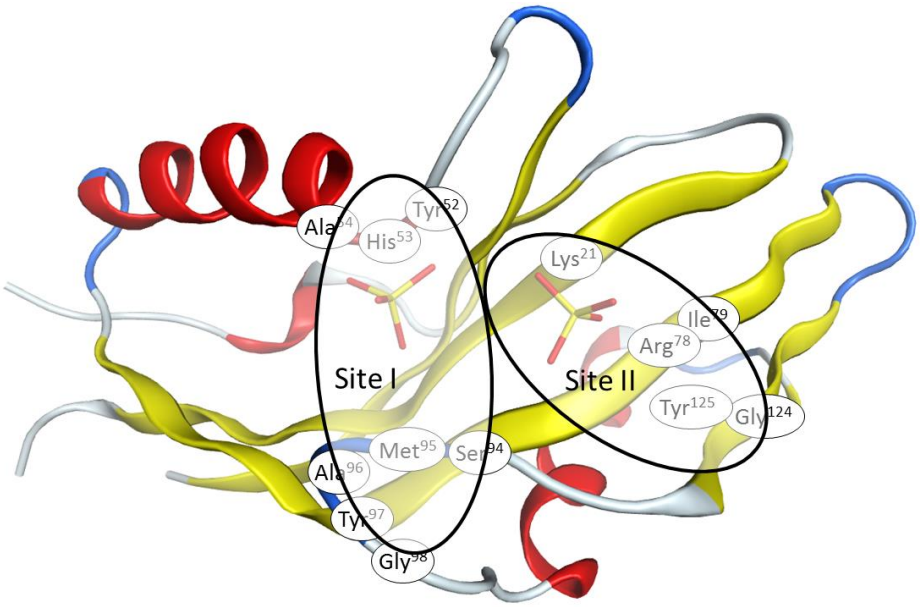

Figure 9: The location of the two proposed sites of catalysis (Site I and Site II) on X-ray structure 2NMM. Based on chemical shift information two possible active sites are proposed; Site I and Site II. See text for details. Figure adapted from Gong et al. 2009.[49]

Based on the suggested phosphate binding a mechanism of hydrolysis of phospho-histidine was proposed with His^{53} as the catalytical residue (see figure 10). In general, a catalytic histidine can act as an attacking nucleophile, a general acid catalyst that protonates the leaving group or as a base, deprotonating a solvent molecule. His^{53} has a predicted pK_a of 3.13, making it unlikely to be a hydrogen donor.[48] Also, the distance to the sulfate (~3.7 Å) is too large for the histidine to act as a nucleophile. This strongly suggests activation of a water molecule by His^{53} (as depicted in figure 10). This mechanism is completely different from the mechanisms used by serine/threonine and tyrosine phosphatase families.

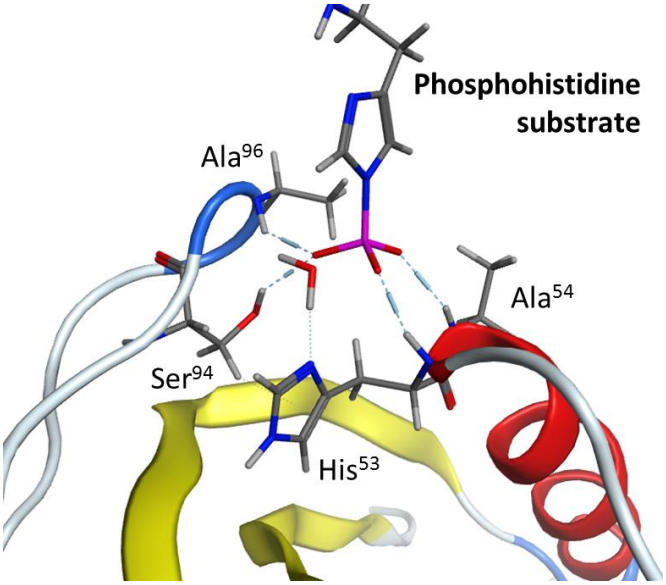

Figure 10: Proposed catalytic mechanism of PHP induced phospho-histidine hydrolysis. The amino acids His^{53}, Ala^{54}, Ser^{94} and Ala^{96} are likely involved in phosphate binding. His^{53}, the only amino acids that is absolutely vital for catalytic activity, is too far away from the phosphate to serve as a nucleophile. His^{53} can also serve as an activator of a water molecule. This water molecule, in close proximity to the phospho-histidine, can act as a nucleophile attacking the phospho-histidine. The assumption is that the phospho-histidine will be 'caught' in the same hydrogen bond network that keeps the sulfate in 2NNM in place due to hydrogen bonds with residues Ala^{54}, Ser^{94} and Ala^{96}. Figure inspired by Gong et al. 2009.[49]

In 2010, Klumpp and co-workers suggested the presence of an ATP binding site on PHP.[50] This would be next to a glycine rich region. Indeed it was shown that PHP can be reversibly labeled with [α-^{32}P]ATP. However, close examination of the crystal-structures makes this highly unlikely. The supposedly responsible triple glycine motive (Gly^{75}-Gly^{76}-Gly^{77}) is located inside the protein underneath the catalytic site. More likely, ATP binds inside the catalytic site and mutations G75A and G77A simply re-model the active site indirectly, explaining the loss of ATP binding and enzyme activity. His^{53} might be pushed up by these mutations altering the solvent exposed catalytical site. It is not unlikely that ATP, with a series of three negatively charged phosphates, will bind to the basic active site directly. More interestingly, this study also looked into the three cysteine residues that are located closely together far away from the active site. Mutation of these residues to alanine did not affect enzyme activity. Truncation of the enzyme from the N-terminus side was possible till amino acid 9 after which amino acid deletion resulted in almost complete loss of catalytic activity. The C-terminus appears to be more important since only 4 amino acids could be deleted without loss of activity.

An extensive survey of tyrosine phosphorylation of proteins isolated from human mammary epithelial cells published in 2009 revealed Tyr^{116} and Tyr^{125} from PHP as targets of phosphorylation.[51] The meaning and relevance of this feature was not addressed and remains to be investigated.

Chapter 2: Aim of the Project

2.1 Prospects and Challenges in Chemical PHP Inhibition

The efforts so far in studying the physiological role of PHP clearly show the need for tools that biology alone cannot provide. These tools can be obtained through chemical means. Especially a small molecule/peptidomimetic inhibitor for PHP can be useful to further elucidate the role that PHP plays in complex processes in cells. Since PHP activity has been linked to neurodegenerative and cardiovascular disorders and cancer, a cellular active PHP inhibitor might be more than a biochemical tool. It can be regarded as a potential therapeutic agent.
For a long time, it was assumed that targeting phosphorylation related enzymes with a small molecule for therapeutic purposes was physiologically impossible. However, the success of the BCR-Abl kinase inhibitor Imatinib (approved in 2001 as Gleevac®) showed that issues of selectivity and related toxicity can be overcome.[52] Since then, several kinase inhibitors successfully reached the market, although the field of phosphatase inhibitors has not taken such a high flight. For inhibition of phosphatases with small molecules, selectivity and poor pharmacokinetic properties remains problematic.[53] The catalytical domains of phosphatases are generally highly conserved and these enzymes exert selectivity in substrate through regulatory domains or subunits and not so much through direct protein-protein selection. Also, localization of the required phosphatase through protein-protein interactions or PTMs (e.g. palmitoylation to achieve membrane binding) is likely to occur and will compartmentalize enzyme catalysis to where it is required.[54] This selectivity issue is less likely to occur with a potent PHP inhibitor. The enzyme uses a unique mechanism of action (as explained in §1.3.4) and lacks the family resemblance to other enzymes in cells. This significantly raises the possibility of a phosphatase inhibitor, selectively targeting PHP, succeeding as a tool and/or drug compound.

2.2 A Strategic Building Block as a Starting Point for PHP Inhibitors

As suggested by molecular modeling, substrate peptides can have significant interaction with the proposed catalytic site of PHP.[48] However, the proposed mechanism and the point mutations reported later, as presented in §1.3.4, suggest otherwise.[49] It remains to be seen how big (or better, how small) and solvent exposed (how 'drug-able') the catalytic site of PHP really is. Also, it is unclear to what extend a peptide sequence will contribute to ligand binding.
Without hits from a high-throughput screen, using a rational design is an attractive option, e.g. a phospho-histidine mimic that cannot be hydrolyzed by the enzyme. This unit would preferably be 'dressed up' in the shape of a Solid Phase Peptide Synthesis (SPPS) compatible building block. Such a strategy has been deployed before, with limited success until recently, in the efforts to generate antibodies against phospho-histidine. The native phospho-histidine (figure 11, **1**) has been mimicked by the use of a furan or pyrrole functionalized as a phosphonate (figure 11, **2** and **3**).[55] Here, the non-hydrolysable C-P bond replaces the acid sensitive N-P bond in **1** in order to prevent the acid catalyzed hydrolysis during the immunization of an animal that is used to generate antibodies. Only the pyrrole **3** has been reported to be used to generate antibodies that recognized the native epitope. The generated antibodies did recognize a peptide with **3** incorporated; however, the native phospho-histidine **1** was not, rendering these antibodies useless.

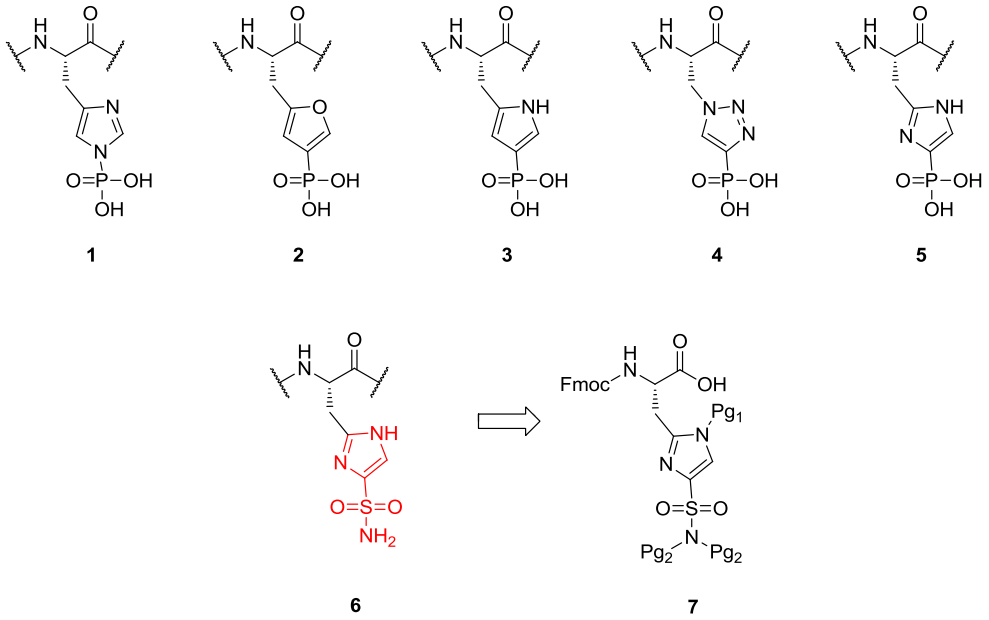

Figure 11: The structures of phospho-histidine (1), reported phospho-histidine mimics 2-5, the novel sulfonamide based mimic 6 and the derived SPPS building block 7. Building block **7** represents a target molecule that can be incorporated in peptides designed as PHP inhibitors. Alternatively, the sulfonamide imidazole motive indicated in red represents a possible starting point for small molecule PHP inhibitor design.

The triazole moiety **4** was used successfully as the generated antibodies indeed recognized the native phospho-histidine **1**.[25] However, the selectivity over phospho-tyrosine was not reported. In our laboratory, similar efforts are ongoing with an imidazole based mimic **5** as a tool to generate antibodies.[56] Improved selectivity over tyrosine is expected based on a more accurate protonation state. The imidazole of **5** will be positively charged under physiological conditions like **1** and unlike **4**.
Using a phospho-histidine mimic (like **2-5**) as a starting point for PHP inhibitors seems reasonable. However, a negatively charged phosphate is likely to give poor cell penetration. Therefore, it was decided to look into the possibility of using a sulfonamide mimic **6** for the transition state of a PHP catalyzed phospho-histidine hydrolysis. In this project the synthesis of a strategic building block **7** is presented. This synthetic amino acid can be incorporated into peptides and upon deprotection these peptides can be tested for PHP inhibition activity. Alternatively, the possibility to generate small molecule inhibitors with this approach is explored. The sulfonamide decorated imidazole motive (indicated in red in figure 11) can serve as a good starting point for small molecule inhibitors as peptide based inhibitors might prove to be too large. Overall, the first steps in this project are the production of the enzyme, setup of biochemical screening and binding assays (described in Chapter 3) and the synthesis/evaluation of building block **7** (described in Chapter 4). The design, synthesis and evaluation of small molecule inhibitors are described in Chapter 5. Chapter 6 is dedicated to the further evaluation of small molecule inhibitors, including cellular experiments. Chapter 7 describes the synthesis and evaluation of several peptides prepared to investigate the histidine phosphorylation of Histone H4. Chapter 8 presents the concluding remarks and future prospects. Finally, the experimental section is described in Chapter 9.

Chapter 3: Assay Development

3.1 Introduction

In order to identify molecules with enzyme inhibitory activity, functional assays are required that are simple, robust and reproducible. A phosphatase assay requires, besides the enzyme, an appropriate substrate that can be de-phosphorylated. Both products of this reaction, the de-phosphorylated substrate or the released phosphate, can be used as readout for enzyme activity (see figure 12).

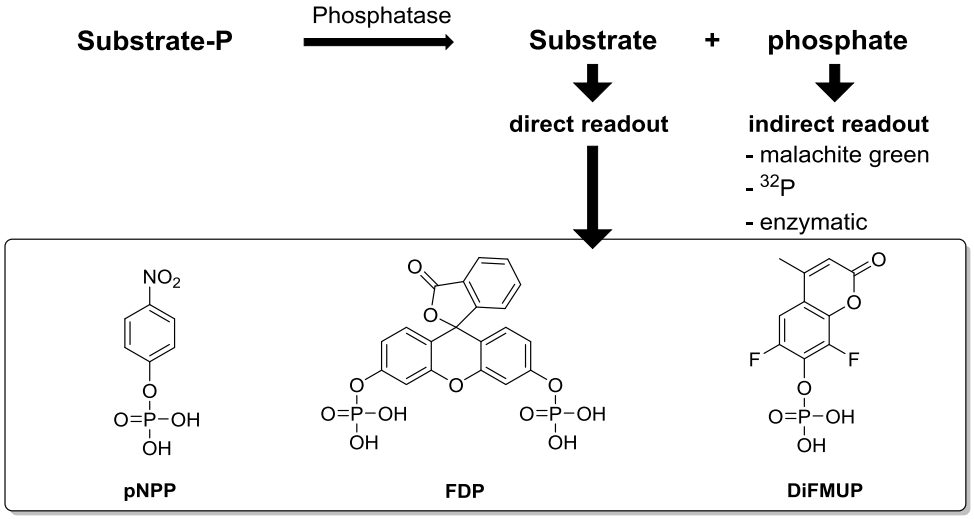

Figure 12: Reaction scheme of a phosphatase catalyzed substrate de-phosphorylation reaction. Both substrate and phosphate can be used as a measure for reaction. In the rectangle are shown the structures of well-known substrates that show fluorescence upon phosphate hydrolysis.

For phosphatases, different activity assaying techniques have been described. Traditionally, phosphatase assays were 'discontinuous', measuring phosphate release after quenching of the reaction using malachite green, ^{32}P-labelled substrates or a second enzymatic reaction.[57] Such an approach is elaborate and does not allow 'real-time' reaction monitoring. More recent, assays have been developed that rely on direct detection of changes in UV absorbance, fluorescence or fluorescence polarization due to the de-phosphorylation of substrate. These assays are called 'continuous' as the readout is measured instantly. For tyrosine phosphatases, substrates like p-nitrophenyl phosphate (pNPP), fluorescein diphosphate (FDP) and 6,8-difluoro-4-methylumbellyferyl phosphate (DiFMUP) are the substrates of choice and allow a direct readout (see figure 12).[58] Also, for serine/threonine phosphatases appropriate fluorescence readout systems have been developed that allow direct continuous detection.[59] As an example, a cleaver chemical instability built into a non-fluorescent peptide is used to release the fluorescent 7-hydroxycoumarin anion upon serine de-phosphorylation (see figure 13).
For PHP activity assaying, only discontinuous methods have been used, e.g. malachite green to detect and quantify the released phosphate. However, for research purposes, a continuous PHP assay is desirable. A continuous assay will allow us to determine important parameters (e.g. K_M) and direct analysis of enzyme inhibition by inhibitors. Both substrate and phosphate readouts were considered and successfully pursued in a continuous set-up (see §3.4 and §3.5).

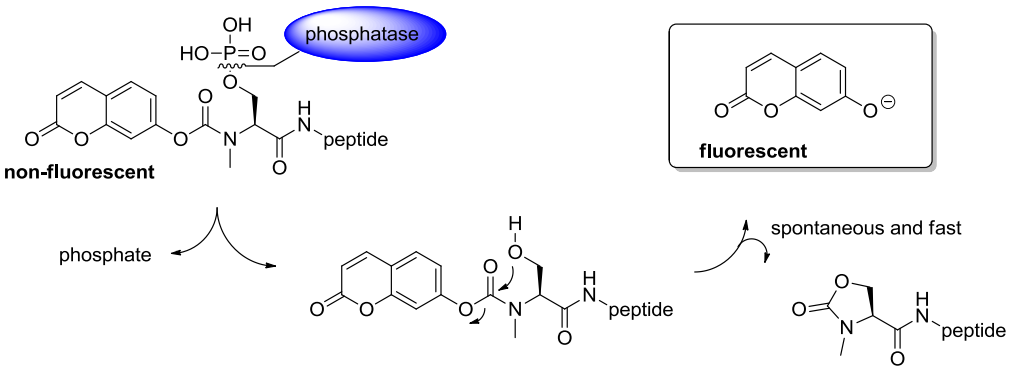

Figure 13: A: Reaction scheme of a Ser/Thr phosphatase assay. A non-fluorescent substrate is de-phosphorylated by the phosphatase of interest and the product is unstable and releases a fluorescent coumarin upon degradation. This anion can be used as a continuous readout. Figure adapted from Xue et al. 2010.[59]

3.2 Cloning and Expression of PHP

The development of PHP assays requires easy access to the non-commercially available enzyme itself. The gene encoding for PHP was supplied to us by Prof. Zetterqvist (Dept. Medical biochemistry, Uppsala University) in the form of a pBADNK vector. This modified expression vector lacked a tag suitable for affinity purification. The gene was cloned into 5 different pBADM expression vectors (see table 1) using the technique of ligation-independent cloning (LIC). These vectors produce the gene product with N-terminal attached His-tag and fusion proteins with different sizes that can increase solubility and expression.[60] Besides the included His-tag the fusion proteins can also be used for affinity chromatography to purify the construct. By use of a TEV cleavage site the fusion protein can be removed leaving just an additional glycine and alanine attached to the N-terminus of the expressed target protein. The cloning and expression in Escherichia coli TOP10 cells upon arabinose addition was successful in all cases as figure 14 shows. The pBADM-60 construct was used for protein production. After His-tag purification (lane 7) the construct was treated with TEV protease (lane 8) and purified using size exclusion chromatography (SEC) as shown in lane 9. Also the product of pBADM-11 was purified but the His-tag was not removed through TEV digestion. This construct was used exclusively for protein X-ray crystallography as described in §3.7.

Vector	*Escherichia coli* derived fusion protein	Size of PHP construct (kDa)
pBADM-11	-	17.0
pBADM-20	Thioredoxin (TrxA)	28.2
pBADM-30	glutathione-S-transferase (GST)	41.6
pBADM-40	Maltose-binding protein (MBP)	56.9
pBADM-60	N utilization substance A (NusA)	70.9

Table 1: overview of the pBADM vectors used for PHP cloning and expression.[60]

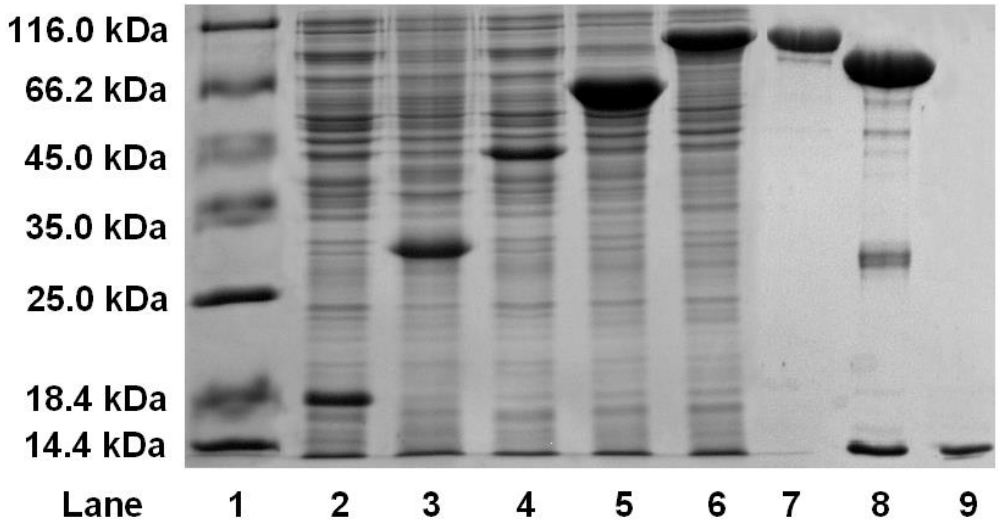

Figure 14: SDS-PAGE gel showing the overexpressed constructs as indicated in Table 1 and the purification and TEV cleavage product: the purified PHP. Lane 1**:** Protein marker, 2: pBADM-11 product His-PHP, 3: pBADM-20 product His-TrxA-PHP, 4: pBADM-30 product His-GST-PHP, 5: pBADM-40 product MBP-PHP, 6: pBADM-60 product His-NusA-PHP, 7: His-NusA-PHP after Ni-NTA purification, 8: PHP, TEV and His-NusA after TEV cleavage, 9: PHP after SEC purification.

Sequencing confirmed successful cloning in case of all five vectors and the mass of the pBADM-60 expressed and purified PHP, with the addition of two N-terminus amino acids, was confirmed using ESI-MS.

3.3 Enzyme activity

The expressed and purified enzyme was aliquoted as 100 µM stock solutions and stored at -80 ^{0}C. To test the viability of the protein and these storage conditions the enzyme activity from a defrozen sample was determined and compared to literature. With the discovery of PHP in 2002, Zetterqvist and co-workers reported a specific activity of 9 µmolmin^{-1}mg^{-1} at pH 7.5 towards a synthetic phospho-histidine peptide.[40] Using a synthetic 20 amino acid phospho-peptide (see §7.3 for details on structure and synthesis) a specific activity of 6.7 µmolmin^{-1}mg^{-1} was established. An anion exchange column was used to separate phosphorylated from non-phosphorylated peptide and determination of conversion.
An interesting issue concerning PHP activity is the question of higher order protein structures. It has been suggested that PHP is active not as a monomer but as a trimer.[38] The X-ray structure 2NMM (as mentioned in §1.3.4) also seems to suggest this (see figure 15). To investigate this, the protein was concentrated to ~100 mg/mL to force quaternary protein structure formation and was analyzed using analytical SEC. The concentrated protein solution was run and compared with a marker solution (see figure 16). A single population of PHP was observed with a molecular weight slightly less than 20 kDa. This strongly suggests that the enzyme is active as a monomer.

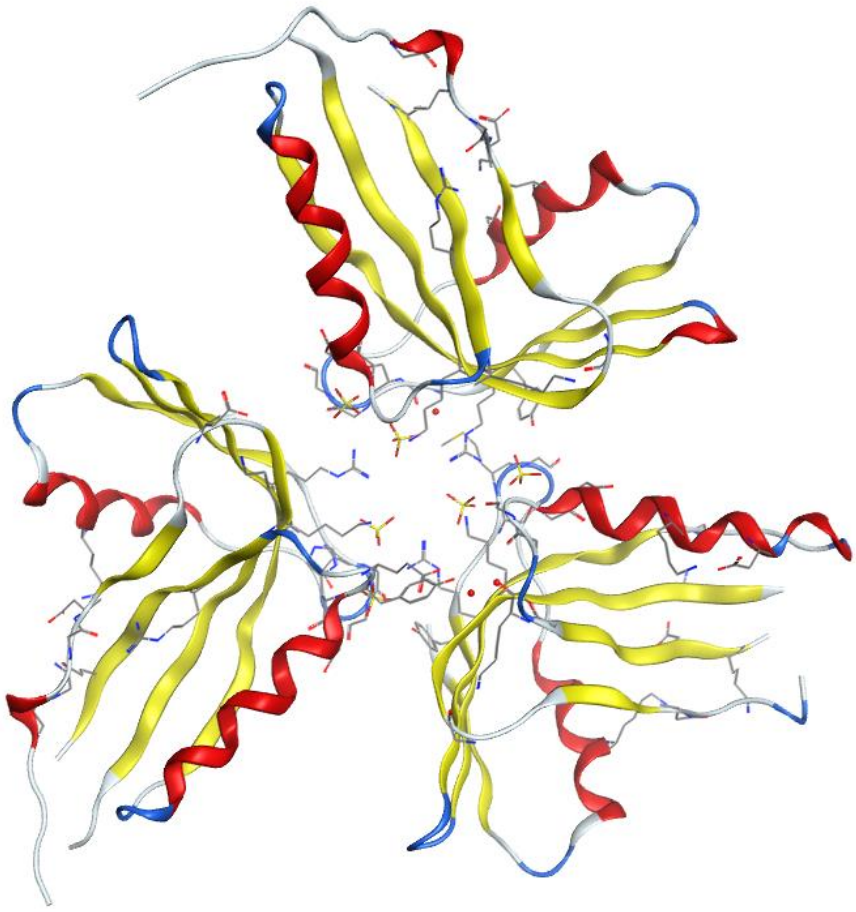

Figure 15: A: X-ray structure 2NMM as submitted to the Protein Database. PHP is crystallized in a clear trimeric shape with the individual catalytic sites (as described in §1.3.4) in close proximity. The lineup of the protein molecules suggests the existence of a quaternary structure.

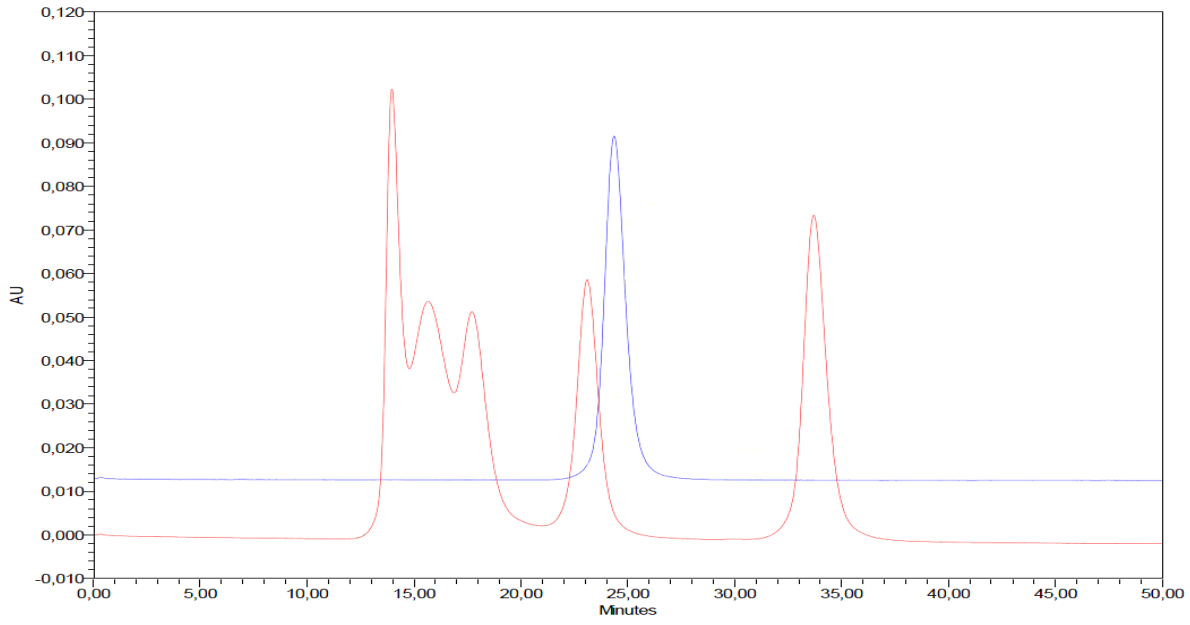

Figure 16: Analytical size exclusion run of PHP. Red line: Marker (Mw: from left to right, 66, 45, 31, 20 and 6.5 kDa). Blue line: PHP (Mw: 14 kDa).

3.4 Continuous Fluorometric Assay

For a PHP activity assay the very sensitive and 'continuous' technique of fluorescence is preferred. For a continuous fluorescence readout generated by an enzyme with a unique mechanism of catalysis (like phospho-histidine phosphatase), the development of new substrates needs to be considered. A phospho-histidine substrate that changes its fluorescence properties upon enzymatic de-phosphorylation is required. A phospho-imidazole analogue of fluorescein (**8**) or coumarin (**9**) can be considered (see figure 17). Such molecules are synthetically not straightforward and it is doubtful that de-phosphorylation of these substrates will indeed display a significant change in fluorescence. Also the approach presented earlier in figure 13 (§3.1) is not feasible for a weak nucleophile like histidine.

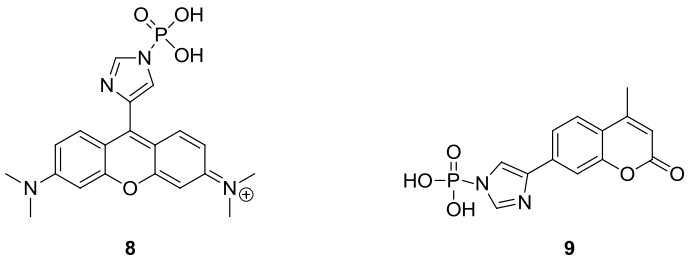

8 **9**

Figure 17: Structure of proposed phospho-histidine fluorescent substrate molecules 8 and 9.

PHP has been reported to have some activity towards p-nitrophenyl phosphate (see pNPP in figure 12) but, it was used in a discontinuous fashion (in combination with addition of base before end point measurement).[49] 6,8-difluoro-4-methyl-2-oxo-2H-chromen-7-yl dihydrogen phosphate or DiFMUP (**13**), a known substrate used in tyrosine phosphatase assays, is functional in a large pH range (5 to 8) and represents an interesting alternative if PHP does remove the phosphate.[61]
This substrate was easily prepared from 6,8-difluoro-7-hydroxy-4-methylcoumarin (**11**) in two steps (see scheme 1). Introduction of the benzyl protected phosphate was achieved using an *in-situ* generated dibenzylphosphoryl chloride and hydrogenation of **12** yielded **13** in 76% yield (over two steps). **11** was synthesized from 2,3,4,5-tetrafluor nitrobenzene (**10**) by Thilo Walther as described in his dissertation.[62]

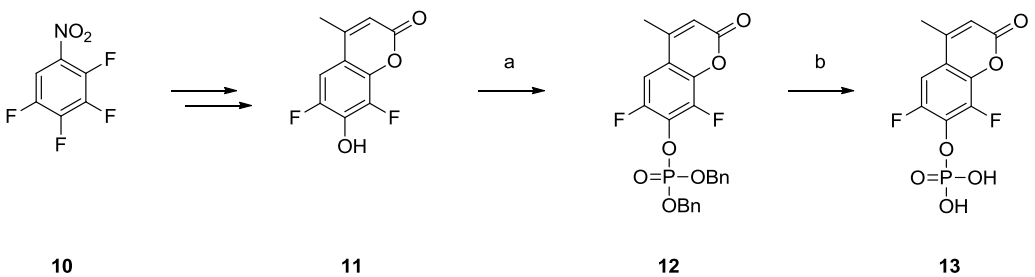

10 **11** **12** **13**

Scheme 1: Synthesis of DiFMUP (13). a: CCl_4, DiPEA, DMAP,dibenzyl phosphite, ACN, -15 ^{o}C. **b:** H_2, Pd/C, EtOH/toluene, rt, 76% (over two steps).

Potential substrate DiFMUP (**13**) was subjected to the enzyme and fluorescence was monitored at 455 nm upon excitation at 355 nm at 37 °C. Conditions were chosen as reported in literature.[62] The pH was set at 8 at which the enzyme is most active.[40, 49] Indeed the substrate proved sensitive to PHP enzymatically induced hydrolysis. To generate a functional assay useful for inhibitor identification significant optimization is required. First, the linearity of detection was established for the plate reader instrument that was used. Plotting the signal obtained against the product (compound **11**) concentration identified a linear range useful for kinetic measurements and a maximal signal beyond where linearity is slowly lost (see figure 18). Above 5 µM of product formation linearity clearly starts to deviate.

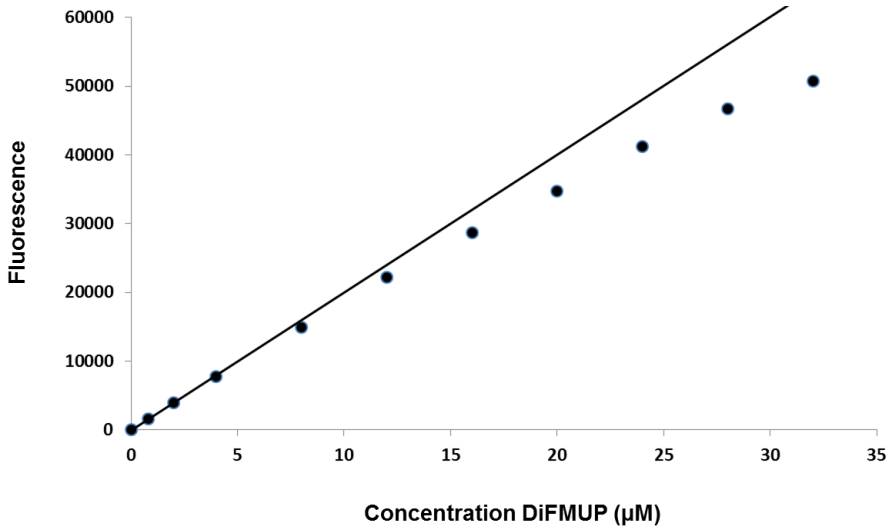

Figure 18: Fluorescence plotted against the concentration of de-phosphorylation reaction product (11). Testing the linearity of signal showed that above a concentration of 5 µM linearity starts to deviate.

When using a setup with a single enzyme (E) and substrate (S), the kinetics can be described by equation 1. ES is the enzyme-substrate complex that is formed prior to the enzyme catalyzed reaction occurring. k_1 is the rate constant for ES formation and k_{-1} the dissociation rate. The overall rate-limiting step in the reaction is the breakdown of the ES complex to yield product (P), which proceeds with rate constant k_2. Assuming rapid equilibrium between reactants (E and S) and the enzyme-substrate complex (ES), the kinetic behavior of enzymes based on the substrate concentration can be described by equation 2. Here, initial velocity of the reaction is related to the substrate concentration [S]. This equation is generally known as the Michaelis-Menten equation.[63]

$$[E] + [S] \underset{k_{-1}}{\overset{k_1}{\rightleftharpoons}} [ES] \xrightarrow{k_2} [E] + [P]$$

Equation 1: General equation describing an enzymetic reaction. [E] = the enzyme concentration, [S] = substrate concentration, [ES] = concentration of a enzyme-substrate complex and [P] = the concentration of the product of the processed substrate.

$$V = \frac{[S] * V_{max}}{[S] + K_M}$$

Equation 2: Michaelis-Menten equation. V = the rate of the reaction, V_{max} = maximal reaction rate, [S] = substrate concentration and K_M = the Michaelis-Menten constant.

The parameter V_{max} is the maximum velocity of reaction that can be reached under substrate saturation conditions. K_M is the Michaelis-Menten constant and represents the concentration of substrate where the velocity of reaction is half the V_{max} (see figure 19). Establishing these parameters is important when identifying enzyme inhibitors. It is essential to run the assay at a substrate concentration at or below the determined K_M value. A higher concentration of substrate will saturate the enzyme and prevent sufficient inhibitor binding to be noticed. Assuming rapid equilibrium between reactants (E and S) and the enzyme-substrate complex (ES) also makes $k_2 = k_{cat}$. The turnover number (k_{cat}) expresses the number of substrate molecules that is being converted to product by the enzyme per second. Also, the parameter k_{cat}/K_M is useful to determine and represents the efficiency of the enzyme towards the substrate and has a physical upper limit of 10^8-10^{10}. Such an enzyme is referred to as superefficient or perfect enzyme.[64]
To determine the K_M the reaction needs to be run at different concentrations of substrate and the initial velocity plotted against the concentration. The equation is only true if the [S] >> [P] and that requires initial velocities to be measured where only a fraction of substrate has been converted to product. This yields a graph like figure 19. K_M and V_{max} can be visually determined from this graph, however this is inaccurate. Nonlinear regression analysis software is preferred in determination of these parameters. The assay was performed at different substrate concentrations ranging from 50 to 1000 µM. The initial velocities were measured and by using the software program XL Fit. A K_M of 765 ± 59 µM and a V_{max} of 8.3 ± 0.6 µM/s was established. k_{cat}/K_M was determined to be 1.08 ± 0.2 $.10^5$ $M^{-1}.s^{-1}$.

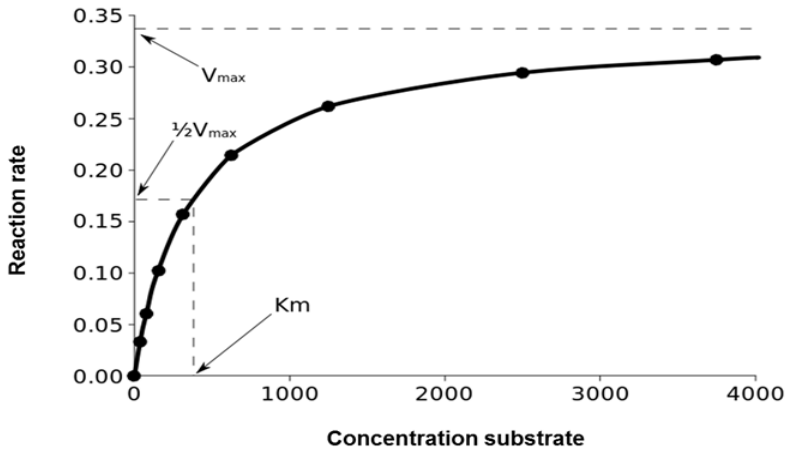

Figure 19: example of the initial velocity plotted against substrate concentration. This graph illustrates an enzyme reaching its maximum rate of substrate conversion V_{max} when increasing the substrate concentration (enzyme saturation). K_M is the concentration of substrate at half the V_{max}.

3.5 Continuous Coupled Enzyme Assay

The assay described in the previous paragraph allows for quick screening and evaluation of PHP inhibitors however, a phospho-tyrosine mimic like DiFMUP (**13**) does not qualify as a physiologically relevant PHP substrate. A control assay utilizing a real phospho-histidine will be required. Consequently, the enzymatically produced 'free' phosphate must be considered as readout. A system to detect phosphate in a continuous fashion has been reported and successfully used in a variety of assays testing for phosphatase, ATPase, GTPase and other enzymatic activity.[65] In this so called coupled assay setup, the enzyme purine nucleoside phosphorylase (PNP, *Bacillus cereus*) rapidly processed free phosphate when provided with cofactor 2-amino-6-mercapto-7-methylpurine riboside (MESG) (see figure 20). This synthetic nucleotide is converted by the enzyme to 2-amino-6-mercapto-7-methylpurine (MES) and the UV absorption of this product can be measured directly at a wavelength of 360 nm. This system is functional in a pH range of 6.5 to 8.5. This is compatible with the pH range required for an acid sensitive phospho-histidine (pH > 7). This assay procedure does require three additional ingredients in the form of a suitable phospho-histidine substrate, the enzyme PNP and the purine derivative MESG.

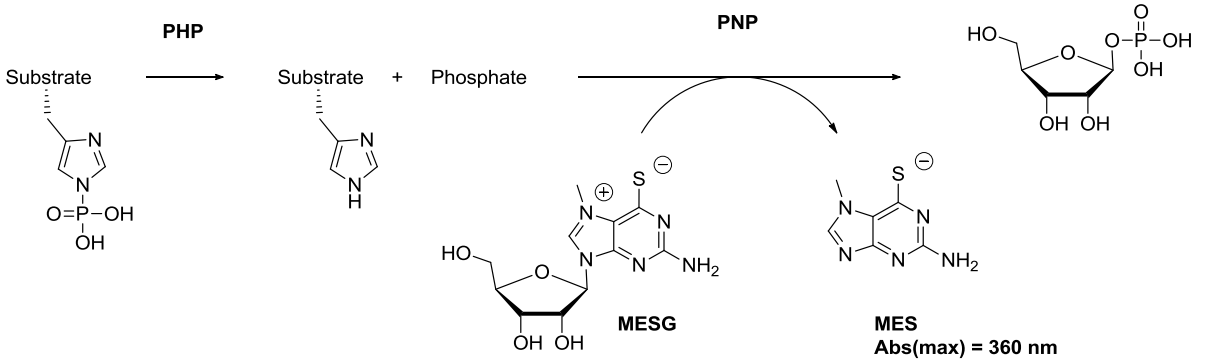

Figure 20: Principle of the coupled assay. The phosphate produced by PHP induced substrate hydrolysis is detected through a second enzyme reaction catalyzed by PNP producing MESP. The formation of this assay product can be monitored through absorption at 360 nm.

Obtaining a phospho-histidine substrate is synthetically feasible. Chemical phosphorylation of histidine itself (or residues in peptides/proteins) has been described in literature as early as 1991.[66] The reagent potassium phosphoramidate (PPA) phosphorylates histidines readily on both the 1- and 3-position. Over time the predominant 1,3-diphospho-histidine is not stable and converts to the more stable 1-phospho-histidine (**15a** see figure 21) and the predominant 3-phospho-histidine (**15b**). Nevertheless, obtaining a chemically pure product is important to guarantee a reproducible stable readout. This procedure requires a purification step upon phosphorylation. Using a single amino acid histidine **14** rather than a peptide seems plausible since the mechanism proposed as PHP catalysis (see §1.3.4) does not necessarily require a substrate peptide recognition. Purification of a single amino acid phospho-histidine **15** has been described using anion exchange chromatography. Indeed chemical phosphorylation of histidine using PPA and purification proved possible and the product **15b** was isolated in pure form.

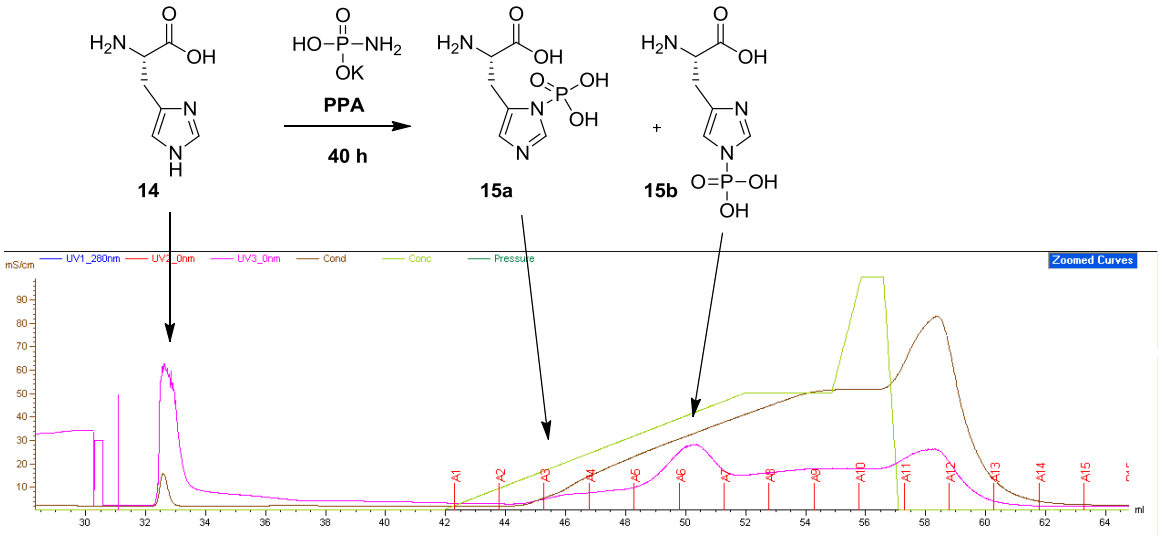

Figure 21: Chemical phosphorylation of histidine. The single amino acid histidine (**14**) was chemically phosphorylated by potassium phosphoramidate (PPA) and 1-phospho-histidine (**15a**) and 3-phospho-histidine (**15b**) were obtained. Purification was performed using a Mono Q anion exchange column.

To generate sufficient quantities of PNP enzyme, a pET-28 vector coding for BcPNP was obtained from Prof. Miller (Cornell University). Expression in *Escherichia coli* TOP10 gave excess to sufficient amounts of working enzyme.
The PNP substrate MESG (**16**) was prepared according to a modified literature procedure from 2-amino-6-chloro-purine ribonucleoside **17** (see scheme 2).[67] Methylation with MeI yielded the ionic intermediate **18**. A reaction with thiourea and methanolic ammonia gave the desired substrate **16** in 64 % yield.

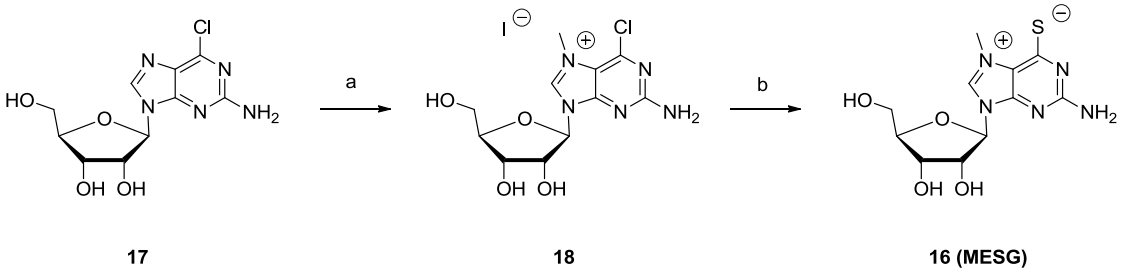

Scheme 2: synthesis of MESG (16). a: MeI. DMF, 18h, rt. b: thiourea, NH_3, 30 min, rt, 64% (two steps).

Mixing all components together in a PNP required buffer and starting the reaction by addition of the phospho-histidine substrate yielded a reaction curve that compared to a background signal (no PHP added) clearly registered the release of phosphate (see figure 22). The pH was set at 7.6 and not 8 due to the increasing instability of MESG at higher pH.

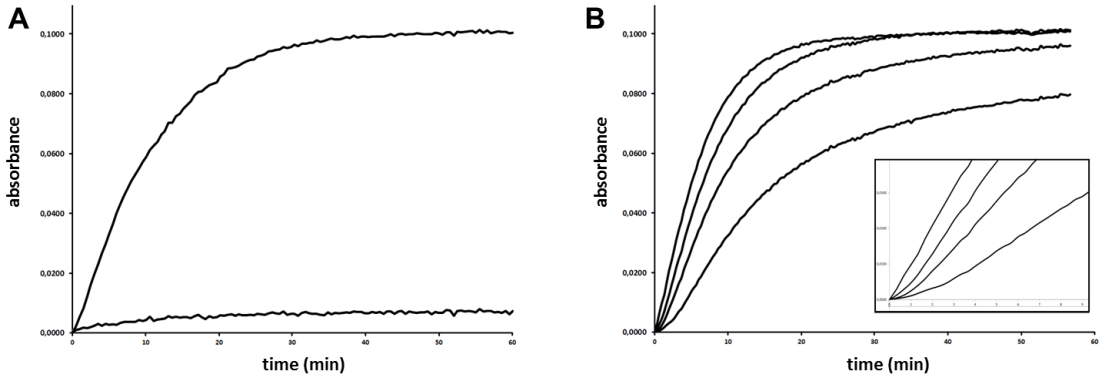

Figure 22: Graphs of the UV absorption at 360 nm plotted against the time. a: the reaction as it runs over time compared to a background reaction (no PHP present). **b:** The reaction run at various amounts of PNP (from left to right 5, 2.5, 1.25, 0.5 µM) in order to eliminate the lag phase. The insert shows a zoom in of the lag phase (see text for details).

A reaction takes place and is clearly detected however, it is unclear from figure 22A which of the two enzymatic reactions is rate limiting. The rate of formation of phosphate is of interest and not the rate of MES formation. To assure this, the PNP reserve should be sufficient to make the phosphate production the limiting factor. This requires an analysis of the reaction at various PNP concentrations. As figure 22B shows, an initial lag phase can be observed at insufficient PNP concentration. Increasing the concentration to 10 µM resulted in a negligible lag time required for conditions of ideal coupled enzyme systems.[68] To further validate this, initial velocities were plotted for reactions with increasing PHP enzyme concentration and found to be linear (see figure 23A and B). This shows that the system is in agreement with Michaelis-Menten kinetics.

In a similar fashion, as described in the previous paragraph, the K_M and V_{max} were determined. A K_M of 3.6 ± 0.2 µM and a V_{max} of 213 ± 12 µM/s was established. k_{cat}/K_M was determined to be 5.9 ± 1.2 $.10^8$ $M^{-1}.s^{-1}$. Clearly the enzyme turns over the phospho-histidine **15b** significantly more efficient compared to DiFMUP (**13**) in the fluorescence assay described in the previous paragraph.

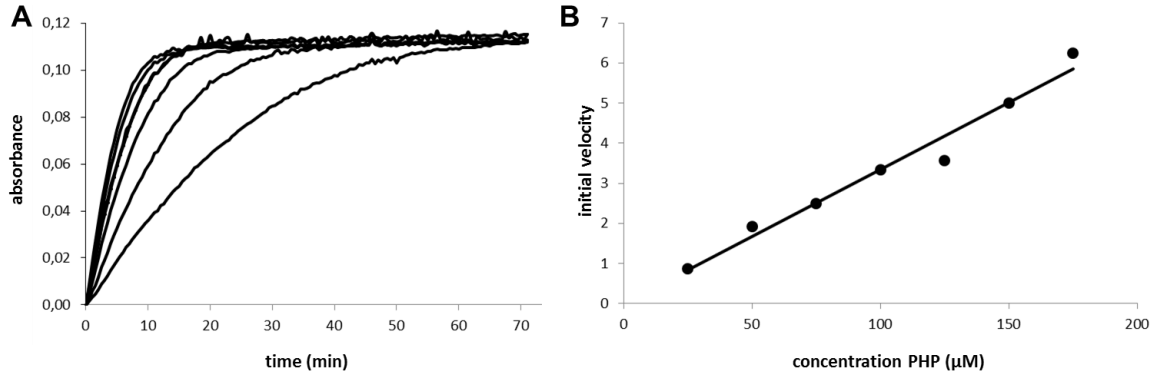

Figure 23: Graph of the reaction run at different concentrations of PHP. plotting the initial velocity against the concentration of PHP yields a straight line. The concentrations of PHP that were used are, from left to right; 175, 150, 125, 100, 75, 50 and 25 µM.

3.6 Determination of K_d with Microscale Thermophoresis

Besides the functional assays suitable for determining IC_{50} values, described in the previous paragraphs, access to a binding assay for PHP is desirable. Determining a binding affinity for PHP inhibitors will be an orthogonal technique to establish interaction between the enzyme and the molecules that are identify as PHP inhibitors. The two enzyme activity assays can be classified as relatively insensitive due to high enzyme concentrations required. A binding assay will not suffer from this and will generate a K_d (dissociation constant) value, describing an affinity independent of enzyme activity and concentration.
Microscale Thermophoresis (MST) is a technique well suited for a sensitive and quantitative analysis of protein-ligand interaction.[69] By means of a nanotemper® device, binding affinity can be determined for either protein-protein interactions but also protein-small molecule interactions. MST is based on applying an infrared laser to homogeneous solutions of a constant concentration of fluorescent labeled protein with a varied ligand concentration added. The laser induces a local temperature gradient in the glass capillaries that contain the sample, and the labeled protein moves away as registered by decrease in fluorescence signal (see figure 24). After reaching steady-state equilibrium, where laser induced motility equals general mass diffusion in the opposite direction, the laser is turned off and back-diffusion restores sample homogeneous distribution. Three different stages of the process are recorded for each sample; the initial fluorescence before laser, the thermophoresis process upon laser initiation and the back diffusion after switching the laser off. The rate of movement is related to the amount of ligand binding (see figure 25).

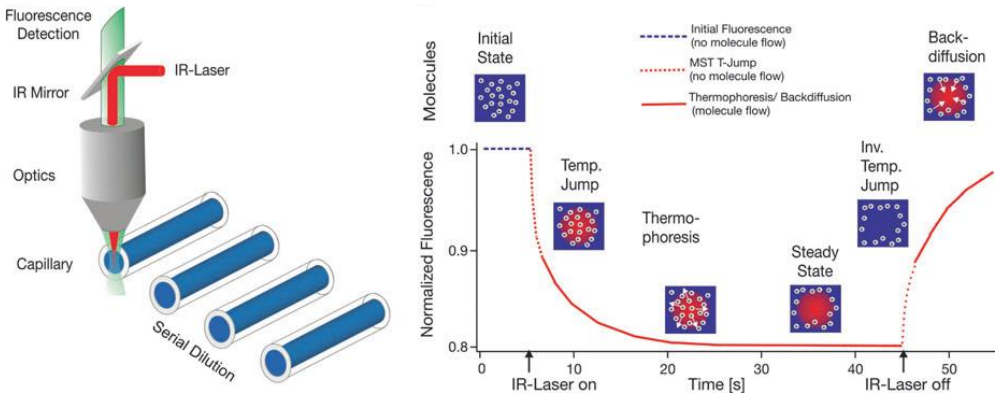

Figure 24 Principle of Nanotemper. The fluorescently labeled protein moved away from a laser induced temperature gradient (thermophoresis) till a steady state is reached. After turning the laser off, the protein moves back (back-diffusion). This process is influenced by ligand binding.[69b] Figure taken from http://www.nanotemper-technologies.com.

This technique is highly sensitive and detects all types of ligand binding induced changes, in size, charge, hydration shell or conformation. Molecular changes in protein structure as small as phosphorylation can be detected using MST. The protein is labeled with an appropriate fluorescent dye, or intrinsic fluorescence (e.g. due to tryptophan) can be used as well. This is especially useful if a protein is to be studied in its native unmodified form.[70]

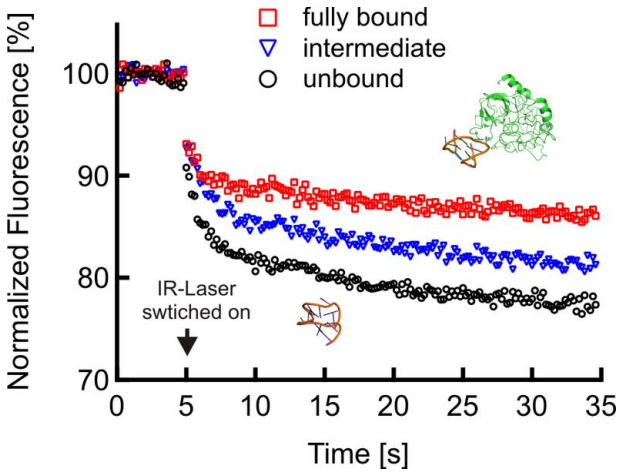

Figure 25: Dependent on ligand binding, the rate of migration of protein away from the laser induced gradient is affected. Figure taken from http://www.nanotemper-technologies.com.

Additionally, there is a complete freedom of buffers and additives (detergents or DMSO) to choose from as it in principle does not affect the MST measurement. Even the use of complete cell lysates has been suggested to be possible mimicking *in vivo* conditions closely.[71]

The Biophysics Department of the Ludwig-Maximilians-University Munich (LMU) studied the principles of MST extensively and identified the solvation entropy and the hydration shell of molecules as the driving force. A change in a primary, secondary, tertiary or quaternary structure due to ligand binding will change the hydration shell around the protein of interest and influences its behavior under MST (see figure 26).[72]

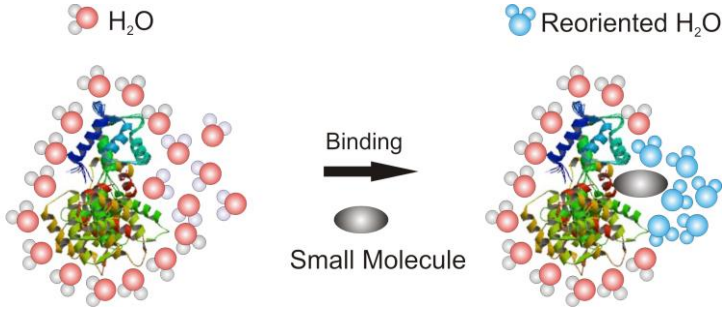

Figure 26: A change in the hydration shell around the fluorescently labeled protein has been found as the mechanism behind MST. Figure taken from http://www.nanotemper-technologies.com.

The availability of a blue/green filter machine limits the possibilities to a small group of possible fluorophores. It was decided to label PHP with a single equivalent of fluorescein by use of a Fluorescein-OSu labeling protocol. The protein was purified with a SEC column and the mass of the mono labeled protein was confirmed with ESI-MS. The protein proved to be stable in the same buffer as used for the non-labeled protein and was stored at 4 ^{0}C.

3.7 PHP Crystallography

The work described in this paragraph has been performed together with Arthur Porfetye under supervision of Dr. Ingrid Vetter.

The X-ray crystal structures published for PHP (described in §1.3.4) have allowed for the development of better models describing PHP its activity and function. However, there is still a lot that remains to be discovered about this protein. This generated a need to have access to in-house crystallization possibilities and to be able to produce crystals of PHP with peptide/protein substrates or small molecule inhibitors.
The X-ray structures published are based on an artificial construct. The enzyme was crystallized as a His-tag labeled protein with 'only' the amino acids 5-125 of the native protein present. This means that the first four amino acid are deleted. For the in-house efforts, crystallization of the native protein construct (with the added Gly-Ala N-terminal amino acids as the only deviation from wild type PHP) and the pBADM-11 derived His-tag labeled PHP construct were attempted. A full screen was launched using commercially available screens and a Mosquito pipetting robot. Two conditions were found that yielded branches of thin needles for the construct without tag (see figure 27A). Optimization led to thicker needles that showed significant diffraction at the Swiss Light Source (SLS, Paul-Scherer Institut Villigen, Switzerland) (see figure 27B). In house, with a less focused X-ray source, no diffraction was observed.

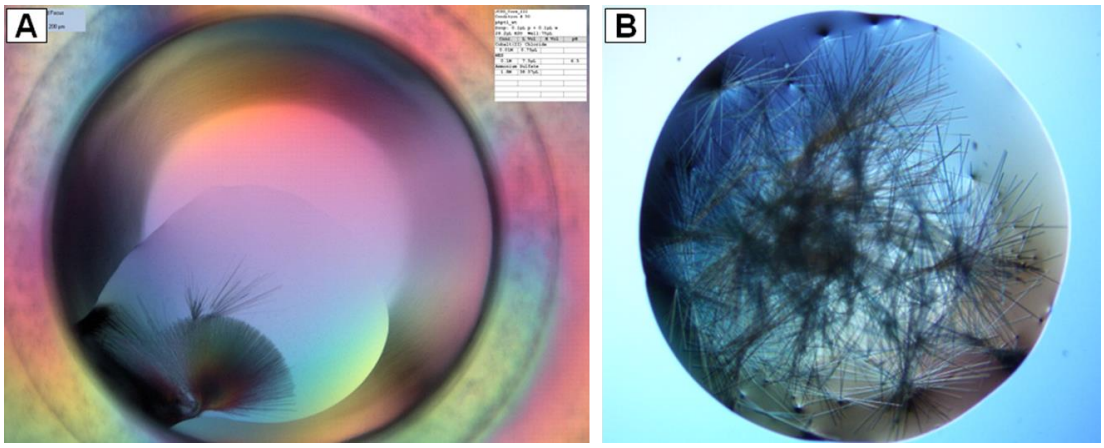

Figure 27: Crystallography results from screening (A) and optimization (B). Conditions for A: $Co(II)Cl_2$ 0.01 M, MES 0.1 M, NH_4SO_4 1.8 M, pH = 6.5 (taken from Core III nr.50). **Conditions for B:** $Co(II)Cl_2$ 0.01 M, MES 0.1 M, NH_4SO_4 1.6-1.8 M, pH = 6.5-8.5.

Comparing the generated structure with the reported structure with pdb code 2HW4 showed an identical fold except for one remarkable difference. The complete C-terminal end of PHP till Tyr^{125} was visible where it is not in 2HW4 (see figure 28B/28C compared to 28A). Due to a more tightly packing, this part of the enzyme becomes visible and leads to a remarkable feature. It significantly reduces the size of the cavity that comprises the active site and it leaves open only a small patch filled with a sulfate ion and a water molecule as shown in figure 28B. This is in good agreement with the proposed catalytic mechanism as presented in §1.3.4, figure 10, and the sulfate is exactly there were the phosphate is proposed (see figure 28D).

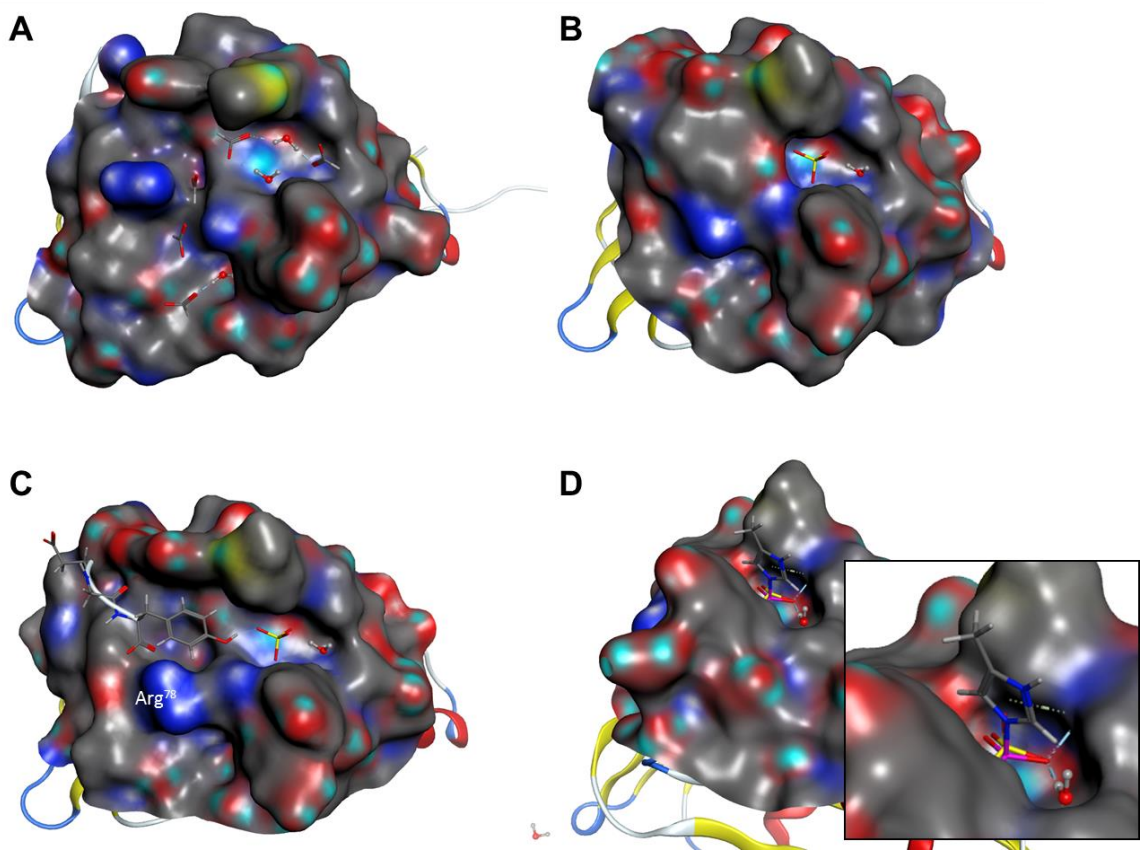

Figure 28: Crystal structure with pdb code 2HW4 compared to the in-house generated structure. A: structure 2HW4 top view, B: own structure top view, C: own structure top view with C-terminal end amino acids visible. The carboxylic acid from Tyr^{125} forms a salt bridge with Arg^{78}. D: side view with a phospho-imidazole placed inside where ligand binding is proposed (as described in §1.3.4). The insert shows a zoom-in.

Different from the proposed model, the water molecule appears to come from the other side and no space is present in between His^{53} and the substrate phosphate. Tyr^{123} covers His^{53} completely with no space for a water molecule (as suggested in figure 10) and the tyrosine phenol forms a hydrogen bond with the substrate phosphate group. The C-terminal carboxylic acid shows a distance to the guanidine of Arg^{78} that justifies the assumption that it is involved in a salt bridge (see figure 28C), as already predicted by the NMR solution structure study reported earlier (see figure 9). Unfortunately, this novel structure does suggest that only a small part of protein can be used for developing a substrate competitive inhibitor. This depends on the role and function of this, likely to be, flexible C-terminal end. In solution, does this 4 amino acid part bend away or is it involved in catalysis? A role in catalysis seems unlikely since deletion of the C-terminus has been reported to be allowed until amino acid 121 (see §1.3.4). Also addressed in that paragraph is the fact that Tyr^{125} is known to be subjected to phosphorylation in a cellular setting. Addition of this phosphate to the tyrosine would block the active site completely! This suggests the presence of a build-in enzyme inhibitory mechanism. Considering the close proximity of the Tyr^{125} phenol group to the substrate-phosphate bound inside the catalytic site, it is also possible that this residue is auto-phosphorylated (see chapter 8 for ongoing research on this topic).

Chapter 4: Design, Synthesis and Application of Building Block 7

4.1 Introduction

The use of peptidomimetics as phosphatase inhibitors is a well-proven concept. In the case of tyrosine phosphatases, potent peptide derived inhibitors have been developed. Originally, a peptide substrate was used and equipped with a non-hydrolysable phosphate mimic, or bioisostere, like difluoro-phosphonomethylphenyl (see compound **19** figure 29; a nanomolar inhibitor for tyrosine phosphatase PTP1B).[73] Drug molecules with negative charges usually display poor cell permeability and **19** is no exception. Ever since the focus has been on developing other phosphate mimics that display improved pharmacodynamic properties. A 1,2,5-thiazolidin-3-one-1,1-dioxide is a well-tolerated alternative (as used in PTP1B inhibitor **20**).[74] Phospho-tyrosine mimics like these, and others, clearly make use of the generally positively charged tyrosine phosphatase active sites. Recently, more and more mimics have been reported usually on small molecules rather than peptide derived structures (see also §5.1).[53b, 75]

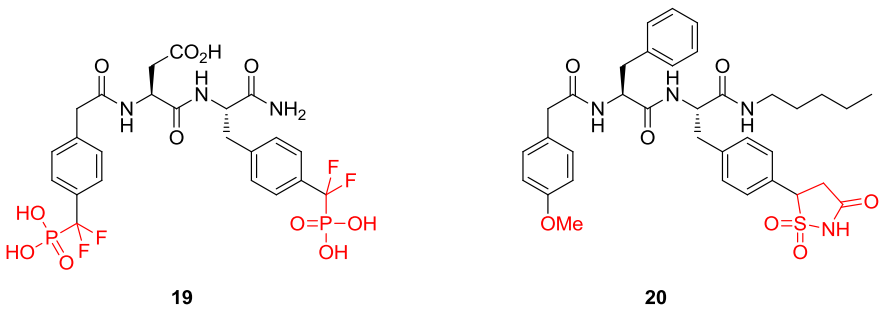

Figure 29: The structures of published phosphatase inhibitors bearing a phospho-histidine mimic.

Based on the proposed mechanism of phospho-histidine hydrolyses presented in §1.3.4 a similar approach can be adopted (see figure 30). A substrate phospho-histidine is recognized by PHP through several H-bond interactions. Then, an activated water molecule acts as a nucleophile that attacks on the phosphorus atom and breaks the N-P bond (figure 30A). Suggested is a synthetic mimic of the transition state of PHP that induces phospho-histidine hydrolysis (figure 30B). Here, the imidazole is maintained and the phosphate is replaced for a non-substituted sulfonamide that mimics the phosphate and the water molecule. In order to prevent hydrolysis the histidine imidazole nitrogen is shifted one position, resulting in a stable and synthetically feasible moiety. To allow incorporation of this transition state mimic into peptides, a building block suited for Fmoc solid-phase peptide synthesis (SPPS); equipped with N-terminal Fmoc and further orthogonal protection, relying on global acidolytic protective group removal (Pg_1 and Pg_2), is required. To our knowledge, a terminal sulfonamide as a phosphate mimic is rare and only a single report has been published.[76] A peptide equipped with different phospho-tyrosine mimics, including a methylene sulfonamide tyrosine (see compound **21** figure 31), was tested as an inhibitor for the phosphatases PTP1B and YopH, a phosphatase from *Yersinia pestis*. Indeed peptide **21** proved active against YopH but not to PTP1B.

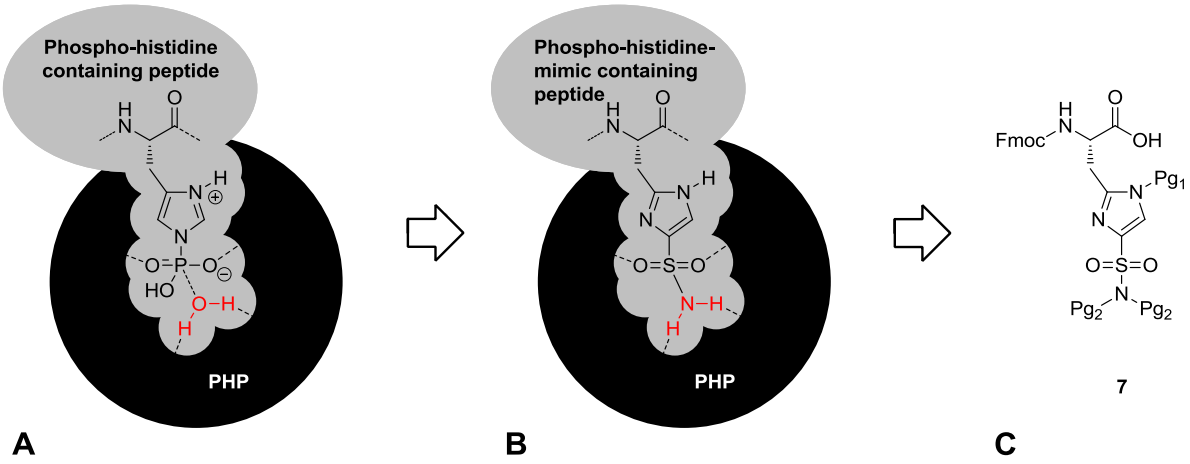

Figure 30: Representation of the recognition of a phospho-histidine substrate by PHP (A), a sulfonamide-based TS-mimic (B) and the corresponding target building block 7 suited for Fmoc SPPS (C).

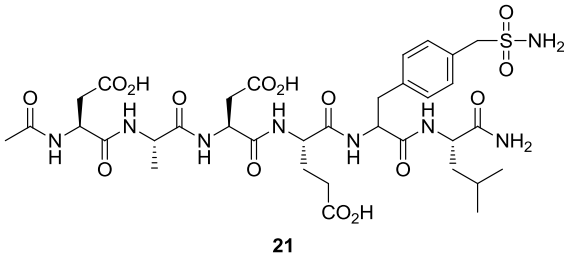

Figure 31: Structure of peptide 21. This peptide was prepared as an inhibitor of phosphatase PTP1B and YopH.[76] The methylene sulfonamide serves as a phosphate isostere.

A sulfonamide has the advantage of bearing no charge at physiological pH. However, until today only this one example employing this group as a phosphate mimic has been reported. There have been many reports on terminal sulfonamides as key elements of carbonic anhydrases inhibitors (see §5.1).

4.2 Synthesis of Building Block 7

A retrosynthetic analysis for the synthesis of this fully protected building block **7** was carried out (see figure 32). Focus is on a linear approach with the formation of a non-saturated amino acid **22** from aldehyde **23** and subsequent asymmetric hydrogenation as key steps in acquiring the amino acid functionality. The imidazole 2-position aldehyde can be introduced by lithiation and quench with DMF. The sulfonamide imidazole is protected with acid labile protective groups (Pg), compatible with the following synthesis steps. A Boc, trityl or similar group can be used for the imidazole. Bis(2,4-dimethoxybenzyl)amine will be used to acquire a protected sulfonamide by direct coupling with the imidazole sulfonyl chloride **24** at an early stage of the synthesis. The 2,4-dimethoxybenzyl protective group has been proven to be an excellent choice for protection of sulfonamides, as well as for carboxamides, and can be removed easily under acidolytic cleavage conditions, similar to Boc or trityl removal.[77]

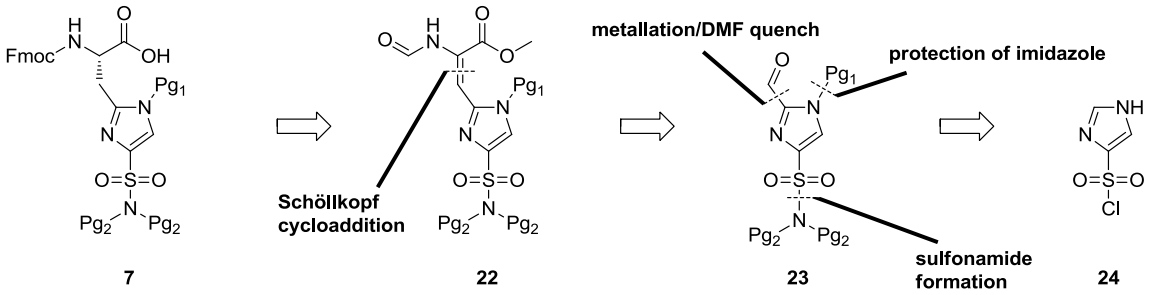

Figure 32: Retrosynthetic analysis of building block 7.

The key step is the asymmetric hydrogenation of the N-formyl dehydroamino ester **22**. This method is a proven strategy towards enantiopure natural and unnatural amino acids.[78] Reduction of a dehydro-amino acid derivative is an elegant method to acquire amino acids and can easily be achieved using a rhodium catalyst and a chiral BINOL derived phosphoramidate like PipPhos (see figure 33A).[79] The α-acetamido group, the C=O moiety in particular, is generally believed to be essential in obtaining high enantioselectivity by directing the catalyst. An acyl group is often used but is difficult to remove after reduction of the double bond without harming the obtained, often delicate, amino acid stereochemistry and substitution pattern. A formyl group has been shown to be an attractive alternative that is effective and easily removed afterwards.[80] Also, the introduction is easily achieved by use of an elegant Schöllkopf procedure combining an aldehyde of choice (in this case aldehyde **23**, see figure 33B for the mechanism) and methyl isocyanoacetate. Through a 2+3 cycloaddition, a Schöllkopf 2-oxazoline is formed and under basic conditions this rearranges into the dehydroamino acid derivative **22**.

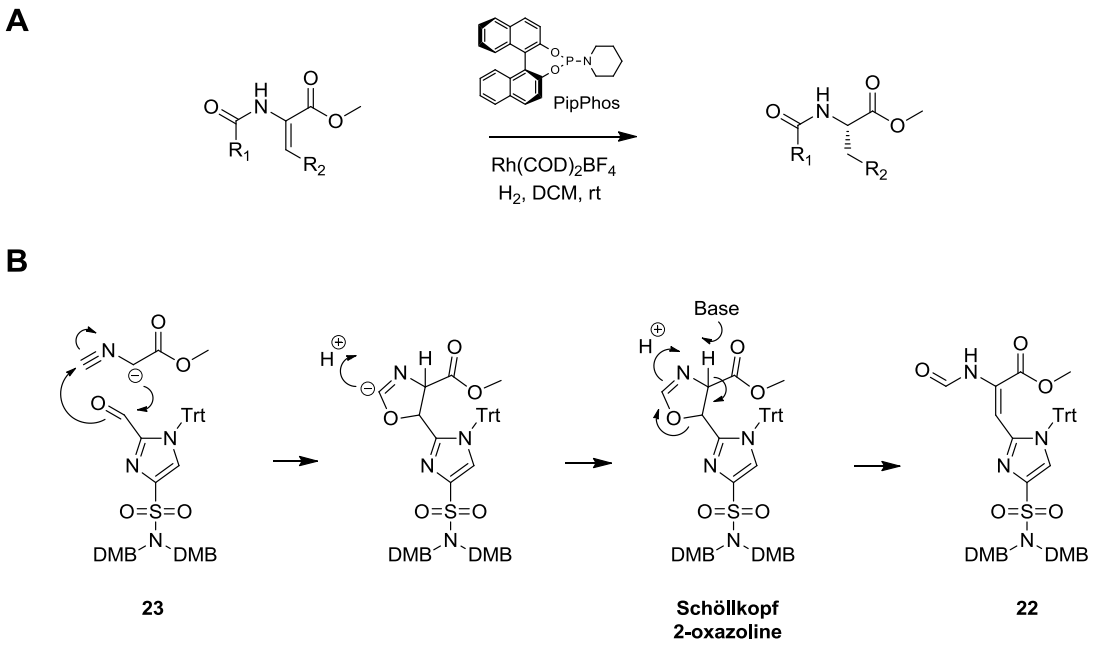

Figure 33: General scheme of an asymmetric hydrogenation (A) and the mechanism of the formation of a Schöllkopf 2-oxazoline and rearrangement into compound 22 (B).

The synthesis of **22** as shown in scheme 3 commenced by heating imidazole (**25**) in chlorosulfonic acid and subsequent addition of thionyl chloride yielded 4(5)-imidazole sulfonyl chloride **24** in 62% after quenching and filtration from water.[81] Reaction of **24** with *N*,*N*-bis(2,4-dimethoxybenzyl)amine (DMB_2NH) in the presence of DIPEA in DCM at 0 °C resulted in sulfonamide **26** in high yield (90%). It was found to be necessary to protect the imidazole (**26**) at *N(1)* before introducing the aldehyde in 2-position through deprotonation and DMF quench. Several protective groups were investigated; tosyl, phenylsulfonyl and *N,N*-dimethylsulfonamine, which all resulted in poor regioselectivity in the deprotonation step (5- vs 2-position), as well as low reproducibility in terms of isolated yield. An *N*(1)-Boc protective group was investigated with good result, but was found to be non-compatible with peptide synthesis.[56] Scrambling of the Boc group between the imidazole and the N^{α}-position upon Fmoc deprotection during peptide synthesis terminated the peptide synthesis prematurely with significantly reduced yield as a result (see figure 34). Eventually, incorporation of a trityl (Trt) group at *N(1)* according to standard conditions, resulted in compound **27** (83%), which underwent complete regio-selective deprotonation on the 2-position with *n*-butyl lithium at -30 °C. Quenching of the lithiate with DMF yielded aldehyde **23**. The condensation with methyl isocyanoacetate proved viable but **22** was obtained in low yield.

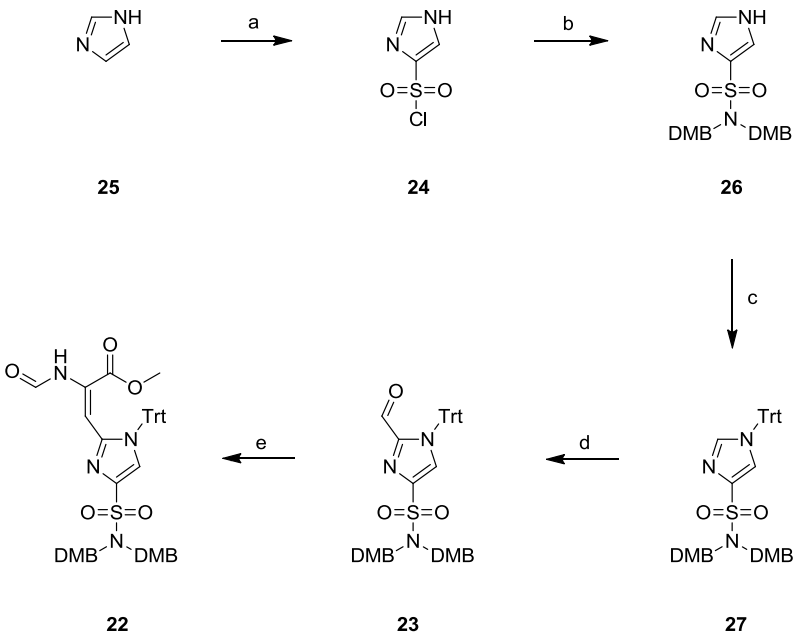

Scheme 3: Synthesis of intermediate 22. a: $ClSO_3H$, 140 ^{0}C, 16h, $SOCl_2$, 5h, till 125 ^{0}C, 62% **b:** N,N-bis(2,4-dimethoxybenzyl)amine (DMB_2NH), DiPEA, DCM, 2h, rt, 90% **c:** KOtBu, TrtCl, DMF, 18h, rt, 83% **d:** n-BuLi, DMF, THF, 1h, -30 ^{0}C, 91% **e:** methyl isocyanoacetate, Cu_2O, KOtBu, 2h, rt, 33%.

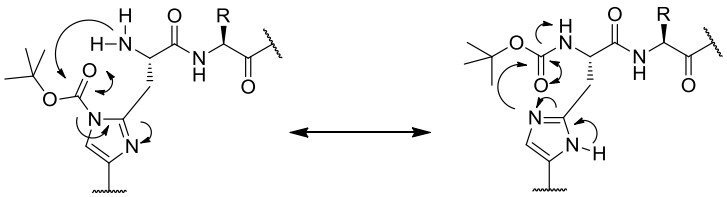

Figure 34: Mechanisms of Boc group scrambling during peptide synthesis. After coupling a building block like **7** on a peptide attached to a resin and the Fmoc is removed from the N terminal amine, scrambling of the Boc group takes place and results in partial termination of SPPS and formation of side-products.[56]

No significant attempts to optimize the methyl isocyanoacetate condensation towards **22** were undertaken since this olefin proved completely immune to hydrogenation. Both asymmetric and symmetric methods were tried in attempts to reduce the double bond but all failed in producing product **28**. The compound was subjected to both homogenous and heterogeneous catalysts and hydrogen pressures up to 28 bar and temperatures up to 60 ^{o}C were applied only to determine complete resistance of **21** to reduction (see table 2 for details).

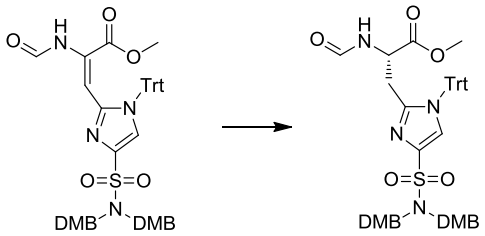

22 **28**

Conditions	Pressure of hydrogen	Temperature	Product formed
Rh(0), THF	atm	25 ^{o}C	No reaction
$Rh(COD)_2Tf$, PPh_3, THF	atm	25 ^{o}C	No reaction
$Rh(COD)_2Tf$, PPh_3, THF	20 bar	25 ^{o}C	No reaction
$Rh(COD)_2Tf$, PPh_3, EtOAc	20 bar	25 ^{o}C	No reaction
Rh(0), THF	atm	40 ^{o}C	No reaction
Rh(0), THF	atm	40 ^{o}C	No reaction
Pd(0), EtOAc	atm	40 ^{o}C	No reaction
Rh(0), THF	28 bar	60 ^{o}C	Degradation of SM
Pd(0), THF	28 bar	60 ^{o}C	Degradation of SM

Table 2: Overview of the attempts that were performed to reduce 22 by hydrogenation. The olefin **22** proved stable towards high temperatures and very high hydrogen pressure. Eventually, increase of temperature and pressure resulted in degradation of starting material (SM) rather than product formation. All reactions were given 18 hours of reaction time.

This inability to reduce the double bond required the development of a new synthetic strategy and a suitable alternative was found in a convergent route where intermediate **27** and 2-position functionalization could still be used (see figure 35). Introduction of iodine instead of an aldehyde gives access to intermediate **29**. This iodine is suitable for an approach where a zinc-iodine serine amino acid derivative **30** can be coupled via a Negishi cross-coupling reaction. Many different unnatural phenylalanine derivatives have been prepared in this fashion.[82] To acquire target molecule **7**, a final step, the orthogonal cleavage of the amino acid methyl ester by trimethyltin-hydroxide (Me_3SnOH) treatment, is required. This non-acidic nor basic methodology should leave both the acid labile protective groups of the imidazole sulfonamide moiety as well as the base-labile Fmoc protection of the N^{α}-position unaffected.[83]

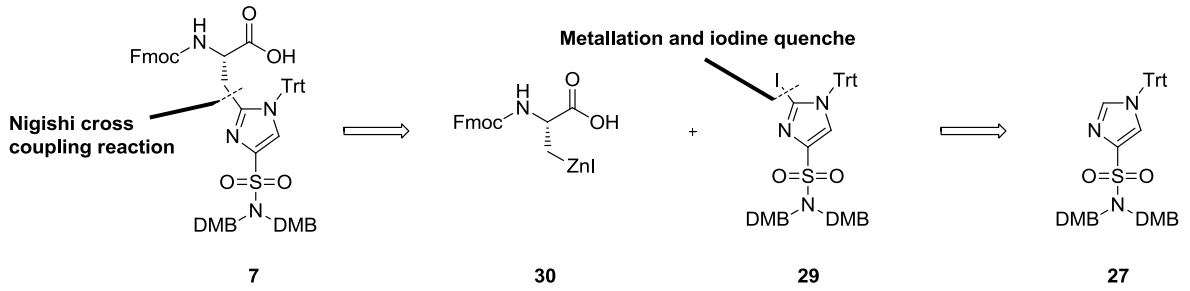

Figure 35: Second retrosynthetic analysis of building block 7 with key intermediate 28.

Indeed, applying the n-BuLi deprotonation as for aldehyde **23** but quenching with I_2 yielded iodine **29** (see scheme 4). After optimization, the procedure resulted in good yield (85%) of **29** on multigram scale. Next, with this intermediate in hand, the Negishi cross coupling with *(R)-*N^{α}-Fmoc-3-zinc iodoalanine methyl ester (**30**) was investigated. This amino acid derived zinc intermediate was prepared from commercially available serine methyl ester **31** (see scheme 5).

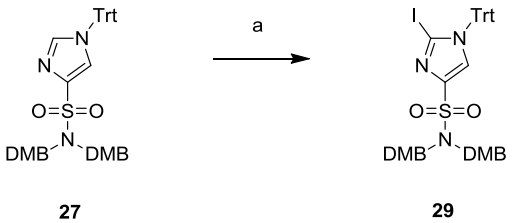

Scheme 4: Introduction of an iodine on the 2-position of intermediate 27, obtaining the product 29. a: n-BuLi, I_2, THF, 1h, -30 ^{0}C, 85%.

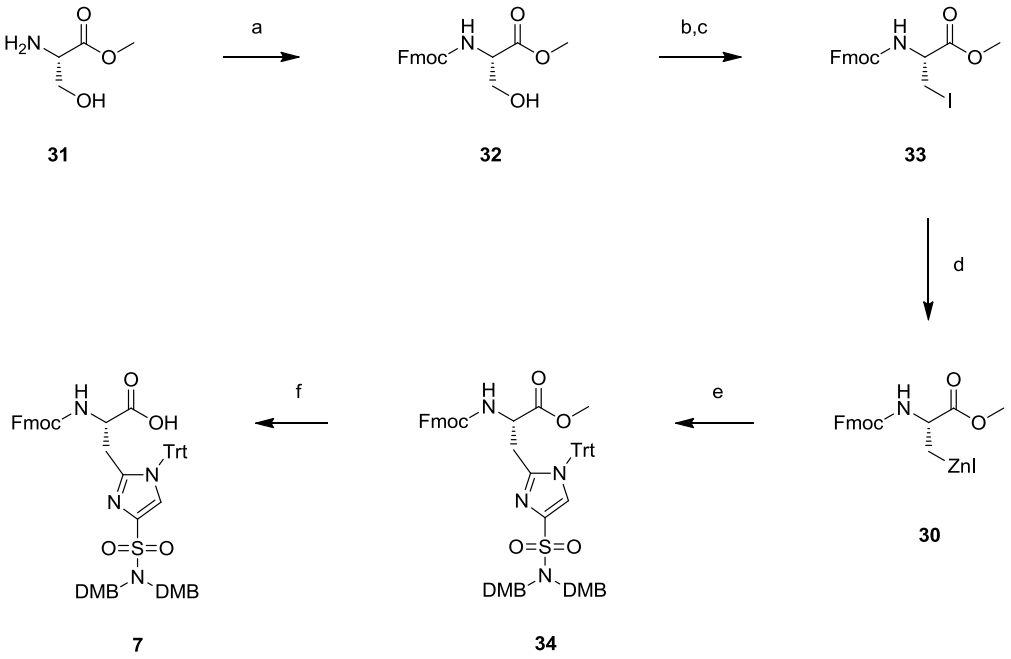

Scheme 5: Negishi coupling based synthesis of building block 7. a: $NaHCO_3$, H_2O, Fmoc-OSu, dioxane, 1h, rt, 98% **b:** pyridine, TsCl, 40h, 4 ^{0}C **c:** NaI, acetone, 18h, rt, 90% (over two steps) **d:** Zn(0), DMF, I_2, **e: 29**, $Pd_2(dba)_3$, XPhos, 2h, 40 ^{0}C, 53% **f:** $Sn(Me)_3OH$, DCE, 18h, 65 ^{0}C, 86%.

After Fmoc protection of **31**, and conversion of the hydroxyl into iodine **33**, zinc species **30** was generated by insertion of activated elemental zinc. Several methods to achieve this conversion have been described.[82a] Zn-activation through ultrasonic treatment or through Knochel's procedure using 1,2-dibromoethane and chlorotrimethylsilane gave variable/irreproducible results. Direct *in-situ* activation of Zn by addition of a small amount of iodine was found to be the best method.[84] In line with earlier reports, a general increase in yield was observed when the reaction was performed in DMF instead of THF.[82a] These serine derived Negishi intermediates are very useful in the preparation of unnatural phenylalanine analogues, although coupling with *ortho*-substituted arylhalides have been reported to be difficult substrates.[84] Our trityl protected iodoimidazole **29** proved to be a very difficult substrate as well, and significant catalyst screening and optimization was required in order to reach isolatable amounts of product. For the Negishi cross-coupling reaction leading to arylalanines, a number of different palladium sources and ligand combinations have been reported in literature. With our substrate (**29**), a strong preference for reduction of the 2-iodo imidazole was observed, leading to rapid formation of the 2-H imidazole **27** as a competing reaction (see figure 36). This is caused by preferential β-hydride elimination/reduction competing with product forming reductive elimination as previously by Buchwald and coworkers.[85] A correlation was found between the amount of equivalents of zinc-reagent added and the yield for the palladium catalyzed coupling reaction. Raising the amount of zinc-reagent usually led to higher yields indicating that the β-hydride elimination/reduction is quick compared to effective coupling.

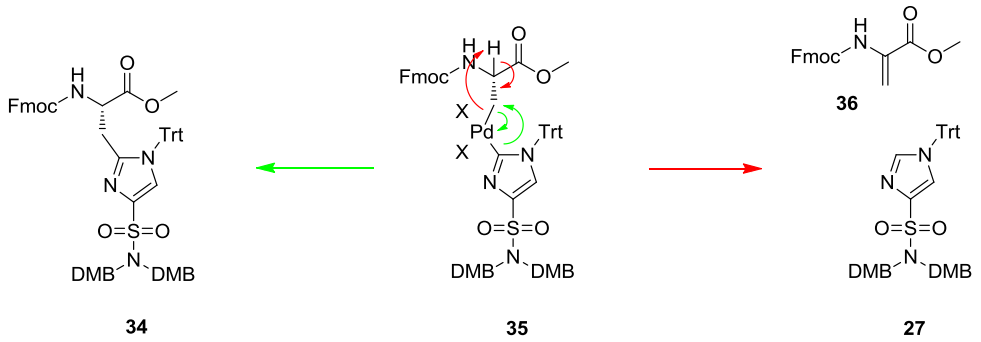

Figure 36: The desired reductive Pd elimination (in green) vs undesired β-elimination (in red). After palladium insertion in the arylhalide and attack of the zinc species intermediate **35** is formed. This complex will collapse and releases the palladium catalyst that can undergo a new catalytic cycle. The collapse of **35** can take place through two distinct mechanisms yielding two different possible products **34** or **27**. A desired reductive Pd elimination will eliminate the catalyst while forming the desired carbon-carbon bond as shown in green. An undesired β-elimination will form an α-β double bond in on the amino acid and eliminates the palladium with the imidazole attached as shown in red. The α-proton is on the palladium and reductive elimination will render the 2-H imidazole **27** as product together with the amino acrylic acid **36**.

Eventually, two equivalents was chosen as a reasonable compromise between higher yield and excessive use of the iodoalanine precursor. For the coupling reaction, different palladium catalysts and ligands were investigated (Table 3). $Pd(PPh_3)_4$ generally showed only traces of product formation at room temperature, at 40 ^oC, 8% conversion was obtained. At this temperature, complete consumption of the iodo-imidazole (**29**) was usually achieved after 2 hours. Use of $PdCl_2(PPh_3)_2$ also did not result in useful amounts of the coupling product. It appeared that only a single turnover took place per equivalent of catalyst (entry 4 and 5). Increasing the temperature to 80 °C (entry 3 and 6) resulted in rapid decomposition of organozinc reagent **30** and no significant product formation was observed. A well-documented palladium catalyst-ligand combination described for Negishi coupling reactions is $Pd(OAc)_2$ or $Pd_2(dba)_3$ with P(*o*-tol)$_3$. Again, only reasonable yields were obtained when using higher loading of palladium catalyst. Next, electron-rich biaryl phosphine ligands were investigated. Such ligands have been reported to perform well and with high substrate tolerance even for the more sterically hindered (mainly ortho-substituted) aryliodides.[86] A ratio between palladium and ligand of 1:1 was maintained.[84] JohnPhos, SPhos and XPhos showed large differences when used in combination with $Pd(OAc)_2$ or $Pd_2(dba)_3$. In both cases, XPhos showed the highest conversion (entries 13 and 16). This is not entirely in agreement with the results from earlier studies where SPhos was shown to be superior over XPhos concerning product formation over β-hydride elimination / reduction.[85] Eventually, entry 16 gave the best result with acceptable catalyst loading, while lowering the amount of palladium resulted in reduced product formation (entry 17). Next, scale up of the reaction to multi-gram scale was performed, resulting in consistent yields. Cleavage of the methyl ester functionality of **34** with trimethyltin hydroxide proved viable, thus providing building block **7** in 86% yield. Overall, the synthesis sequence resulted in 18% of building block **7** over six steps.

Entry	Pd Precursor	Equiv. Pd	Ligand	Equiv. Ligand	Temperature coupling reaction	% conversion into coupling product[a]
1	$Pd(PPh_3)_4$	0.1	-	-	25 °C	0
2	$Pd(PPh_3)_4$	0.1	-	-	40 °C	8
3	$Pd(PPh_3)_4$	0.1	-	-	80 °C	0
4	$PdCl_2(PPh_3)_2$	0.1	-	-	40 °C	13
5	$PdCl_2(PPh_3)_2$	0.2	-	-	40 °C	21
6	$PdCl_2(PPh_3)_2$	0.1	-	-	80 °C	5
7	$Pd_2(dba)_3$	0.1	$P(o\text{-}tol)_3$	0.4	40 °C	0
8	$Pd(OAc)_2$	0.05	$P(o\text{-}tol)_3$	0.2	40 °C	7
9	$Pd(OAc)_2$	0.1	$P(o\text{-}tol)_3$	0.2	40 °C	23
10	$Pd(OAc)_2$	0.1	$P(o\text{-}tol)_3$	0.4	40 °C	20
11	$Pd(OAc)_2$	0.1	JohnPhos	0.2	40 °C	0
12	$Pd(OAc)_2$	0.1	SPhos	0.2	40 °C	19
13	$Pd(OAc)_2$	0.1	XPhos	0.2	40 °C	43
14	$Pd_2(dba)_3$	0.1	JohnPhos	0.1	40 °C	0
15	$Pd_2(dba)_3$	0.1	SPhos	0.1	40 °C	22
16	$Pd_2(dba)_3$	0.1	XPhos	0.1	40 °C	75 (53)[b]
17	$Pd_2(dba)_3$	0.05	XPhos	0.05	40 °C	44

Table 3: Optimization of the Negishi reaction towards 34. a: HPLC-based as detected (absolute intensity) by a corona CAD detector. % conversion into coupling product = area coupling product / (area coupling product +area reduction product)x100. Starting material was fully converted in all cases. **b:** Isolated yield after silica gel purification.

4.3 Synthesis of Peptides 37 and 38

Next, building block **7** was evaluated in standard SPPS according to the Fmoc protocol. It was decided to prepare a peptide with the sequence AH*PFG originating from Zetterqvist and co-workers original studies on PHP (scheme 6, peptide **37**).[40] The peptide was synthesized on Tentagel-resin functionalized with a RAM-anchored Fmoc-glycine (Scheme 6, **A**-**D**). Coupling of the Fmoc-amino acids (step **A** and **C**) was carried out using standard HBTU/HOBt activation, except for the protected sulfonamide building block **7** (step **B**), which was coupled employing HATU/HOAt as activating reagents. Capping after coupling of building block **7** was not possible as treatment with acetic anhydride/HOBt resulted in imidazole *N*-acetylation and Trt removal at the imidazole moiety, leading to acyl migration from the imidazole core to the N^{α}-position after subsequent Fmoc removal (mechanism similar to described for Boc scrambling in figure 34). This shift stopped further amino acid coupling and significantly reduced yield. Cleavage from the resin (**D**), as well as global deprotection, was carried out by applying a mixture of trifluoroacetic acid (TFA)/triisopropylsilane (TIPS)/H_2O (90:5:5).

After preparative reverse phase HPLC purification (C18) and subsequent lyophilization, peptide **37** was isolated in 42% yield (from resin loading). An additional peptide sequence carrying the sulfonamide histidine was synthesized (RH*RKG, peptide **38**, 59% yield). This peptide was based on the sequence from histone H4 and carries positively charged amino acids rather than neutral amino acids as in peptide **37**. A distinction in ligand binding should be expressed in IC_{50} values if the peptide sequence is of importance for substrate recognition.

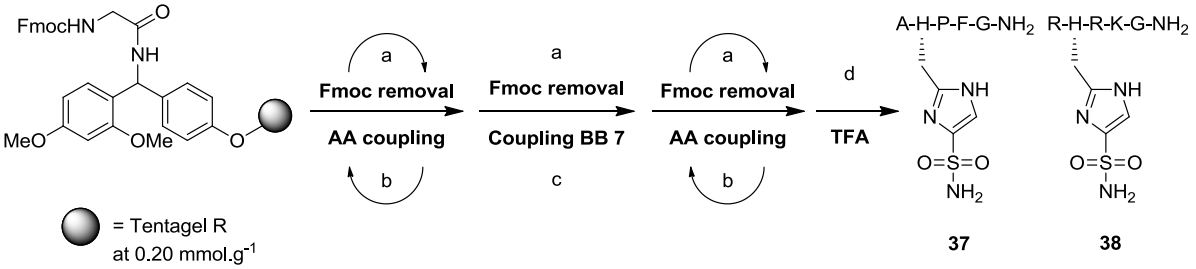

Scheme 6: The peptide synthesis performed with building block 7 to yield the PHP peptide inhibitors 37 and 38.

4.4 Evaluation of Peptides 37 and 38 as PHP Inhibitors

The two peptides were tested in both fluorescence as the enzyme coupled activity assay at a concentration of 100 µM and failed to show any effect. This suggests that either the presentation of the sulfonamide histidine in a peptide form is not working or the sulfonamide is not a good mimic. The de-protected amino acid itself (see scheme 7, compound **39**) also failed to show any activity at all. Clearly peptide based inhibitors with this sulfonamide imidazole moiety are not suited as a basis for PHP inhibitor design.

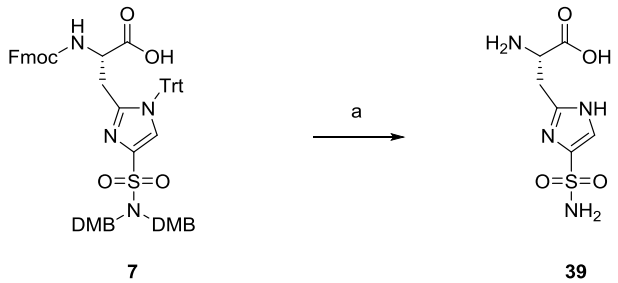

Scheme 7: The deprotection of building block 7 that yielded the non-natural amino acid 39. a: piperidine, DMF, 1h, rt **b:** TFA, water, TiPS, 2h, rt, 34% (over two steps).

Chapter 5: Design, Synthesis and Evaluation of Small Molecules as PHP Inhibitors

5.1 Introduction

As already introduced in the previous chapter, the development of inhibitors bearing groups that serve as phosphate bioisosteres is a common theme in medicinal chemistry programs directed at phosphatases. The difficulties that are associated with peptide based inhibitors did move the focus from peptidomimetics to small molecule inhibitors. Also, the discovery of allosteric sites boosted the development of inhibitors that do not directly compete with substrate binding.[53a] Nevertheless, the use of mimics for phosphate is still very common for substrate competitive inhibitors. Small molecule inhibitors generally use the same or similar phospho-tyrosine mimics as the peptide inhibitors. Mimics like difluoro-phosphono-methylphenyl or difluoromethylene sulfonic acid (used in PTP1B inhibitors **40** and **41**, see figure 37) found their use in various small molecule phosphatase inhibitors. The mimics based on heterocyclic rings generally display improved stability and effectiveness compared to phosphonic or sulfonic acids. Popular examples are 1,2,5-thiazolidin-3-one-1,1-dioxide (compound **42**) and various thiazolidinone derivatives (e.g. compounds **43** and **44**).[53b]

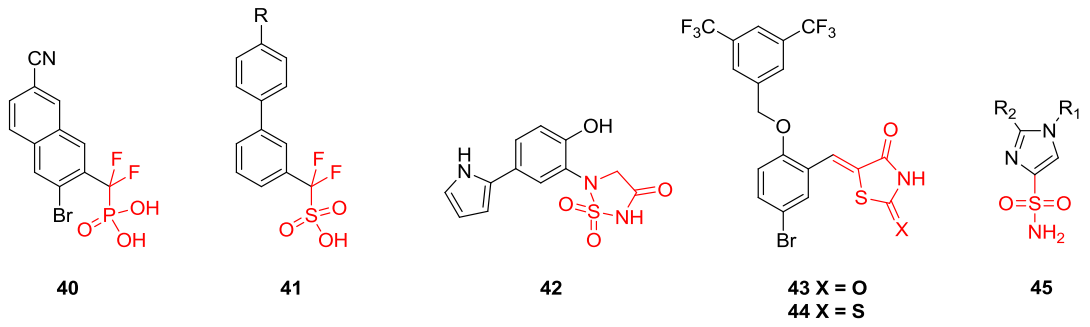

40 **41** **42** **43 X = O** **44 X = S** **45**

Figure 37: The structures of small molecule phosphatase inhibitors 40-44, bearing various phospho-histidine mimics, and imidazole sulfonamide general structure 45.

The failure of peptides **37** and **38** to show PHP inhibitor activity made us look into the possibility of exploring small molecules based on the same 4-sulfonamide imidazole bioisostere principle (structure **45**). To our knowledge a terminal sulfonamide has never been reported as a part of a small molecule phosphatase inhibitor but this feature is common for inhibitors targeting carbonic anhydrases (CAs).[87] These ubiquitously expressed enzymes catalyze the reversible reaction of hydration or formation of bicarbonate ions to or from CO_2. In humans, fifteen different isoforms have been identified. Important roles for these enzymes have been addressed for many of them and inhibitor development has received considerable attention in this field. Today the largest class of CA inhibitors that have been reported are indeed sulfonamides, as exemplified by binding of benzene sulfonamide in CA II (figure 38A). The anion form has a direct interaction with the zinc cation conserved inside the active site of the CA. In terms of catalysis, this zinc is responsible for activation of the water molecule that attacks the CO_2 molecule to form the bicarbonate enzymatic product. The Zn sits at the bottom of a conical cavity lined partially by hydrophobic and hydrophilic amino acid residues and is stabilized by three histidines. A terminal sulfonamide serves as a mimic for the water molecule as well as the CO_2 molecule.[88]

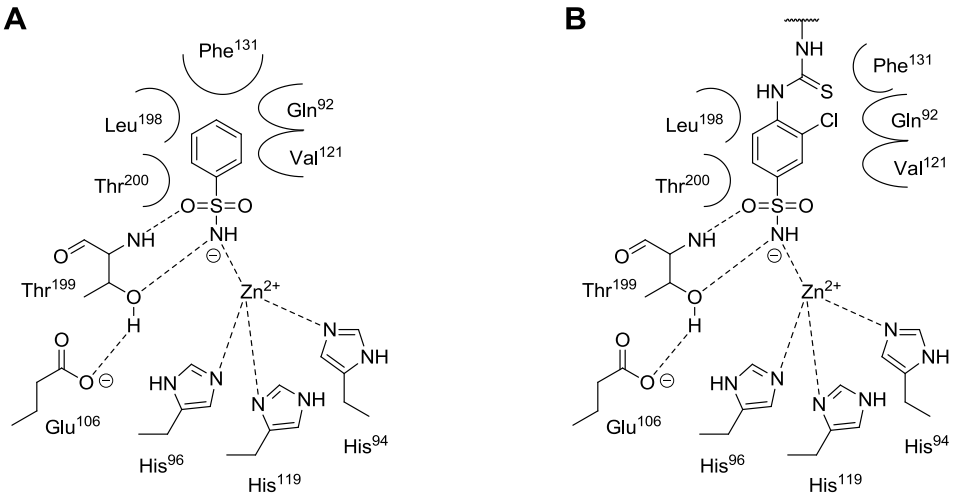

Figure 38: Representation of benzene sulfonamides binding inside the catalytic site of human CA II. Both a simple benzene sulfonamide (A) or more decorated inhibitors (B), inducing selectivity, have been reported. Figure redrawn from Alterio et al. 2012.[88]

Optimization around the benzene sulfonamide theme led to the identification of extended series of CA inhibitors. Especially functionalization patterns like **46** and **47** were reported (figure 39). The R-group represents a substituent varying from a peptide tail to an aliphatic spacer. Selectivity within the family of carbonic anhydrases can be achieved by modifications in this position as well as optimization of physicochemical properties. Also, urea (example **48**) and thiourea (example **49**/figure 38B) derivatives have been reported. Several carbonic anhydrase inhibitors are currently in clinical trials but no compound has been FDA approved so far.[87]
Besides benzene ring based inhibitors many different sulfonamide functionalized heterocyclic rings, like **50-52**, have found their way into CA inhibitor design as well. Surprisingly, a functionalized imidazole, like compound **45** (figure 37), has never been reported. Important to keep in mind is that the design of an imidazole sulfonamide PHP inhibitor like **45** can come with additional activity towards members of this CA enzyme family. This is not necessary a problem as carbonic anhydrase inhibitory activity is associated to antitumor activity but can limit its usefulness as a tool compound.[88]

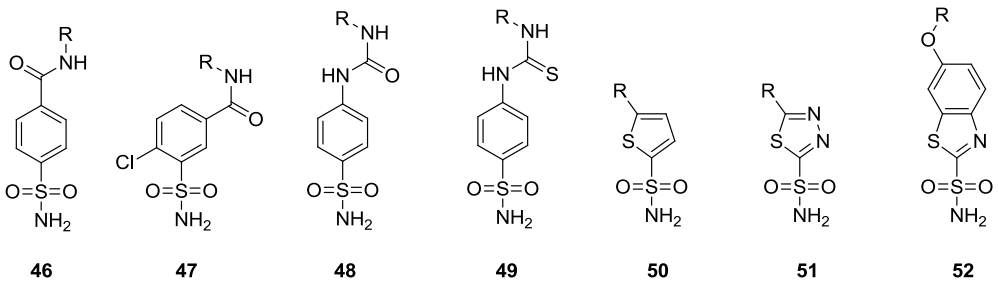

Figure 39: Examples of carbonic anhydrase inhibitors bearing a sulfonamide motive. Many different aromatic rings found their way into carbonic anhydrase inhibitors. However, a sulfonamide directly attached to an imidazole has never been reported as a carbonic anhydrase inhibitor.

5.2 Synthesis and Evaluation of Imidazole Sulfonamide PHP Inhibitors

The chemistry that was developed to synthesize building block **7** included the intermediates **27** and **29**. Removal of the protective groups gives access to small molecules **53a** and **53b** (see scheme 8). Using the same 2-position lithiation protocol and quenching with various electrophiles, introduction of various groups (intermediates **54c-f**) was proven to be possible. Immediate acid treatment and HPLC purification gave direct access to a set of four additional small molecules, **53c-f** (see table 4 for structures). To broader scan the imidazole 2-position, aromatic rings were introduced by performing palladium catalyzed cross-coupling reactions on iodine **29**. The products **55a-d** were continued without purification in an TFA deprotection step and products **56a-d** were isolated upon HPLC purification. This set of compounds was tested in the continuous fluorometric assay and remarkable results were obtained (see table 4). Small 2-position substituents like H, Me, Et and Cl failed to show significant activity at 100 µM concentration whereas larger substituents like bromine (**53f**) or iodine (**53b**) do give 100% inhibitory activity at this concentration. An IC_{50} value of 11.1 ± 5.9 µM and 6.2 ± 2.5 µM respectively was determined. The aromatic substituents **56a-d** showed little activity with a phenyl substituent showing as little as 34% inhibition at 100 µM as best.

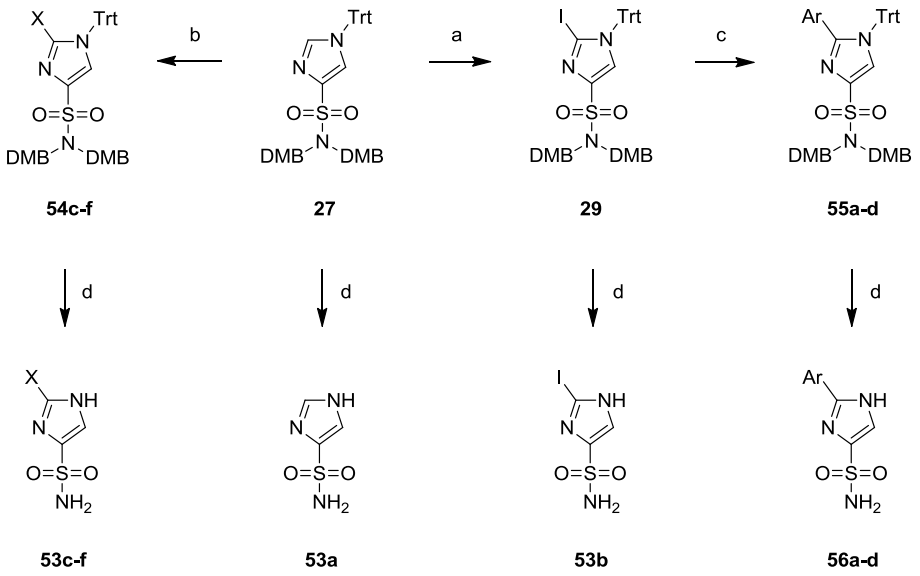

Scheme 8: Deprotection of building block 27 and 29 and synthesis of derivatives 53a-f and 56a-d. a: BuLi, I_2, THF, 1h, -30 ^{0}C, 85% **b:** BuLi, electrophile, THF, 1h, -30 ^{0}C **c:** $Pd(PPh_3)_4$, K_2CO_3, dioxane/water, 80ºC (for **54d**: Zn(0), BnI, DMF, $PdCl_2(PPh_3)_2$, 40 ºC) **d:** TFA, water, TiPS, 18h, RT.

These results were clearly encouraging and also the activity assay showed consistent and reproducible results. Clearly the 2-position substituent is of major influence but limited in what size substituent is allowed by the enzyme. To further investigate the imidazole 2-position it was decided to exploit the versatile possibilities of the metallation protocol and functionalize with more polar oxygen containing substituents.

Entry	Substituent X/Ar	Yield (%)	Activity Fluorescence assay % inhibition at 100 µM (IC_{50} in µM)
53a	H	32	0
53b	I	60	100 (6.2 ± 2.5)
53c	Me	58[a]	2
53d	Et	40[a]	3
53e	Cl	32[a]	0
53f	Br	57[a]	100 (11.1 ± 5.9)
56a	Phenyl	51[a]	34
56b	2-furan	17[a]	0
56c	3-pyridine	6[a]	0
56d	CH_2-phenyl	18[a]	2

Table 4: Yield and inhibitor activity of compounds 53a-f and 56a-d. a: yields over two steps.

Aldehyde **23**, another intermediate prepared originally for the synthesis for building block **7**, represents a useful starting point and the aldehyde was easily converted into **57** with MeMgBr. A reduction of **23** with $NaBH_4$ gave access to intermediate **58** that could be methylated directly using MeI, yielding **59**. The general TFA deprotection protocol used on the previous set of molecules was also used here and the molecules **60a**, **60c** and **60d** were isolated in good yield. **60b** was not isolated successfully, most likely due to chemical instability.

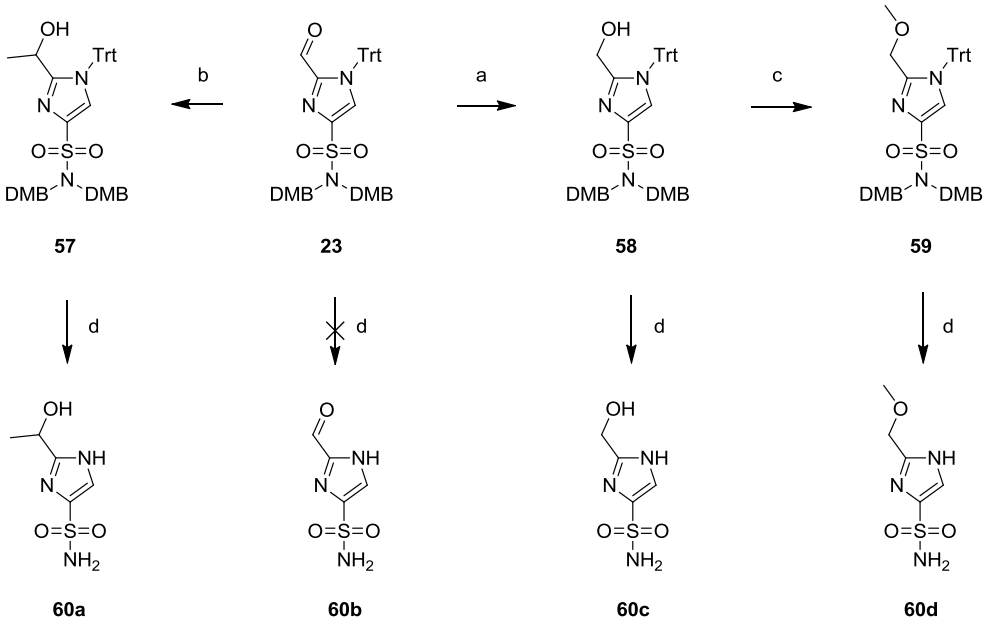

Scheme 9: The aldehyde functionality of 23 was manipulated to yield 57-59 and general TFA deprotection yielded the compound series 60a,c,d. **a:** $NaBH_4$, MeOH, 45 ºC, 96% **b:** MeMgBr, THF, 1h, 0 ^{0}C **c:** NaH, MeI, THF, 0 ºC **d:** TFA, water, TiPS, 18h, RT.

Furthermore, a carboxylic acid was introduced on the imidazole 2-position through quenching of the lithiated imidazole by canuling it into a stirred slurry of dry ice in dry THF (see scheme 10). Upon isolation of the product the trityl protective group proved instable, most likely due to internal protonation of the imidazole by the carboxylic acid. Eventually, the non-protected imidazole **61** was isolated in high yield. Removal of the DMB groups from **61** yielded carboxylic acid **62**. Additionally, the carboxylic acid was converted into three small amides, **63a-c** (see table 5 for structures). The unprotected imidazole did not interfere with amide formation as conversion was generally complete after one hour. Deprotection of **63a-c** yielded amides **64a-c**.

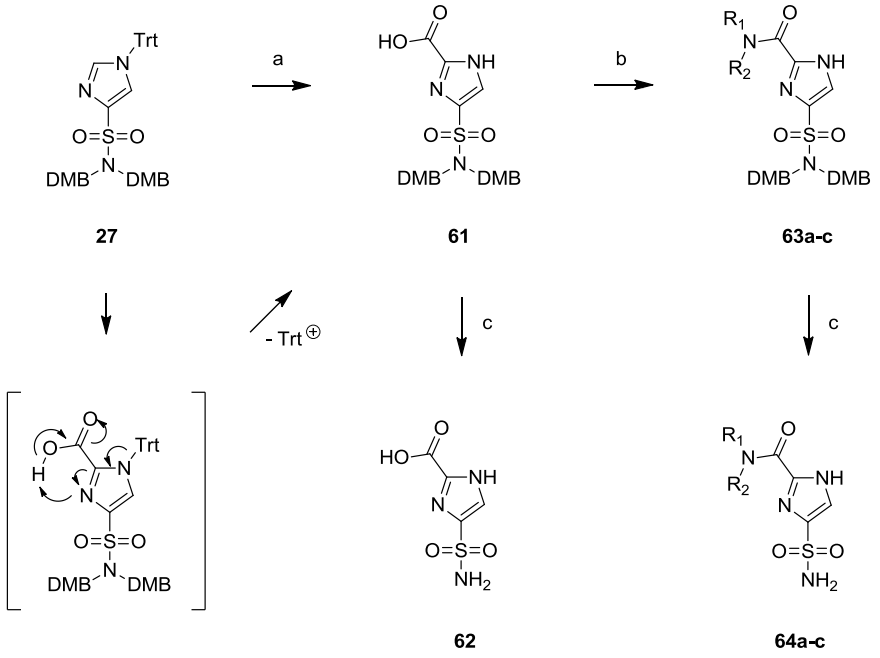

Scheme 10: Introduction of a carboxylic acid on the 2-position, the instability of the trityl protective group and the derived small molecules 62 and 64a-c. a: BuLi, CO_2, THF, 1h, -30 ^{0}C, 93% **b:** R_1R_2NH, PyBOP, DiPEA, DMF, RT **c:** TFA, water, TiPS, 18h, RT.

Compounds **60a-d**, **62** and **64a-c** were subjected to the fluorescence activity assay and **60c**, bearing a methylhydroxy substituent, showed full inhibition at 100 µM. An IC_{50} value was determined for this compound and a value of 9.9 ± 4.0 µM was found. The methoxymethyl (**60d**) and dimethylcarbonamide (**64c**) substituents showed significantly less activity with 37 and 31 % respectively. Among the other substituents very little activity was established (see table 5).
The initial results of screening the 2-position substituent showed encouraging results and the available X-ray structures were investigated in an attempt to explaining the established SAR. It is unclear whether the fully visible C terminal end X-ray structure, as was generated in-house, is a better model compared to the structure as reported in literature. It is clear that the in-house generated ‘closed’ structure shows little space for substituent binding compared to the reported structure 2HW4 (see figure 28b-d compared to 28a). Therefore it was decided to use 2HW4 as the basis for *in silico* modeling.

Entry	Substituent	Yield (%)	Activity Fluorescence assay % inhibition at 100 µM (IC_{50} in µM)
60a	$-CH(CH_3)OH$	54[a]	3
60c	$-CH_2OH$	44[a]	99 (9.9 ± 4.0)
60d	$-CH_2OCH_3$	42[b]	37
62	-COOH	44	22
64a	$-CONH_2$	12[a]	23
64b	$-CONHCH_3$	75[a]	0
64c	$-CON(CH_3)_2$	62[a]	31

Table 5: yield and inhibitor activity of compounds 60a-d, 62 and 64a-c. a: yields over two steps

Docking experiments performed using X-ray structure 2HW4, with **60c** as the ligand, showed a strong preference for two possible binding conformations. The inhibitor can adopt a conformation with the sulfonamide in the same pocket as where the binding with a phospho-histidine was predicted (figure 40A). Alternatively, an inverse binding mode was proposed (figure 40B) where the sulfonamide interacts with Arg[78] (see also figure 40A and 40B inserts for an interaction graph). Interestingly, the results from such a docking exercise are very similar when using a rigid receptor or an induced fit method when amino acid residue flexibility is taken into consideration. The tautomerisation of the imidazole seems to be of little influence on the docking experiment outcome and again these two possible binding modes are favored.

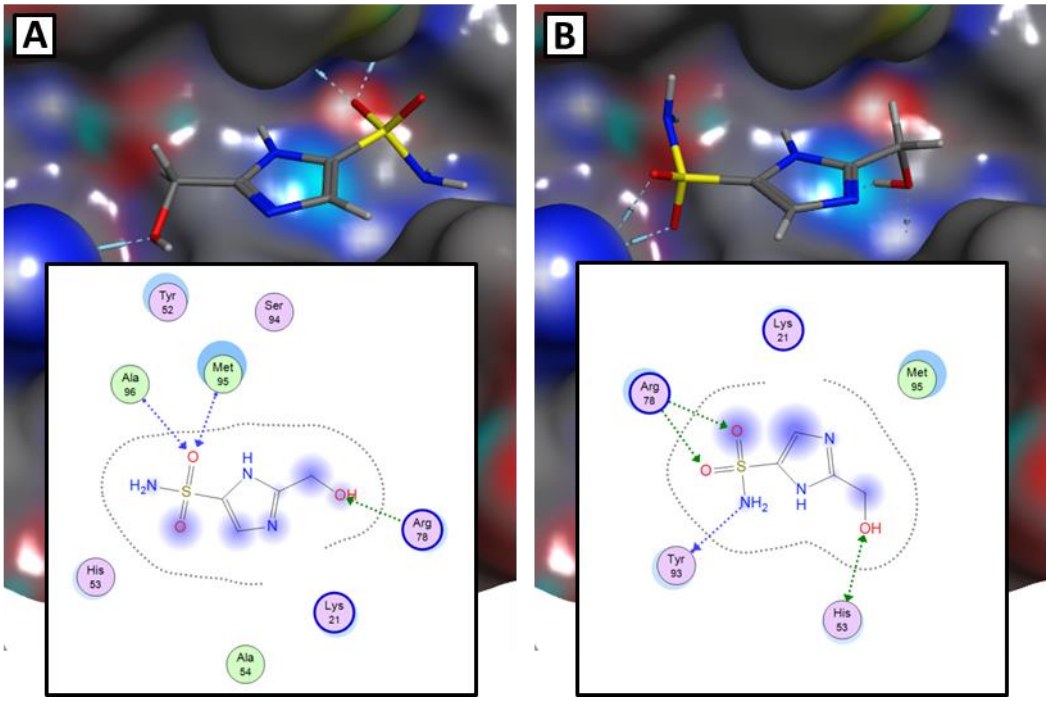

Figure 40: Two possible binding modes for compound 60c as predicted by docking experiments. See text for details.

In both cases, the essential His^{53} is covered by the ligand and is non-accessible for interaction with a phospho-histidine substrate. This clearly suggests competitive inhibition of the enzyme as the mechanism of action for these molecules.
For compound **53b** no clear trend was found when docking experiments were performed in the pdb reported structure 2HW4. This is likely to be caused by the under appreciation of the van-der-waals interaction possibilities compared to hydrogen bond formation possibilities in the strongly polar protein surface of the catalytic site. The relatively lipophilic iodine will give less strong interactions compared to the polarized methylene hydroxyl substituent in the 2-position of compound **60c**. One predicted conformation seems particularly attractive. This is where the large iodine is locked nicely in between the residues Met^{95}, Ser^{94}, His^{53} and Tyr^{52} (see figure 41). The imidazole is lying flat on the bottom of the pocket forming one hydrogen bond with the backbone amine of Met^{95}. The sulfonamide hydrogens are lined up perfectly for the formation of a pair of hydrogen bonds with Arg^{78}. The $-NH_2$ of the sulfonamide finds its way into a tunnel formed by the standing upright residues Arg^{78} and Tyr^{93}.

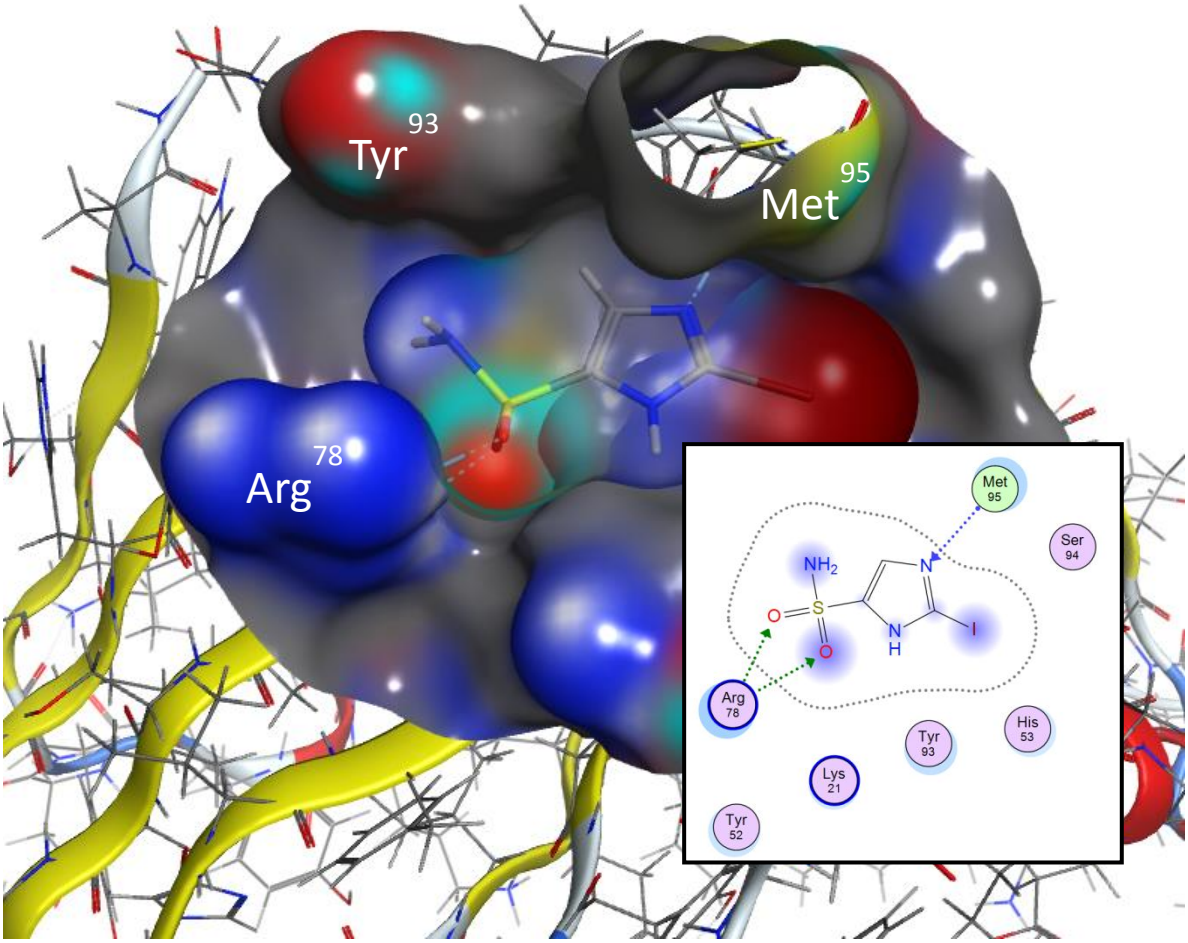

Figure 41: proposed binding mode based on docking studies for compound 53b. In this proposed binding mode the inhibitor lies flat on the bottom of the catalytic cavity locked in place by three hydrogen bonds with Arg^{78} and Met^{95}. The insert shows a graph of the identified ligand-receptor protein interactions.

Next, it was decided to look into the possibility to further functionalize the sulfonamide or move to a sulfonyl derivative. Expanding the molecule in this direction is an opportunity to reduce the polarity of the molecule by increasing the logP value together with increasing the surface area of the ligand interaction with the protein. Low logP values are generally associated with poor cell permeability. The compounds **53b** and **60c** display clogP values of 0.11 and -1.64 respectively, rendering them likely to suffer from poor cell permeability (calculated using the software MarvinSketch 6.0.6). Addition of a methyl or benzyl group attached to the sulfonamide of **53b** will raise this value to 0.33 and 2.05 respectively. For **60c** these modifications will lead to values of -1.08 and 0.31. The arrow in figure 42 shows the space in between the upstanding residues Arg^{78} and Tyr^{93}. The conformation of these residues forms a tunnel that seems suited for ligand extension.

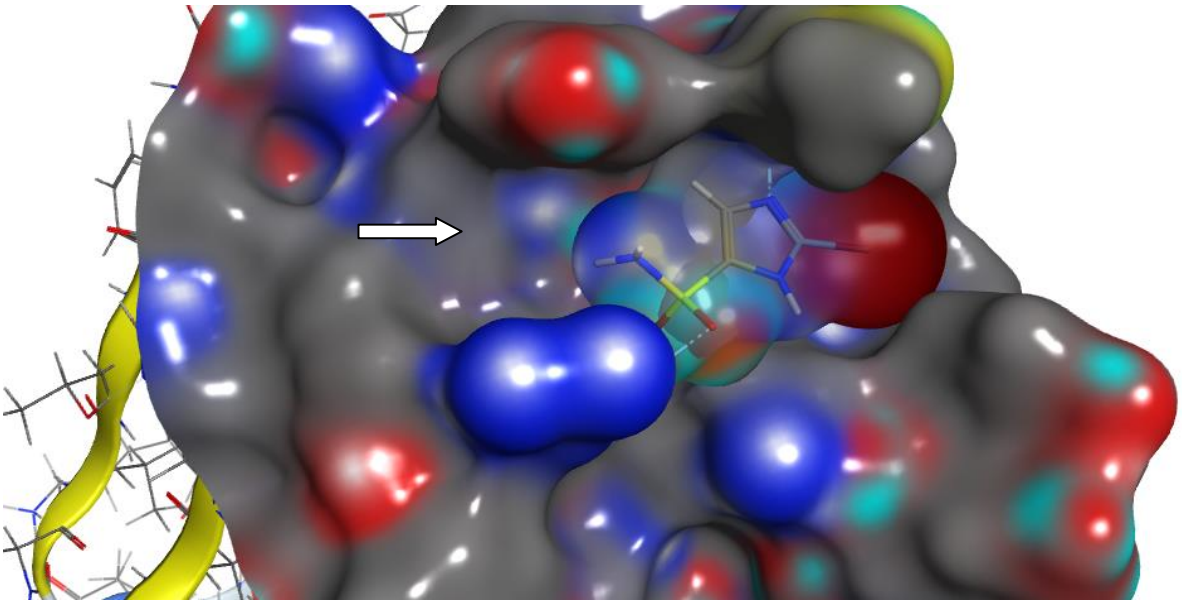

Figure 42: the proposed binding mode of 53b predicts space for extension on the sulfonamide, as indicated by the arrow. Substitution of the sulfonamide nitrogen with alkyl or aromatic groups will give access to such molecules.

A strategic building block like sulfonyl chloride **65** was required to provide easy access to a series of compounds with substituted sulfonamide (see scheme 11). A bromine or iodine substituent on the imidazole 2-position is favored over the methyl hydroxyl substituent due to synthetic feasibility. The possibility to directly introduce a bromine or iodine at the 2-position of intermediate **24** was investigated but failed due to the instability of the product (**65**) during formation. The protection of the imidazole was considered and a benzyl chloromethyl ether (BOM) group was successfully introduced on the imidazole. Subsequently, bromination on the 2-position of **66** was possible in reasonable yield. The introduction of iodine failed and did not yield isolatable amounts of product. Again, instability of the product was observed and this significantly lowered the yield. Reacting sulfonylchloride **68** with different amines yielded compounds **69a-f**.

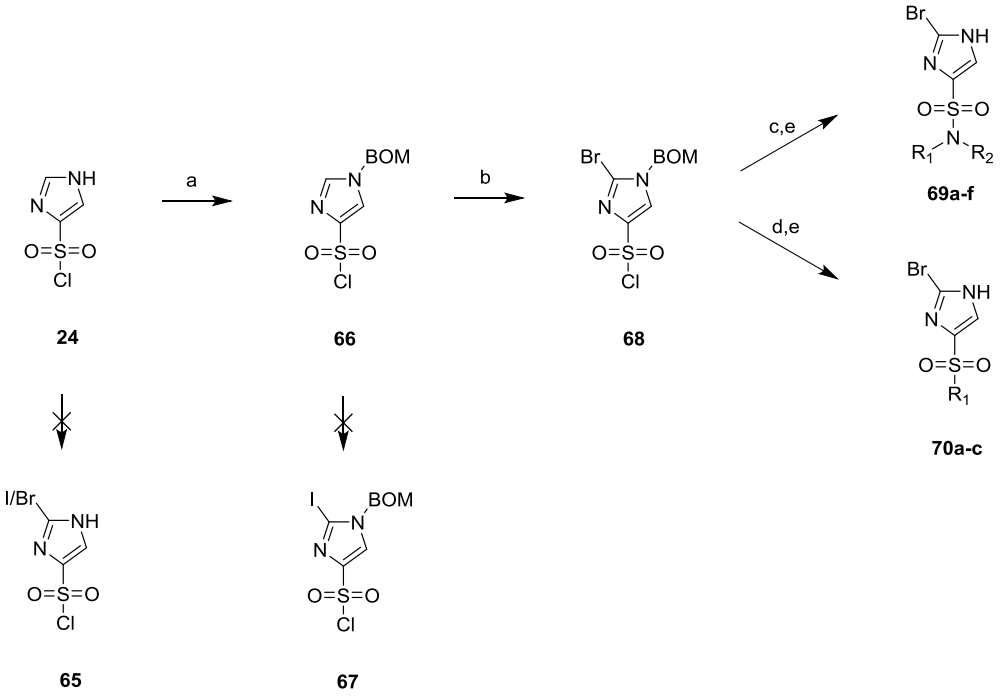

Scheme 11: The synthesis of compounds 69a-f and 70a-c through strategic intermediate 68. a: BOMCl, MeCN, 18h, RT, 79% **b:** NBS, $CHCl_3$, 4h, 50 ^oC 43% **c:** HNR_1R_2, DiPEA, DCM, 18h, RT **d:** Na_2SO_3, $NaHCO_3$, water, tetra-*n*-butylammonium bromide, R_1X, 18h, RT **e:** TFA, water, TiPS, 18h, RT.

An interesting procedure described by King and Beatson, using Na_2SO_3 as a reducing agent and an alkylhalide, gave excess to alkyl sulfonyl derivatives **70a-c**.[89] Unfortunately, inhibitory activity was lost in almost all entries (see table 6). In this series a methyl sulfonyl substituent (entry **70a**) showed some activity with 16% inhibition at the highest concentration of 100 µM.

Entry	Substituent R1	Substituent R2	Yield (%)[a]	Activity Fluorescence assay % inhibition at 100 µM (IC_{50} in µM)
69a	-H	$-CH_3$	35	0
69b	$-CH_3$	$-CH_3$	57	0
69c	-H	$-CH_2CH_2OCH_3$	45	7
69d	-H	$-CH_2-CH=CH_2$	24	0
69e	-H	-Phenyl	46	0
69f	-H	$-CH_2$-phenyl	43	0
70a	$-CH_3$	-	53	16
70b	$-CH_2-CH=CH_2$	-	35	7
70c	$-CH_2$-phenyl	-	50	0

Table 6: activity of compounds 69a-f and 70a-c. a; yields over two steps

It is clear that there is little room for improvement and the molecule appears to bind in a small pocket making the proposed binding mode of figure 42 less plausible. This suggests that the X-ray structure generated in-house (see §3.7) is a better basis for a model. However, the exposed pocket is too small to fit even the small molecules like **53b** or **60c**. The question is how does the C-terminal Tyr^{125} behave in solution and does the C-terminal end pressed against the active site represent a relevant conformation or is it an artifact caused by tight crystal packing? Closer analysis of the X-ray structure and comparing it to 2HW4 does show significant movement of the amino acids Arg^{78} and Lys^{21}. These residues seem to be pressed in a tight conformation next to Tyr^{52} due to Tyr^{125} being pushed into the catalytic site. Lifting up this tyrosine residue just a few angstrom exposes a deepened binding pocket that fits the identified inhibitors remarkable well. Further underneath the lifted Tyr^{125}, appears to be more space but this is likely to be filled with a water molecule present in the non-manipulated X-ray structure. Figure 43 shows a representation of iodine **53b** docked inside the Tyr^{125} lifted structure.

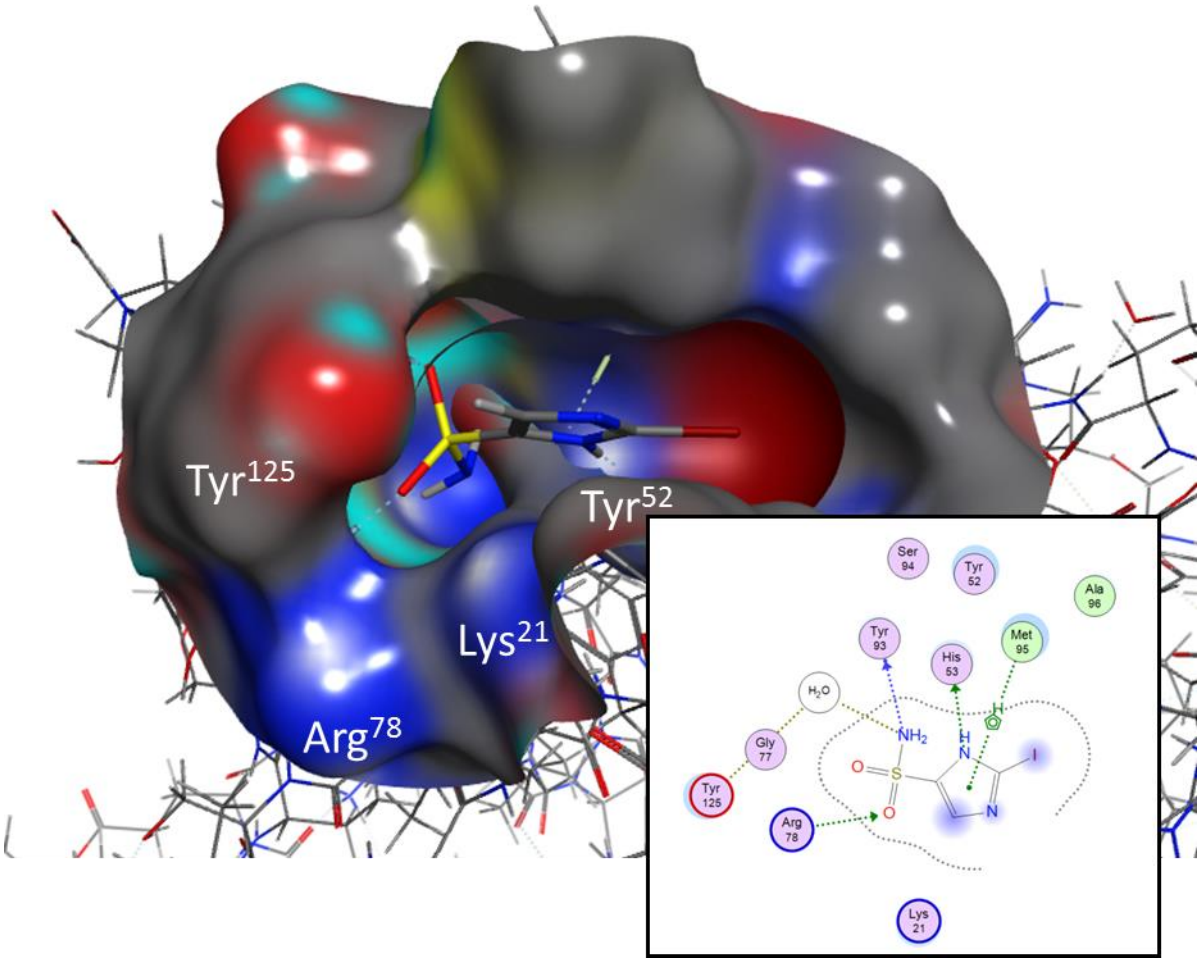

Figure 43: The proposed binding mode of 53b in the in house generated X-ray structure. A single manipulation was made in lifting up the C-terminal Tyr^{125} slightly. In doing so, an ideal binding pocket for these small molecules was obtained.

For the final stage of optimization, focused was on smaller variations directly on the imidazole core since larger substituents on the premises of the molecule led to significant loss of activity. Three methyl variations (1-,3- or 5-methylimidazole) were pursued in order to see if such additions are allowed (see figure 44, entries **71**, **72** and **73**). Again, a bromine or iodine as 2-position substituent is preferred over the methyl hydroxyl substituent.

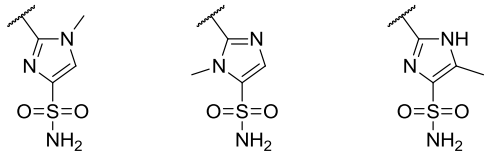

71 **72** **73**

Figure 44: The structures of the methyl imidazole regioisomers 71, 72 and 73.

The synthesis of the 1-methyl regioisomer commenced with commercially available 1-N-methylimidazole **74** (see scheme 12). In line with the previously described synthesis of the 1-H version the sulfonyl chloride moiety was readily introduced using chlorosulfonic acid and thionyl chloride. Conversion of the sulfonylchloride **75** into a sulfonamide was again achieved by the use of a dimethoxybenzyl protected amine. Introduction of the 2-position halide on **76** proved more difficult as selectivity during lithiation between the 2- and the 5-position was completely lost with the small 1-position methyl substituent compared to the earlier used trityl group. The 2,5-dihalide **77** was readily obtained, unlike the desired 2-position mono iodide. It has been reported in literature that a 5-position halogen-imidazole is not stable under acidic conditions.[90] This would allow for the synthesis of the desired 2-position mono-halide. Indeed upon acid treatment to remove the DMB protective groups, the 5-positon iodide was nicely removed and only the desired mono iodide **71** was identified as product.
Synthesis of **72** proved difficult due to instability problems. Precursor **24** could be methylated selectively on the 3-position using dimethyl sulfate in formic acid. However, converting the sulfonylchloride **78** into sulfonamide **79** was not possible and methylated amine **81** was isolated as the only product. A mechanism for this unforeseen instability is proposed in the box in scheme 13.
The 5-methyl regioisomer **73** was prepared in a method similar to the preparation of the compounds **69a-f**. Here, a commercially available 4/5-methylimidazole (**82**) was used as starting material and the sulfonylchloride and BOM protection group were introduced successfully and in similar yield as compared to compound **68**. For entry **73** it was decided to prepare the bromide since introduction of the iodide failed before (see scheme 11). Introduction of the bromide on the 2-position was achieved and consequent conversion into sulfonamide gave compound **85**. Final acidic cleavage of protective groups yielded the desired 5-methyl derivative **73**.

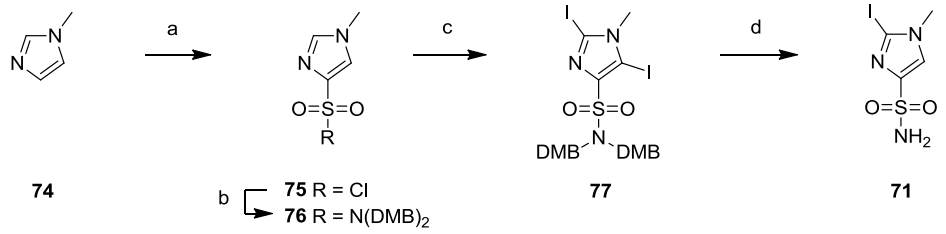

Scheme 12: Synthesis of compound 71. a: $ClSO_3H$, 140 ^{0}C, 16h, $SOCl_2$, 5h, till 125 ^{0}C, 31% **b:** N,N-bis(2,4-dimethoxybenzyl)amine (DMB_2NH), DiPEA, DCM, 2h, 0 ºC - rt, 82% **c:** BuLi, I_2, THF/ HMPA, 18h, -30 ºC, 83% **d** TFA, water, TiPS, 18h, rt, 41%.

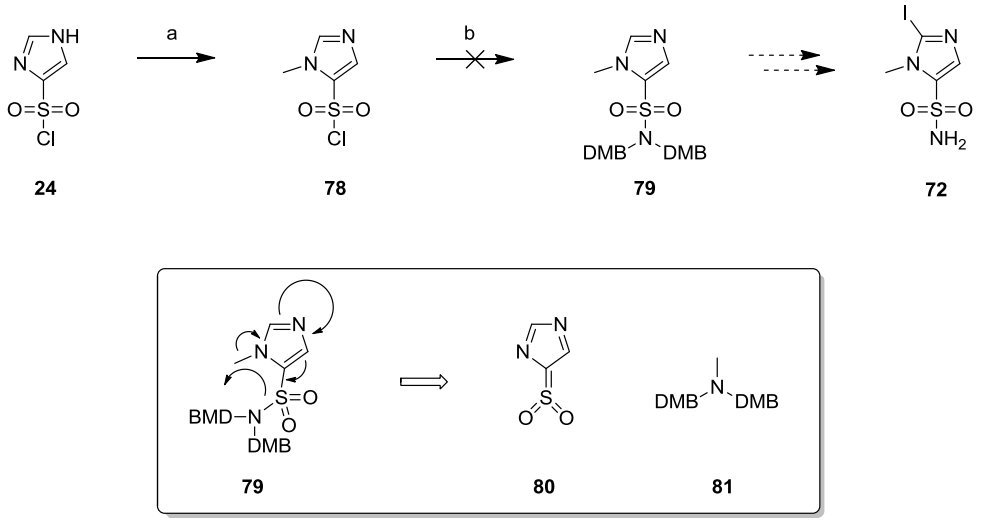

Scheme 13: Attempt of synthesis of compound 72. a: 78% formic acid, Me_2SO_4, 18h, RT, 58% **b:** N,N-bis(2,4-dimethoxybenzyl)amine (DMB_2NH), DiPEA, DCM, 2h, 0ºC-rt. Instead of obtaining the desired **79**, compound **81** was isolated. The mechanism explaining this product involves a nucleophilic attack of the $(DMB)_2N$ on the adjacent methyl. Byproduct **80** is quenched upon aqueous workup and lost during extraction.

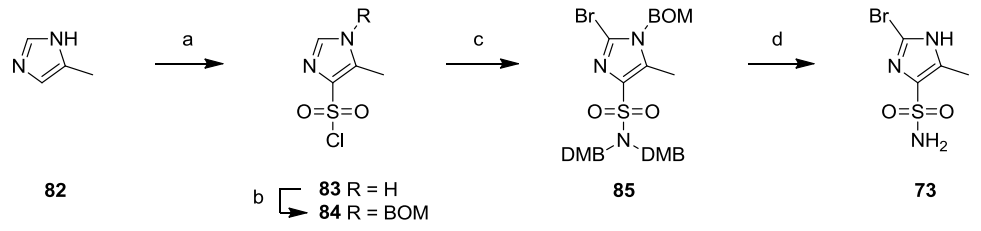

Scheme 14: Synthesis of compound 73. a: $ClSO_3H$, 140 ^{0}C, 16h, $SOCl_2$, 5h, till 125 ^{0}C, 39% **b:** BOMCl, MeCN, 18h, rt, 50% **c:** NBS, $CHCl_3$, 3h, 50 ^{o}C, N,N-bis(2,4-dimethoxybenzyl)amine (DMB_2NH),, DiPEA, DCM, 3h, 0 ºC - rt, 16% **d** TFA, water, TiPS, 18h, rt, 50%.

Besides adding substituents to the imidazole core, the role of imidazole core tautomerism needs to be investigated. The imidazole proton can be on the 1- or on the 3-position (see figure 45A and 45B respectively). The model proposed in figure 43 shows the formation of a hydrogen bond between the imidazole core and the His[53] lining the bottom of the cavity. If this assumed interaction is important for inhibitor activity the tautomeric form that the inhibitor adopts, becomes essential. His[53] is under physiological conditions not protonated.[48] The imidazole inhibitors have a hydrogen bond donating proton but due to tautomerism the hydrogen can point the wrong way. Also, the pK_a will be of influence on the imidazole protonation state. Imidazole itself has a pK_a of 6.9. The electron withdrawing groups generally found on the inhibitor 2-position and the sulfonamide will lower the pK_a significantly, assuring a non-charged imidazole at physiological pH. This means that the imidazole 3-position is not necessarily a hydrogen bond donor when the ligand meets the enzyme in solution. To establish a constitutive proton on the imidazole 3-position, a molecule like compound **86** (figure 45) was considered. Introduction of a hetero-atom directly on the 2-position will generate a molecule that is likely to adopt a urea-like conformation resulting in a constitutively protonated 1- and 3-position nitrogen. A thiourea (X = S) would be preferred due to the larger size compared to an oxygen or nitrogen.

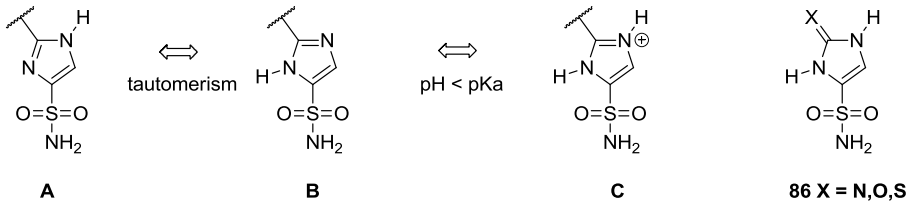

Figure 45: Influence of tautomerisation and pK_a on the form an imidazole is in and structure 86 the can lock the ring in a urea form. The urea of **86** will generate a molecule with permanent protonation on both imidazole nitrogens.

To introduce the sulfur on the 2-position of the imidazole the lithiation protocol deployed so successfully before can also be used. Quenching the 2-position lithiate with elemental sulfur led to disappearance of starting material **27** and formation of a variety of sulfurated compounds due to the use of an excessive amount of S_8. Treatment with trifluoro acetic acid yielded only a single compound, the desired thiourea **86**. H- and F-NMR analysis showed no sign of molecule protonation by a TFA counter ion that indeed could be observed for all the other imidazoles. This shows that **86** is indeed only present in the thiourea form.

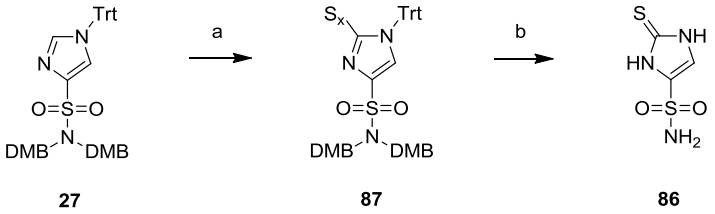

Scheme 15: Synthesis of compound 86. a: BuLi, S_8, THF, 30min, -30 ºC **d** TFA, water, TiPS, 18h, RT, 12% (over two steps).

Eventually, the compounds **71**, **73** and **86** were subjected to the fluorescence activity assay and remarkably, the entries **71** and **73** failed to show any activity. Perhaps these substituents interfere with an important hydrogen bond. Entry **86** however, showed full inhibition at 100 µM and an IC_{50} value of 3.1 ± 1.7 µM was determined.

Thiourea **86** is indeed the most active compound that was identified during this synthesis and testing campaign. The explanation on the previous page stating that the permanent protonation of both imidazole nitrogens will be beneficial seems very plausible and is supported by docking experiments. Using the Tyr^{125} lifted structure, described earlier in figure 43, it becomes evident that **86** fits convincingly in the same configuration as found for 2-iodo inhibitor **53b**. The added 2-position sulfur shows multiple possibilities for hydrogen bond formation, either as a thiourea or as a 2-position –SH tautomer. However, it is doubtful that this will be of mayor contribution to the binding affinity. Sulfur has been reported to be a poor hydrogen bond acceptor and a moderate hydrogen bond donor.[91] It is more likely that the tautomeric permanent 3-position NH hydrogen bond donor is the major contributor in this case. This constitutive hydrogen bond donation to the underlying His^{53} (see insert of figure 46) will lock the compound more tightly inside the enzyme active site.

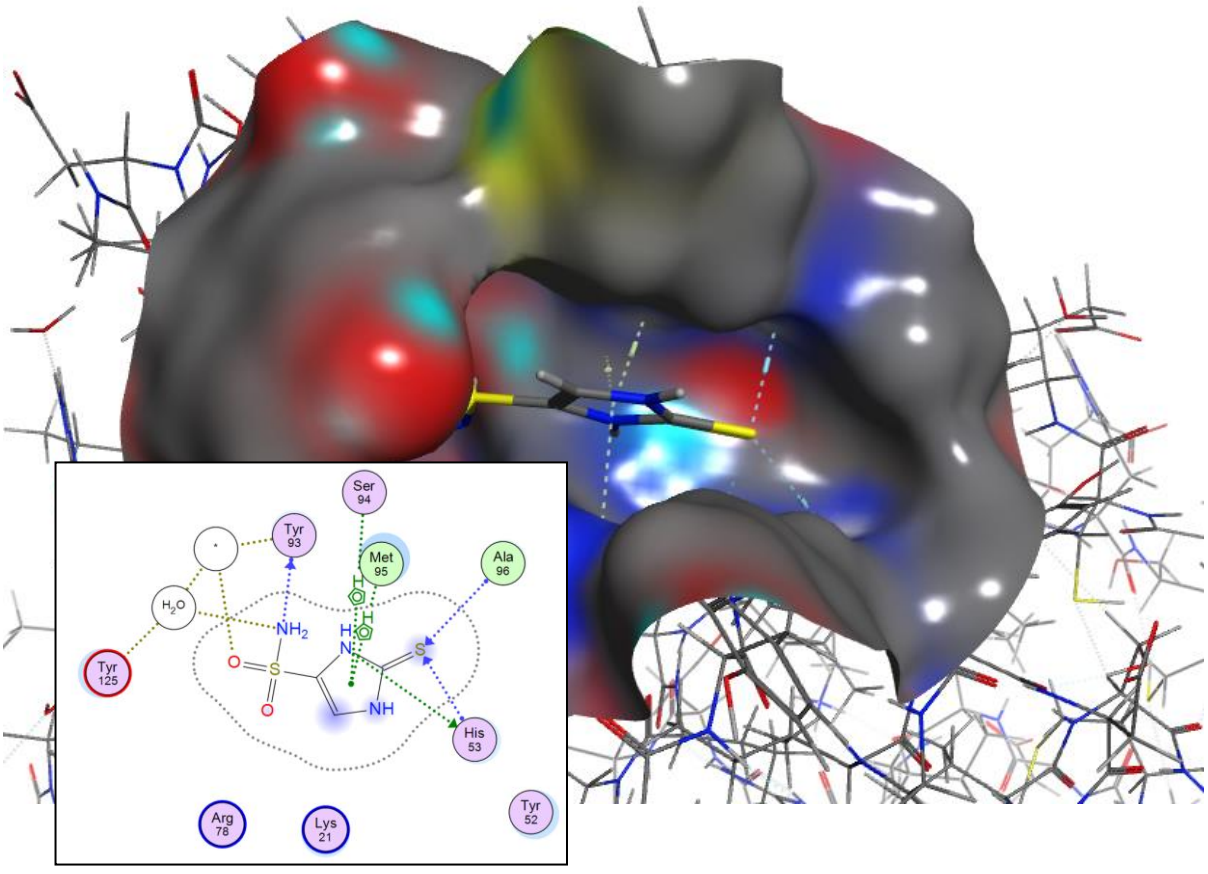

Figure 46: The proposed binding mode of 86 as predicted by docking. The insert shows the multitude of H-bond interaction possibilities between ligand and protein and also a conserved water molecule underneath Tyr^{125}.

5.3 Synthesis and Evaluation of Phosphonate and Carboxamides/Carbonic Acid Derivatives as PHP Inhibitors

The success of the sulfonamide functionality raises the question if other bioisosteres for phosphate would also be allowed. A phosphonate group (compound **88**, figure 47) would be desirable but also a carboxylic acid (**89**) or amide (**90**) are interesting substituents. The phosphonate and carboxylic acid are not very attractive options since such negative charges often prevent drug molecules from diffusing through a cell membrane. However, both the phosphonate and carboxylic acid have been employed successfully as phosphate mimics in numerous occasions, unlike the sulfonamide or amide bioisosteres.[75] It is interesting to see the scope of the enzyme's sensitivity towards these small molecule inhibitors when decorated like the sulfonamide series. It was decided to use iodine as the 2-position substituent. Introduction of the iodo group is easily achieved and the acidic instability of a 5-position iodine, described in the synthesis of **71**, can also be used in the synthesis of these compounds when regioselective introduction of the iodine is problematic.

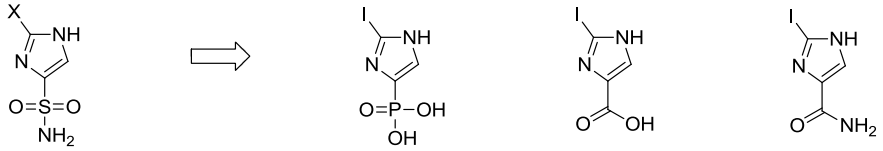

88 **89** **90**

Figure 47: Translating the sulfonamide based inhibitors to phosphonate (88), carboxylate (89) and amide (90) versions.

To substitute the sulfonamide for a (benzyl protected) phosphonate, a halogen metal exchange on the 4-position of trityl protected 4-iodo imidazole **92** (see scheme 16) is required. This chemistry was employed successfully before, in our group, in an attempt to synthesize a phosphonate based phospho-histidine building block **98** (see figure 48). For this compound, the same chemistry was used that was developed for the sulfonamide based mimic **7** synthesis (as described in chapter 4).[56] Nevertheless, the introduction of an iodine on the 2-position of **93** through n-butyllithium induced lithiation failed. The presence of the phosphonate heavily influenced the regioselectivity of the deprotonation and the 5-position iodo imidazole isomer (**95**) was formed instead. Indeed acidic removal of the benzyl protective groups gave **97** as the sole product rather than **96** (or **88**), indicating that the iodine was indeed introduced on the 5-position and lost upon acid treatment.
To achieve the desired 2-position lithiation over the favorable 5-position lithiation on intermediate **93**, the thermodynamically favored lithiation (**93b**, figure 49) needs to be overcome to achieve the kinetically favored 2-position lithiation (**93a**). Lowering the temperature during lithiation from -30 ºC to -78 ºC did not change regioselectivity nor did replacing the n-BuLi by s-BuLi, LDA or Li-TMP.

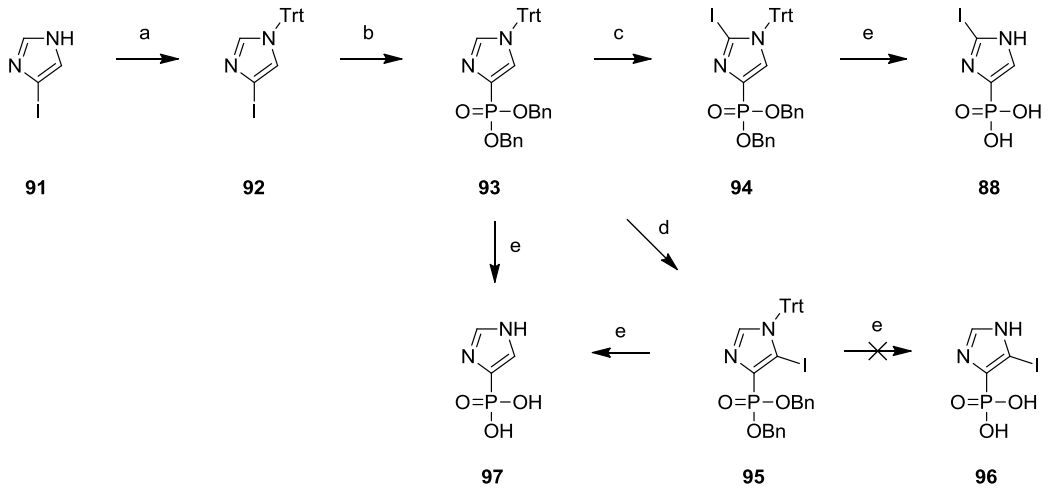

Scheme 16: Synthesis of compound 88. a: TrtCl, DiPEA, THF, 18h, 60 ºC, 84% **b:** iPrMgCl:LiCl, bis(diethylamino)phosphine chloride, 2h, -78 ºC - rt, BnOH, MeCN, tetrazole, 0 ºC - rt, 18h, 53% **c:** *t*-BuLi, I_2, THF, 2min, -100 ºC, 62% **d:** BuLi, I_2, THF, 30min, -30 ºC, 53%[67] **e:** TFA, water, TiPS, 18h, rt, (**88** from **94**: 64% and **97** from **93**: 29%).

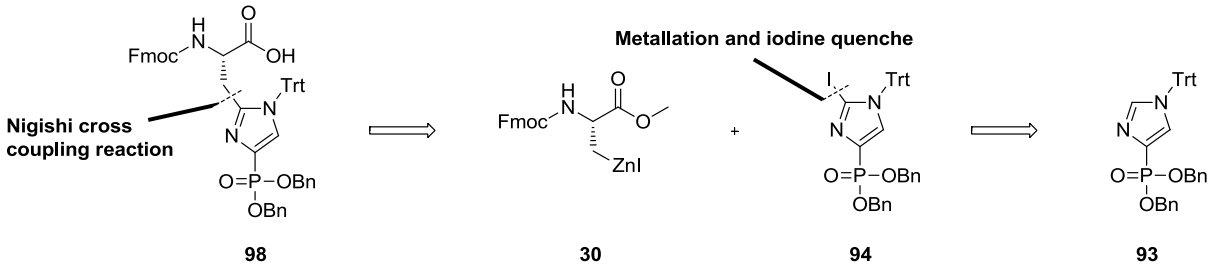

Figure 48: Retrosynthetic analysis of compound 98 with intermediate 93 and 94. This synthesis is described in the thesis from Bart van Vliet.[56]

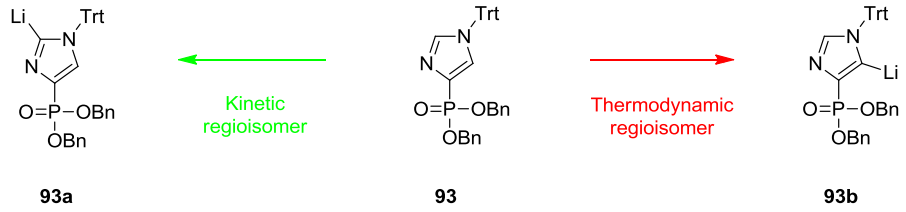

Figure 49: Lithiation of 93 going either kinetically on the 2-position (93a) or thermodynamically on the 5-position (93b).

An elegant method for influencing the regioselectivity of lithiation of 2-methoxypyridine **99** was described by Caubere and coworkers (see figure 50).[92] Treating this heterocycle with different lithiating reagents and quenching with an electrophile generally failed to give the desired 6-position substituted product **100**. For example, LDA yielded the 3-position lithiate **101** due to the directing effect of the methoxy group. Use of n-BuLi resulted in nucleophilic addition yielding lithiate **102**. The *in-situ* generated non-nucleophilic reagent complex BuLi-$Me_2N(CH_2)_2OLi$ (BuLi-LiDMAE was used successfully on **99**, generating lithiate **103**, and desired pyridine **100** could be isolated with E being a variety of substituents. The formation of a complex as shown in figure 50 (insert 1) was given as explanation for the obtained regioselectivity. Hypothetically, this sterically hindered and non-nucleophilic complex can also use the presence of the imidazole nitrogen and phosphonate P=O to coordinate and facilitate deprotonation on the adjacent carbon in a similar fashion as with **99** (see figure 50, insert 2). Unfortunately, when applying this method, no desired 2-position deprotonation of **93** was observed and again, only 5-position iodo product was found after quenching.

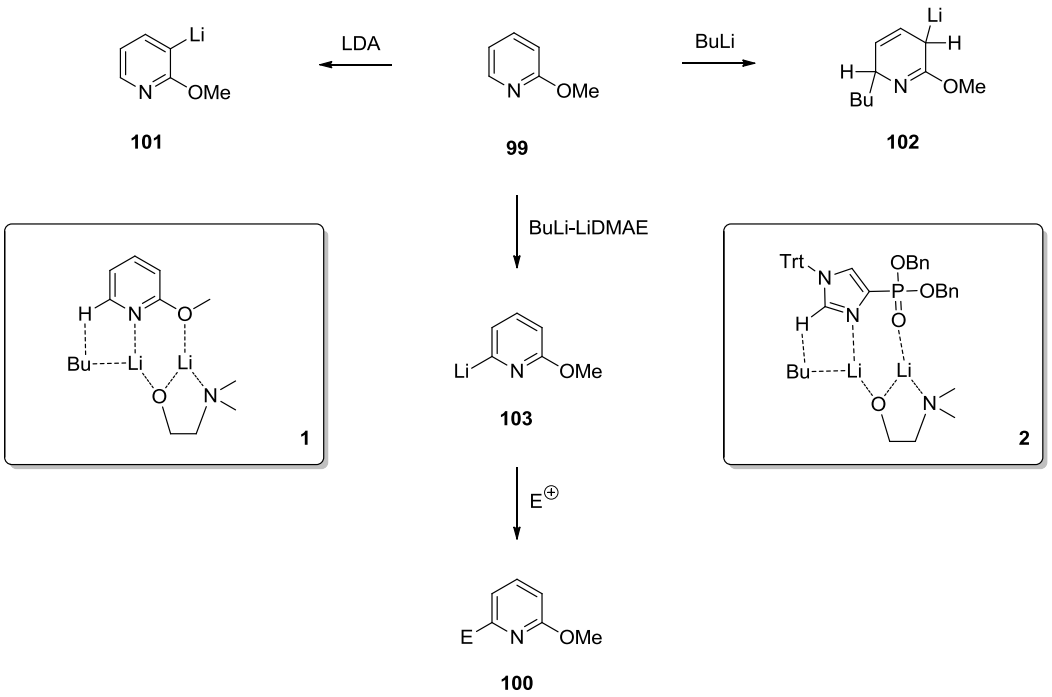

Figure 50: The lithiation of 2-methoxypyridine. Successful 2-position lithiation of pyridines can be achieved by using BuLi-DMAE. This complex associates with the pyridine nitrogen and methoxy oxygen and directs a second equivalent of BuLi towards the pyridine 2-position hydrogen.[92] It was hypothesized that 2-position lithiation of **93** could be achieved in a similar fashion.

A more successful method was found in the use of a stronger and more kinetic base like t-BuLi. Simply replacing n-BuLi from the original protocol by t-BuLi yielded the desired iodo regioisomer **94**. Optimization of the protocol by lowering the temperature to -100 ºC and addition of the iodine immediately upon t-BuLi addition resulted in a 62% yield with no formation of the 5-position isomer observed. Indeed, acidic removal of the protective groups from **94**, showed stability of the halide and allowed us to acquire the desired phosphonate **88**.

To complete the set of alternative bioisosteres the commercially available 4-carboxylic acid imidazole **104** was protected with a trityl group. The carboxylic acid **105** was reacted with the same double dimethoxybenzyl protected amine used for the sulfonamides, obtaining compound **106**. Like for the sulfonamide the DMB protective group is a suitable protection for a terminal amide group.[93] With these two building blocks in hand the lithiation and regioselectivity of these carbonyl attached imidazoles was investigated. Again, regioselectivity proved to be an issue for the lithiation. In both cases a clear lack of selectivity was observed as both 2- and 5-position isomers were formed in similar amounts. Using n-BuLi or t-BuLi did not influence the ratio much in both cases. The mixture of isomers also seemed hard to separate by normal or reversed phase chromatography. However, this was assumed not to be a serious issue since the 5-position isomers were likely to be unstable under acidic deprotection conditions. This was already observed for the sulfonamide and phosphonate compounds. Indeed upon TFA treatment and HPLC purification only the 2-position iodo-imidazoles, **89** and **90** were isolated in pure form.

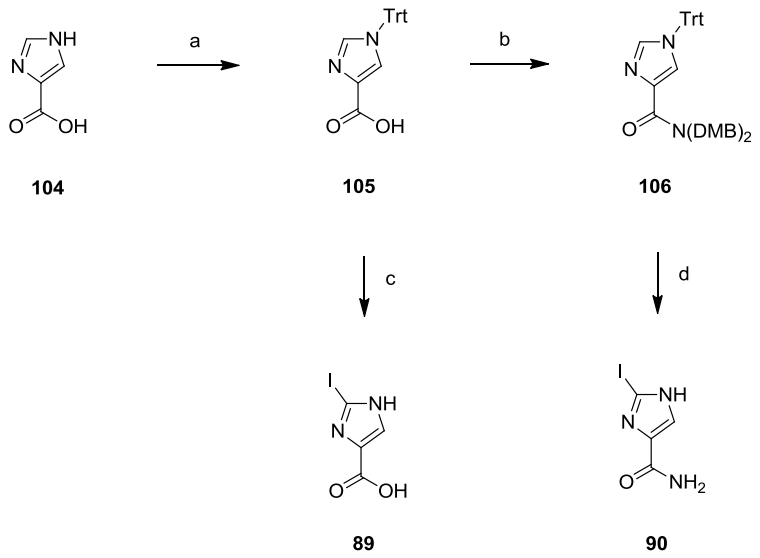

Scheme 17: Synthesis of compounds 89 and 90. a: TrtCl, pyridine, DMF, 18h, rt, 73% **b:** *N*,*N*-bis(2,4-dimethoxybenzyl)amine, HOBt, EDC.HCl, DiPEA, 2h, rt, 95% **c:** t-BuLi, I_2, THF/HMPA, 2 min., -100 ºC, TFA, water, TiPS, 18h, rt, 45% **d:** t-BuLi, I_2, THF, 2 min., -100 ºC, TFA, water, TiPS, 18h, rt, 38%.

Compounds **88**, **89**, **90** and phosphonate **97** were tested for PHP enzyme inhibition and remarkably, showed no enzyme inhibitory activity. The sulfonamide is clearly superior to carboxylic acid, carboxamide and even the phosphonate. This result suggests a binding mode for the imidazole sulfonamides different to the way a phospho-histidine substrate binds to the enzyme prior to enzymatic hydrolysis. This is in line with the various binding modes already proposed predicting the 2-position substituent of the imidazole sulfonamide inhibitors at the place where substrate phosphate is likely to bind.

5.4 Encore: Structure Based Design: 3,5-diphenyl-isothiazolidine-dioxides as PHP inhibitors?

The availability of X-ray structures for PHP allows the application of structure based (ligand) design as an alternative means of novel inhibitor identification. With this technique, the structural information available directs the design of new ligands.
X-ray structure 2HW4 shows a significantly larger catalytic cleft compared to the in-house generated structure (see figure 28). Assuming that 2HW4 is a real, *in situ*, conformation for PHP, an inhibitor design can be envisioned that contains a central core with two aromatic rings attached (see figure 51). The most convincing binding modes for the imidazole sulfonamides place the sulfonamide in the center close to Arg^{78}. This sulfonamide is easily incorporated in a ring system. This ring should be able to position the aromatic ring features correctly to fill the two pockets on both left- and right-hand side. Preferably, this center ring is saturated to induce a certain amount of flexibility. An isothiazolidine 1,1-dioxide ring presents a viable option and a 3,5-diphenyl decoration as the best orientation for the phenyl rings. This test compound, **107** in figure 52, can be prepared in a racemic fashion to obtain a total of 4 different stereoisomers. Docking experiments were performed and all four possible isomers, SR, RR, SS and RS were docked inside 2HW4. Three out of four compounds were docked convincingly, placing the ligand nicely in the catalytic site (see figure 53). The RS isomer poses a problem as the cis-orientation prevents the ligand from adopting a suitable conformation. For the other cis-isomer, SR, this was not a limitation.

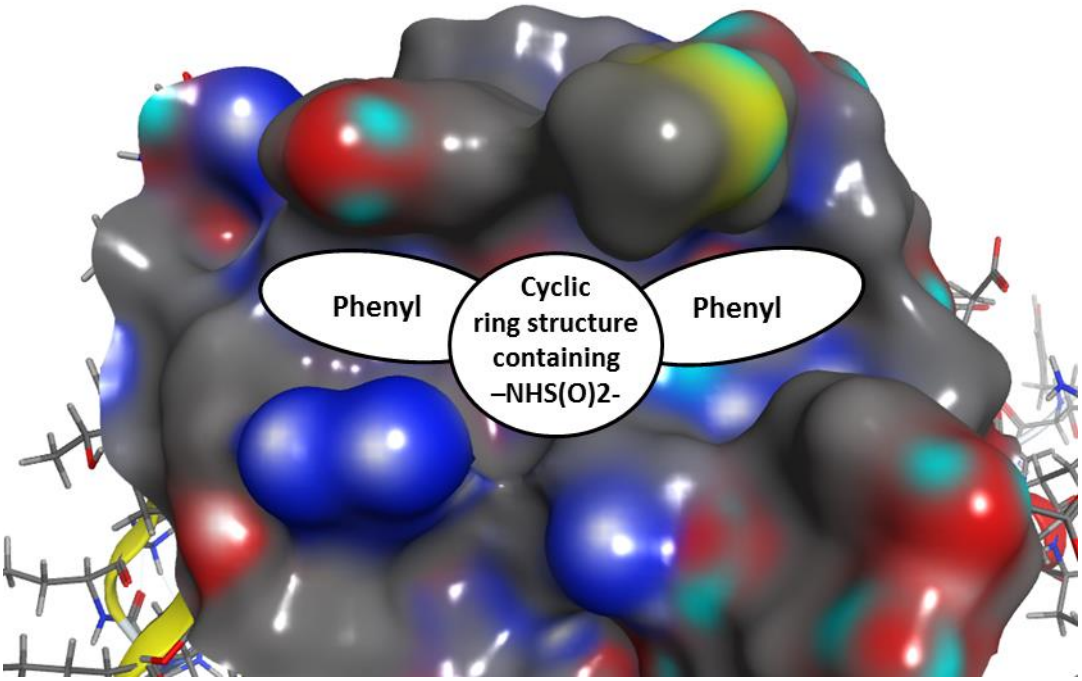

Figure 51: Depiction of a proposed layout for novel PHP inhibitors based on pdb 2HW4. Performing a structure based ligand design, the available binding pocket can be filled with a molecule based on a cyclic ring structure containing a sulfonamide. The two additional spaces can be filled with a phenyl ring attached to the central ring.

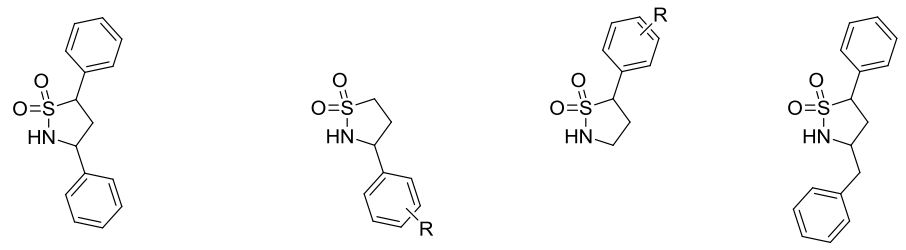

107 **108** **109** **110**

Figure 52: Structure of the proposed compound 107 and the structures of the in literature reported compounds 108, 109 and 110.

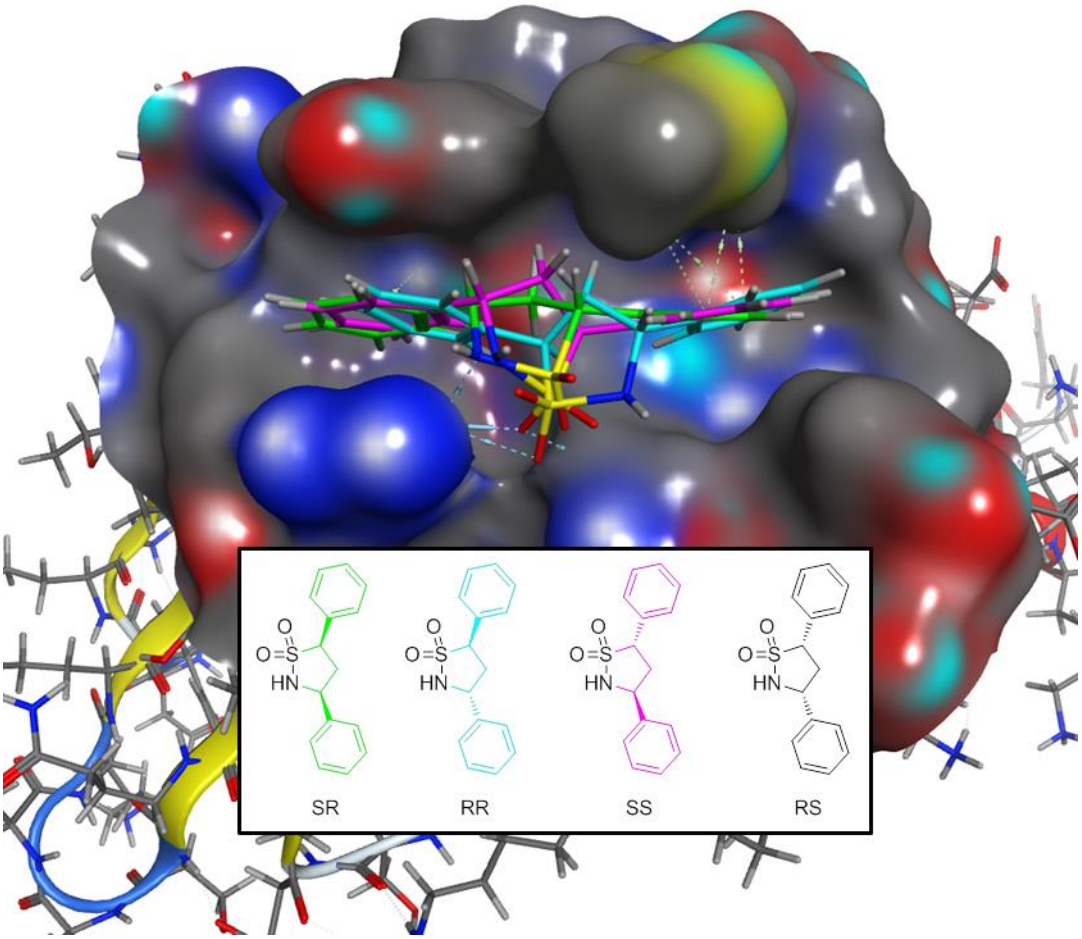

Figure 53: Docking of the four different stereoisomers of 107 in pdb 2HW4. Isomers SR, RR and SS dock well inside the active site, obtaining the configuration as designed with the sulfonamide in close proximity to Arg[78]. Isomer RS did not fit in the protein due to the cis configuration.

Unlike for the 3,5-diphenyl-isothiazolidine-dioxides, the mono-phenyl versions **108** and **109** are known in literature and their synthesis reported.[94] Also, a benzyl decorated alternative, compound **110**, has been reported before.[77] Nevertheless, **107** would be an interesting, and above all, feasible target for synthesis and a promising scaffold for novel bioactive molecules. Alternatively, the phenyl substituents can be replaced by heterocyclic or aliphatic substituents when **107** shows promising activity
In order to design a synthetic procedure to prepare **107**, the reported synthesis of **108** and **109** proved useful. These compounds were prepared by two different synthetic routes disconnecting the centre isothiazolidine 1,1-dioxide either in between the C3 and C4 atom or in between the C5 and N1 atom (see figure 54). Disconnecting in between C3 and C4 of **107** and disconnecting further to sulfonyl chloride **112** and amine **113** leads back to a non-natural amino acid, phenylglycine **114**.[94a] This route allows for a quick optimization program starting from various commercially available sulfonyl chlorides and (un)natural amino acids if the test compound shows inhibitory activity. Alternatively, **107** can be prepared from a Boc protected sulfonamide **116** and epoxide **117**, derived from styrene **118**.[94b] The readily availability of starting materials and the absence of protective groups strongly favors the first synthetic strategy.

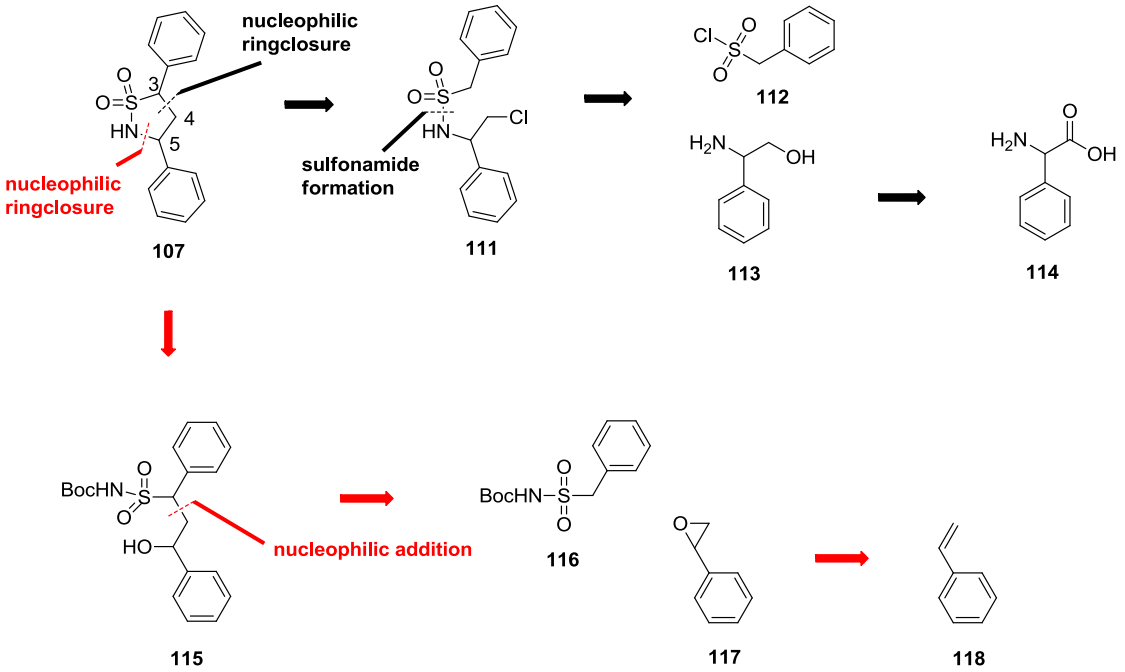

Figure 54: Retrosynthetic analysis for 107. Either a disconnection in between C3 and C4 or in between C5 and N1 will generate a synthetic procedure starting from commercially available starting materials. Favorable is the route starting from amino acid **114**. This route starts with easily available starting materials and does not require the use of protective groups. This route is also more suitable for parallel synthesis if compound **107** is followed up by an optimization program

Commercially available racemic phenyl glycine **114** was treated with an excess of $LiAlH_4$ (see scheme 18). The primary alcohol product was immediately reacted with benzyl sulfonylchloride **112**. Two equivalents of the sulfonyl chloride were used in order to directly obtain the chloride **111** rather than a primary alcohol. A ring closure induced with two equivalents of n-BuLi allowed the isolation of **107** in moderate yield. Care was taken in isolating the two pairs of diastereomers that were formed separately. After the final ring closure four different products are formed when a racemic amino acid starting material **114** is used. The trans-enantiomers were isolated separately from the cis enantiomers (see figure 55).

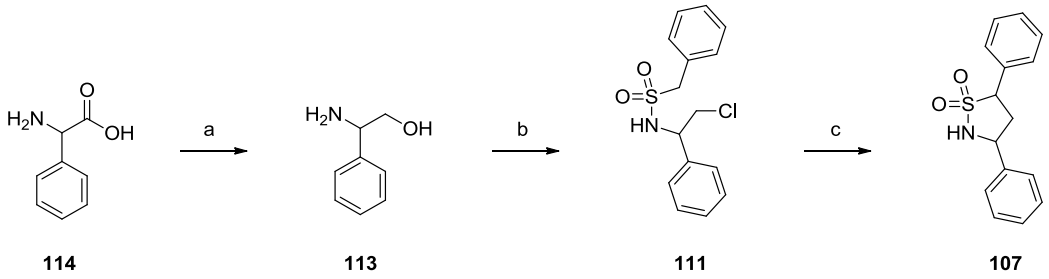

Scheme 18: Synthesis of compound 107. a: $LiAlH_4$, THF, 18h, 0 ^oC - rt **b: 112**, TEA, THF, 8h, 0 ^oC - rt, 68% (over two steps) **c:** diisopropylamine, BuLi, THF, 3h, -70 ºC – 0 ^oC, 64%.

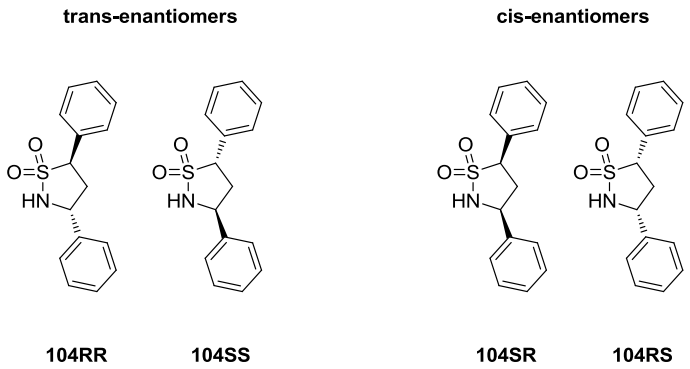

Figure 55: Depiction of all possible stereoisomers of 107. Using ordinary straight fase chromatography the diastereoisomers were obtained separately. The compounds were tested as two sets of enantiomers.

Both enantiomeric mixtures were isolated in pure state and assayed separately for PHP enzyme inhibition. Unfortunately, both compound mixtures failed to show any inhibition at a 100 µM concentration.

Chapter 6: Further Evaluation of the Sulfonamide Imidazoles as PHP Inhibitors

6.1 Introduction

The biochemical screening assay results presented so far are based on the fluorescence assay described in §3.4. The substrate used in this assay is DiFMUP and this phospho-tyrosine mimic cannot be considered a realistic substrate for a phospho-histidine phosphatase. A phospho-histidine containing substrate would be a more realistic probe in a biochemical assay setup. The development of this assay was described in §3.5 and phospho-histidine itself was successfully prepared and used for this assay. The assay is significantly less 'high throughput' but perfectly suitable as a backup assay to validate the results from the fluorescence screening assay. Based on the results of this secondary assay, a subset of compounds was continued and investigated in the Microscale Thermophoresis (nanotemper) binding assay described in §3.6.
The next step is profiling in cellular assay systems. An important requirement for cellular active compounds is good water solubility and cell membrane permeability. This was assayed for the compound selection using a PAMPA type permeability screen as described in §6.4. The cellular assays that were performed are a patch clamp ion channel current experiment with HCT116 colon cancer cells and a scratch type migration assay with MCF-7 breast cancer cells. The results are described in §6.5 and §6.6 respectively. Monitoring the behavior of these compounds inside living cells using fluorescence microscopy is a very attractive alternative technique to use. It will allow pinpointing the location of increased concentrations of fluorescently labeled compound *in vivo*. It can also show the interaction between a labeled inhibitor compound and a labeled receptor protein in live cells. The efforts to obtain a fluorescently labelled imidazole sulfonamide are described in §6.7.
Finally, structural information regarding the interaction between the inhibitors and the enzyme would be a great achievement. Attempts to co-crystallize and soak the developed inhibitors with the PHP enzyme are discussed in §6.8.

The compounds that were selected for further profiling, based on the fluorescent screening assay results, are **53f**, **60c** and **86** (see figure 56). These compounds all display inhibitory activity in the 1-10 µM IC_{50} range. Added for solubility and cell permeability assaying, is the structurally different sulfonyl compound **70a**. This compound displays only minor PHP inhibitory activity but is different in chemotype, since it is lacking the sulfonamide that can lead to poor cell permeability properties.

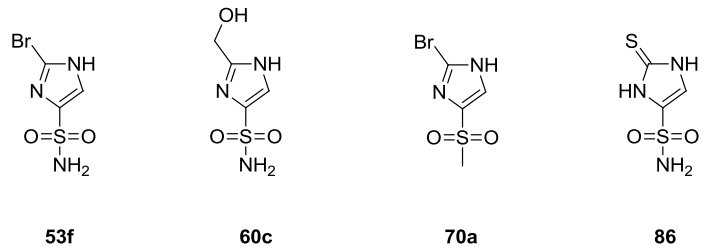

53f **60c** **70a** **86**

Figure 56: Structures of the compounds 53f, 59c, 70a and 86. This set of compounds was selected for further profiling.

6.2 Continuous Coupled Enzyme Assay

The continuous coupled assay that was developed as a control assay (see §3.4) uses phospho-histidine as a substrate and a second enzyme reaction to generate a readout. However, the principle is the same as for the fluorescence screening assay used during the synthesis and testing cycles described in chapter 5. Consequently, the inhibitory results should be in the same range. The compounds **53f**, **60c**, **70a** and **86** were subjected to a full IC_{50} determination. The results are presented in table 7. As expected, the determined IC_{50} values are indeed comparable underlining the robustness of both assay systems. Generally, activity is lower in the coupled assay but clearly within the margin of error. A typical IC_{50} curve is shown in figure 57.

Entry	Activity Fluorescence assay (IC_{50} in µM)	Activity Continuous Coupled assay (IC_{50} in µM)
53f	11.1 ± 5.9	13.6 ± 5.6
60c	9.9 ± 4.0	20.8 ± 9.0
70a	16% inhib. @ 100 µM	0% inhib. @ 100 µM
86	3.1 ± 1.7	6.2 ± 2.0

Table 7: Comparison of the activity determined in both biochemical assay for the selected compounds.

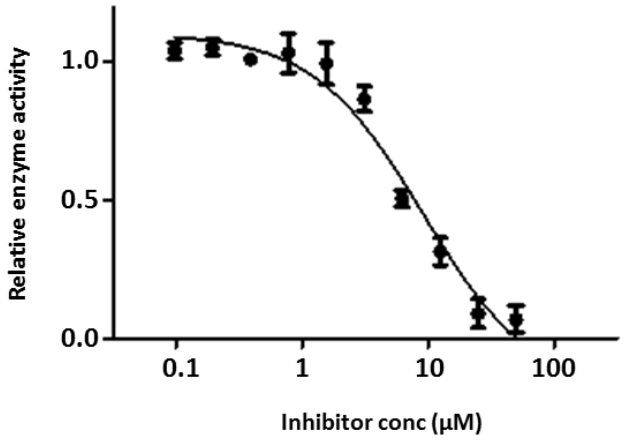

Figure 57: Typical inhibition curve shown for compounds 60c. Figure generated using the software Prism 5.0.

To provide a full perspective of the assay, a complete screen was performed. All compounds that were synthesized in the project were tested at a 100 µM concentration comparing both active and inactive compounds on both assays.
Indeed, no surprises were obtained and compounds that failed to show inhibitory activity in the fluorescence screening assay did not show inhibition in the coupled assay (data not shown).

6.3 Determination of K_d values using Microscale Thermophoresis (MST)

Unlike a biochemical assay, where the substrate conversion is used as readout, a binding assay will give direct information about the interaction between protein and ligand. As described in §3.6, PHP was labelled with fluorescein in order to measure equilibrium binding constants between protein and the inhibitor molecules.

In the selection of compounds used for K_d determination, **70a** was replaced by **53e** (see figure 58). This compound is structurally more similar to the other three imidazole sulfonamides but, completely inactive in both functional assays. This compound serves as a negative control and should not show any binding with the fluorescein labelled PHP protein.

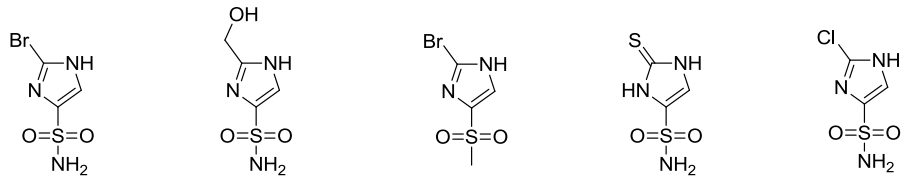

53f **60c** **70a** **86** **53e**

Figure 58: Structures of the compounds 53f, 60c, 86 and 53e. These compounds were selected for MST K_d determination. **70a** was replaced by the structurally more similar but inactive chloride **53e**.

The determined dissociation constants are given in table 8. The K_d values match well to the IC_{50} values generated in the two biochemical functional assays. **60c** displays a somewhat lower binding. Also, for the continuous coupled assay this compound was less active compared to the fluorescence assay. Negative control **53e** clearly underlines the validity of the binding assay showing no effect even at the highest concentration of measurement, being 200 µM.

Entry	Activity Fluorescence assay (IC_{50} in µM)	Binding constant K_d (IC_{50} in µM)
53f	11.1 ± 5.9	12.8 ± 2.0
60c	9.9 ± 4.0	22.3 ± 2.1
86	3.1 ± 1.7	2.0 ± 0.5
53e	0% inhib. @ 100 µM	>200

Table 8: Comparison of the inhibitory activity determined in the fluorescence biochemical assay and the K_d values for the compounds 53f, 60c, 86 and non-active negative control 53e.

6.4 Solubility and Cell Permeability

As mentioned in the introduction of this chapter, solubility and cell permeability for the compounds is essential for obtaining useful data from cellular assays. The intention is to show cellular efficacy, making these parameters essential for forwarding these compounds into more complex assays using living cells. The selected compounds were subjected to measurements determining kinetic solubility and Parallel Artificial Membrane Permeability Assays (PAMPA).[95] The obtained results are outlines in table 9.

Entry	Solubility [µM]	PAMPA [%Flux][a]	cLogP[b]	Sulfonamide pK_a[b]
53f	498.3	5.9	0.12	7.92
60c	482.6	0.6	-1.88	8.64
70a	434.4	110.6	0.70	-
86	498.3	66.5	-0.01	11.74
121	495.3	0.5	-1.03	-
122	418.3	4.9	0.95	-

Table 9: Determination of the kinetic solubility as determined by a direct LCMS based measurement (assay wall: 500 µM) and PAMPA permeability. a: %Flux defined as concentration (test well)/concentration (control well) x 100. Solubility and PAMPA data generated by the Lead Discovery Center, Dortmund**. b:** calculated using the software MarvinSketch 6.0.6.

The kinetic solubility is excellent for all compounds and can be considered higher than the assay maximum of 500 µM. The low molecular weight and high polarity of these compounds assure good water solubility. The passing over a membrane as expressed by %Flux is very low for entries **53f** and **60c**. For these molecules a relatively acidic sulfonamide and an extremely low lipophilicity respectively, negatively influences their ability to passively diffuse through a membrane. This is underlined by entries **70a**, lacking the sulfonamide, and **86**, with a much higher pK_a for the sulfonamide. These compounds display significantly better cell permeability. This clearly sets apart compound **86** as the prime candidate for further investigation.
In an attempt to improve the cell permeability of **60c** the preparation of prodrugs was considered. Decided was to acylate and benzylate the primary hydroxyl group and resubmit these esters for permeability measurements. The compounds were prepared as shown in scheme 19. Hydroxyl precursor **58** was converted into the esters **119** and **120**. Fortunately, acidic removal of the protective groups did not harm the ester functionality and the compounds **121** and **122** were isolated in good yield.
As shown in table 9, addition of a large lipophilic group significantly improved cell permeability for entry **122** compared to **60c**. Addition of a simple acyl group however, did not affect the PAMPA permeability as compound **121** did not display increased membrane passing compared to **60c**.
Compounds **121** and **122** were also tested in the fluorescence biochemical screening assay and were found to be inactive.

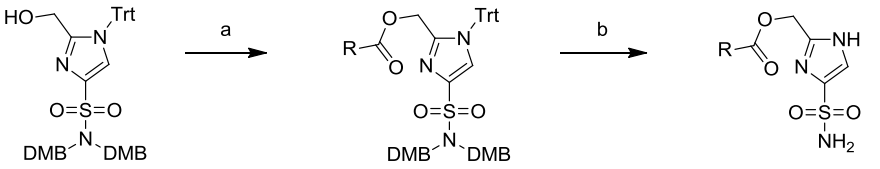

58

119 R = Me
120 R = Ph

121 R = Me
122 R = Ph

Scheme 19: Synthesis of prodrugs 121 and 122. a: pyridine, RCOCl, DCM, 2h, 0 ^{o}C - rt **b:** TFA, TiPS, 18h, rt, 56% and 76% respectively (yield over two steps).

6.5 KCa3.1 Ion Channel Patch Clamp

The experiments described in this paragraph have been performed by Prof. Dr. Frank Wehner (Max Planck Institute, Dortmund)

The potassium channel KCa3.1 is the prime known example where histidine phosphorylation is essential for a physiological event in eukaryotes. This calcium-activated potassium channel is vital in CD4 T cells for maintaining the cell membrane potential relatively negative. This is the driving force for Ca^{2+} influx when required inside the cell upon T cell activation. PHP negatively regulates channel activity through dephosphorylation of His^{358} (see §1.2.2).[35] As mentioned in §1.3.3, PHP activity has also been related to human lung cancer cell migration and invasion.[45] The cells that were used in this study are highly metastatic lung cancer CL1-5 cells. It was suggested that the mechanism involves an effect on cytoskeletal rearrangement but KCa3.1, as a possible target for PHP in this process, was not mentioned.
To investigate if KCa3.1 is involved in cell metastasis, whole cell patch clamp experiments were performed with readily available, highly metastatic, HCT116 colon cancer cells. Upon treatment of the cells with either a KCa3.1 channel activator (DCEBIO, figure 59A) or inhibitor (TRAM-34, figure 59A), a significant difference in current was observed compared to untreated cells (see figure 59B, red trace and green trace respectively compared to the blue trace representing untreated cells). Clearly the ion channel is present and fully functioning in this cell line.
Secondly, the influence of PHP inhibition on the ion channel behavior was investigated. The same experiment was now performed with 10 µM of inhibitor **53f**, **86** or **122** pre-incubated cells. No effect was observed except with inhibitor **86** present. Unexpectedly, the effect of addition of channel activator DCEBIO seems to be impaired by the PHP inhibitor. The experiment was repeated with a concentration of 100 µM (see figure 59C) and indeed the compound significantly inhibited the action of channel activator DCEBIO (red trace). This is different than expected as PHP inhibition was reported in T cells to activate channel flow. A PHP inhibitor would be expected to increase the channel current of untreated cells (blue trace). With the current knowledge this different effect cannot be explained. A direct antagonistic action of the compound on the ion channel is a possible mechanism. To investigate if **86** influences channel activity through a different mechanism the experiment needs to be repeated with PHP siRNA knock-down. This experiment has not been performed yet.

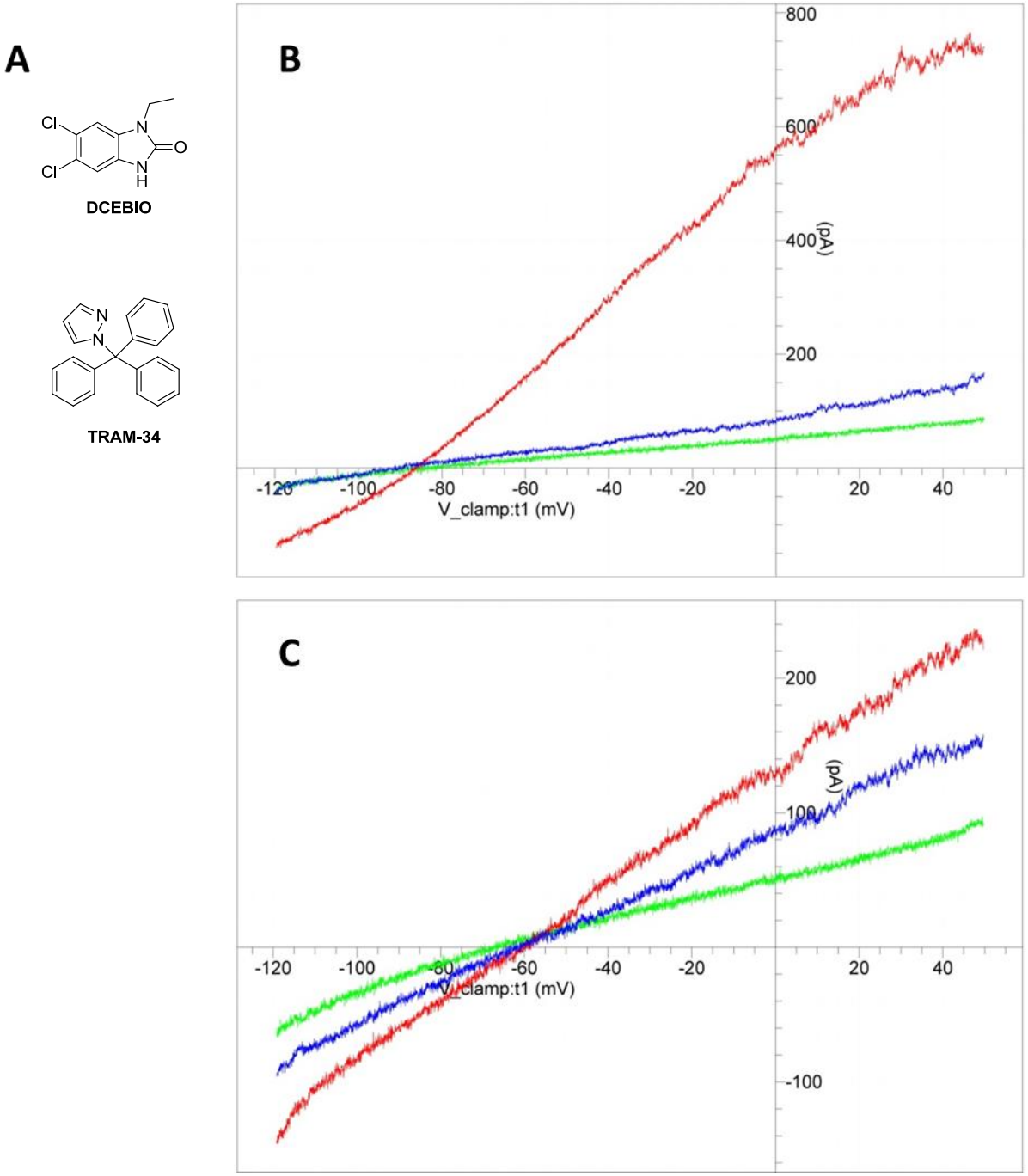

Figure 59: Investigation of the role PHP has in KCa3.1 channel activity in HCT116 colon cancer cells. A: The chemical structures of ion channel activator DCEBIO and channel blocker TRAM-34. **B:** The current-voltage (*i-v*) plot of the HCT116 cells. The effect on channel current at different voltage membrane potential is plotted with the presence of a channel activator DCEBIO (red trace) or channel blocker TRAM-34 (green trace). Untreated cells are represented by the blue trace. **C:** The current-voltage (*i-v*) plot of the HCT116 cells pre-incubated with 100 µM concentration of PHP inhibitor **86**. Again, the effect on channel current at different voltage membrane potential is plotted with the presence of a channel activator DCEBIO (red trace) or channel blocker TRAM-34 (green trace). Untreated **86** pre-incubated cells are represented by the blue trace. Surprisingly, the presence of PHP inhibitor **86** has no effect on the cells except when channel activator DCEBIO is added. Here, the channel remains predominantly in a closed state.

6.6 Wound Healing Scratch Assay

The work described in this paragraph has been performed by Dr. Rosemarie Marchan in the lab of Prof. Dr. med. Jan G. Hengstler (Leibniz Research Centre for Working Environment and Human Factors)

A wound healing scratch assay is a widely used assay testing for the ability of cells to migrate *in vitro* under the influence of chemical compounds or applied genetic changes, e.g. gene knockdown, under carefully chosen conditions.[96] The role of a particular protein in the migration of cells can be studied in detail using this technique. A monolayer of cells is grown on a plate under medium and a scratched opening is created using a pipet tip. The closing of this gap is monitored in time. The increased or decreased rate of closing can be quantified and related to the added chemical (concentration dependent) or genetic change.
The vital role that has been found for PHP in CL1-5 lung cancer cell lines, was also investigated in a wound healing scratch assay as reported by Dacheng and coworkers.[45] In order to investigate PHP through means of chemical inhibition, CL1-5 cells were requested and obtained from Pan-Chyr Yang, Dean and Professor of Medicine at the National Taiwan University College of Medicine. The obtained cells were also subjected to the scratch assay protocol, however growing a monolayer of the CL1-5 cells in our lab proved impossible. A tendency to grow on top of each other rather than creating a monolayer was observed. It was decided to test the PHP inhibitors in MCF-7 breast cancer cells instead. These cells are known to behave well in this type of scratch assay and do express detectable levels of intracellular PHP (data not shown).
The compounds selected for the assay were the same as used for the patch clamp experiments, **53f**, **86** and benzylic prodrug **122**. The compounds were tested at 5 and 10 µM concentration and compared to non-treated cells. Pictures were taken at time points 0,1,2 and 3 with 24 hour increments. The results were disappointing as none of the three compounds showed a significant effect at either 5 or 10 µM concentrations. Increasing the concentration, as was required for the patch clamp experiment, was also no option as cell toxicity was observed for compound **86** at a 10 µM concentration (see figure 60). This is in line with the higher cell permeability that was established for this compound and supports a conclusion that this compound is cytotoxic for MCF-7 cells. Possibly, compounds **53f** and **122** have a similar toxicity but fail to enter the cell. The mechanism to this toxicity is unknown and not necessarily PHP mediated. Also, the outcome of the patch clamp experiments suggests an unexpected pharmacology for **86**. The cytotoxicity might also be an expected effect as sulfonamides like **86** can possess carbonic anhydrase inhibitory activity (see §5.1). Several carbonic anhydrase inhibitors are indeed being evaluated as anti-tumor drugs.[88] Also the role of certain carbonic anhydrases in breast cancer is being investigated.[97] In MCF-7 cells, upregulation of carbonic anhydrase XII by various growth factors has been established.[98]
Besides the PHP knockdown experiments performed in CL1-5 lung cancer cells, siRNA PHP knockdown has been shown to inhibit both cell growth and proliferation in hepatocellular carcinoma (HCC) cell lines.[46] This suggest that also selection of the right cell line is essential for a successful outcome in an experiment to study the effect of PHP inhibition. Additionally, the cytotoxic properties of the PHP inhibitors should be considered as a subject of investigation next to their alleged ability to impair cell migration.

New experiments with different cell lines are currently being considered in order to further study PHP in cells and the cellular effectiveness of the inhibitors. Overexpression of PHP might be required to distinguish the effect of PHP inhibition from compound related side effects. CL1-5 cells do express the enzyme in far higher concentrations compared to other many other cell lines that are more readily available. Additionally, the inhibitory effect of the compounds on carbonic anhydrases needs to be evaluated. This activity can limit the usefulness of these compounds as tools to investigate PHP.

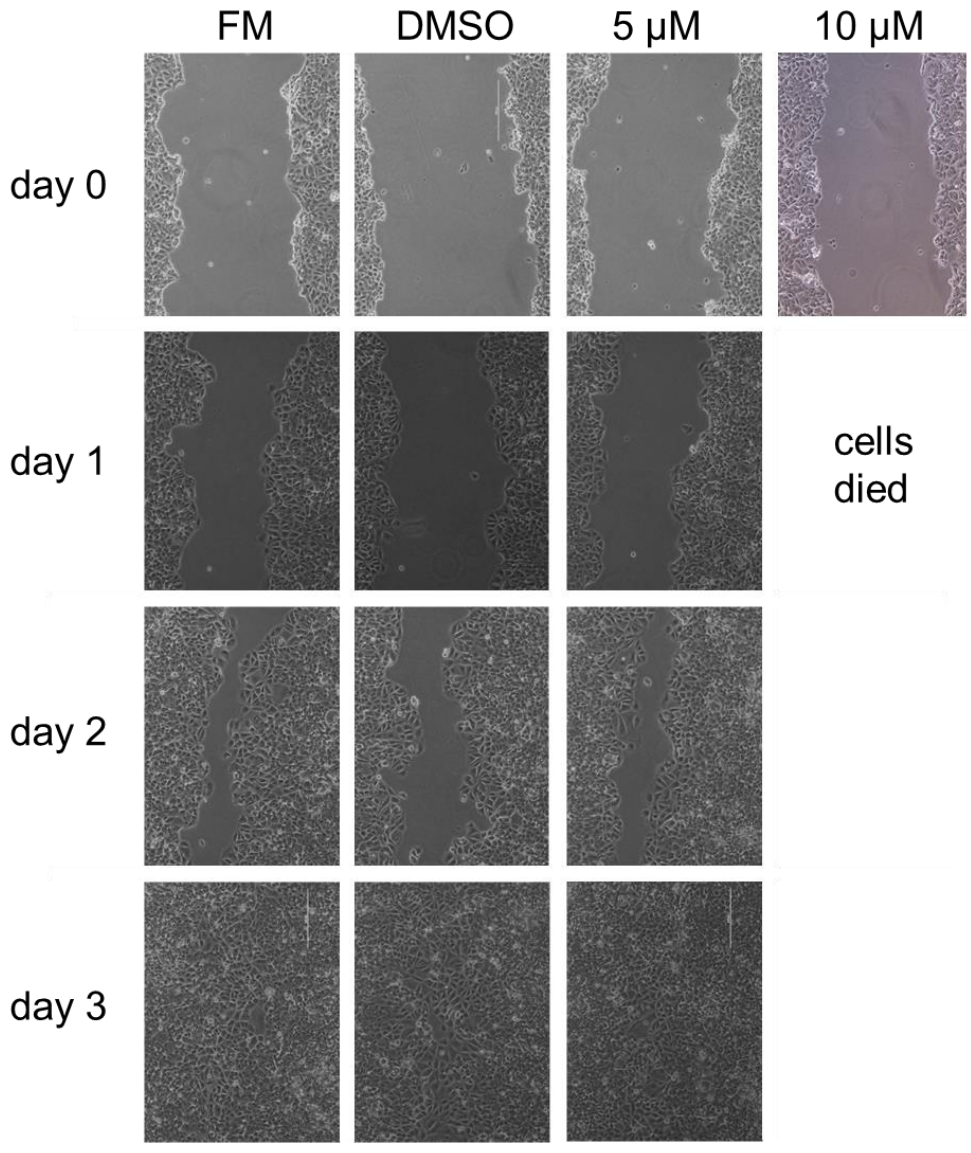

Figure 60: Results for compound 86 in the wound healing scratch assay. The experiment was performed in full media (FM), with DMSO or at a concentration of 5 or 10 µM. At concentrations of 5 and 10 µM the rate of scratch closing was monitored using microscopy in time. At 5 µM concentration the created opening closed just as rapidly as for the untreated and DMSO control experiments indicating no effect at this concentration. Raising the concentration of inhibitor compound **86** to 10 µM resulted in immediate cell death.

6.7 Fluorescence Microscopy

A powerful technique that can yield solid evidence for an interaction between two (bio-)molecules in living cells is Förster (or Fluorescence) Resonance Energy Transfer (FRET). What made this technique possible was the discovery of an entire class of auto-fluorescent proteins, e.g. Green Fluorescent Protein (GFP), found in jellyfish.[99] A protein of interest can be labelled through cloning of the protein gene into an expression vector linking a fluorescent protein to the N- or C-terminal end. This vector can then be transfected into the cell of interest. Energy transfer from one excited fluorophore (donor) to another (acceptor) when in close proximity (10 to 100 Å) leads to an emission of light from the acceptor fluorophore (see figure 61).[100]

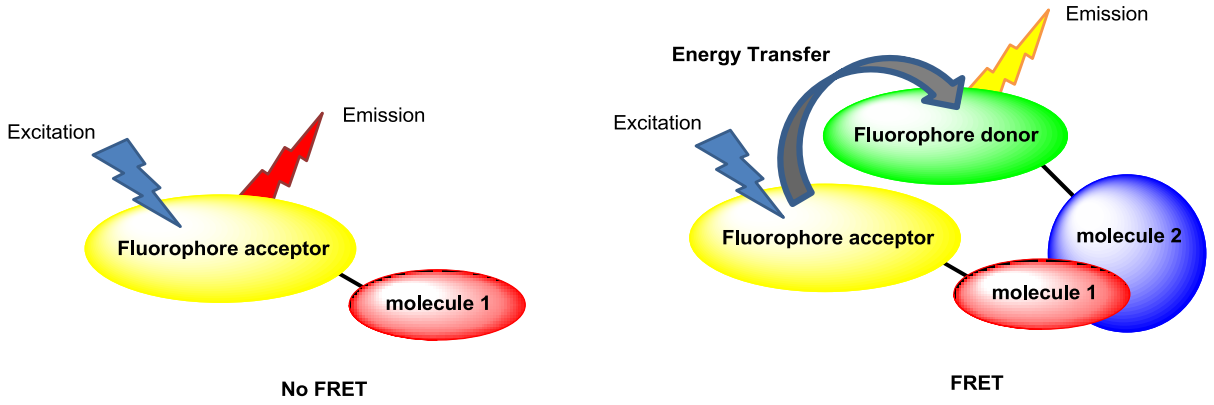

Figure 61: Principle of Förster Resonance Energy Transfer (FRET). Excitation of the fluorophore acceptor leads to energy transfer to the fluorophore donor when in close proximity due to interaction of molecule 1 and 2. The amount of emitted light by the donor is a measure for the interaction of molecule 1 and 2.

Besides an interaction between two biomolecules, interaction between a small molecule inhibitor and a target molecule can also be visualized if the right fluorescently labelled tools can be obtained. Labelling the PHP inhibitor molecule with a fluorescent tag and generating a PHP-fluorescent protein construct can generate an interesting opportunity to study the inhibitor-enzyme interaction in various cellular set-ups.
The spectroscopic properties of the two fluorophores need to be considered in selecting the right labels in order to obtain a workable FRET pair. It is essential that there is sufficient separation in excitation spectra to achieve selective stimulation of the donor fluorophore. Also, an overlap is required (approximately 30%) between the emission spectrum of the donor and the excitation spectrum of the acceptor to obtain efficient energy transfer. Finally, a reasonable separation in emission spectra between donor and acceptor is required to allow independent measurement of the fluorescence of each fluorophore.[101] A good combination of fluorophores for this approach is an mCitrine labelled PHP and the inhibitor molecule labelled with fluorescein derivative TAMRA (see figure 62). In this combination all requirements are met.

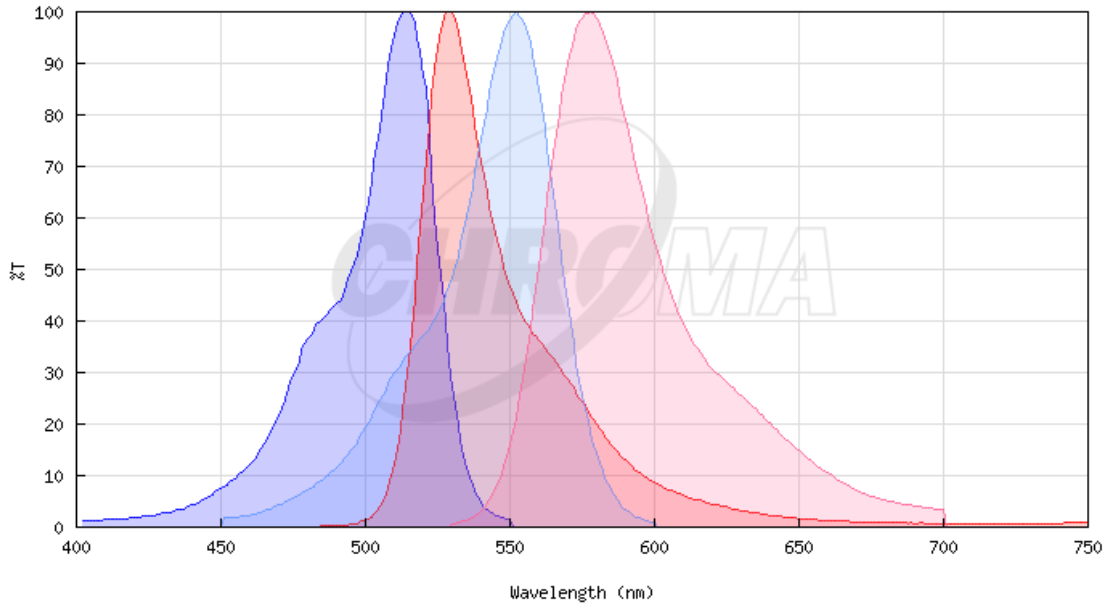

Figure 62: Excitation and emission spectra from mCitrine and TAMRA. blue: mCitrine excitation spectrum; **red:** mCitrine emission spectrum; **light blue:** TAMRA excitation spectrum; **light red:** TAMRA emission spectrum. Generated online through www.chroma.com

Besides FRET there is the possibility to use Fluorescence Lifetime Imaging or FLIM.[102] With this technique the unique properties of either the fluorophore donor or acceptor is being used. A fluorophore is not only characterized by its excitation and emission spectrum, but also by its unique lifetime. This lifetime is defined as the average time that a fluorophore remains in an excited state before returning to the ground state. FLIM does not depend on changes in fluorophore molecule concentration, excitation intensity and other factors that limit intensity-based measurements. The fluorescence lifetime is influenced by changes in the cellular environment including the occurrence of FRET, which shortens the excited state lifetime. Also, the use of FLIM allows the monitoring of intracellular events at very high resolution, allowing accurate pinpointing of the event.[103] Combination of FRET and FLIM data provides direct evidence of interactions between labelled molecules. By measuring the donor lifetime in the presence and the absence of acceptor it is possible to accurately calculate the distance between the donor- and acceptor-labeled molecules.[104]

PHP was N- and C-terminal labelled with mCitrine using standard cloning techniques. TAMRA is a suitable label for a small molecule since it is commercially available as N-hydroxysuccinimide ester and is superior to many other fluorescent labels regarding loss of fluorescence due to bleeding during experiments.[105]
Adding a fluorescent label to the imidazole sulfonamide PHP inhibitors is challenging. Trivial from a synthetic point of view, but analyzing the SAR that was established around the imidazole sulfonamides, showed that only minor structural modifications are allowed around the core without significant loss of activity. Adding a large additional molecule in the form of a fluorophore is likely to disrupt the binding to PHP. **60c** did show some activity (37% at 100 µM) and attaching the TAMRA through a linker would result in target molecule **123** (see figure 63).

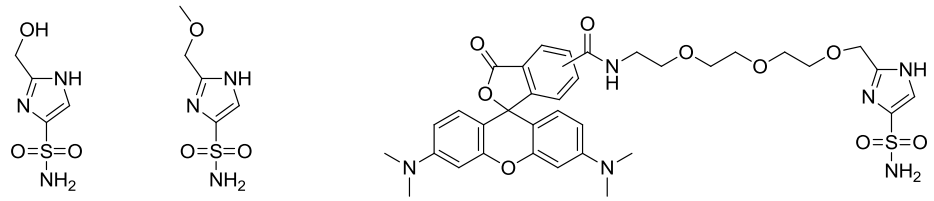

53f **60c** **123**

Figure 63: Structures of the compounds 53f, 60c and TAMRA labeled target molecule 123. Compound **60c** forms a small opening in the SAR around **53f**. The oxygen of **53f** is the only site where a linker can be attached without losing all activity.

For the TAMRA labelled sulfonamide imidazole compound **123**, synthesis started with triethylene glycol **124** (see scheme 20). Converting one alcohol into an azide was achieved by applying methanesulfonyl chloride and secondly, sodium azide. From **125**, the other terminal alcohol was activated as a tosylate and used to alkylate synthetic intermediate **58** obtaining azide **127**. To convert the terminal azide in a primary amine, triphenylphosphine was used and attaching the TAMRA fluorophore was achieved through coupling with the commercially available OSu ester. The protective groups were removed using TFA and preparative HPLC afforded target molecule **123** in 10% yield from **127**. The low yield was caused by significant cleavage of the first ether bond from the linker under the acidic protective group removal conditions. During purification, a large amount of **53f** was observed indicating acid catalyzed degradation of the product.

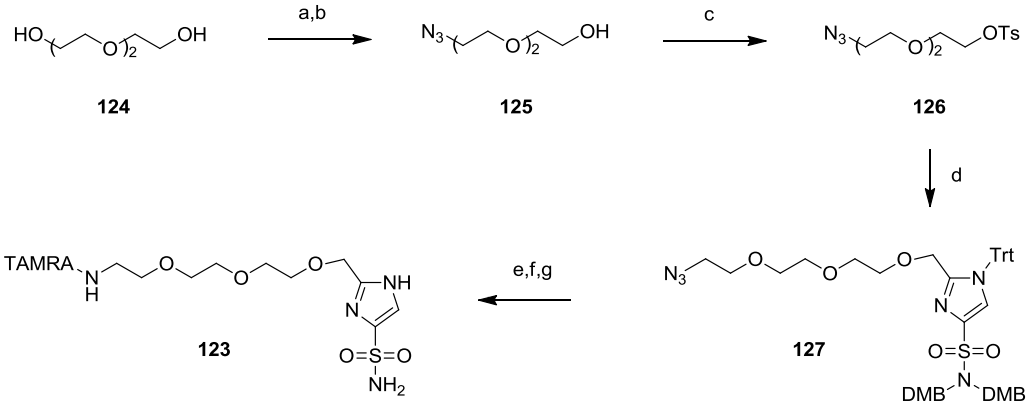

124 **125** **126** **127** **123**

Scheme 20: Synthesis of fluorescently labelled imidazole sulfonamide 123. a: $MeSO_2Cl$, TEA, THF, 18h, 0 ºC - rt, **b:** NaN_3, EtOH, 6h, 80 ºC, 45% over two steps **c:** TsCl, pyridine, DCM, 18h, rt, 66% **d: 58**, NaH, DMF, 18h, rt, 41% **e:** PPh_3, H_2O, THF, 24h, rt **f:** TAMRA-OSu, TEA, DMF, 18h, rt **g:** TiPS, H_2O, TFA, 2h, rt, 10% over three steps .

The labelled PHP was obtained through cloning of the PHP gene into two mCitrine PET vectors attaching the fluorescent label at both terminal ends. This work was performed by the Dortmund Protein Facility.[106] The cellular experiments, transfecting the labelled enzyme into CL1-5 cells and monitoring FRET and/or FLIM upon addition of compound **123**, has not been performed yet.

6.8 X-ray Co-Crystallization and Soaking

The work described in this paragraph has been performed together with Arthur Porfetye under supervision of Dr. Ingrid Vetter.

The successful crystallization of the wild type PHP in-house initiated trials for co-crystallography and soaking of the identified inhibitors. However, despite extensive screening of conditions no structure was obtained showing the inhibitors bound in the catalytic site. What was observed in the X-ray structure was an electron density in the active site that can be assigned with high likelihood to a sulfate ion. All conditions that were used for successful PHP crystal formation contain concentrations of sulfate ions in excess of 1.5 molar.
Close examination of the X-ray structures that were obtained in-house revealed a network of hydrogen bonding to this sulfate ion from catalytically essential amino acids like His^{53} and Lys^{21} (see figure 64). The adjacent PHP molecule in the tightly packed matrix revealed a glutamine residue (Gln^{84}) making contact with the sulfate. This renders the sulfate essential in forming important contacts from one PHP molecule to another stabilizing the protein matrix. This interaction can be considered to be essential for obtaining crystals that diffract well. Competition between the inhibitors and the excessively high sulfate concentration will render attempts to obtain a co-crystal nearly impossible. Also soaking did not result in a replacement of the sulfate by inhibitor underlining the sulfate as a key element of the crystal matrix.

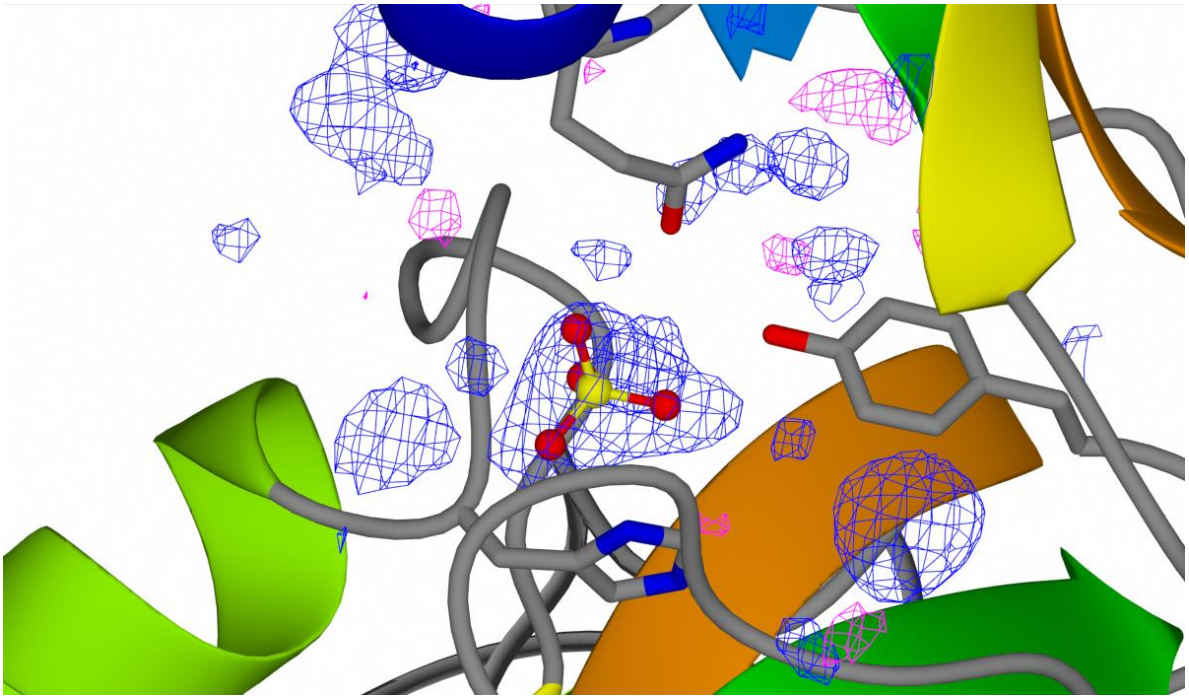

Figure 64: The importance of a conserved sulfate ion in the X-ray matrix. The electron density found in the active site matches a sulfate ion. Besides hydrogen bonds between the sulfate and the protein catalytic cavity, an additional interaction with Gln^{84} from an adjacent PHP molecule is observed. This interaction shows that the sulfate plays an essential role in the protein stacking of the X-ray matrix. This explains why a high concentration of sulfate is so important for obtaining crystals.

Chapter 7: Peptide Pull-down Probes and Phospho-histidine Peptides; in Search of Histone H4 Phospho-histidine Interacting Partners

7.1 Introduction

Building block **7** was designed as a tool that can be incorporated into different peptides. Depending on the chosen amino acid sequence, these peptides can be used to study different aspects of histidine phosphorylation. Besides the attempts to create PHP inhibitor peptides as described in chapter 4, the sulfonamide imidazole mimic of phospho-histidine can be incorporated into peptides that are designed as pull-down probes. Such tools are then used to extract previously unidentified phospho-histidine interacting partners out of various cell lysates. Clearly more important in this set-up is a genuine phospho-histidine mimic. The building block **128** (as depicted in figure 65) would be required and peptide synthesis and protective group removal would result in a peptide **129** carrying the desired phospho-histidine mimic. This non-hydrolysable phosphonate building block **128** was prepared previously in our group and has already been used successfully in raising antibodies that recognize native phospho-histidine peptides as represented by **130**.[56]

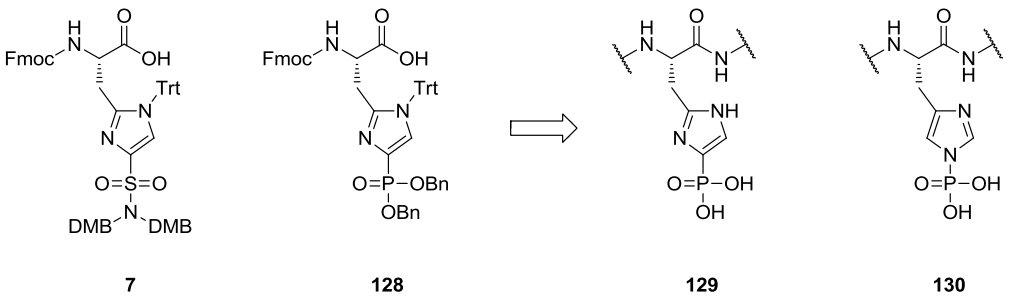

Figure 65: The structures of previously described building block 7, phospho-histidine mimic building block 128 and its peptide incorporated form 129, and a true phospho-histidine 130 as topic of investigation.

The days when histones were seen as proteins used just for storage of DNA are far behind us. Histones and their post-translational modifications are now fully recognized as integral parts of the genetic information stored in a cell nucleus.[6a] As mentioned in §1.2.2, histone H4 is known to be phosphorylated on two histidine residues, His[18] and His[75]. These PTMs were discovered a long time ago but did not receive the same attention dedicated to other histone PTMs like acetylation, methylation and O-phosphorylation.[6b] Therefore, the physiological function and importance remains to be discovered. Also here, the proper tools are essential for successful investigation of N-phosphorylation.[107]
It has been shown that O-phosphorylation on histones is an essential part of DNA repair and transcription regulation.[108] Additionally, a phospho-serine or phospho-threonine can directly influence the activity of other PTM applying enzymes, e.g. Histone Acetyl Transferase (HAT) on adjacent residues.[109] The phosphorylation of histones can also serve for the generation of docking sites for proteins involved in DNA expression like transcription factors.[110] In this line it is easily hypothesized that the N-phosphorylation on histone H4 His[18] can serve a similar purpose.

In investigating this hypothesis, the identification of interacting partners for histone H4 with the phospho-histidine of interest is essential. Two pull-down probes, peptides with building blocks **7** and **128** incorporated, were designed and prepared. These peptides were deployed to identify proteins from various cell lysate mixtures. To eliminate false positive protein hits, a negative control, an analogous peptide with non-modified histidine, was prepared as well. This work is described in §7.2.
Alternatively, the role of Histone H4 His^{18} phosphorylation was studied in an *in vitro* set up enzyme assay. The rate of lysine acetylation or methylation by either HAT or histone H4 Lys^{20} specific lysine methylase Suv420h1 is measured on a His^{18} phosphorylated peptide and compared to the non-phosphorylated peptide counterpart. This work is described in §7.3.

7.2 Preparation and Evaluation of Sulfonamide and Phosphonate Containing Pull-down Probes 131 and 132

The design of the pull-down probe peptides is based on 20 amino acids corresponding with AAs 9-28 from histone H4 (indicated in red in figure 66). Besides the two phospho-histidine mimics, replacing His^{18}, a desthiobiotin attached through a linker was added in the design. This moiety will allow pulling the construct out of a cell lysate mixture through the use of streptavidin on magnetic beads.[111] To prevent the linker and desthiobiotin from interfering with the protein recognition, it is attached to an additional lysine at the C terminal end of the peptide. Finally, a glycine with amide end is added in the design for synthetic purposes preventing problems with detaching the finished peptide from the resin. The Rink Amide (RAM) Tentagel resin was selected as it is a suitable resin for a challenging SPPS campaign. Peptides **131** and **132** are intended to solely identify proteins that interact with a native phospho-histidine. This requires a control probe **133** that contains a normal histidine to identify proteins that bind to other parts of the peptide besides the phospho-histidine mimic. These proteins can then be excluded from a list of hits (see figure 67 for a detailed description of the experiment).

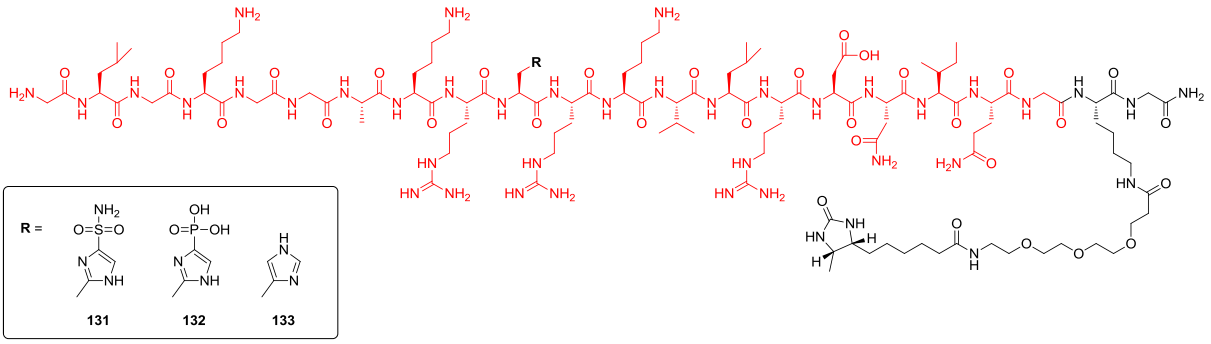

Figure 66: The structures of pull-down probes 131 and 132, and control peptide 133. In red are the amino acids derived from histone H4 (AAs 9-28). Probe **133** bears a normal histidine and serves as a negative control to eliminate false positive hits.

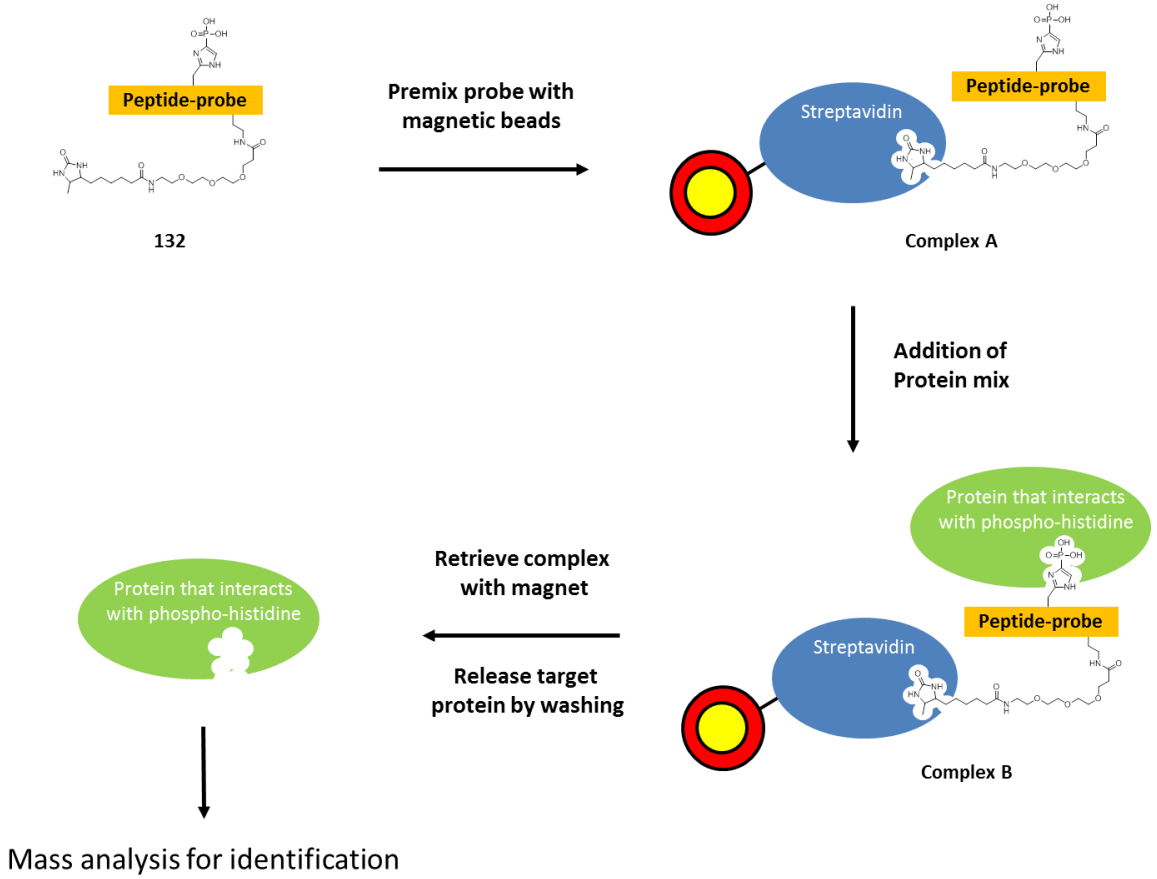

Figure 67: Principe of the pull-down experiment as exemplified with probe 132. Premixing probe **132** with streptavidic coated magnetic beads gives a complex (A) that can bind to a protein that interacts with phospho-histidine. Addition of a cell lysate protein mixture will lead to complex B that can be retrieved by using a magnet. Washing will release the target protein that can be identified by mass analysis. Any protein that is identified by probe **131** or **132** and not by control probe **133** interacts with the phospho-histidine mimic. This identified protein is worth further investigation.

Before the synthesis of the probes on the resin could begin, the desthiobiotin linker attached to Fmoc protected lysine was prepared. Synthesis of building block **134** is described in scheme 21. Starting from triethylene glycol **124** a tert-butylester was introduced by 1,4-addition to tert-butylacrylate. Conversion of the second terminal alcohol into an azide gave **136** in good yield. The azide was reduced using PPh_3 and the desthiobiotin was attached. **137** was coupled to an Fmoc protected lysine through the succinimide activated carboxylic acid **138** obtaining building block **134**.
For the SPPS a Tentagel RAM resin was selected. These low loading (0.24 mmol/g) resins are suited for complex peptide synthesis. After loading of the resin with Fmoc-glycine and Fmoc deprotection, building block **134** was coupled to the functionalized resin **139** using standard HBTU coupling conditions (see scheme 22). Unfortunately, coupling to the resin was unsuccessful. A test cleavage of **140** failed to show the Fmoc protected dipeptide in analysis. Also, an Fmoc protected glycine was not found indicated that the coupling reaction of **134** with **139** failed. Coupling with an alloc protected Fmoc lysine towards **141** was successful showing that the biotin linker of **134** interfered with peptide coupling. The alloc of the obtained **141** can be removed selectively and this allows for attachment of the desthiobiotin linker at a later stage.

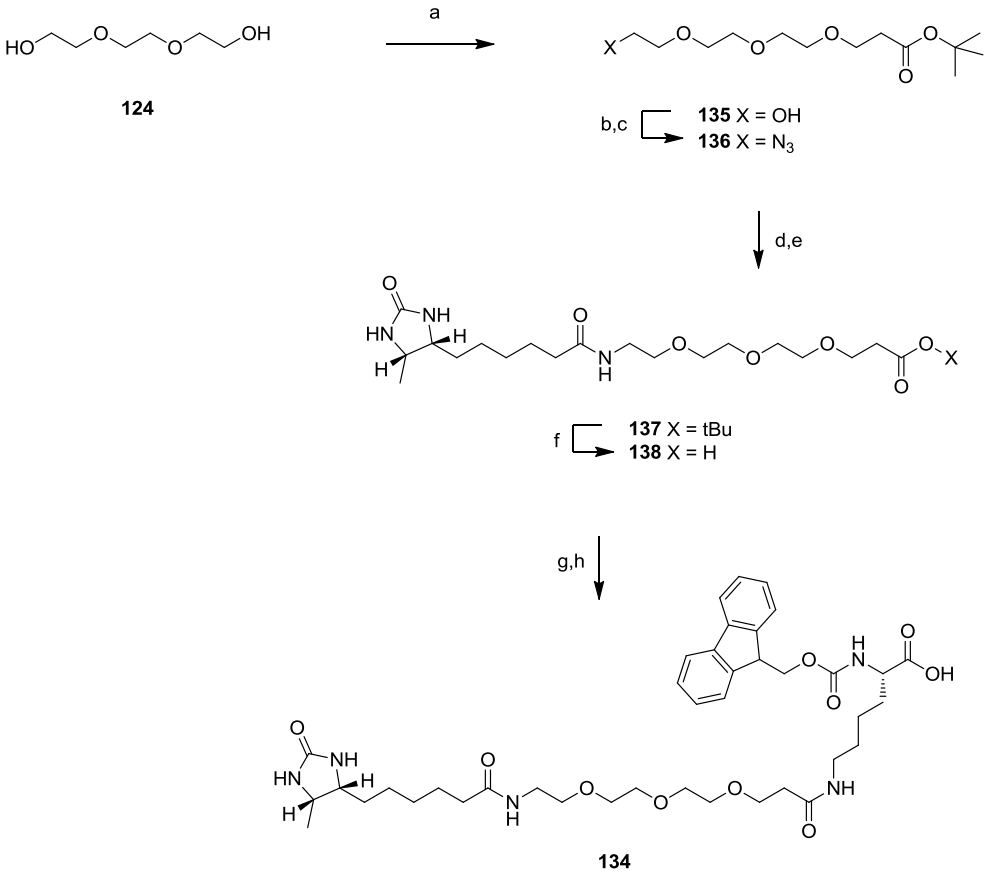

Scheme 21: Synthesis of building block 134. a: t-butyl acrylate, Na, THF, 18h, rt, 29% **b:** MsCl, TEA, DCM, 4h, 0 °C - rt **c:** NaN_3, DMF, 18h, 60 ºC, 87% over two steps **d:** PPh_3, dioxane/H_2O, 18h, rt **e:** desthiobiotin, EDC.HCl, DMAP, DMF, 18, rt, 43% over two steps **f:** TFA, DCE, 30min, rt **g:** N-hydroxysuccinimide, EDC.HCl, DCM, 18h, 0 ºC - 25 ºC **h:** Fmoc-lysine, dioxane/$NaHCO_3$(aq), 3h, 0 ºC - rt, 31% over three steps.

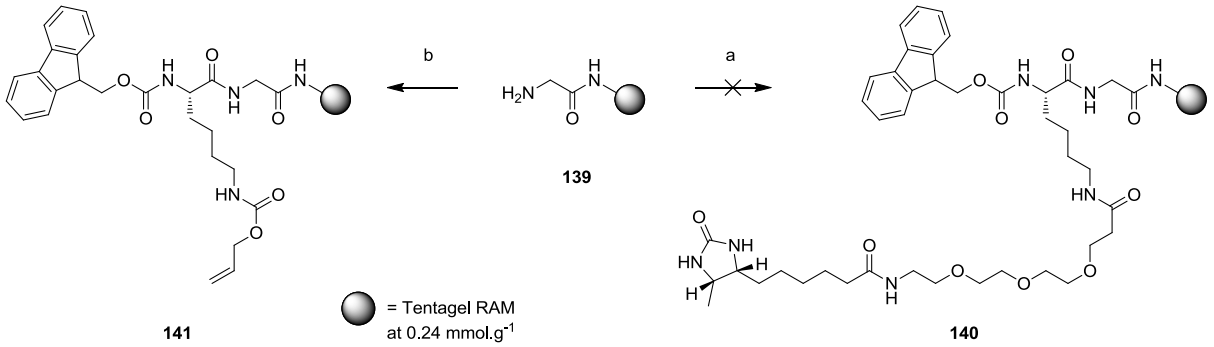

Scheme 22: Initiation of peptide synthesis on the resin. a: 134, HOAt, HATU, DiPEA, DMF, 3h, rt (coupling performed 2x) **b:** Fmoc-allyl lysine, HOAt, HATU, DiPEA, DMF, 2h, rt (coupling performed 2x).

The three peptides were synthesized, starting from **141** using SPPS and ten more amino acids were coupled using an automated peptide synthesizer (see scheme 23). Before manual coupling of the building blocks, the resin material was split in three batches. Besides coupling of the two building blocks, a normal Fmoc histidine was attached for the synthesis of peptide **133**. The three peptides were completed separately and for the final amino acid a Boc protected glycine was used. The alloc from the lysine was removed using $Pd(PPh_3)_4$ and the desthiobiotin linker was attached using carboxylic acid **138** with HATU as coupling reagent. In this fashion, all three peptides **142a-c** were prepared. The peptides were cleaved from the resin and deprotected in one step using TFA. Peptides, **131**, **132** and **133** were purified using preparative HPLC and isolated in 22 %, 20 % and 17 % overall yield respectively.

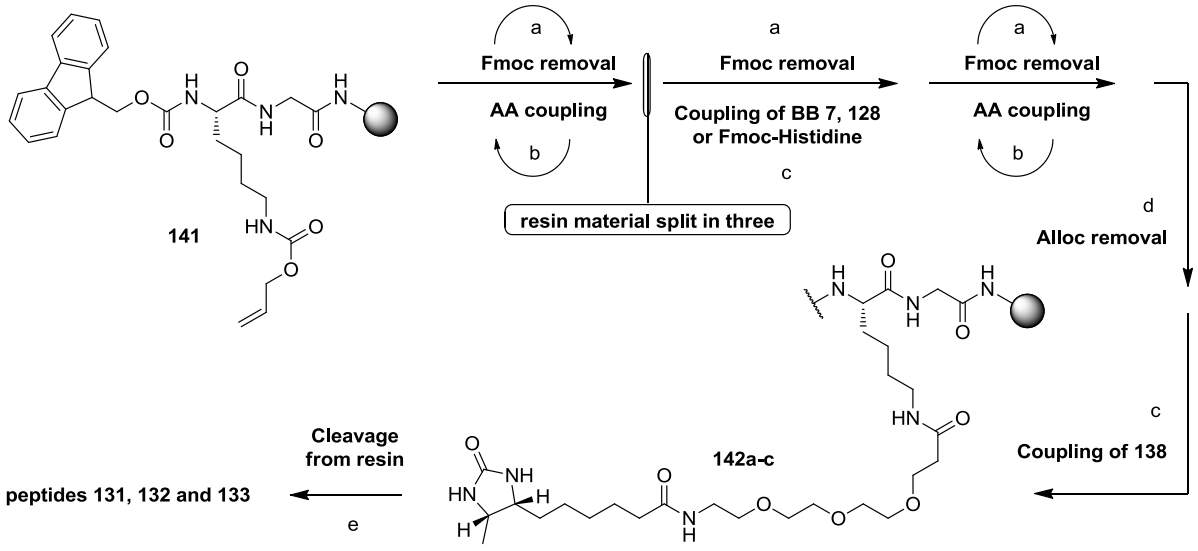

Scheme 23: Synthesis of peptides 131, 132 and 133. a: piperidine, DMF, 10 min, rt (performed 3x) **b:** Fmoc-AA, HOAt, HATU, DiPEA, DMF, 1h, rt (coupling performed 2x) **c: 7** or **131** or Fmoc-histidine, HOAt, HATU, DiPEA, DMF, 1h, rt (coupling performed 2x) **d:** $Pd(PPh_3)_4$, DMF, 2h, rt (performed 2x) **e:** TFA, H_2O, TiPS, 1h, rt (performed 3x).

The peptides were used in pull-down experiments performed in the lab of Prof. Dr. Robert Schneider at the Max-Planck-Institute of Immunobiology Freiburg. For these experiments Hela cell nuclear extracts were used. These cells are easy to grow and a large amount of nuclear extract can be obtained. The potential interacting partners are supposed to reside in the nucleus and discarding the cytosolic proteins reduces the chance of obtaining false positives. Unfortunately, comparing the results from the control peptide equipped with a natural imidazole with both modified histidine peptides, did not result in the identification of proteins that interact with a phospho-histidine. It can be hypothesized that the 20 amino acid peptide does not mimic the tertiary structure of the 102 amino acid histone H4 properly. Alternatively, the two mimics might simply fail to be a good mimic for the native phospho-histidine. However, building block **128** has been used successfully to generate antibodies recognizing the native phospho-histidine. These antibodies can be used as a positive control but, this control experiment has not been performed yet.

7.3 Preparation and Evaluation of Histone H4 Derived Peptides 143 and 144

The peptidic fragment of histone H4 that contains His^{18} is rich in lysines (containing Lys^5, Lys^8, Lys^{12}, Lys^{16} and Lys^{20}) that are targeted by HATs for acetylation and methyl transferases (MTs) for methylation.[112] This modification releases the attached DNA from the histone. If the His^{18} phospho-histidine is influencing HAT activity, the rate of lysine acetylation should be affected by offering a phosphorylated peptide (**144**, figure 68) to a HAT and compare it with a non-phosphorylated peptide (**143**, figure 68). These peptides need to be prepared synthetically through SPPS. Phospho-peptide **144** is prepared from **143** through chemical phosphorylation. As previously demonstrated in §3.5, chemical phosphorylation of peptides with potassium phosphoramidate (PPA) is a powerful procedure for obtaining chemically pure phospho-histidine peptides.
The experiment was performed in the presence of ^{14}C-labelled acetyl-CoA. The relative amount of incorporated radioactivity is a measure for the amount of acetylation and allows for acetylation reaction rate determination. This experiment was also performed with recombinant human lysine methylase Suv420h1. Here, the influence of His^{18} phosphorylation on lysine methylation is investigated.

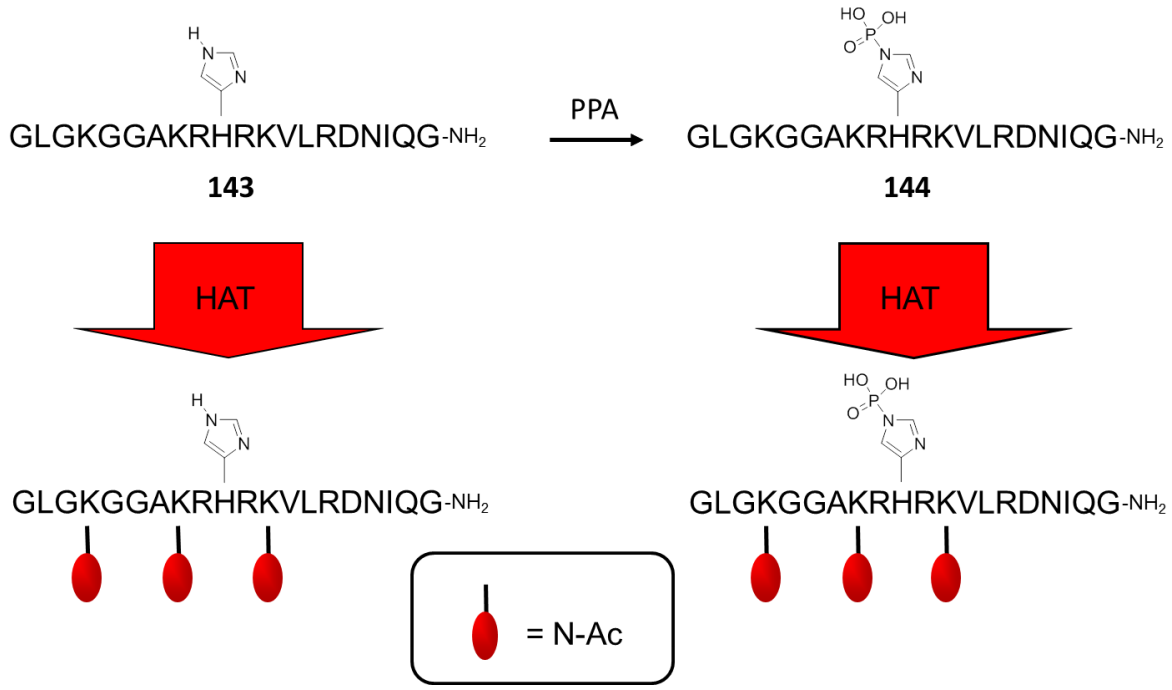

Figure 68: The principle of probing the influence of the N-phosphorylation of histone H4 on His^{18}. By comparing the rate of peptide acetylation by human Histone Acetyl Transferase (HAT) with (peptide **144**) and without (peptide **143**) the presence of the phosphate on His^{18}, the influence of N-phosphorylation of histone H4 is assayed.

Again the amino acids 9-28 from the histone H4 were chosen and phospho-histidine peptide **144** is obtained by chemical phosphorylation of **143**. For analytical purposes a strong UV absorbing 4-nitroaniline, attached to glutamic acid 26, is incorporated in the design (see figure 69 for the detailed structure of the peptides).

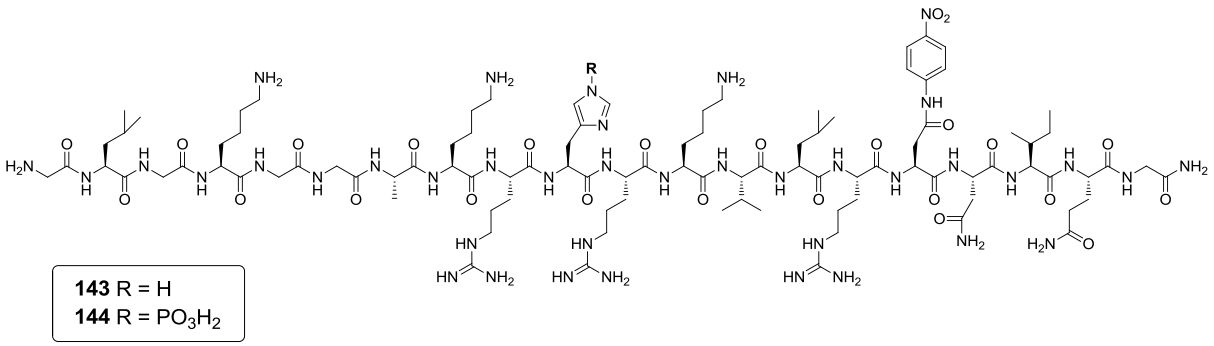

Figure 69: The structures of peptides 143 and 144. Peptide **143** is based on the amino acids 9-28 from histone H4. Glu[26] is equipped with a 4-nitroaniline for analytical purposes. Chemical phosphorylation of **143** on His[18] gives access to peptide **144**.

Peptide **143** was synthesized using automated SPPS on a Tentagel glycine preloaded resin (0.25 mmol/g). The synthesis was performed in a similar fashion as was described for peptides **131**-**133** (scheme 23). The Fmoc protected 4-nitroaniline glutamic acid **145** was prepared starting from commercially available Boc/tertbutyl protected glutamic acid **146** (see scheme 24). Attachment of the 4-nitroaniline was achieved through the activation of the carboxylic acid using HOAT. The Boc and tertbutyl protective groups from **147** were removed using strong acid and the Fmoc protective group was attached to obtain the required building block **145** in 40 % overall yield.

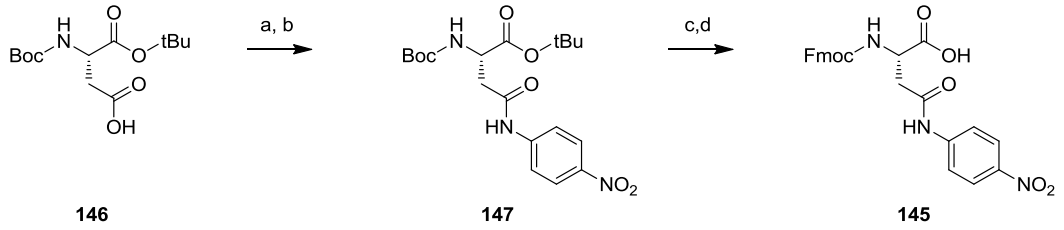

Scheme 24: Synthesis of building block 152. a: HOAt, EDC.HCl, DCM, 18h, 0 ^{o}C - rt **b:** 4-nitroaniline, DBU, DCM, 18h, 0 ^{o}C – 35 ºC, 68% over two steps **c:** TFA, H_2O, DCM, 4h, rt **d:** Fmoc-OSu, $NaHCO_3$, dioxane/H_2O, 18h, 0 ^{o}C - rt, 57% yield over two steps.

Phosphorylation of peptide **143** with potassium phosphoramidate followed the familiar pattern that is always observed for chemical histidine phosphorylation.[66] Rapid formation of the 1- and 1,3-diphosphate isomer, **148** and **149** respectively, was initially obtained (see figure 70). Upon standing the 3-isomer, the desired mono phospho-peptide **144**, became dominant due to the instable nature of the 1-position isomer **148**. After 48 hours, peptide **144** is the main component and purification using a Source 15S cation exchange column was performed. An increasing gradient of NH_4HCO_3 salt solution was used to separate the components. A second run was required to obtain chemically pure material (purity >95%).

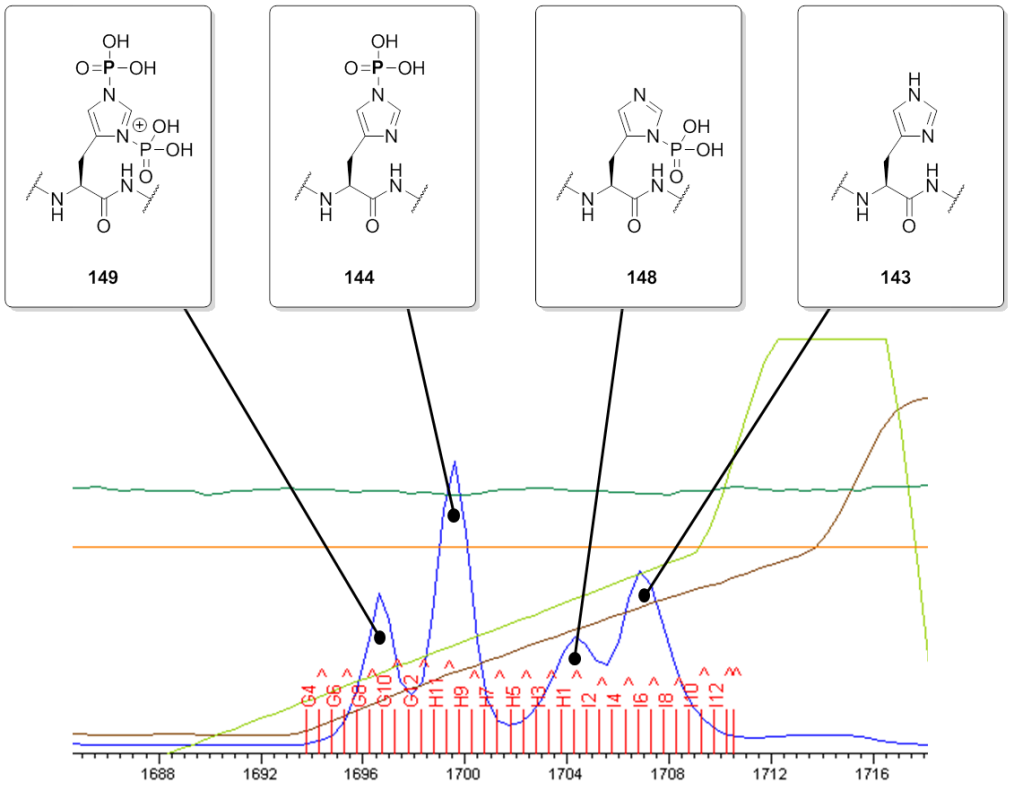

Figure 70: Purification of phospho-histidine peptide 144. The incubation of **143** with potassium phosphoramidate generates three products; the quickly formed 1-isomer **148** and 1,3-isomer **149**. Upon standing the more stable 3-isomer **144** becomes predominant. **144** was purified using a Source 15S cation exchange column and a NH_4HCO_3(aq) gradient to elute the peptide.

The biochemical experiments, investigating the influence of phosphorylation of His^{18} on HAT and Suv420h1 activity, were also performed in the lab of Prof. Dr. Robert Schneider at the Max-Planck-Institute of Immunobiology Freiburg. For the HAT activity, cell extracts were used and Suv420h1 was obtained from a commercial recombinant source. The AcCoA and SAM cofactors are radioactively labeled allowing the quantification of lysine modification. Again, for both the HAT and HMT assays there was no significant effect comparing the His^{18} phosphorylated peptide with the control non-modified histidine peptide. For the HAT assay, it can be proposed that the possible effect is diluted, since there are multiple targeted lysines in the peptide masking the impact. Potentially all lysines in the peptide are targets for the enzyme and a smaller peptide incorporating a single lysine close to the His^{18}, e.g. only Lys^{20}, would be a better substrate to investigate the effect of histidine phosphorylation on HAT. Alternatively it can again be proposed to use the complete histone H4 for this study in order to obtain the entire tertiary protein structure as for the pull-down experiments. However, obtaining such a selectively phosphorylated protein is not trivial. Other than for the HAT activity, the Suv420h1 is specific for Lys^{20} and also here no alteration in lysine methylation was observed with or without the phosphate present on His^{18}.

Chapter 8: Concluding Remarks and Future Prospects

The systematic unraveling of the secrets of N-phosphorylation has only recently begun. It still remains to be seen if it will be found to be just as important as O-phosphorylation. Clear examples of vital roles for N-phosphorylation are still scarce. Essential for revealing more N-phosphorylation driven processes is the development of the right tools to identify N-phosphorylation events *in vitro* and *in vivo*. Antibodies that can recognize phospho-histidine have only recently been reported and are likely to boost the research in this field in the next coming years.[25, 56] Also, inhibitors for the kinases and phosphatases involved in N-phosphorylation can improve our understanding of the role of these enzymes. Besides using these compounds as tools to investigate the role of an enzyme, there might be opportunities to further develop them as therapeutics for various illnesses. The kinases involved are known to be promiscuous and do not limit themselves to N-phosphorylation alone. Many enzymes that are known to be out there have not been isolated and characterized yet. For now, Phospho-histidine Phosphatase (PHP) remains the only dedicated N-phosphorylation related enzyme.

The assays described in this thesis, probing PHP phosphatase activity, are the first continuous assays for this enzyme to be reported. Methods that were used so far required a purification step before determination of phosphate release.[40, 49-50] The validation that was performed on these novel assays, the hits that were identified and the reproducibility underline the value for further research in this field.

Synthesis of building block **7**, an imidazole sulfonamide based phospho-histidine mimic, proved viable and two peptide molecules, designed as PHP inhibitors, were prepared. Unfortunately, these peptides failed to inhibit the enzyme. More successful was the approach of using small molecules based on the same imidazole sulfonamide feature. Figure 71A shows the SAR that was established around the imidazole sulfonamide core. Initially, optimization focused on the imidazole 2-position. Here, significant steepness in SAR was found and various substituents showed activity in the range of 5-12 µM. Halogens I (compound **53b**, 6.2 ± 2.5 µM) and Br (**53f**, 11.1 ± 5.9 µM) were identified (see figure 71B). A smaller halogen like a Cl or only hydrogen showed no inhibitory activity at 100 µM. Larger 2-position substituents like phenyl, furan or benzyl failed to show significant inhibition even at a concentration of 100 µM. A methylhydroxy group was the third substituent displaying significant activity (compound **60c**, 9.9 ± 4.0 µM). A methyl or ethyl substituent was not allowed, showing that the hydroxyl group of **60c** is an essential feature for activity. The possibility of forming a hydrogen bond is likely to cause this potency gain. Other hetero atom containing groups at the imidazole 2-position, like ether, carboxylic acid or amides did not lead to active compounds. Attempts to gain more potency focused on the substitution pattern on both the sulfonamide nitrogen and the imidazole ring. Surprisingly, addition of alkyl groups to the sulfonamide nitrogen is not allowed as all potency was lost. Also, the addition of a methyl to the 1-position nitrogen or 5-position resulted in complete loss of activity. Here, the influence on the tautomerism of the imidazole can be considered. It can be hypothesized that essential for activity is the presence of a proton on the 3-position nitrogen. This would allow for a hydrogen bond to the imidazole of His^{53} (see figure 43, §5.2). To test this concept, compound **86**, containing a 2-position sulfur substituent, was designed. This compound was shown to be completely in the thiourea form resulting in a constitutively protonated 3-position nitrogen. **86** is the most active compound identified with an IC_{50} of 3.1 ± 1.7 µM. Finally, replacement of the sulfonamide by phosphonate, amide or substituted sulfonyl resulted in complete loss of activity.

A

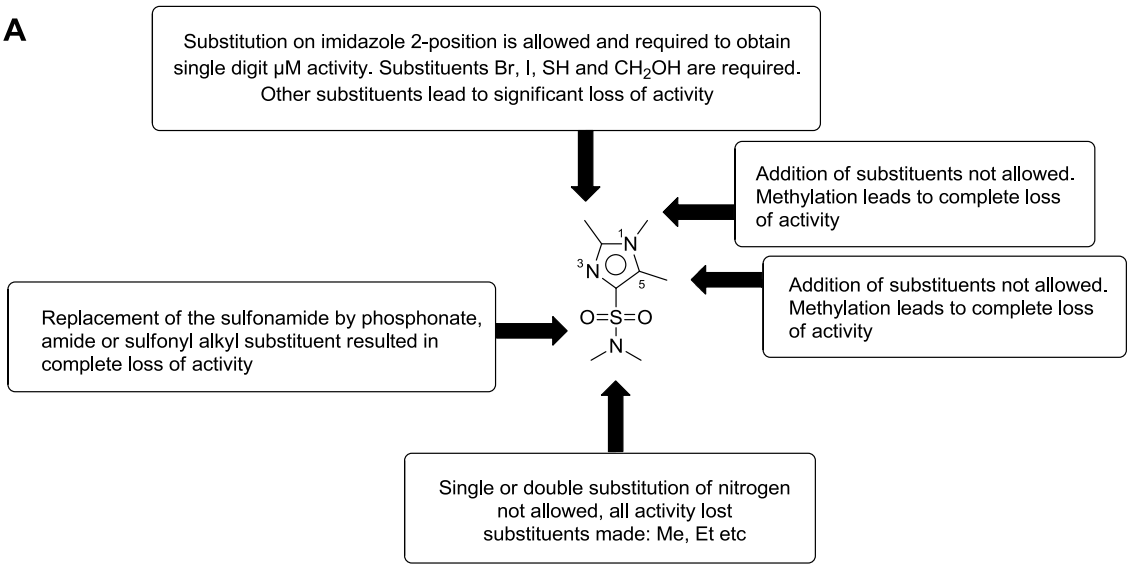

B

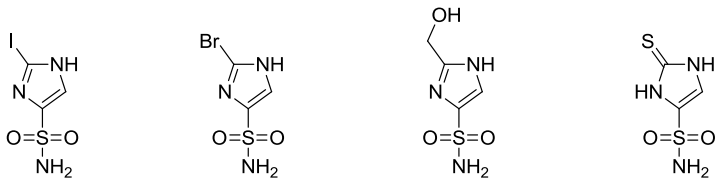

	53b	**53f**	**60c**	**86**
Fluorescence assay IC_{50} (µM):	**6.2 ± 2.5**	**11.1 ± 5.9**	**9.9 ± 4.0**	**3.1 ± 1.7**
Coupled assay IC_{50} (µM):	**n.d**	**13.6 ± 5.6**	**20.8 ± 9.0**	**6.2 ± 2.0**
Binding K_d (µM):	**n.d**	**12.8 ± 2.0**	**22.3 ± 2.1**	**2.0 ± 0.5**
solubility ():	**n.d**	**498.3**	**482.6**	**498.3**
PAMPA [%Flux]:	**n.d**	**5.9**	**0.6**	**66.5**

Figure 71: The established SAR around the imidazole sulfonamide core and the identified µM active PHP inhibitors. In general, addition of substituents led to complete loss of activity. The only exception is the imidazole 2-position were the substituents I, Br, CH_2OH and =S resulted in activity ranging from 3 to 12 µM inhibitory activity.

The identified inhibitors were tested in an alternative functional assay, using a more native phospho-histidine as substrate, and similar activities were established. Also in the MST binding assay very similar values for K_d were established. Overall biochemical assay results appear to be remarkable reproducible and universal for the different assay systems.

The solubility was measured and generally these compounds are highly soluble in aqueous media. This is due to the small and polar nature of the compounds. Cell permeability was also established using a PAMPA assay and found to be low for all compounds except for imidazole sulfonamide **86**, that showed significant cell permeability with 66%. Altogether, **86** displays the best combination of properties making it our prime PHP inhibitor for use in cellular assays.

Testing the compounds in cellular assays did not yield promising results so far. Compounds **53f**, **60c** and **86** were tested in the patch clamp assay and an effect was observed at a 100 µM concentration of **86** but the effect seems contrary to what was expected. With the current stand in science it cannot be explained as KCa3.1 activity was blocked rather than activated with compound **86**. Overexpression of PHP can overrule a different side effect caused by the inhibitors and might be required for further studies. It can also be argumented that a 1-10 µM activity is insufficient for achieving cellular activity. However, the optimization program that was performed suggests little room for optimization. The available X-ray structures and the proposed catalytic site reveals a shallow pocket predominantly lined with polar substituents. X-ray structures of PHP were also generated in-house and revealed a remarkable feature. The C terminal end was visible as not seen before in published structures. A significant part of the catalytic cleft is then occupied by this loop rendering only a small pocket that fits little substrate beyond a single phosphate group (see figure 28, §3.7). This is in line with the small nature of the active inhibitors that were identified.
Obtaining sub-micromolar activity generally requires lipophilic patches or deep pockets to obtain a strong binding affinity. PHP lacks this and the already small catalytic site is completely solvent exposed. This is also reflected by the promiscuous nature of the enzyme. In the literature, there is only a single example of a phospho-histidine containing peptide that was shown to be not a substrate for PHP.[107] Also in our hands the enzyme was able to dephosphorylate various substrate peptides. It is likely that the localization of either substrate or PHP determines selectivity rather than structure and mechanism of the PHP-substrate interaction *in vivo*. In general, this is not uncommon for phosphatases.[113] Put together, is seems that achieving sub-micromolar PHP inhibitory activity is a near impossible task.
Alternatively, activity of the sulfonamide inhibitors might be improved by covalent attachment to the enzyme. The catalytic site contains a residue that can be used for covalent attachment of a substrate. An electrophilic ligand, if presented properly, can react with Lys[21] found in the active site. Introducing a CF_3 group on the 2-position of the imidazole is likely to yield a compound with an intrinsic liability (see figure 67). Deletion of HF in **150** generates an electrophile (**151**) that forms an easy target for a nucleophile like a lysine. Essential is that the inhibitor binds to the enzyme, and so that the lysine can react, generating **152**. Taking into consideration the binding mode that was proposed, this is not the case. However, no definite structural proof for a particular binding mode has been found so far. Compound **150** has not been prepared yet.

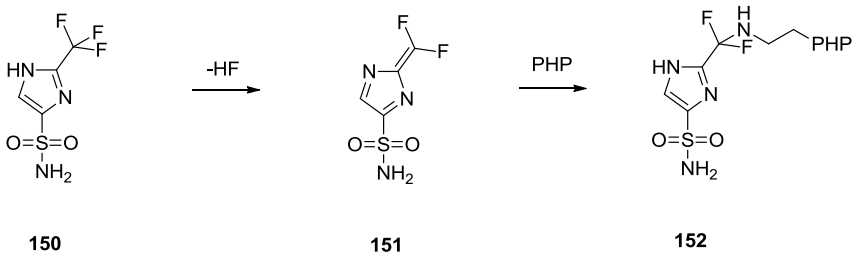

150 151 152

Figure 72: Structure and suggested mechanism of action of proposed inhibitor 150. Compound **150** is expected to be able to eliminate HF and form the reactive intermediate **151**. Reaction with Lys[21] can give covalently inhibition of PHP as represented by structure **152**.

A powerful alternative technique that can be deployed to identify inhibitors for PHP is High Throughput Screening (HTS).[114] The continuous fluorescence assay that is described can easily be adapted to a 384 well plate format and used to screen large numbers of compounds in an automated fashion. This approach can generate new chemical structures able to inhibit the enzyme and a new optimization program can be commenced.

X-ray crystallography of the PHP protein was performed successfully in order to investigate the enzyme its shape and function. Co-crystallization with the inhibitors, unfortunately, did not lead to successful crystal formation. Also, soaking experiments failed to trap the inhibitor into the matrix and obtain a binding conformation. All conditions established for successfully obtaining crystals, required a high concentration of sulfate ions in the excess of 1.5 molar. Analysis of the structures that were obtained showed a highly conserved sulfate ion in the active site of the enzyme that facilitates protein stacking. In order to obtain an X-ray structure that shows the ligand bound, a modification of the enzyme will be required. Only then new conditions can be found for crystallizing the enzyme without a sulfate blocking the active site.
The amino acid Gln^{84} was found to be involved in hydrogen binding to the sulfate found in the catalytic site from an adjacent PHP molecule. Modification of this amino acid to a different one can alter the crystallography dynamics for this enzyme and might give a micromolar active ligand a chance to appear in the crystal grid.

The phospho-histidine peptides that were prepared to study histone H4 did not lead to a major breakthrough in the elucidation of the role of His^{18} phosphorylation of histidine H4. Expression of the entire histone followed by chemical phosphorylation might result in a different outcome in the experiment investigating the PTMs that are applied to the lysines that bind the DNA. Also, the pull-down peptide probes that were prepared with building block **7** and **128** failed to identify proteins that interact with phospho-histidine. Here, a similar remark can be made, that the chosen peptide sequence might be too small and using an entire Histone H4 protein, equipped with a non-hydrolysable phospho-histidine mimic, will represent a better ‘bate’ in fishing for phospho-histidine interacting partners. However, this is not a trivial target. Obtaining such a protein would require a chemical ligation approach.

Finally, the study of the protein-protein interacting dynamics of the enzyme remains an undiscovered part of the enzyme’s function. The role of the loosely attached C terminal end is unknown. It has been established that the C terminal Tyr^{125} is a target for phosphorylation and the X-ray structure generated in-house shows how closely this residue can reach the catalytic site. Is this residue prone to get auto-phosphorylated by this protease? Or is an attached phosphate a target for autocatalytic cleavage? The fluorescence assay that uses DiFMUP shows that the enzyme has some phospho-phenol cleaving activity. A phospho-tyrosine can also serve as a docking site for other proteins. To study these possibilities, the preparation of the phosphorylated enzyme is required. Also, deletion of the C terminal end will yield a protein that with likely have altered properties, e.g. catalytic activity. Further investigation of this C-terminal end represents the most promising direction for continuation of this research.

Chapter 9: Experimental Section

9.1 General Materials and Remarks

Microbiology

Used machines

PCR	Eppendorf Mastercycler ep gradient S
Centrifuge	Eppendorf 5810 R Tabletop
Electroporation	Biorad Pulse Xcell
Incubator	Memmert Model 100
Microfluidizer	Microfluidics Corporation
Protein purification	GE Healtcare Akta Purifier
Affinity purification	His-Trap FF crude Ni^{2+}-NTA-(5mL Matrix)
Gelfiltration	Highload 26/60 Sephadex 75 prep grade
Protein conc. determination	Thermo Scientific Nanodrop
UV absorbance and Fluorescence	Tecan Infinite 200Pro instrument.

Cells

OmniMAX and electrocompetent TOP10 cells were kindly supplied by Prof. Dr. Frank Schulz (Ruhr-Universität Bochum).

Sequencing

Sequencing was performed by StarSEQ

Media

LB	Yeast extract	5.0	g/L	
	NaCl	10.0	g/L	
	Trypton	10.0	g/L	pH = 7.5
TB	Yeast extract	24.0	g/L	
	Trypton	12.0	g/L	
	Glycine	4.0	mL/L	
	KH_2PO_4	2.13	g/L	
	K_2HPO_4	12.54	g/L	pH = 7.0
SOB	Yeast extract	5.0	g/L	
	Trypton	20.0	g/L	
	NaCl	0.6	g/L	
	KCl	0.2	g/L	
	$MgCl_2$ (10 mM)	10.0	mL/L	
	$MgSO_4$ (10 mM)	10.0	mL/L	
SOC	SOB-medium			
	Glucose	20.0	mM	

Primers

Obtained from Eurofins MWG

LIC primer forwards:
CTTTATTTTCAGGGCGCCATGGCAGTGGCGGACCTCGCTC
LIC primer rev:
CAAAACAGCCAAGCTCTCGATTATTAGTAGCCGTCGTTAGCCCAGGTG

Enzymes

NcoI	Obtained from New England Biolabs
XhoI	Obtained from New England Biolabs
Phu polymerase	Obtained from New England Biolabs
TEV protease	Provided by the Dortmund Protein Facility[106]
HindIII	Obtained from Fermentas

Kits

Plasmid isolation	Qiagen QIAprep Spin Miniprep Kit
Gel extraction	Qiagen QIAquick Gel Extraction Kit

Chemistry

All chemicals were obtained from Acros, Aldrich, Alfa Aesar, Merck or Rapp Polymere and were used without further purification except when noted. Solvents were used as received; except dichloromethane, which was distilled from CaH_2 and THF, which was distilled from sodium. ^{1}H, ^{13}C and ^{31}P NMR spectra were recorded on Varian Mercury 400- or a Bruker DRX 500 NMR spectrometer. Chemical shifts are reported in δ values relative to residual solvent peaks (Abbreviations: s: singlet, bs: broad singlet, bd: broad doublet, d: doublet, dd: doublet of doublets, dt: doublet of triplets, t: triplet, q: quartet, m: multiplet). Specific optical rotations were measured on a Schmidt + Haensch Polartronic HH8 Polarimeter. Column chromatography was performed using silica gel for chromatography (0.035-0.070 mm, 60A) purchased from Acros Organic. Compounds on TLC were visualized by UV and/or basic $KMnO_4$ staining. High resolution mass spectra (HR-MS, 70 eV) were measured on a Thermo Orbitrap, coupled to a Thermo Accela nano-HPLC machine, using electron spray ionization (ESI). Analytical HPLC-MS data were recorded on an Agilent HPLC (1100 series) coupled to a Finnigan LCQ ESI spectrometer, using a Nucleodur C18 gravity column, ID 4 mm, length 125 mm, particle size 3 µm from Macherey-Nagel. A gradient was applied beginning at 10% acetonitrile and ending at 90% after 15 min, followed by 3 min at 90% acetonitrile; finally, the column was washed for 5 min with 100% acetonitrile. The column was equilibrated for 3 min with 10% acetonitrile. All RP-HPLC solvents contained TFA (0.1% v/v). Preparative HPLC purifications were performed with an Agilent 1100 series instrument, connected to an Agilent MSD VL mass spectrometer andequipped with a fraction collector. All RP-HPLC solvents contained TFA (0.1% v/v) and products with basic amines were isolated as a TFA salt.

9.2 Cloning and Expression of PHP

The gene encoding for PHP was supplied to us by Prof. Zetterqvist (Dept. Medical biochemistry, Uppsala University) in the form of a pBADNK vector. The pBADM vectors were supplied to us by Prof. Frank Schultz (Ruhr-Universität Bochum).

PCR

requirements:

- Buffer solution 5x 20 µL
- dNTPs 10 µL
- primer 1 (10pmol/µL) 5 µL
- primer rev (10pmol/µL) 5 µL
- Phu polymerase 1.25 µL
- plasmid 2.5 µL
- steril water 56.25 µL

The solution was divided over 5 PCR tubes

program

1. 98°C – 20 sec
2. 98°C – 5 sec (30x)
3. 72°C – 20 sec (30x)
4. 72°C – 5 min
5. 4°C -

To the PCR reaction mixture was added loading buffer/color dye (5x) and loaded on an agarose gel. The gel was run at 100V constant voltage and the desired DNA was cut out and purified using a gel extraction kit.

Plasmid digestion

The five different pBADM vectors were digested using the enzymes NcoI and XhoI.

- NcoI-HF mix 1.0 µL
- XhoI mix 1.0 µL
- pBADM vector 10.0 µL
- steril water 8.0 µL

To the digestion reaction mixture was added loading buffer/color dye (5x) and loaded on an agarose gel. The gel was run at 100V constant voltage and the desired DNA was cut out and purified using a gel extraction kit.

From the isolated PCR product and the linearized vector solution the concentration was determined by nanodrop measurement:

PCR product	35.0	ng/µL	pBADM-30	9.7	ng/µL
pBADM-10	10.6	ng/µL	pBADM-40	19.1	ng/µL
pBADM-20	15.5	ng/µL	pBADM-60	16.8	ng/µL

Ligation-independent cloning

100 ng of purified insert and 50 ng of linearized and purified vector were mixed together in a total volume of 5 µL. On ice, 5 vial of 50 µL OmniMAX chemically competent cells were thawed. The insert/vector mixtures from all five vectors were carefully added to and mixed with the cells and incubated for 30 min. on ice. Heat-shock was applied to the cells for 1 min. and 15 sec. at 42 ^{0}C. The cells were places on ice for 1 min. and 600 µL SOC medium was added and the mixture was transferred to a shaker and incubated for 45 min. at 37 ^{0}C. The mixture was divided over 3 LB agar plates (with 100 µg/mL ampicillin) with 5/50/500+ division and incubated overnight at 37 ^{0}C. For all five vectors 5 clear single clones were selected and incubated in 10 mL LB medium (100 ug/mL ampicillin) and grown overnight at 37 ^{0}C. The cells were harvested by centrifuge for 15 min. at 4,000 rpm and 4 ^{0}C. Vectors were isolated by use of a miniprep kit and sequenced.

Expression and purification of PHP

1 µL vector solution (pBADM60) was mixed with a 50 µL aliquot of TOP10 electrocompetent cells on ice. The mixture was then transferred to the electroporation cuvette and the reaction was carried out (bacteria\Ecoli\1.8kV). SOC-medium (0.6 mL) was then added and the cells were transferred back into the eppendorf tube. The eppendorf tube was then transferred to a shaker and heated at 37 ºC for 1 hour. The resulting solution was plated on plates (LB+100 µg/mL carbenicillin). Incubated at 37 ºC overnight. 100 mL LB medium with 100 µg/mL ampicillin was inoculated with one colony from the plate and incubated at 30 °C and 150 rpm overnight. 2000 mL LB medium (100 µg/mL ampicillin) was inoculated with the pre-culture so that the OD_{600} was 0,05. The culture was incubated at 37 °C and 150 rpm to an OD_{600} = 0.8 - 1. The culture was cooled to 20 °C and the expression was started by addition of arabinose (0.05 % w/v). The culture was further incubated overnight at 20 °C and 150 rpm. The cells were harvested by centrifugation for 10 min at 4000 rpm by 4 °C. After re-suspension in wash buffer (25 mM HEPES, 150 mM NaCl, pH 7.5) in 1/10 of the volume of the main culture, the cells were harvested again by centrifugation. The cells were re-suspended in lysis buffer (25 mM HEPES, 150 mM NaCl, 50 mM imidazole, pH 7.5) (0.5 g pellet per mL buffer) and sonicated (90 % power, 5 x 20 sec, 1 min on ice in between). The lysed cells were centrifuged for 15 min by 10,000 rpm at 4 °C. The supernatant was pipetted off and transferred to a fresh tube and loaded on a 5 mL HisTrap FF column (GE Healthcare) pre-equilibrated with lysis buffer at a rate of 1 mL/min. The column was washed with 50 mL lysis buffer (1 mL/min). The protein was eluted with 25 mL elution buffer (25 mM HEPES, 150 mM NaCl, 250 mM imidazole, pH 7.5) and concentrated with an Amicon tube (10 kDa MWCO). The concentrated protein was incubated with TEV protease and cleavage was analyzed using SDS PAGE. The sample was directly loaded onto the SEC column pre-equilibrated with storage buffer (20 mM HEPES, 20 mM NaCl, pH 7.5), eluted and concentrated with an Amicon (10 kDa MWCO) to 25 mg/mL. The enzyme solution was used as such for crystallography or was aliquoted as 100 µM stock solutions and stored at -80 ^{0}C for enzymatic assay purposes. The molecular weight was confirmed with mass analysis.

Expression and purification of the pBADM-11 PHP-His Tag protein

Expression performed the same way as described for pBADM-60 derived PHP with exception that the TEV digestion was not performed. Stored in the same buffer (20 mM HEPES, 20 mM NaCl, pH 7.5) at a concentration of 25 mg/mL.

9.3 Continuous Fluorometric Assay

Synthesis of DiFMUP (13)

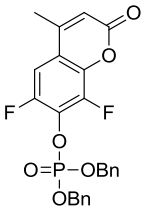

dibenzyl (6,8-difluoro-4-methyl-2-oxo-2H-chromen-7-yl) phosphate (12) 200 mg (0.94 mmol) **11** was suspended in 6 mL dry acetonitril under argon in a flame-dried flask. 0.46 mL (4.71 mmol) CCl_4, 0.34 mL (1.98 mmol) DiPEA and 10 mg DMAP were added before cooling the RM to -15 ^{0}C. 300 µL (1.37 mmol) dibenzyl phosphite was added dropwise and the RM was allowed to reach -5 ^{0}C in 2 h. The RM goes from bright yellow to almost colorless and TLC indicated full conversion. 2 mL 0.5 M K_2HPO_3-solution was added and the RM was allowed to reach RT over 1 h. Water was added and extracted with EtOAc. The EtOAc was washed with brine, dried over Na_2SO_4 and evaporated. Filtration through a plug of silica yielded 398 mg **12**. ^{1}H-NMR(400 MHz, DMSO-d_6) δ: 7.40 – 7.32 (m, 10H), 7.16 (dd, J=2.0, 10.7Hz, 1H), 6.35 (s, 1H), 5.24 (d, J = 8.4Hz, 4H), 2.39 (d, J = 1.2Hz, 3H). Analytical data in agreement with literature.[73]

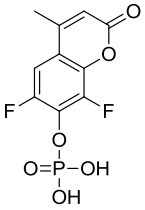

6,8-difluoro-4-methyl-2-oxo-2H-chromen-7-yl dihydrogen phosphate (13) 360 mg (0.76 mmol) **12** was dissolved in 6 mL ethanol and 3 mL toluene. The flask was rinsed with argon before replacing the argon with hydrogen gas. The RM was stirred overnight at RT. TLC indicated complete conversion and the RM was filtered through celite. Evaporation yielded 210 mg **13** (76 % yield over two steps). ^{1}H-NMR(400 MHz, DMSO-d_6) δ: 7.60 (dd, J=2.0, 10.7Hz, 1H), 6.46 (s, 1H), 4.30 (bs, 2H), 2.39 (d, J = 1.2Hz, 3H). Analytical data in agreement with literature.[73]

Determination of K_M and V_{max}

Assay buffer:
20 mM Tris
20 mM NaCl
0.02% NP40
pH = 8.0

In a 96 well microtiter plate, DiFMUP substrate solution (80 µL in assay buffer, endconcentration ranging from 50 to 1000 µM) were mixed with enzyme solution (20 µL in assay buffer, endconcentration of 100 nM) and the fluorescence at 455 nm (excitation wavelength: 358 nm) was measured every 30 seconds for 5 minutes at 37 °C. The experiment was performed in triplo. The initial velocities were measured and by using the software program 'XL Fit' a K_M of 765 ± 59 µM and V_{max} of 8.3 ± 0.6 µM/s was established. k_{cat}/K_M was determined to be 1.08 ± 0.2 $.10^5$ $M^{-1}.s^{-1}$.

Determination of inhibitor activity

Assay buffer:
20 mM Tris
20 mM NaCl
0.02% NP40
pH = 8.0

In a 96 well microtiter plate, inhibitor solutions (50 µL in assay buffer, endconcentration of 100 µM for screening purposes and 10 different concentrations around the IC_{50} for a full curve) were mixed with enzyme solution (20 µL in assay buffer, endconcentration of 100 nM) and incubated for 10 minutes at RT (total volume was filled to 90 µL with assay buffer for every well). Immediately after addition of the DiFMUP substrate solution (10 µL in assay buffer, endconcentration of 200 µM) the fluorescence at 455 nm (excitation wavelength: 358 nm) was measured every 30 seconds for 5 minutes at 37 °C. The relative increase in fluorescence in 5 minutes is the measure for inhibition. As a control a reaction with only substrate (background experiment with 90 µL assay buffer) and a reaction without inhibitor (positive control experiment with 50 µL extra assay buffer) was run in parallel. Every inhibitor was tested from the solid material twice and both separate experiments performed in duplo.

Inhibitor solutions:
10 mM in DMSO diluted to 200 µM stock in assay buffer (final DMSO concentration is 1%, should be held constant for all inhibitor concentration solutions for an IC_{50} determination).

9.4 Continuous Coupled Enzyme Assay

Synthesis of substrate 3-phosphohistidine (15) and MESG (16)

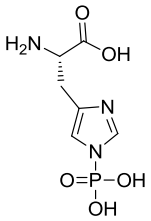

3-phosphohistidine (15) 25 mg (0.16 mmol) histidine was dissolved in 2 mL water before adding 217 mg (1.6 mmol) potassium phosphoramidate. The RM was stirred for 40 hours at RT, filtered and loaded onto a monoQ anion exchange column (0.5 mL mixture per run diluted with 0.5 mL buffer) equilibrated with 0.5 mL/min 50mM NH_4HCO_3(aq) on an akta system. The product was eluted with a gradient to 50 % 1.5 M NH_4HCO_3(aq) in 20 min and in 1 min to 100%. A second purification of the obtained product solution was required to obtain highly pure material. The concentration was determined (see below for procedure) and diluted with buffer to obtain 4.7 mL of 1.0 mM solution. The substrate solution was aliquoted in 100 µL amounts, shock frozen and stored at -80 ºC. ^{31}P-NMR(161 MHz, $CDCl_3$) δ: 3.50.

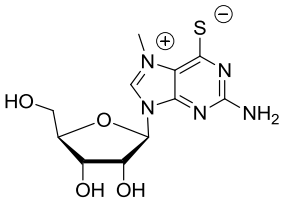

2-amino-6-mercapto-7-methylpurine riboside MESG (16) 200 mg (0.66 mmol) 2-amino-6-chloropurine riboside (**17**) was dissolved in 1 mL dry DMF. 0.4 mL (6.4 mmol) MeI was added and the RM was stirred overnight at RT. The excess MeI was removed under vacuum before adding 200 mg thiourea. After 30 minutes the pH was corrected from 2 to 7 using methanolic ammonia before drop wise addition of the RM into 10 mL acetone. A yellow precipitate was formed, after stirring for 10 minutes before the acetone was decanted off. This step was repeated before filtration yielded a yellow solid. This material was suspended in MeOH, the MeOH was decanted off (repeated 3x). The solid material was dried under vacuum yielding 132 mg **16** as a yellowish solid (64 % yield from **17**). ^{1}H-NMR(400 MHz, DMSO-d_6) δ: 9.64 (s, 1H), 7.68 (bs, 2H), 5.81 (d, J=2.5Hz, 1H), 5.67 (d, J=6.0Hz, 1H), 5.27 (d, J=6.0Hz, 1H), 5.17 (t, J=6.0Hz, 1H), 4.35 (m, 1H), 4.22 (s, 3H), 4.14 (q, J=5.0Hz, 1H), 3.97 (dd, J=5.7Hz, J=3.2Hz, 1H), 3.75-3.55 (m, 2H). Analytical data in agreement with literature.[83]

Expression of Bacillus cereus Purine Nucleoside Phosphorylase (BcPNP)

The gene encoding for PNP was supplied to us by Prof. Steve Ealick (Cornell University).

50 µL chemical competent *E. coli* BL21 DE3 cells were thawed on ice. 2.0 µL plasmid solution (pBcPNP2_28) was added and incubated for 30 min. The cells were heated to 42 °C for 1 min (heat shock) and immediately cooled for 2 min on ice. After addition of 700 µL SOC medium the cells were incubated for 40 min at 37 °C. Cells were streaked out on LB agar plates with 50 µg/mL kanamycin and incubated overnight at 37 °C. 4 mL LB medium with 50 µg/mL kanamycin was inoculated with one colony and incubated over night at 30 °C. The plasmid DNA was isolated by use of a miniprep kit and sequenced. The digested DNA (HindIII) was analyzed by agarose gel electrophoresis (1 % Agarose (w/v) in TAE buffer, 120 V). 150 mL LB medium with 50 µg/mL kanamycin was inoculated with one colony from a LB agar plate and incubated at 30 °C and 150 rpm overnight.
1000 mL LB medium with 50 µg/mL kanamycin was inoculated with the pre-culture so that the OD_{600} was 0.05. The culture was incubated at 37 °C and 150 rpm to an OD_{600} = 0.8 – 1. The culture was cooled to 20 °C and the expression was started by addition of IPTG (1 mM in the culture). The culture was further incubated for 18 h (overnight) at 20 °C and 150 rpm. The cells were harvested by centrifugation for 10 min at 4000 rpm by 4 °C. After resuspension in wash buffer (25 mM HEPES, 150 mM NaCl, pH 7.5) in 1/10 of the volume of the main culture, the cells were harvested again by centrifugation. The cells were resuspended in lysis buffer (25 mM HEPES, 150 mM NaCl, 50 mM imidazole, pH 7,5) (0,5 g pellet per mL buffer) and sonicated (90 % power, 5 x 20 sec, 1 min on ice between). The lysed cells were centrifuged for 15 min by 10000 rpm at 4 °C. The protein was in the supernatant which was pipetted off and transferred to a fresh tube. The supernatant was loaded on a 5 mL HisTrap FF column (GE Healthcare) pre equilibrated with lysis buffer at a rate of 1 mL/min. The column was washed with 50 mL lysis buffer (1 mL/min). The protein was eluted with 25 mL elution buffer (25 mM HEPES, 150 mM NaCl, 250 mM imidazol, pH 7,5) and concentrated with an Amicon (10 kDa MWCO). The buffer was changed (wash buffer) by adding several times (at least 3 times) fresh buffer (10 mL) to the Amicon.

Determination of the concentration of phospho-histidine (15) and determination of K_M and V_{max}

Assay buffer:
20 mM Tris
1 mM $MgCl_2$
0.02% NP40
pH = 7.5

To determine the concentration of the purified 3-phospho-histidine (**15**) the enzyme reaction was run at various concentrations of phosphate to create a calibration graph. In a 96 well microtiter plate, various KH_2PO_4 solutions (80 µL in assay buffer, endconcentration ranging from 2 to 50 µM) were mixed with MESG substrate solution (40 µL in assay buffer, endconcentration of 100 µM). PNP solution (80 µL in assay buffer, endconcentration of 5 µM) was added and the absorbance at 360 nm was measured every 30 seconds for 1 hour at 30 °C. The maximum absorbance reached was plotted against the concentration. The experiment was repeated with various concentrations of **15** premixed with 500 nM PHP to assure complete hydrolysis. Comparison with the generated calibration line revealed a concentration of 1.6 mM.

To determine the K_M and V_{max} values, PHP (10 µL in assay buffer, endconcentration of 100 nM), MESG (40 µL in assay buffer, endconcentration of 100 µM) and PNP (20 µL in assay buffer, endconcentration of 10 µM) were mixed in a 96 well microtiter plate. The volume was filled up to 190 µL with assay buffer and substrate **15** (10 µL in assay buffer, endconcentration of 25 µM) was added and the absorbance at 360 nm was measured every 30 seconds for 10 minutes at 30 °C. The experiment was performed in triplo. The initial velocities were measured and by using the software program 'XL Fit' a K_M of 3.6 ± 0.2 µM and a V_{max} of 213 ± 12 µM/s was established. k_{cat}/K_M was determined to be 5.9 ± 1.2 .108 M-1.s-1.

Determination of inhibitor activity

Assay buffer:
20 mM Tris
1 mM $MgCl_2$
0.02% NP40
pH = 7.5

In a 96 well microtiter plate, inhibitor solutions (100 µL in assay buffer, endconcentration of 100 µM for screening purposes and 10 different concentrations around the IC_{50} for a full curve) were mixed with PHP solution (10 µL in assay buffer, endconcentration of 100 nM) and incubated for 10 minutes at RT. MESG (40 µL in assay buffer, endconcentration of 100 µM) and PNP (20 µL in assay buffer, endconcentration of 10 µM) were added. The volume was filled up to 190 µL with assay buffer. The substrate **15** (10 µL in assay buffer, endconcentration of 25 µM) was added and the absorbance at 360 nm was measured every 30 seconds for 10 minutes at 30 °C. The relative increase in absorbance in 5 minutes is the measure for inhibition. As a control a reaction without PHP (background) and a reaction without inhibitor was run in parallel. Every inhibitor was tested from the solid material twice and both separate experiments performed in duplo. Additionally, all inhibitor compounds were tested on PNP solely in order to exclude PNP inhibition as the mechanism of action. No compound was found to be active on the coupled PNP enzyme confirming the inhibitors to be genuine PHP inhibitors.

Inhibitor solutions:
10 mM in DMSO diluted to 200 µM stock in assay buffer (final DMSO concentration is 1%, should be held constant for all inhibitor concentration solutions for an IC_{50} determination).

9.5 Determination of K_d with Microscale Thermophoresis

PHP fluorescein labeling:
5 mL (1 mg/mL) PHP solution (in PBS buffer) was treated with 0.5 mL (1.5 mg/mL) carboxyfluorescein succinimidyl ester in DMSO. The mixture was allowed to react overnight at 4 ºC. The labelled protein was purified by SEC (20 mM Tris/20 mM NaCl, pH = 8.0) and concentrated to 0.5 mL. Concentration was determined to be 4 mg/mL.

Assay buffer:
20 mM Tris
20 mM NaCl
0.02% NP40
pH = 8.0

The labelled protein was diluted to correct fluorecence intensity (generally 750 nM) and incubated with 12 different inhibitor solutions in a 1:1 dilution row around the K_d value. Samples were incubated for 20 min before measurements. Laser-on and -off times were adjusted to 30 s and 5 s, respectively. The measurements were carried out at 20 ºC and generally performed at 50% LED power and 60% infrared-laser power. The measurements were performed on NanoTemper Monolith NT.115 instruments in standard treated capillaries and analyzed with NanoTemper Analysis version 1.2.205 (NanoTemper Technologies GmbH).

9.6 PHP Crystallography

A search for new crystal forms for PHP was initialized with both histag labeled and label free protein (~30 mg/ml). A full screen was launched using commercially available screens and a Mosquito pipetting robot. New crystal forms were obtained in $Co(II)Cl_2$ 0.01 M, MES 0.1 M, NH_4SO_4 1.8 M, pH = 6.5 (taken from Core III nr.50). After optimization, the best diffracting crystals were grown in $Co(II)Cl_2$ 0.01 M, MES 0.1 M, NH_4SO_4 1.6-1.8 M, pH = 6.5-8.5. Thicker needles were obtained that showed significant diffraction at the Swiss Light Source (SLS, Paul-Scherer Institut Villigen, Switzerland).

9.7 Synthesis of Building Block 7

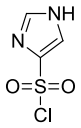

1H-imidazole-4-sulfonyl chloride (24) 20.0 g (294 mmol) imidazole (**25**) was melted (theoretical mp = 90 °C / heated to 115 °C) in an argon flushed 250 mL flask. 60.0 mL (900 mmol) $ClSO_3H$ was added drop wise (Caution! the first 15 mL reacted violently, with excessive HCl(g) formation). The reaction mixture was heated at 140 ^oC for 16 hours. The resulting dark reaction mixture (RM) was cooled to 40 ^oC before adding 22.0 mL (302 mmol) thionyl chloride drop wise over 5 minutes (immediate gas evolution visible). The RM was heated until gas evolution ceased, during which time the temperature was slowly raised to 125 °C. The RM was allowed to cool to rt before pouring it into a slurry of 300 g crushed ice with 20.0 g NaCl. A white precipitate was formed and the suspension was filtered after the ice had completely melted. The white solid was washed with a small amount of cold water and dried overnight under vacuum over KOH. The filtrate was re-filtered once and the collected solid was washed with a small amount of water and dried overnight under vacuum over KOH. Combining the two solids yielded 30.2 g **24** as a fine white powder (62% yield from **25**). ^{1}H-NMR(400 MHz, DMSO-d_6) δ: 14.22 (broad s, 1H), 8.99 (d, J=1.2Hz, 1H), 7.64 (d, J=1.2Hz, 1H) Analytical data in agreement with literature.[120]

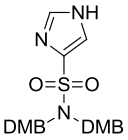

***N,N*-bis(2,4-dimethoxybenzyl)-1H-imidazole-4-sulfonamide (26)** 4.00 g (24.0 mmol) **24** was added in small portions to a solution of 6.34 g *N*,*N*-bis(2,4-dimethoxybenzyl)amine (20.0 mmol) in 100 mL DCM with 6.60 mL (5.17 g/40 mmol) DIPEA at 0 °C. The RM was stirred at 0 $^\circ$C for 30 minutes, followed by 2 hours at rt. When TLC indicated complete conversion, the RM was poured into 20.0 mL 5% citric acid and was shaken once before adding 200 mL sat. $NaHCO_3$(aq) and shaking it carefully (gas evolution). The layers where separated and the DCM was washed with brine, dried over $MgSO_4$(s), concentrated and dried under vacuum. The product was purified by SiO_2 column chromatography, eluted with EtOAc to obtain 8.02 g of **26** as a pale yellow foam (90% yield from bis(2,4-dimethoxybenzyl)amine). R_f = 0.46 (DCM/MeOH 9:1); ^{1}H-NMR(400 MHz, $CDCl_3$) δ: 7.92 (d, J=1.2Hz, 1H), 7.23 (d, J=1.2Hz, 1H), 7.05 (d, J=8.4Hz, 2H), 6.28 (dd, J=8.4Hz J=2.4Hz, 2H), 9.19 (d, J=2.4Hz, 2H), 5.35 (broad s, 2H), 4.34 (s, 4H), 3.66 (s, 6H), 3.54 (s, 6H); ^{13}C-NMR(101 MHz, $CDCl_3$) δ: 160.3, 158.1, 137.3, 136.4, 130.4, 120.7, 116.6, 104.0, 97.7, 55.2, 54.9, 46.6; ESI HRMS calculated for $C_{21}H_{26}O_6N_3S$ $[M+H]^+$ = 448.15368. Mass found $[M+H]^+$ = 448.15358.

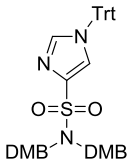

(*N,N*-bis(2,4-dimethoxybenzyl)-1-trityl-1H-imidazole-4-sulfonamide (27) In a 100 mL round bottom flask, 2.00 g (4.47 mmol) **26** was dissolved in 30.0 mL dry DMF. After adding 1.00 g (8.91 mmol) KOtBu (RM became yellow) and allowing it to stir (20 minutes), 1.87 g (6.71 mmol) trityl-Cl was added at 0 ^{o}C and the RM was stirred for 18 hours at rt. The DMF was evaporated and the residue was suspended in sat. $NaHCO_3$(aq) and extracted with EtOAc twice. The combined EtOAc layers were washed with brine, dried over $MgSO_4$(s), concentrated and dried under vacuum. The product was purified by SiO_2 column chromatography, eluted with toluene/EtOAc (85:15) to obtain 2.53 g of **27** as a white/yellow foam (83% yield from **26**). R_f = 0.69 (toluene/EtOAc 1:1); ^{1}H-NMR(400 MHz, $CDCl_3$) δ: 7.46 (d, J=1.2Hz, 1H), 7.34 (m, 10H), 7.20 (d, J=8.4Hz, 2H), 7.05 (m, 6H), 6.33 (dd, J=8.4Hz, J=2.4Hz, 2H), 6.29 (d, J=2,4Hz, 1H), 4.48 (s, 4H), 3.74 (s, 6H), 3.62 (s, 6H); ^{13}C-NMR(101 MHz, $CDCl_3$) δ: 160.2, 158.3, 141.8, 140.2, 140.1, 130.3, 129.9, 128.7, 128.5, 124.8, 117.9, 104.1, 98.1, 76.5, 55.5, 55.2, 46.3; ESI HRMS calculated for $C_{40}H_{40}O_6N_3S$ $[M+H]^+$ = 690.26323. Mass found $[M+H]^+$ = 690.26366.

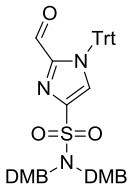

N,N-bis(2,4-dimethoxybenzyl)-2-formyl-1-trityl-1H-imidazole-4-sulfonamide (23 2.0 g (2.9 mmol) **27** was dissolved in 20.0 mL dry THF in a flame-dried Schlenk flask. The reaction mixture was cooled to -30 ^{o}C under argon atmosphere. 2.20 mL (3.52 mmol) of a 1.6 M *n*-butyl lithium solution in hexane was added drop wise at -30 ^{o}C and the RM became red. After 20 minutes, 1 mL dry DMF (5 equiv.) was added drop wise. The RM was allowing the RM to warm up for 1 hour. The RM was poured into sat. $NaHCO_3$ solution and was extracted twice with EtOAc. The combined EtOAc layers were washed with brine, dried over $MgSO_4$(s), concentrated and dried under vacuum. The product was purified by SiO_2 column chromatography, eluted with toluene/EtOAc (9:1) to obtain 1.89 g of **23** as a white foam (91% yield from **27**). R_f = 0.68 (cyclohexane/EtOAc 1:1); ^{1}H-NMR(400 MHz, $CDCl_3$) δ: 9.23 (d, J=6Hz, 1H), 7.33 (m, 10H), 7.24 (d, J=8.4Hz, 2H), 7.01 (m, 6H), 6.35 (dd, J=8.4Hz, J=2.4Hz, 2H), 6.33 (d, J=2,4Hz, 1H), 4.56 (s, 4H), 3.74 (s, 6H), 3.68 (s, 6H); ^{13}C-NMR(101 MHz, $CDCl_3$) δ: 178.7, 160.4, 158.6, 145.4, 141.8, 141.5, 130.8, 129.7, 128.7, 128.4, 128.3, 117.5, 104.1, 98.2, 78.2, 55.5, 55.3, 46.5; ESI HRMS calculated for $C_{41}H_{40}O_7N_3S$ $[M+H]^+$ = 718.25815. Mass found $[M+H]^+$ = 718.25885.

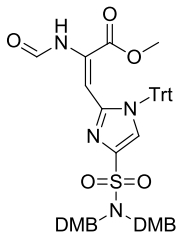

(E)-methyl 3-(4-(N,N-bis(2,4-dimethoxybenzyl)sulfamoyl)-1-trityl-1H-imidazol-2-yl)-2-formamidoacrylate (22) 820 mg (1.14 mmol) **23** and 105 µL (1.15 mmol) methyl isocyanoacetate were dissolved in 8 mL dry THF. 8 mg Cu_2O was added and the RM was stirred for 1h at RT. 135 mg KOtBu was added at to the RM at 0 ^oC and stirred for 2 hours at RT. The RM was poured into a sat. $NaHCO_3$ and was extracted using EtOAc. The EtOAc was dried and evaporated, yielding 350 mg **22** (33% yield from **23**). R_f = 0.90 (EtOAc); ^{1}H-NMR(400 MHz, $CDCl_3$) δ: 10.68 (bs, 1H), 8.60 (bs, 1H), 7.37-7.35 (m, 9H), 7.23-720 (m, 2H), 7.05-7.02 (m, 6H), 6.35-6.32 (m, 4H), 5.60 (bs, 1H), 4.58 (s, 4H), 3.74 (s, 6H), 3.68 (s, 6H), 3.60 (s, 3H); ^{13}C-NMR(101 MHz, $CDCl_3$) δ: 163.9, 160.4, 158.5, 145.4, 141.3, 139.3, 130.8, 129.9, 128.8, 128.7, 124.6, 117.5, 106.1, 104.0, 98.2, 77.1, 55.5, 55.3, 53.6, 52.7, 46.7; ESI HRMS calculated for $C_{45}H_{45}O_9N_4S$ $[M+H]^+$ = 817.29018. Mass found $[M+H]^+$ = 817.29039.

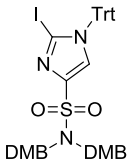

***N,N*-bis(2,4-dimethoxybenzyl)-2-iodo-1-trityl-1H-imidazole-4-sulfonamide (29)** 1.0 g (1.45 mmol) **27** was dissolved in 20.0 mL dry THF in a flame-dried Schlenk flask. The reaction mixture was cooled to -30 ^oC under argon atmosphere. 1.20 mL (1.74 mmol) of a 1.41M *n*-butyl lithium solution in hexane was added drop wise at -30 ^oC and the RM became dark red. After 20 minutes, 1.00 g iodine (3 equiv.) dissolved in 5.00 mL THF was added drop wise. The first equivalent of iodine was consumed as seen by disappearance of color. An additional 1 mL of iodine solution was added. The RM was stirred at -30 ^oC for 10 minutes before removing the cooling bath and allowing the RM to warm up for 10 minutes. The still relatively cold (-5 °C) RM was poured into a sat. $Na_2S_2O_3$ solution and was extracted twice with EtOAc. The combined EtOAc layers were washed with brine, dried over $MgSO_4$(s), concentrated and dried under vacuum. The product was purified by SiO_2 column chromatography, eluted with toluene/EtOAc (95:5) to obtain 1.01 g of **29** as a white foam (85% yield from **27**). R_f = 0.73 (toluene/EtOAc 1:1); ^{1}H-NMR(400 MHz, $CDCl_3$) δ: 7.34 (m, 10H), 7.20 (d, J=8.4Hz, 2H), 7.05 (m, 6H), 6.33 (dd, J=8.4Hz, J=2.4Hz, 2H), 6.29 (d, J=2,4Hz, 1H), 4.48 (s, 4H), 3.74 (s, 6H), 3.62 (s, 6H); ^{13}C-NMR(101 MHz, $CDCl_3$) δ: 160.3, 158.5, 142.1, 141.0, 130.8, 130.6, 128.6, 128.3, 128.2, 117.7, 104.1, 98.1, 92.1, 78.1, 55.5, 55.3, 46.2; ESI HRMS calculated for $C_{40}H_{39}O_6N_3IS$ $[M+H]^+$ = 816.15988. Mass found $[M+H]^+$ = 816.16011.

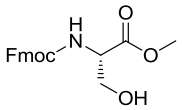

(S)-methyl 2-((((9H-fluoren-9-yl)methoxy)carbonyl)amino)-3-hydroxypropanoate (32) 1.88 g (22 mmol) $NaHCO_3$ and 1.43 g (9.0 mmol) Serine-OMe.HCl (**31**) were dissolved in 20 mL water and cooled to 0 ^{0}C. 3.05 g (9 mmol) Fmoc-OSu dissolved in 20 mL dioxane was added dropwize. The resulting suspension was allowed to reach RT and was stirred for an additional hour. 10 mL water was added and the RM was extracted 4x with EtOAc. The combined EtOAc was washed with 0.2 M HCl solution and with brine. Drying and evaporation yielded a transparent oil. Toluene was added and evaporated to remove traces of dioxane and 3.07 g (8.9 mmol) **32** was isolated as a white powder (98% yield from **31**). ^{1}H-NMR(400 MHz, $CDCl_3$) δ: 7.77 (2H, d, *J* = 7.2), 7.61 (2H, d, *J* = 6.8), 7.41 (2H, t, *J* = 7.6), 7.32 (2H, t, *J* = 7.6), 5.70 (1H, d, *J* = 6.8), 4.44 (3H, m), 4.23 (1H, t, *J* = 6.8), 3.98 (2H, m), 3.80 (3H, s), 1.86 (1H, br s). Analytical data in agreement with literature.[121]

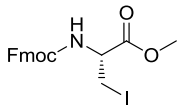

(R)-methyl 2-((((9H-fluoren-9-yl)methoxy)carbonyl)amino)-3-iodopropanoate (33) 3.0 g **32** was dissolved in 30 mL pyridine. The mixture was cooled to -5 ^{0}C before adding 3.3 g (2 equiv.) TsCl. The RM was stirred at 4 ^{0}C for 40h. The RM was poured in ice-water and was extracted using EtOAc. The EtOAc was washed with 1 M citric acid (3x), sat $NaHCO_3$, 1 M HCl (2x), sat $NaHCO_3$ and sat NaCl. The organic layer was dried and evaporated. To the oil was added ether and a crystaline solid was formed that was dried under vacuum overnight. The solid was dissolved in 20 mL acetone and the flask flushed with argon. A solution of 2.42g (2equiv.) NaI in 10 mL acetone was added dropwise and the RM was stirred overnight at RT (flask was wrapt in alumina foil). The RM was filtered and the filtrate was concentrated. The residue was suspended in chloroform and washed with water, sat. $Na_2S_2O_3$ and $NaHCO_3$.. The chloroform was dried and evaporated. The solid material was redissolved in 200 mL 1:1 Ethanol/petroleum ether and the volume was reduced with vacuum and the concentrated solution was stored at 4 ^{0}C overnight. The solid material was filtered off yielding 3.3 g **33** as a white powder (90% yield from **32**). ^{1}H-NMR(400 MHz, $CDCl_3$) δ: 7.77 (2H, d, *J* 7.5), 7.62 (2H, d, *J* 7.5), 7.41 (2H, t, *J* 7.5), 7.35-7.32 (2H, m), 5.66 (1H, d, *J* 7.0), 4.65-4.56 (1H, m), 4.45-4.36 (2H, m), 4.25 (1H, t, *J* 7.5), 3.83 (3H, s), 3.62-3.59 (2H, m). Analytical data in agreement with literature.[122]

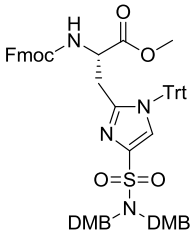

(S)-methyl-2-(((9H-fluoren-9-yl)methoxy)carbonylamino)-3-(4-(N,N-bis(2,4-dimethoxybenzyl)-sulfamoyl)-1-trityl-1H-imidazol-2-yl)propanoate (34) 65 mg (1 mmol) Zn(0) (dust) was weighted into a pear-shaped flask and flame-dried. 20 mg I_2 dissolved in 3 mL dry DMF was added (the yellow color disappeared after approx. 1 minute). 160 mg (0.36 mmol) (R)-methyl 2-(((9H-fluoren-9-yl)methoxy)-carbonylamino)-3-iodopropanoate **33** together with 20 mg iodine was added and the RM was stirred until TLC indicated full consumption of **33**.[25] The stirring was stopped and the unreacted Zn was allowed to precipitate. 2 mL of the supernatant was taken out in a syringe and directly added to a pre-stirred solution of 6 mg (0.006 mmol) $Pd_2(dba)_3$, 6 mg (0.012 mmol) Xphos and 100 mg (0.12 mmol) **29** suspended in 1 mL dry DMF. The RM was aged for 2 hours at 40 ^oC, poured into sat. $NaHCO_3$(aq) and extracted twice with EtOAc. The combined EtOAc layers were washed with sat NaCl(aq), dried over $MgSO_4$(s), concentrated and dried under vacuum. The product was purified by SiO_2 column chromatography, eluted with toluene/EtOAc (9:1) to obtain 66 mg of **34** as a pale yellow foam (53% yield from **29**). R_f = 0.63 (toluene/EtOAc 1:1). $[\alpha]_D^{20}$ +22.2° (c = 0.4, $CHCl_3$); ^{1}H-NMR(400 MHz, $CDCl_3$) δ: 7.73 (d, J=8.0Hz, 2H), 7.58 (t, J=8.0Hz, 2H), 7.35 (m, 11H), 7.22 (m, 5H), 7.06 (m, 6H), 6.45 (d, J=8.8Hz, 1H), 6.39 (dd, J=8.4Hz, J=2.4Hz, 2H), 6.28 (d, J=2.4Hz, 1H), 4.60 (d, 16.0Hz, 1H), 4.45 (d, 16.0Hz, 1H), 4.39 (m, 2H), 4.20 (m, 2H), 3.74 (s, 6H), 3.71 (s, 3H), 3.58 (s, 6H), 2.57 (dd, J=17.2Hz, J=4.0Hz, 1H)), 2.07 (dd, J=17.2Hz, J=4.0Hz, 1H); ^{13}C-NMR(101 MHz, $CDCl_3$) δ: 171.7, 160.2, 158.4, 156.5, 149.2, 144.2, 144.0, 141.4, 141.4, 141.1, 137.7, 130.5, 130.1, 128.7, 128.6, 127.9, 127.8, 127.4, 127.4, 125.6, 125.5, 125.0, 120.1, 117.9, 104.3, 98.1, 76.3, 67.6, 55.5, 55.2, 52.7, 51.7, 47.3, 46.5, 32.8; ESI HRMS calculated for $C_{59}H_{57}O_{10}N_4S$ $[M+H]^+$ = 1013.37899. Mass found $[M+H]^+$ = 1013.37950.

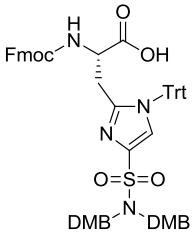

(S)-2-(((9H-fluoren-9-yl)methoxy)carbonylamino)-3-(4-(N,N-bis(2,4-dimethoxybenzyl)sulfamoyl)-1-trityl-1H-imidazol-2-yl)propanoic acid (7) 500 mg (0.49 mmol) **34** was dissolved in 10 mL DCE. 894 mg (5.0 mmol) $Sn(Me)_3OH$ was added. The RM was heated at 65 °C for 18 hours, when TLC indicated complete disappearance of SM. The RM was poured into citric acid and extracted with DCM (2x 20 mL). The DCM was dried over $MgSO_4$(s), concentrated and dried under vacuum. The product was purified by SiO_2 column chromatography, eluted with toluene/EtOAc (1:1) to obtain 425 mg of **7** as a pale yellow foam (86% yield from **34**). R_f = 0.20 (toluene/EtOAc 1:1); $[\alpha]_D^{20}$ +19.8° (c = 0.3, $CHCl_3$). ^{1}H-NMR(400 MHz, $CDCl_3$) δ: 7.76 (d, J=8.0Hz, 2H), 7.56 (d, J=8.0Hz, 1H), 7.51 (d, J=8.0Hz, 1H), 7.35 (m, 11H), 7.22 (m, 5H), 7.06 (m, 6H), 6.45 (d, J=8.8Hz, 1H), 6.39 (dd, J=8.4Hz, J=2.4Hz, 2H), 6.28 (d, J=2.4Hz, 1H), 4.60 (d, 16.0Hz, 1H), 4.45 (d, 16.0Hz, 1H), 4.39 (m, 2H), 4.20 (m, 2H), 3.74 (s, 6H), 3.71 (s, 3H), 3.58 (s, 6H), 2.57 (dd, J=17.2Hz, J=4.0Hz, 1H)), 2.07 (dd, J=17.2Hz, J=4.0Hz, 1H). ^{13}C-NMR(101 MHz, $CDCl_3$) δ: 172.2, 160.4, 158.5, 155.6, 148.9, 144.1, 144.0, 141.5, 141.4, 140.6, 137.0, 130.8, 130.0, 128.8, 128.1, 128.0, 127.5, 127.3, 125.4, 125.3, 124.9, 120.2, 117.5, 104.3, 98.3, 67.4, 55.5, 55.4, 53,7, 51.7, 47.2, 46.6, 34.2, 29.9; ESI HRMS calculated for $C_{58}H_{55}O_{10}N_4S$ $[M+H]^+$ = 999.36334. Mass found $[M+H]^+$ = 999.36386.

Peptides 37 and 38 Synthesized manually on Tentagel Rink-amide resin preloaded with glycine (0.25 mmol/g). Coupling of the Fmoc-amino acids (10 equiv) was carried out using standard HBTU/HOBt activation, except for the protected sulfonamide building block **7** (2 equiv.), which was coupled employing HATU/HOAt as activating reagents. Cleavage from the resin, as well as global deprotection, was carried out by applying a mixture of trifluoroacetic acid (TFA)/triisopropylsilane (TIPS)/H_2O (90:5:5). After filtration from the resin, an additional 10% H_2O was added to the cleavage mixture, which was allow to stir for 30 min. to ensure complete hydrolysis of the DMB-protective groups from the sulfonamide moiety. Concentration under reduced pressure at ambient temperature and trituration with diethyl ether yielded the crude peptide. After preparative reverse phase HPLC purification (C18) and subsequent lyophilization the peptides **37** and **38** were isolated as white solids.

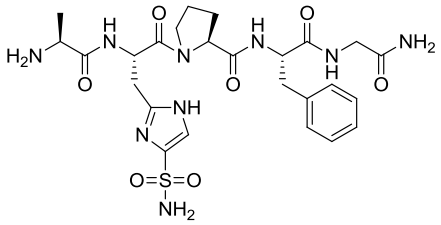

Peptide 37; Isolated was 88 mg (42% yield from 1.0 g resin). ESI HRMS calculated for $C_{25}H_{36}O_7N_9S$ $[M+H]^+$ = 606.24529. Mass found $[M+H]^+$ = 606.24433.

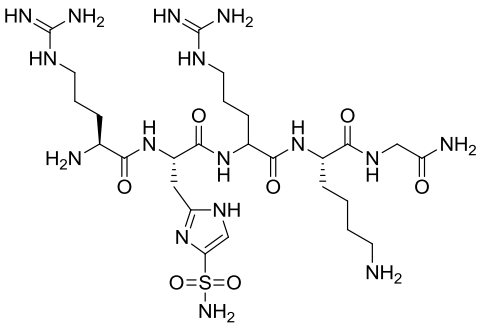

Peptide 38; Isolated was 82 mg (59% yield from 0.43 g resin). ESI HRMS calculated for $C_{26}H_{51}O_7N_{16}S$ $[M+H]^+$ = 731.38419. Mass found $[M+H]^+$ = 731.38311.

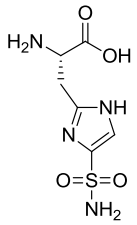

(S)-2-amino-3-(4-sulfamoyl-1H-imidazol-2-yl)propanoic acid (39) 100 mg **7** (0.1 mmol) was treated with 4 mL piperidine/DMF 2:8 for 30 min. The RM was evaporated to dryness and was co-evaporated with toluene (2x) before dissolving in 4 mL TFA/water/TiPS 90:5:5 and was stirred for 4 hours. The solvents were evaporated and the residue was taken up in methanol, filtered and was purified with prep HPLC yielding 23 mg **39** (66% yield from **7**). R_f = 0.45 (EtOAc/MM 1:2); $[\alpha]_D^{20}$ +9.9° (c = 0.2, $CHCl_3$) ; ^{1}H-NMR(400 MHz, D_2O) δ: 7.80 (s, 1H), 4.49 (t, J=..Hz, 1H), 3.52 (m, 2H); ^{13}C-NMR(101 MHz, CD_3OD) δ: 168.6, 144.8, 138.8, 120.3, 50.6, 27.2; ESI HRMS calculated for $C_6H_{11}O_4N_4S$ $[M+H]^+$ = 235.04955. Mass found $[M+H]^+$ = 235.04960.

9.8 Synthesis and evaluation of Sulfonamide-Imidazole PHP Inhibitors

General procedure A 150 mg (0.22 mmol) **27** was dissolved in 3 mL dry THF and treated dropwise with 0.2 mL 1.6 M BuLi solution (1.5 equiv) at -30 ^{0}C under argon. The red solution was stirred at this temperature for 20 minutes before 2 equiv of the appropriate electrophile dissolved in a minimum of dry THF was added dropwise. The RM was stirred for 30 minutes at -30 ^{0}C before pouring into a saturated solution of $NaHCO_3$ ($Na_2S_2O_3$ for entries: **53b**, **53e**, **53f** and **86**). The water layer was extracted 2x with EtOAc and the combined organic layers were washed with saturated NaCl solution. The EtOAc was dried over anhydrous Na_2SO_4 and evaporated to dryness. The residue was taken up in 2 mL TFA/water/TiPS 90:5:5 and stirred overnight. The solvent was removed under vacuum and the residue was suspended in MeOH, filtered and purified using preparative HPLC.

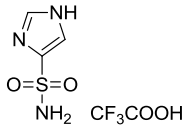

1H-imidazole-4-sulfonamide 2,2,2-trifluoroacetate (53a) Synthesized according to the TFA deprotection step from general procedure A from compound **27**, imidazole **53a** was obtained as a sticky oil (18.3 mg, 32% yield from **27**). R_f = 0.12 (DCM/MeOH 9:1); ^{1}H-NMR(400 MHz, CD_3OD) δ: 8.21 (d, J=1.2Hz, 1H), 7.74 (d, J=1.2Hz, 1H); ^{13}C-NMR(101 MHz, CD_3OD) δ: 139.9, 136.7, 119.8; ESI HRMS calculated for $C_3H_6O_2N_3S$ $[M+H]^+$ = 148.01752. Mass found $[M+H]^+$ = 148.01737.

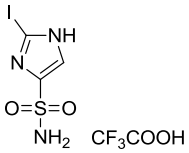

2-iodo-1H-imidazole-4-sulfonamide 2,2,2-trifluoroacetate (53b) Synthesized according to the TFA deprotection step from general procedure A from compound **27**, imidazole **53b** was obtained as an off-white solid (42.0 mg, 60% yield from **27**). R_f = 0.34 (DCM/MeOH 9:1); ^{1}H-NMR(400 MHz, CD_3OD) δ: 7.60 (s, 1H); ^{13}C-NMR(101 MHz, CD_3OD) δ: 144.8, 123.3, 110.0; ESI HRMS calculated for $C_3H_5O_2N_3IS$ $[M+H]^+$ = 273.91417. Mass found $[M+H]^+$ = 273.91407.

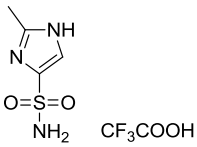

2-methyl-1H-imidazole-4-sulfonamide 2,2,2-trifluoroacetate (53c) According to general procedure A and MeI as electrophile, imidazole **53c** was obtained as a sticky oil (35,0 mg, 58% yield from **27**). Isolated as a mixture of two isomers (2- and 5-methyl). R_f = 0.15 (DCM/MeOH 9:1); ^{1}H-NMR(400 MHz, CD_3OD) δ: 8.39/7.72 (s, 1H), 2.57/2.51 (s, 3H); ^{13}C-NMR(101 MHz, CD_3OD) δ: 147.1, 137.1, 134.1, 132.9, 131.2, 119.9, 10.9, 8.8; ESI HRMS calculated for $C_4H_8O_2N_3S$ $[M+H]^+$ = 162.03317. Mass found $[M+H]^+$ = 162.03306.

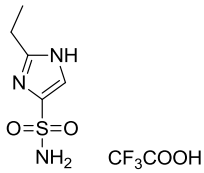

2-ethyl-1H-imidazole-4-sulfonamide 2,2,2-trifluoroacetate (53d) According to general procedure A and EtI as electrophile, imidazole **53d** was obtained as a white solid (25.4 mg, 40% yield from **27**). R_f = 0.2 (DCM/MeOH 9:1); ^{1}H-NMR(400 MHz, CD_3OD) δ: 7.71 (s, 1H), 2.91 (q, J=8.0Hz, 2H) 1.36 (t, J=8.0, 3H); ^{13}C-NMR(101 MHz, CD_3OD) δ: 151.9, 137.5, 119.8, 20.1, 10.9; ESI HRMS calculated for $C_5H_{10}O_2N_3S$ $[M+H]^+$ = 176.04882. Mass found $[M+H]^+$ = 176.04864.

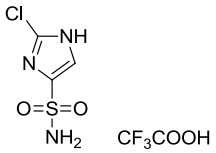

2-chloro-1H-imidazole-4-sulfonamide 2,2,2-trifluoroacetate (53e) According to general procedure A and NCS as electrophile, imidazole **53e** was obtained as a white solid (21,0 mg, 32% yield from **27**). R_f = 0.18 (DCM/MeOH 9:1); ^{1}H-NMR(400 MHz, CD_3OD) δ: 7.68 (s, 1H), 2.91 (q, J=8.0Hz, 2H) 1.36 (t, J=8.0, 3H); ^{13}C-NMR(101 MHz, CD_3OD) δ: 135.13; ESI HRMS calculated for $C_3H_5O_2N_3ClS$ $[M+H]^+$ = 181.97855. Mass found $[M+H]^+$ = 181.97844.

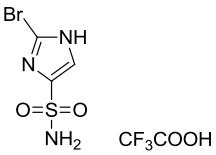

2-bromo-1H-imidazole-4-sulfonamide 2,2,2-trifluoroacetate (53f) According to general procedure A and CBr_4 as electrophile, imidazole **53f** was obtained as a white solid (42,8 mg, 57% yield from **27**). R_f = 0.28 (DCM/MeOH 9:1); ^{1}H-NMR(400 MHz, CD_3OD) δ: 7.77 (s, 1H); ^{13}C-NMR(101 MHz, CD_3OD) δ: 141.4, 122.4, 119.1; ESI HRMS calculated for $C_3H_5O_2N_3BrS$ $[M+H]^+$ = 225.92804/227.92599. Mass found $[M+H]^+$ = 225.92837/227.92624.

General procedure B 150 mg (0.18 mmol) iodine **29** was dissolved in 3 mL dioxane and 0.3 mmol boronic acid, 0.5 mL 2M K_2CO_3 solution and 10 mg $Pd(PPh_3)_4$ were added under argon atmosphere. The mixture was stirred at 80 ^{0}C till TLC indicated complete conversion of the starting material. The mixture was poured into a saturated solution of $NaHCO_3$. The water layer was extracted with EtOAc (2x) and the combined organic layers were washed with saturated NaCl solution. The EtOAc was dried over anhydrous Na_2SO_4 and evaporated to dryness. The residue was taken up in TFA/water/TiPS 90:5:5 and stirred overnight. The solvent was removed under vacuum and the residue was suspended in MeOH, filtrated and purified using preparative HPLC.

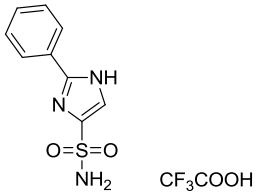

2-phenyl-1H-imidazole-4-sulfonamide 2,2,2-trifluoroacetate (56a) According to general procedure B and using phenylboronic acid, imidazole **56a** was obtained as a white solid (38,0 mg, 51% yield from **29**). R_f = 0.80 (DCM/MeOH 9:1); ^{1}H-NMR(400 MHz, CD_3OD) δ: 7.94-7.89 (m, 2H), 7.80 (s, 1H), 7.56-7.51 (m, 3H); ^{13}C-NMR(101 MHz, CD_3OD) δ: 148.1, 140.7, 130.8, 129.2, 127.0, 126.4, 120.7; ESI HRMS calculated for $C_9H_{10}O_2N_3S$ $[M+H]^+$ = 224.04882. Mass found $[M+H]^+$ = 224.04888.

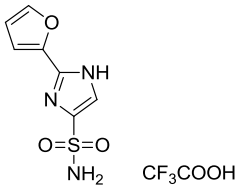

2-(furan-2-yl)-1H-imidazole-4-sulfonamide 2,2,2-trifluoroacetate (56b) According to general procedure B and using 2-furanylboronic acid, imidazole **56b** was obtained as a white solid (12.0 mg, 17% yield from **29**). R_f = 0.77 (DCM/MeOH 9:1); ^{1}H-NMR(400 MHz, CD_3OD) δ: 7.69 (m, 1H), 7.66 (s, 1H), 7.05 (m, 1H), 6.62 (m, 1H); ^{13}C-NMR(101 MHz, CD_3OD) δ: 144.4, 143.7, 141.8, 140.4, 119.8, 111.9, 109.9; ESI HRMS calculated for $C_7H_8O_3N_3S$ $[M+H]^+$ = 214.02809. Mass found $[M+H]^+$ = 214.02819.

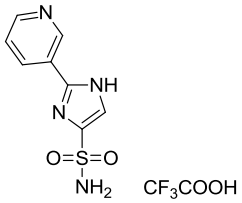

2-(pyridin-3-yl)-1H-imidazole-4-sulfonamide 2,2,2-trifluoroacetate (56c) According to general procedure B and using 3-pyridinylboronic acid, imidazole **56c** was obtained as a white solid (4.2 mg, 6% yield from **29**). R_f = 0.33 (DCM/MeOH 9:1); ^{1}H-NMR(400 MHz, $CDCl_3$) δ: 9.21 (d, J=2.0Hz, 1H), 8.71 (dd, J=2.0Hz, J=5.0Hz, 1H), 8.62 (dt, J=2.0Hz, J=8.0Hz, 1H), 7.82 (m, 1H), 7.78 (s, 1H); ESI HRMS calculated for $C_8H_9O_2N_4S$ $[M+H]^+$ = 225.04407. Mass found $[M+H]^+$ = 225.04342.

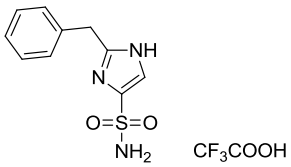

2-benzyl-1H-imidazole-4-sulfonamide 2,2,2-trifluoroacetate (56d) 52 mg (0.8 mmol) Zn(0) (dust) was weighted into a pear-shaped flask and flame-dried. 18 mg I_2 dissolved in 2 mL dry DMF was added (the yellow color disappeared after approx. 1 minute). 65 mg (0.33 mmol) benzyl iodine together with 18 mg iodine was added and the RM was stirred until TLC indicated full consumption. The stirring was stopped and the unreacted Zn was allowed to precipitate. 2 mL of the supernatant was taken out in a syringe and directly added to a pre-stirred solution of 8 mg (0.006 mmol) $PdCl_2(PPh_3)_2$ and 200 mg (0.18 mmol) iodine **29** suspended in 1.5 mL dry DMF. The RM was aged for 2 hours at 40 ^{0}C, poured into sat. $NaHCO_3$ (aq) and extracted (2x) with EtOAc. The combined EtOAc layers were washed with sat NaCl (aq), dried over $MgSO_4$ (s), concentrated and dried under vacuum. The residue was taken up in TFA/water/TiPS 90:5:5 and stirred overnight. The solvent was removed under vacuum and the residue was purified using preparative HPLC. Imidazole **56d** was obtained as a white solid (16 mg, 18% yield from **29**). R_f = 0.60 (DCM/MeOH 9:1); ^{1}H-NMR(400 MHz, D_2O) δ: 7.74 (s, 1H), 7.35-7.20 (m, 5H), 4.24 (s, 2H); ^{13}C-NMR(101 MHz, D_2O) δ: 149.9, 134.2, 133.4, 129.5, 129.1, 128.3, 121.7, 32.1; ESI HRMS calculated for $C_{10}H_{12}O_2N_3S$ $[M+H]^+$ = 238.06447. Mass found $[M+H]^+$ = 238.06459.

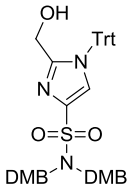

2N,N-bis(2,4-dimethoxybenzyl)-2-(hydroxymethyl)-1-trityl-1H-imidazole-4-sulfonamide (58) 1.2 g (1.67 mmol) **23** was suspended in 22 mL dry MeOH and warmed to 45 ^{0}C. The solid dissolved and 126 mg (3.34 mmol) $NaBH_4$ was added and the RM stirred for 2 hours at 45 ^{0}C. The RM was diluted with DCM and was washed with sat $NaHCO_3$, dried over Na_2SO_4 and evaporated to obtain alcohol **58** as an off-white foam (1.15 g, 96% yield from **23**). R_f = 0.45 (cyclohexane/EtOAc 1:1); ^{1}H-NMR(400 MHz, $CDCl_3$) δ: 7.37-7.33 (m, 10H), 7.27 (d, J=8.4Hz, 2H), 7.03 (m, 6H), 6.37 (dd, J=8.4Hz, J=2.4Hz, 2H), 6.33 (d, J=2,4Hz, 1H), 4.51 (s, 4H), 3.74 (s, 6H), 3.66 (s, 6H), 3.57 (s, 2H), 2.85 (bs, 1H); ^{13}C-NMR(101 MHz, $CDCl_3$) δ: 160.3, 158.5, 151.3, 141.1, 137.9, 130.7, 129.9, 128.8, 128.7, 125.1, 117.8, 104.1, 98.1, 76.2, 59.3, 55.5, 55.3, 46.1; ESI HRMS calculated for $C_{41}H_{42}O_7N_3S$ $[M+H]^+$ = 720.27380. Mass found $[M+H]^+$ = 720.27378.

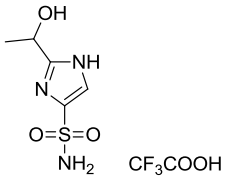

2-(1-hydroxyethyl)-1H-imidazole-4-sulfonamide 2,2,2-trifluoroacetate (60a) 100 mg (0.14mmol) **23** was dissolved in 2 mL dry THF and cooled to 0 ^{0}C. 75 µL (0.22 mmol) MeMgBr (3M in ether) was added dropwize and the RM was allowed to stir for 30 min. at 0 ^{0}C and 1 hour ar RT. The RM was diluted with DCM and washed with sat. $NaHCO_3$ solution. The DCM was dried over $MgSO_4$ and evaporated. Deprotection was performed according to the TFA deprotection step from general procedure A and imidazole **60a** was obtained as an off-white solid (23 mg, 54% yield from **23**). R_f = 0.10 (DCM/MeOH 9:1); ^{1}H-NMR(400 MHz, CD_3OD) δ: 7.69 (s, 1H), 5.00 (q, J=8.0Hz, 1H), 1.55 (d, J=8.0Hz, 3H); ^{13}C-NMR(101 MHz, CD_3OD) δ: 154.0, 138.7, 119.7, 62.9, 21.6; ESI HRMS calculated for $C_5H_{10}O_3N_3S$ $[M+H]^+$ = 192.04374. Mass found $[M+H]^+$ = 192.04368.

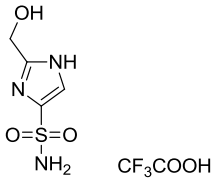

2-(hydroxymethyl)-1H-imidazole-4-sulfonamide 2,2,2-trifluoroacetate (60c) Synthesized according to the TFA deprotection step from general procedure A from compound **58**, imidazole **60c** was obtained as an off-white solid (18 mg, 44% yield from **58**). R_f = 0.08 (DCM/MeOH 9:1); ^{1}H-NMR(400 MHz, D_6-DMSO) δ: 12.40 (bs, 1H), 7.44 (s, 1H), 7.06 (bs, 2H), 4.45 (s, 2H); ^{13}C-NMR(101 MHz, D_6-DMSO) δ: 149.9, 142.5, 119.1, 57.4; ESI HRMS calculated for $C_4H_8O_3N_3S$ $[M+H]^+$ = 178.02809. Mass found $[M+H]^+$ = 178.02798.

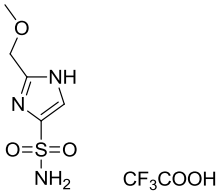

2-(methoxymethyl)-1H-imidazole-4-sulfonamide 2,2,2-trifluoroacetate (60d) 100 mg (0.14 mmol) **23** was reduced as described for **58** and the solid material was dissolved in 5 mL dry THF, cooled to 0 ^{0}C and 28 mg (0.7 mmol) NaH was added. The RM was stirred for 30 min. at 0 ^{0}C and 30 min. at RT. 35 µL MeI (0.56 mmol) was added and the RM was allowed to stir overnight. The RM was diluted with DCM and washed with sat. $NaHCO_3$ solution. The DCM was dried over $MgSO_4$ and evaporated. Deprotection was performed according to the TFA deprotection step from general procedure A and imidazole **60d** was obtained as an oil (45 mg, 42% yield from **23**). R_f = 0.22 (DCM/MeOH 9:1); ^{1}H-NMR(400 MHz, CD_3OD) δ: 7.70 (s, 1H), 4.58 (s, 2H), 3.43 (s, 2H); ^{13}C-NMR(101 MHz, CD_3OD) δ: 147.2, 139.8, 120.1, 65.7, 58.1; ESI HRMS calculated for $C_5H_{10}O_3N_3S$ $[M+H]^+$ = 192.04374. Mass found $[M+H]^+$ = 192.04361.

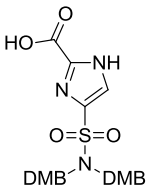

4-(N,N-bis(2,4-dimethoxybenzyl)sulfamoyl)-1H-imidazole-2-carboxylic acid (61) 500 mg (0.72 mmol) **27** was dissolved in 10 mL dry THF and cooled to -30 ^{0}C. 0.68 mL (1.5 equiv) 1.6 M BuLi solution was added dropwise and the RM was stirred for 20 min. before transferring it through a cannula into a suspension of crushed CO_2 pallets in 5 mL dry THF. The mixture was allowed to reach RT over 2 hours and was taken up in diluted 5% citric acid solution. The product was extracted using EtOAc (3x) and the combined organic layers were washed with sat $NaHCO_3$ solution, dried over Na_2SO_4(s) and concentrated. The product was purified by SiO_2 column chromatography, eluted with DCM/MeOH (from 98:2 to 9:1) to obtain 330 mg of **61** as an off-white foam (93% yield from **27**). R_f = 0.13 (DCM/MeOH 9:1); ^{1}H-NMR(400 MHz, CD_3OD) δ: 7.71 (s, 1H), 7.05 (d, J=8.4Hz, 2H), 6.36-6.30 (m 4H), 4.49 (s, 4H), 3.73 (s, 6H), 3.64 (s, 6H); ^{13}C-NMR(101 MHz, CD_3OD) δ: 160.8, 159.6, 158.5, 136.2, 130.4, 128.3, 116.9, 104.0, 97.6, 54.6, 54.4, 46.9; ESI HRMS calculated for $C_{22}H_{26}O_8N_3S$ $[M+H]^+$ = 492.14351. Mass found $[M+H]^+$ = 492.14294.

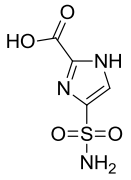

4-sulfamoyl-1H-imidazole-2-carboxylic acid (62) Synthesized according to the deprotection step from general procedure A from 60 mg (0.12 mmol) carboxylic acid **61**, imidazole **62** was obtained as a sticky oil (16 mg, 44% yield from **61**). R_f = 0.03 (DCM/MeOH 9:1); ^{1}H-NMR(400 MHz, D_6-DMSO) δ: 13.40 (bs, 1H), 7.70 (s, 1H), 7.28 (bs, 2H); ^{13}C-NMR(101 MHz, D_6-DMSO) δ: 175.1, 171.9, 136.7, 73.1; ESI HRMS calculated for $C_4H_6O_4N_3S$ $[M+H]^+$ = 192.00735. Mass found $[M+H]^+$ = 192.00735.

General procedure C 90 mg (0.18 mmol) **61** was dissolved in 1 mL dry DMF and the appropriate amine (0.22 mmol), 112 mg (0.22 mmol) PyBOP and 38 µL DiPEA (0.36 mmol) were added. The RM was stirred till TLC indicated complete conversion before concentration under vacuum. The residue was dissolved in EtOAc and washed with a saturated solution of $NaHCO_3$. The organic layer was washed with saturated NaCl(aq) solution. The EtOAc was dried over anhydrous Na_2SO_4 and evaporated to dryness. The residue was taken up in 2 mL TFA/water/TiPS 90:5:5 and stirred overnight. The solvent was removed under vacuum and the residue was suspended in MeOH, filtered and purified using prep HPLC.

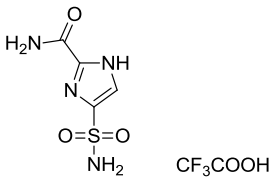

4-sulfamoyl-1H-imidazole-2-carboxamide 2,2,2-trifluoroacetate (64a) According to general procedure C and *N,N*-bis(2,4-dimethoxybenzyl)amine as nucleophile, imidazole **64a** was obtained as a white solid (12 mg, 22% yield from **61**). R_f = 0.21 (DCM/MeOH 9:1); ^{1}H-NMR(400 MHz, CD_3OD) δ: 8.08 (bs, 1H), 7.82 (bs, 2H), 7.62 (s, 1H); ESI HRMS calculated for $C_4H_7O_3N_4S$ $[M+H]^+$ = 191.02334. Mass found $[M+H]^+$ = 191.02331.

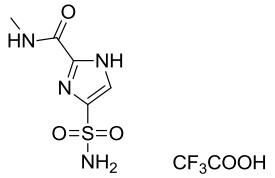

N-methyl-4-sulfamoyl-1H-imidazole-2-carboxamide 2,2,2-trifluoroacetate (64b) According to general procedure C and methylamine HCl as nucleophile, imidazole **64b** was obtained as a white solid (43 mg, 75% yield from **61**). R_f = 0.08 (DCM/MeOH 9:1); ^{1}H-NMR(400 MHz, D_6-DMSO) δ: 13.40 (bs, 1H), 8.53 (bs, 1H), 7.83 (s, 1H), 7.62 (bs, 2H), 2.79 (s, 3H); ^{13}C-NMR(101 MHz, D_6-DMSO) δ: 107.63, 26.54; ESI HRMS calculated for $C_5H_9O_3N_4S$ $[M+H]^+$ = 205.03899. Mass found $[M+H]^+$ = 205.03910.

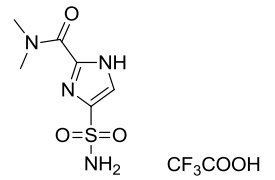

N,N-dimethyl-4-sulfamoyl-1H-imidazole-2-carboxamide 2,2,2-trifluoroacetate (64c) According to general procedure C and *N,N*-dimethylamine HCl as nucleophile, imidazole **64c** was obtained as a white solid (37 mg, 62% yield from **61**). R_f = 0.15 (DCM/MeOH 9:1); ^{1}H-NMR(400 MHz, CD_3OD) δ: 7.98 (s, 1H), 3.09 (s, 3H), 3.00 (s, 3H); ^{13}C-NMR(101 MHz, CD_3OD) δ: 162.5, 136.4, 136.1, 128.2, 37.9, 34.2; ESI HRMS calculated for $C_6H_{11}O_3N_4S$ $[M+H]^+$ = 219.05464. Mass found $[M+H]^+$ = 219.05464.

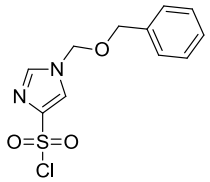

1-((benzyloxy)methyl)-1H-imidazole-4-sulfonyl chloride (66) 5.0 g (30.0 mmol) **24** was dissolved in 100 mL acetonitrile and 4.5 mL (33.0 mmol) BOM-Cl was added and the RM was stirred overnight at RT. The RM was concentrated, resuspended in DCM and loaded onto a silica column. The product was eluted with cyclohexane/EtOAc 2:1 to 1:1 and 6.8 g **66** was obtained as a transparent oil that turns solid upon freezer storage (79% yield from **24**). R_f = 0.55 (chex/EtOAc 1:1); ^{1}H-NMR(400 MHz, $CDCl_3$) δ: 7.76 (s, 1H), 7.70 (s, 1H), 7.41-7.27 (m, 5H), 5.40 (s, 2H), 4.56 (s, 2H); ^{13}C-NMR(101 MHz, $CDCl_3$) δ: 144.2, 138.9, 135.3, 129.2, 129.1, 128.3, 124.0, 76.3, 71.7.

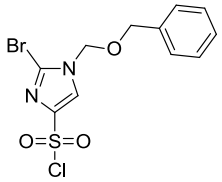

1-((benzyloxy)methyl)-2-bromo-1H-imidazole-4-sulfonyl chloride (68) 2.0 g (7.0 mmol) **66** was dissolved in 50 mL chloroform and 1.4 g NBS (7.87 mmol) was added. The reaction was stirred for 4 hours at 50 ^{0}C. The RM was concentrated to an oil and loaded onto a silica column. The product was eluted with cyclohexane/EtOAc 4:1 to 2:1 and 1.1 g **68** was obtained as a transparent oil that turns solid upon freezer storage (43% yield from **66**). R_f = 0.67 (chex/EtOAc 1:1); ^{1}H-NMR(400 MHz, $CDCl_3$) δ: 7.75 (s, 1H), 7.41-7.28 (m, 5H), 5.41 (s, 2H), 4.61 (s, 2H); ^{13}C-NMR(101 MHz, $CDCl_3$) δ: 143.8, 135.4, 129.11, 129.07, 128.2, 126.3, 122.9, 77.1, 72.2.

General procedure D 100 mg (0.27 mmol) **68** was dissolved in 1.5 mL DCM and the appropriate amine (0.5 mmol) and 175 µL (1.0 mmol) DiPEA were added. The RM was stirred overnight at RT. The RM was washed with sat $NaHCO_3$ solution, dried over Na_2SO_4(s) and evaporated the residue was taken up in 1 mL TFA and 1 mL 48% HBr in water and stirred overnight. The solvent was removed and the residu purified with prep HPLC.

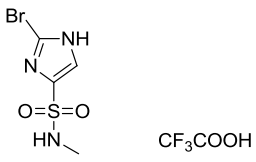

2-bromo-N-methyl-1H-imidazole-4-sulfonamide 2,2,2-trifluoroacetate (69a) According to general procedure D and using methylamine HCl, imidazole **69a** was obtained as a white solid (33 mg, 35% yield from **68**). R_f = 0.50 (DCM/MeOH 9:1); ^{1}H-NMR(400 MHz, CD_3OD) δ: 7.76 (s, 1H), 2.61 (s, 1H); ^{13}C-NMR(101 MHz, CD_3OD) δ: 138.5, 124.0, 119.4, 28.1; ESI HRMS calculated for $C_4H_7O_2N_3BrS$ $[M+H]^+$ = 239.94369. Mass found $[M+H]^+$ = 239.94380.

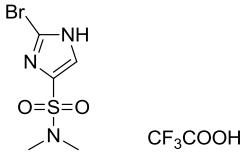

2-bromo-N,N-dimethyl-1H-imidazole-4-sulfonamide 2,2,2-trifluoroacetate (69b) According to general procedure D and using *N,N*-dimethylamine HCl, imidazole **69b** was obtained as a white solid (57 mg, 57% yield from **68**). R_f = 0.70 (DCM/MeOH 9:1); ^{1}H-NMR(400 MHz, CD_3OD) δ: 7.48 (s, 1H), 2.76 (s, 6H); ^{13}C-NMR(101 MHz, CD_3OD) δ: 137.0, 124.6, 119.5, 38.0; ESI HRMS calculated for $C_5H_9O_2N_3BrS$ $[M+H]^+$ = 253.95934. Mass found $[M+H]^+$ = 253.95950.

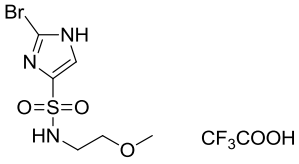

2-bromo-N-(2-methoxyethyl)-1H-imidazole-4-sulfonamide 2,2,2-trifluoroacetate (69c) According to general procedure D and using 2-methoxyethylamine, imidazole **69c** was obtained as a white solid (48 mg, 45% yield from **68**). R_f = 0.60 (DCM/MeOH 9:1); ^{1}H-NMR(400 MHz, CD_3OD) δ: 7.64 (s, 1H), 3,41 (t, J=5.6Hz, 2H), 3.29 (s, 3H), 3.12 (t, J=5.6Hz, 2H); ^{13}C-NMR(101 MHz, CD_3OD) δ: 140.87, 123.49, 118.92, 71.08, 57.70, 42.55; ESI HRMS calculated for $C_6H_{11}O_3N_3BrS$ $[M+H]^+$ = 283.96990. Mass found $[M+H]^+$ = 283.97001.

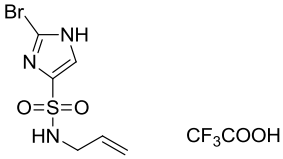

N-allyl-2-bromo-1H-imidazole-4-sulfonamide 2,2,2-trifluoroacetate (69d) According to general procedure D and using allylamine, imidazole **69d** was obtained as a white solid (25 mg, 24% yield from **68**). R_f = 0.54 (DCM/MeOH 9:1); ^{1}H-NMR(400 MHz, CD_3OD) δ: 7.64 (s, 1H), 5.76 (m, 1H), 5.18 (m, 1H), 5.05 (m, 1H), 3.58 (m, 2H); ^{13}C-NMR(101 MHz, CD_3OD) δ: 140.78, 134.04, 123.62, 118.98, 115.84, 45.38; ESI HRMS calculated for $C_6H_9O_2N_3BrS$ $[M+H]^+$ = 265.95934. Mass found $[M+H]^+$ = 265.95946.

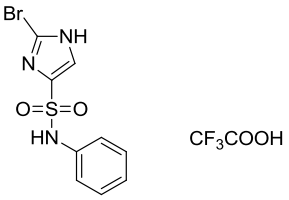

2-bromo-N-phenyl-1H-imidazole-4-sulfonamide 2,2,2-trifluoroacetate (69e) According to general procedure D and using aniline, imidazole **69e** was obtained as a white solid (52 mg, 46% yield from **68**). R_f = 0.57 (DCM/MeOH 9:1); ^{1}H-NMR(400 MHz, CD_3OD) δ: 7.57 (s, 1H), 7.22 (dt, J=1.2Hz, J=8.8Hz, 2H), 7.13 (dd, J=1.2Hz, J=8.8Hz, 2H), 7.04 (tt, J=1.2Hz, J=8.8Hz, 1H); ^{13}C-NMR(101 MHz, CD_3OD) δ: 137.56, 128.84, 124.71, 124.42, 120.88, 119.02; ESI HRMS calculated for $C_9H_9O_2N_3BrS$ $[M+H]^+$ = 301.95934. Mass found $[M+H]^+$ = 301.95938.

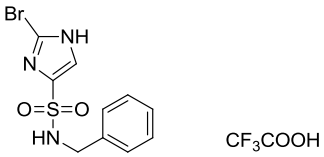

N-benzyl-2-bromo-1H-imidazole-4-sulfonamide 2,2,2-trifluoroacetate (69f) According to general procedure D and using benzylamine, imidazole **69f** was obtained as a white solid (40 mg, 43% yield from **68**). R_f = 0.58 (DCM/MeOH 9:1); ^{1}H-NMR(400 MHz, CD_3OD) δ: 7.54 (s, 1H), 7.27-7.18 (m, 5H), 4.15 (s, 2H); ^{13}C-NMR(101 MHz, CD_3OD) δ: 140.93, 137.50, 128.14, 127.72, 127.21, 123.65, 118.91, 46.68; ESI HRMS calculated for $C_{10}H_{11}O_2N_3BrS$ $[M+H]^+$ = 315.97499. Mass found $[M+H]^+$ = 315.97517.

General procedure E 50 mg (0.13 mmol) **68**, 34 mg (0.26 mmol) Na_2SO_3 and 23 mg (0.26 mmol) $NaHCO_3$ were suspended in 0.5 mL water. The RM was allowed to run for 3 hours during which the sulfonylchloride slowly goes into solution. 4.2 mg (0.013 mmol) tetra-*n*-butylammonium bromide and 0.20 mmol halide was added and the RM was stirred overnight. The RM was evaporated, the residue was taken up in 1 mL TFA and 1 mL 48% HBr in water and the mixture was stirred overnight at RT. The solvent was removed and the residu purified with prep HPLC.

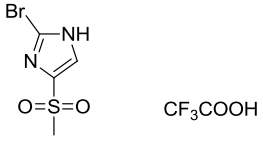

2-bromo-4-(methylsulfonyl)-1H-imidazole 2,2,2-trifluoroacetate (70a) According to general procedure E and using iodomethane, imidazole **70a** was obtained as a white solid (25 mg, 53% yield from **68**). R_f = 0.37 (DCM/MeOH 9:1); ^{1}H-NMR(400 MHz, CD_3OD) δ: 7.79 (s, 1H), 3.12 (s, 3H); ^{13}C-NMR(101 MHz, CD_3OD) δ: 141.50, 124.39, 119.66, 42.16; ESI HRMS calculated for $C_4H_6O_2N_2BrS$ $[M+H]^+$ = 224.93279. Mass found $[M+H]^+$ = 224.93299.

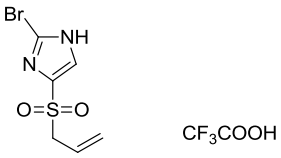

4-(allylsulfonyl)-2-bromo-1H-imidazole 2,2,2-trifluoroacetate (70b) According to general procedure E and using allylbromide, imidazole **70b** was obtained as a white solid (18 mg, 35% yield from **68**). R_f = 0.50 (DCM/MeOH 9:1); ^{1}H-NMR(400 MHz, CD_3OD) δ: 7.77 (s, 1H), 5.79 (m, 1H), 5.34 (m, 1H), 5.23 (m, 1H), 3.97 (m, 2H); ^{13}C-NMR(101 MHz, CD_3OD) δ: 139.19, 126.10, 124.93, 123.67, 119.76, 58.92; ESI HRMS calculated for $C_6H_8O_2N_4BrS$ $[M+H]^+$ = 250.94844. Mass found $[M+H]^+$ = 250.94804.

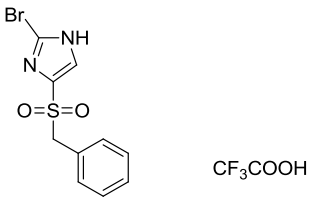

4-(benzylsulfonyl)-2-bromo-1H-imidazole 2,2,2-trifluoroacetate (70c) According to general procedure E and using benzylbromide, imidazole **70c** was obtained as a white solid (29 mg, 50% yield from **68**). R_f = 0.60 (DCM/MeOH 9:1); ^{1}H-NMR(400 MHz, CD_3OD) δ: 7.50 (s, 1H), 7.33-7.27 (m, 3H), 7.21-7.17 (m, 2H), 4.50 (s, 2H); ^{13}C-NMR(101 MHz, CD_3OD) δ: 138.50, 130.87, 128.55, 128.53, 128.34, 126.38, 119.83, 60.69; ESI HRMS calculated for $C_{10}H_{10}O_2N_2BrS$ $[M+H]^+$ = 300.96409. Mass found $[M+H]^+$ = 300.96418.

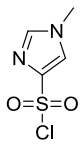

1-methyl-1H-imidazole-4-sulfonyl chloride (75) 24.1 g (294 mmol) N-methylimidazole (**74**) was melted in an argon flushed 250 mL flask. 60.0 mL (900 mmol) $ClSO_3H$ was added drop wise (Caution! the first 15 mL reacted violently, with excessive HCl(g) formation). The reaction mixture was heated at 140 ^oC for 16 hours. The resulting dark reaction mixture (RM) was cooled to 40 ^oC before adding 22.0 mL (302 mmol) thionyl chloride drop wise over 5 minutes (immediate gas evolution visible). The RM was heated until gas evolution ceased, during which time the temperature was slowly raised to 125 °C. The RM was allowed to cool to RT before pouring it into a slurry of 300 g crushed ice with 20.0 g NaCl. A white precipitate was formed and the suspension was filtered after the ice had completely melted. The white solid was washed with a small amount of cold water and dried overnight under vacuum over KOH. The filtrate was re-filtered once and the collected solid was washed with a small amount of water and dried overnight under vacuum over KOH. Combining the two solids yielded 16.2 g **75** as a fine white powder (31% yield from **74**). ^{1}H-NMR(400 MHz, DMSO-d_6) δ: 8.93 (d, J=1.2Hz, 1H), 7.68 (d, J=1.2Hz, 1H) Analytical data in agreement with literature.[115]

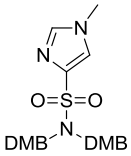

N,N-bis(2,4-dimethoxybenzyl)-1-methyl-1H-imidazole-4-sulfonamide (76) 1.0 g (5.54 mmol) **75** was added in portions to a solution of 1.27 g (4.0 mmol) *N*,*N*-bis(2,4-dimethoxybenzyl)amine in 40 mL DCM with 2.1 mL (12.0 mmol) DiPEA at 0 ^{0}C. The RM was stirred at 0 ^{0}C for 30 min. before allowing it to warm to RT. The RM was stirred at RT overnight. The RM was washed with $NaHCO_3$, dried over $MgSO_4$(s), concentrated and dried under vacuum. The product was purified by SiO_2 column chromatography, eluted with toluene/EtOAc (1:1 to 1:3) to obtain 1.52 g of **76** as a white foam (82% yield from **75**). R_f = 0.15 (toluene/EtOAc 1:1); ^{1}H-NMR(400 MHz, $CDCl_3$) δ: 7.40 (d, J=1.2Hz, 1H), 7.23 (d, J=8.4Hz, 2H), 7.12 (d, J=1.2Hz, 1H), 6.35 (dd, J=8.4Hz, J=2.4Hz, 2H), 6.24 (d, J=2,4Hz, 1H), 4.46 (s, 4H), 3.75 (s, 6H), 3.61 (s, 6H), 3.60 (s, 3H); ^{13}C-NMR(101 MHz, $CDCl_3$) δ: 160.3, 158.4, 141.5, 138.7, 130.8, 123.8, 117.9, 103.9, 97.9, 55.6, 55.2, 47.1, 33.9; ESI HRMS calculated for $C_{22}H_{28}O_6N_3S$ $[M+H]^+$ = 462.16933. Mass found $[M+H]^+$ = 462.16875.

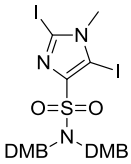

N,N-bis(2,4-dimethoxybenzyl)-2,5-diiodo-1-methyl-1H-imidazole-4-sulfonamide (77) 400 mg (0.87 mmol) **76** was suspended in 10 mL dry THF and 2 mL HMPA in a flame dried Schlenk flask. The reaction mixture was cooled to -30 ^{0}C under argon. 1.1 mL (1.76 mmol) 1.6 M BuLi solution is added dropwize. The RM becomes dark blue. After 10 min. at -30 ^{0}C 400 mg iodine (1.76 mmol) dissolved in 3 mL dry THF was added dropwize. The RM was stirred at -30 ^{0}C for 10 min and allowed to reach RT when it was poured into a sat. $Na_2S_2O_3$ solution and was extracted twice with EtOAc. The combined EtOAc layers were washed with brine, dried over $MgSO_4$(s), concentrated and dried under vacuum. The product was purified by SiO_2 column chromatography, eluted with toluene/EtOAc (4:1) to obtain 514 mg of **77** as a white foam (83% yield from **76**). R_f = 0.75 (EtOAc); ^{1}H-NMR(400 MHz, $CDCl_3$) δ: 7.21 (d, J=8.4Hz, 2H), 6.35 (dd, J=8.4Hz, J=2.4Hz, 2H), 6.28 (d, J=2,4Hz, 1H), 4.51 (s, 4H), 3.76 (s, 6H), 3.68 (s, 6H), 3.59 (s, 3H); ^{13}C-NMR(101 MHz, $CDCl_3$) δ: 160.3, 158.4, 148.2, 130.9, 117.7, 104.0, 97.9, 92.3, 55.6, 55.3, 47.2, 39.0; ESI HRMS calculated for $C_{22}H_{26}O_6N_3I_2S$ $[M+H]^+$ = 713.96262. Mass found $[M+H]^+$ = 713.96321.

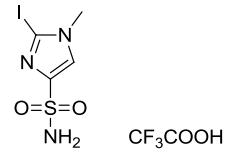

2-iodo-1-methyl-1H-imidazole-4-sulfonamide 2,2,2-trifluoroacetate (71) Synthesized according to the deprotection step from general procedure A from 100 mg **77**, imidazole **71** was obtained as a sticky oil (23 mg, 41% from **77**). R_f = 0.18 (DCM/MeOH 9:1); ^{1}H-NMR(400 MHz, CD_3OD) δ: 9.15 (s, 1H), 3.89 (s, 3H); ^{13}C-NMR(101 MHz, CD_3OD) δ: 139.32, 138.58, 82.92, 37.58; ESI HRMS calculated for $C_4H_7O_2N_3IS$ $[M+H]^+$ = 287.92982. Mass found $[M+H]^+$ = 287.92969.

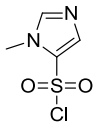

1-methyl-1H-imidazole-5-sulfonyl chloride (78) 3 g (18 mmol) **24** was suspended in 10 mL 78% formic acid. 1.8 mL (19 mmol) Me_2SO_4 was added and the RM was stirred overnight at RT. The RM was poored carefully into a saturated $NaHCO_3$ solution and extracted with DCM (3x). The DCM was dried over Na_2SO_4(s) and evaporated to dryness giving 2.1 g **78** as a white powder (58% yield from **24**). ^{1}H-NMR(400 MHz, DMSO-d_6) δ: 9.02 (d, J=1.2Hz, 1H), 7.63 (d, J=1.2Hz, 1H), 3.89 (s, 3H). Analytical data in agreement with literature.[116]

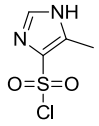

5-methyl-1H-imidazole-4-sulfonyl chloride (83) 20 g (244 mmol) 4(5)-methylimidazole (**82**) was melted in an argon flushed 250 mL flask. 60.0 mL (900 mmol) $ClSO_3H$ was added drop wise (Caution! the first 15 mL reacted violently, with excessive HCl(g) formation). The reaction mixture was heated at 140 ^{o}C for 16 hours. The resulting dark reaction mixture (RM) was cooled to 40 ^{o}C before adding 22.0 mL (302 mmol) thionyl chloride drop wise over 5 minutes (immediate gas evolution visible). The RM was heated until gas evolution ceased, during which time the temperature was slowly raised to 125 °C and was stirred for 6 hours. The RM was allowed to cool to RT before pouring it into a slurry of 300 g crushed ice with 20.0 g NaCl. A white precipitate was formed and the suspension was filtered after the ice had completely melted. The white solid was washed with a small amount of cold water and dried overnight under vacuum over KOH. The filtrate was re-filtered once and the collected solid was washed with a small amount of water and dried overnight under vacuum over KOH. Combining the two solids yielded 17.1 g **83** as a fine white powder (39% yield from **82**). ^{1}H-NMR(400 MHz, DMSO-d_6) δ: 12.24 (bs, 1H), 8.83 (s, 1H), 2.32 (s, 3H).

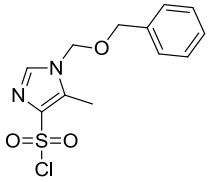

1-((benzyloxy)methyl)-5-methyl-1H-imidazole-4-sulfonyl chloride (84) 5.0 g (27.7 mmol) **83** was dissolved in 150 mL acetonitrile and 4.12 mL (30.0 mmol) BOM-Cl was added and the RM was stirred overnight at RT. The RM was concentrated, resuspended in DCM and loaded onto a silica column. The product was eluted with cyclohexane/EtOAc 2:1 to 1:1 and 4.2 g **84** was obtained as a transparent oil that turns solid upon freezer storage (50 % from **83**). R_f = 0.45 (chex/EtOAc 1:1); ^{1}H-NMR(400 MHz, $CDCl_3$) δ: 7.56 (bs, 1H), 7.42-7.25 (m, 5H), 5.34 (s, 2H), 4.54 (s, 2H), 2.60 (s, 3H); ^{13}C-NMR(101 MHz, $CDCl_3$) δ: 140.5, 138.3, 135.5, 135.1, 129.1, 129.0, 128.3, 74.8, 71.4, 9.7.

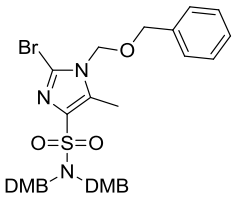

2-iodo-5-methyl-1H-imidazole-4-sulfonamide (85) 1.0 g (3,3 mmol) **84** was dissolved in 25 mL $CHCl_3$ and 700 mg NBS (3.9 mmol) was added. The reaction mixture was stirred for 3 hours at 50 ºC. The RM was poured into a sat. $Na_2S_2O_3$ solution and was extracted twice with DCM. The DCM was dried over Na_2SO_4(s) and evaporated to dryness. The solid material was dissolved in 5 mL DCM and added dropwise to a solution of 1.27 g (4.0 mmol) *N*,*N*-bis(2,4-dimethoxybenzyl)amine and 0.9 mL (1.0 mmol) DiPEA in 30 mL DCM at 0 ^{0}C. The RM was for 3 hours at RT and was poured into a sat. $NaHCO_3$ (aq) solution and was extracted twice with DCM. The combined DCM layers were washed with brine, dried over $MgSO_4$(s), concentrated and dried under vacuum. The residue was taken up in DCM and purified using silica chromatography (cyclohexane/EtOAc 4:1 to 1:1) obtaining 356 mg imidazole **85** as a white solid (16 % yield from **84**). Rf = 0.60 (chex/EtOAc 1:1); ^{1}H-NMR(400 MHz, $CDCl_3$) δ: 7.33 (m, 5H), 7.22 (d, J=8.4Hz, 2H), 6.34 (dd, J=8.4Hz, J=2.4Hz, 2H), 6.26 (d, J=2,4Hz, 2H), 5.24 (s, 2H), 4.49 (s, 2H), 3.73 (s, 6H), 3.66 (s, 6H), 2.41 (s, 3H); ^{13}C-NMR(101 MHz, $CDCl_3$) δ: 160.26, 158.41, 138.34, 136.32, 134.66, 130.67, 128.87, 128.59, 127.96, 119.91, 117.84, 103.93, 97.92, 74.12, 70.96, 55.53, 55.23, 47.12, 10.11; ESI HRMS calculated for $C_{30}H_{35}O_7N_3BrS$ $[M+H]^+$ = 660.13736. Mass found $[M+H]^+$ = 660.13747

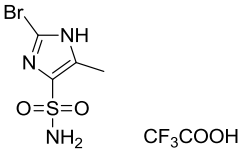

2-iodo-5-methyl-1H-imidazole-4-sulfonamide 2,2,2-trifluoroacetate (73) Synthesized according to the deprotection step from general procedure A from 200 mg (0.30 mmol) **85**. Imidazole **73** was obtained as a white solid (53 mg, 50% yield from **85**). R_f = 0.40 (DCM/MeOH 9:1); ^{1}H-NMR(400 MHz, DMSO-d_6) δ: 13.12 (bs, 1H), 7.12 (bs, 2H), 2.31 (s, 3H); ^{13}C-NMR(101 MHz, DMSO-d_6) δ: 139.5, 132.1, 115.5, 10.8; ESI HRMS calculated for $C_{58}H_{55}O_{10}N_4S$ $[M+H]^+$ = 239.94369. Mass found $[M+H]^+$ = 239.94380.

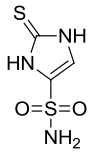

2-mercapto-1H-imidazole-4-sulfonamide (86) According to general procedure A and S_8 as electrophile (added as a suspension in dry THF). Imidazole **86** was obtained as a white solid (18 mg, 12% yield from **27**). R_f = 0.27 (DCM/MeOH 9:1); ^{1}H-NMR(400 MHz, DMSO-d_6) δ: 12.78 (bs, 1H), 12.43 (bs, 1H), 7.43 (bs, 2H), (t, J=2.4Hz, 1H); ^{13}C-NMR(101 MHz, CD_3OD) δ: 163.5, 131.1, 118.5; ESI HRMS calculated for $C_3H_6O_2N_3S_2$ $[M+H]^+$ = 179.98959. Mass found $[M+H]^+$ = 179.98944.

9.9 Synthesis and evaluation of Phosphonate and Amide/Carbonic Acid Derivatives as PHP Inhibitors

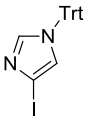

4-iodo-1-trityl-1H-imidazole (92) 5.0 g (25.8 mmol) **91** and 7.5 g (27.1 mmol) TrCl were suspended in 50 mL THF. After stirring for 10min. 9.4 mL (57 mmol) DiPEA was added. The RM was stirred for 30 min. before raising the temp to 60 ^{0}C and was stirred overnight. The RM was evaporated to dryness, the residue was redissolved in chloroform and washing with 10% Na_2CO_3 (aq), water and sat. NaCl. The chloroform was dried over Na_2SO_4 and evaporation afforded solid material that was suspended in 5 mL MeOH and 50 mL diethyl ether and stirred for 1 hour. The white solid was filtered off and washed with diethyl ether. The filtrate was concentrated and co-evaporated with toluene before re-suspension in 1 mL MeOH and 10 mL diethyl ether. After stirring for one hour the solvent was decanted and the white solid was washed with ether. The solids were combined and 9.45 g **92** was obtained as an off-white solid (84% yield from **91**). ^{1}H-NMR(400 MHz, $CDCl_3$) δ: 7.36-7.32 (m, 10H), 7.13-7.09 (m, 6H), 6.91 (d, J=1.4Hz, 1H). Analytical data in agreement with literature.[123]

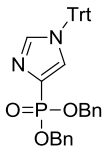

dibenzyl (1-trityl-1H-imidazol-4-yl)phosphonate (93) 4.0 g (9.2 mmol) **92** was dissolved in 50 mL dry THF under argon. The RM was cooled to 0 ^{0}C and 7.4 mL i-PrMgCl:LiCl 1.3M in THF (9.6 mmol) was added dropwise. The RM was stirred for 20 min. at 0 ^{0}C and 20 min. at RT before cooling to -78 ^{0}C. 2.4 g (10 mmol) bis(diethylamino)phosphine chloride was added dropwise and the RM was stirred for 1 hour at -78 ^{0}C before allowing the RM to reach RT and letting it stir for 1 addition hour. The THF was evaporated and under argon 5.0 g benzyl alcohol (40 mmol) and 30 mL dry acetonitril was added. The mixture was cooled to 0 ^{0}C and 2 mL tetrazole 0.45 M in acetonitrile (0.9 mmol) was added and the RM was stirred overnight at RT. The yellow suspension was cooled to 0 ^{0}C and 4 mL (35.3 mmol) 30% hydrogen peroxide was added dropwise. The RM was stirred for 2 hours at 0 ^{0}C and 30 min. at RT. 50 mL 5% Na_2CO_3 and 50 mL EtOAc were added and stirred for 10 min. The layers were separated and the water was extracted with EtOAc (2x). The combined organic layers were washed with water and sat. NaCl(aq) solution, dried over Na_2SO_4(s) and evaporated to dryness. The product was purified by SiO_2 column chromatography (cyclohexane/EtOAc 4:1 to 3:5) to obtain 2.8 g of **93** as a sticky oil (53% yield from **92**). ^{1}H-NMR(400 MHz, $CDCl_3$) δ: 7.58-7.53 (m, 1H), 7.53-7.50 (m, 1H), 7.36-7.29 (m,4H), 7.29-7.15 (m, 15H), 7.10-6.97 (m, 6H), 5.20-5.04 (m, 4H). Analytical data in agreement with literature.[67]

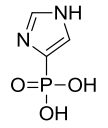

(1H-imidazol-4-yl)phosphonic acid (97) Synthesized according to the TFA deprotection step from general procedure A from **93**, imidazole **97** was obtained as a sticky oil (17 mg, 29% yield from **93**). R_f = 0.25 (DCM/MeOH 8:2); ^{1}H-NMR(400 MHz, DMSO-d_6) δ: 8.83 (s, 1H), 7,57 (s, 1H), 5.75-4.25 (bs); ^{13}C-NMR(101 MHz, DMSO-d_6) δ: 135.70, 132.12, 130.09; ^{31}P-NMR(161 MHz, DMSO-d_6) δ: -7.60; ESI HRMS calculated for $C_3H_6O_3N_2P$ $[M+H]^+$ = 149.01106. Mass found $[M+H]^+$ = 149.01090.

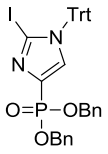

dibenzyl (2-iodo-1-trityl-1H-imidazol-4-yl)phosphonate (94) To 1.6 g (2.3 mmol) **93** dissolved in 10 mL freshly distilled THF in a flame dried flask at -100 ^{0}C was added 1.47 mL 1.7 M t-BuLi (2.5 mmol) dropwize. The red solution was stirred for 2 min. at -100 ^{0}C and a solution of 760 mg (3.0 mmol) I_2 in 4 mL dry THF was added dropwize and the RM was stirred for 5 min. at -100 ^{0}C. The cold RM was poured directly into saturated $Na_2S_2O_3$ solution and was extracted with EtOAc (3x), the combined EtOAc was washed with sat. NaCl(s) solution, dried over Na_2SO_4(s) and evaporated to dryness. The product was purified by SiO_2 column chromatography (toluene/EtOAc (3:1) to obtain 1.0 g of **94** as a white powder (62% yield from **93**). R_f = 0.30 (toluene/EtOAc 1:1); ^{1}H-NMR(400 MHz, $CDCl_3$) δ: 7.43 (d, J=0.8Hz, 1H), 7.38-7.29 (m, 19H), 7.10-7.07 (m, 6H), 5.19-5.09 (m, 4H); ^{13}C-NMR(101 MHz, $CDCl_3$) δ: 147.1, 141.1, 136.4, 136.3, 134.8, 134.4, 132.7, 130.8, 130.3, 129.9, 128.7, 128.6, 128.52, 128.46, 128.30, 128.26, 128.20, 128.15, 128.13, 127.5, 93.9, 93.7, 77.9, 68.30, 68.24; ^{31}P-NMR(161 MHz, $CDCl_3$) δ: 11.42; ESI HRMS calculated for $C_{36}H_{3103}N_2IP$ $[M+H]^+$ = 687.11115. Mass found $[M+H]^+$ = 697.11097.

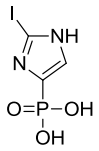

(2-iodo-1H-imidazol-4-yl)phosphonic acid (88) Synthesized according to the TFA deprotection step from general procedure A from compound **94** imidazole **88** was obtained as a white solid (35 mg, 64% yield from **94**). R_f = 0.40 (DCM/MeOH 8:2); ^{1}H-NMR(400 MHz, DMSO-d_6) δ: 11.00-8.00 (bs), 7.57 (s, 1H), 7.45 (s, 1H); ^{13}C-NMR(101 MHz, DMSO-d_6) δ: 188.90, 146.67, 146.47; ^{31}P-NMR(161 MHz, DMSO-d_6) δ: -11.34; ESI HRMS calculated for $C_3H_5O_3N_2IP$ $[M+H]^+$ = 274.90770. Mass found $[M+H]^+$ = 274.90707.

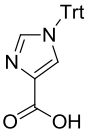

1-trityl-1H-imidazole-4-carboxylic acid (105) A suspension of 224 mg **104** (2.0 mmol) and 613 mg trityl chloride (2.2 mmol) in 3 mL pyridine and 6 mL DMF was stirred at RT overnight. The RM was poured into water and extracted with EtOAc (2x). The combined organic layers were washed with 10% citric acid and sat NaCl solution, dried over Na_2SO_4 and concentrating . The residue was washed with EtOAc to afford 520 mg **105** as a white powder (73% yield from **104**). ^{1}H-NMR(400 MHz, $CDCl_3$) δ: 7.65 (d, J=1.4Hz, 1H), 7.51 (d, J=1.4Hz, 1H), 7.38-7.33 (m, 9H), 7.12-7.08 (m, 6H); Analytical data in agreement with literature.[124]

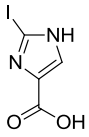

2-iodo-1H-imidazole-4-carboxylic acid (89) 100 mg (0.28 mmol) **105** was dissolved in 3 mL dry THF with 1 mL HMPA and cooled to -100 ^{0}C. 0.2 mL (0.34 mmol, 1.7M) tBuLi was added dropwize and the RM was stirred for 2 minutes. 125 mg (0.5 mmol) I_2 dissolved in 2 mL dry THF was added dropwize and the RM was stirred for 5 min. at -100 ^{0}C. The cold RM was poured directlly into sat. $Na_2S_2O_3$(aq) solution and was extracted with EtOAc (3x), the combined EtOAc was washed with sat. NaCl(s) solution, dried over Na_2SO_4(s) and evaporated to dryness. The residue was taken up in 2 mL TFA/water/TiPS 90:5:5 and stirred overnight. The solvent was removed under vacuum and the residue was purified using preparative HPLC. Imidazole **89** was obtained as a white solid (44 mg, 45% yield from **105**). R_f = 0.15 (DCM/MeOH 8:2); ^{1}H-NMR(400 MHz, $CDCl_3$) δ: 8.18 (s, 1H); ^{13}C-NMR(101 MHz, $CDCl_3$) δ: 139.76, 129.12, 127.76; ESI HRMS calculated for $C_4H_4O_2N_2I$ $[M+H]^+$ = 238.93120. Mass found $[M+H]^+$ = 238.93114.

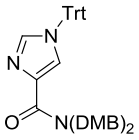

N,N-bis(2,4-dimethoxybenzyl)-1-trityl-1H-imidazole-4-carboxamide (106) 1.2 g **105** (3.4 mmol) and 1.27 g *N*,*N*-bis(2,4-dimethoxybenzyl)amine (4.0 mmol) were dissolved in 25 mL DMF. 460 mg HOBt (3.4 mmol) was added and the RM was cooled to 0 ^{0}C before adding 127 mg EDC.HCl (6.0 mmol) and 2.2 mL DiPEA (12 mmol) and the RM was stirred for 2 hours at RT under argon. The solvent was removed under vacuum and the product was purified by SiO_2 column chromatography, eluted with cyclohexane/EtOAc (1:1 to 100% EtOAc) to obtain 2.1 g of **106** as a white foam (95% yield from **105**). R_f = 0.20 (cyclohexane/EtOAc 1:1); ^{1}H-NMR(400 MHz, $CDCl_3$) δ: 7.50 (d, J=1.4Hz, 1H), 7.35-7.26 (m, 11H), 7.11-7.07 (m, 7H), 6.45-6.37 (m, 4H), 5.20 (bs, 2H), 4.57 (bs, 2H), 3.78 (bs, 6H), 3.71 (bs, 3H), 3.65 (bs, 3H); ^{13}C-NMR(101 MHz, $CDCl_3$) δ: 165.1, 160.0, 158.7, 158.7, 158.5, 142.3, 138.1, 137.2, 130.0, 128.4, 128.3, 126.9, 119.2, 118.7, 104.2, 104.0, 98.5, 75.9, 55.6, 55.3, 53.6, 46.7, 43.7; ESI HRMS calculated for $C_{41}H_{40}O_5N_3$ $[M+H]^+$ = 654.29625. Mass found $[M+H]^+$ = 654.29638.

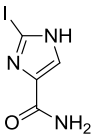

2-iodo-1H-imidazole-4-carboxamide (90) 100 mg (0.15 mmol) **106** was dissolved in 2 mL dry THF and cooled to -100 ^{0}C. 0.12 mL (0.19 mmol) 1.7M tBuLi was added dropwize and the RM was stirred for 2 min. 75 mg (0.3 mmol) I_2 dissolved in 1 mL dry THF was added dropwize and the RM was stirred for 5 min. at -100 ^{0}C. The cold RM was poured directly into saturated $Na_2S_2O_3$(aq) solution and was extracted with EtOAc (3x), the combined EtOAc was washed with sat. NaCl(aq) solution, dried over Na_2SO_4(s) and evaporated to dryness. The residue was taken up in 2 mL TFA/water/TiPS 90:5:5 and stirred overnight. The solvent was removed under vacuum and the residue was purified using preparative HPLC. Imidazole **90** was obtained as a white solid (20 mg, 38% yield from **106**). R_f = 0.38 (DCM/MeOH 8:2); ^{1}H-NMR(400 MHz, CD_3OD) δ: 8.23 (s, 1H); ^{13}C-NMR(101 MHz, $CDCl_3$); 162.58, 139.13, 132.75, 114.53; ESI HRMS calculated for $C_4H_5ON_3I$ $[M+H]^+$ = 237.94718. Mass found $[M+H]^+$ = 237.94736.

9.10 Synthesis of 3,5-diphenyl isothiazolidine 1,1-dioxide

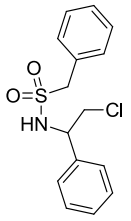

N-(2-chloro-1-phenylethyl)-1-phenylmethanesulfonamide (111) 0.55 g (14.5 mmol) $LiAlH_4$ was weight in a flask (carefully not to make a dust cloud). The flask was flushed with argon before adding 20 mL of THF. The suspension was cooled to 0 ^{0}C and 1.0 g (6.6 mmol) **114** was added in portions. The RM was stirred for one hour at RT and at 50 ^{0}C overnight. The RM was cooled to 0 ^{0}C and 0.5 mL water was added dropwise. The RM became thick and 10 mL THF was added before 3 mL 2M K_2CO_3(aq) solution was added. Filtration and evaporation of the solvent gave a yellow solid that was dissolved in 25 mL THF and 2 mL TEA was added. The RM was cooled to 0 ^{0}C. and 2.86 g (15 mmol) **112** was added portion wise. The ice bath was removed and the RM was stirred at RT for 8 hours. The precipitated salt was filtered off and washed with EtOAc. The filtrate was evaporated to dryness and dissolved in 16 mL DMF. 0.6 g NaCl(s) was added and the RM was stirred overnight at 80 ^{0}C. The RM was allowed to cool before adding water and was extracting with EtOAc (3x). The combined EtOAc was washed with 1M HCl and sat. NaCl(aq) solution. Drying over Na_2SO_4 and evaporation yielded a yellow solid that was purified by SiO_2 column chromatography, eluted with cyclohexane/EtOAc (8:2) to obtain 1540 mg of **111** as an off-white solid (68% yield from **114**). R_f = 0.38 (cyclohexane/EtOAc 1:1); ^{1}H-NMR(400 MHz, $CDCl_3$) δ: 7.42-7.17 (m, 10H), 5.11 (d, J=8.0Hz, 2H), 4.66 (q, J=8.0Hz, 2H), 4.11 (m, 2H), 3.73 (m, 2H); ^{13}C-NMR(101 MHz, $CDCl_3$) δ: 138.2, 131.0, 129.2, 129.0, 128.91, 128.88, 127.2, 60.4, 59.0, 48.8; ESI HRMS calculated for $C_{15}H_{17}O_2NClS$ $[M+H]^+$ = 310.06630. Mass found $[M+H]^+$ = 310.06641.

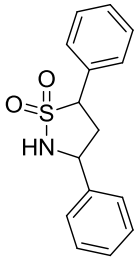

3,5-diphenylisothiazolidine 1,1-dioxide (107) 600 mg chloride **111** (1.94 mmol) and 68 µL (0.49 mmol) diisopropylamine were dissolved in 20 mL dry THF and cooled to -70 ^{o}C. 2.8 mL 1.6 M BuLi solution (4.36 mmol) was added dropwise and the reaction mixture was allowed to warm to 0 ^{0}C over 1 hour. The mixture was stirred at 0 ^{0}C for 2 hours and quenched with a 1.0 M HCl solution. The reaction mixture was extracted with EtOAc (3x). The combined organic layers were washed with sat. NaCl(aq) solution, dried over $MgSO_4$ and concentrated to dryness. The residue was purified by SiO_2 column chromatography, eluted with cyclohexane/EtOAc (1:1) to obtain 188 mg of **107 isomer 1** and 153 mg of **107 isomer 2** as off-white solids (64% total yield from **111**). **Isomer 1**: R_f = 0.25 (cyclohexane/EtOAc 1:1); ^{1}H-NMR(400 MHz, $CDCl_3$) δ: 7.50-7.34 (m, 10H), 4.89 (m, 1H), 4.77 (bd, 1H), 4.52 (m, 1H) 3.19 (m, 1H) 2.70 (m, 1H); ^{13}C-NMR(101 MHz, $CDCl_3$) δ: 141.5, 130.5, 129.44, 129.41, 129.2, 129.1, 128.6, 61.3, 55.1, 37.4; ESI HRMS calculated for $C_{15}H_{16}O_2NS$ $[M+H]^+$ = 274.08963. Mass found $[M+H]^+$ = 274.08985. **Isomer 2**: R_f = 0.15 (cyclohexane/EtOAc 1:1); ^{1}H-NMR(400 MHz, $CDCl_3$) δ: 7.50-7.31 (m, 10H), 5.02 (bd, 1H), 4.78 (m, 1H), 4.51 (m, 1H) 2.94 (m, 1H) 2.70 (m, 1H); ^{13}C-NMR(101 MHz, $CDCl_3$) δ: 140.7, 129.9, 129.5, 129.20, 129.17, 129.15, 128.6, 65.4, 56.0, 38.3; ESI HRMS calculated for $C_{15}H_{16}O_2NS$ $[M+H]^+$ = 274.08963. Mass found $[M+H]^+$ = 274.08989.

9.11 Synthesis of Prodrugs 121 and 122

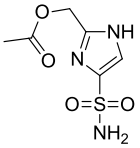

(4-sulfamoyl-1H-imidazol-2-yl)methyl acetate (121) 50 mg (0.07 mmol) **58** was dissolved in 0.5 mL dry DCM and 0.5 mL pyridine was added before cooling the RT to 0 ^{0}C. 6 µL acetyl chloride (0.08 mmol) was added and the RM was stirred for 2 hour at RT. The solvent was evaporated and the residue was suspended in 2 mL TFA with 50 µL TiPS and 50 µL water and stirred overnight at RT. The solvent was evaporated and the residue taken up in MeOH and purified using prep HPLC yielding 13 mg **121** (56% yield from **58**). R_f = 0.40 (DCM/MeOH 9:1); ^{1}H-NMR(400 MHz, CD_3OD) δ: 7.60 (s, 1H), 5.14 (s, 2H), 2.10 (s, 3H); ^{13}C-NMR(101 MHz, CD_3OD) δ: 170.8, 144.9, 141.9, 120.1, 58.1, 19.2; ESI HRMS calculated for $C_6H_{10}O_4N_3S$ $[M+H]^+$ = 220.03865. Mass found $[M+H]^+$ = 220.03859.

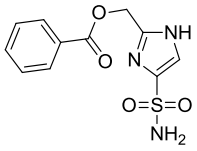

(4-sulfamoyl-1H-imidazol-2-yl)methyl benzoate (122) 50 mg (0.07 mmol) **58** was dissolved in 0.5 mL dry DCM and 0.5 mL pyridine was added before cooling the RT to 0 ^{0}C. 10 µL benzoyl chloride (0.08 mmol) was added and the RM was stirred for 2 hour at RT. The solvent was evaporated and the residue was suspended in 2 mL TFA with 50 µL TiPS and 50 µL water and stirred overnight at RT. The solvent was evaporated and the residue taken up in MeOH and purified using prep HPLC yielding 21 mg **122** (76% yield from **58**). R_f = 0.55 (DCM/MeOH 9:1); ^{1}H-NMR(400 MHz, CD_3OD) δ: 8.04 (dt, J=8.4Hz, J=2.4Hz, 1H), 7.64 (s, 1H), 7.61 (dd, J=2.4Hz, J=8.4Hz, 2H), 7.48 (dt, J=2.4Hz, J=8.4Hz, 2H), 5.4 (s, 2H)); ^{13}C-NMR(101 MHz, CD_3OD) δ: 166.1, 144.8, 141.9, 133.5, 129.6, 129.4, 128.5, 120.3, 58.5; ESI HRMS calculated for $C_{11}H_{12}O_4N_3S$ $[M+H]^+$ = 282.05430. Mass found $[M+H]^+$ = 282.05422.

9.12 Synthesis of TAMRA labeled Probe 123

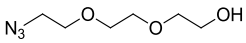

2-(2-(2-azidoethoxy)ethoxy)ethanol (125) 38.6 g (257 mmol) triethylene glycol (**124**) was dissolved in 250 mL anhydrous THF under argon atmosphere and cooled to 0 ^{0}C. 5.0 mL methanesulfonyl chloride (64.4 mmol) and 9.0 mL TEA (64.4 mmol) were added dropwise. The RM was allowed to stir at room temperature overnight under an argon atmosphere. The reaction mixture was concentrated and the residue was dissolved in 250 mL dry ethanol. 20.9 g sodium azide (322.0 mmol) was added and the reaction mixture was heated to reflux for 6 hours. After cooling to room temperature the mixture was concentrated and dissolved in water. The product was extracted with DCM (3x), and the combined organic fractions were dried over magnesium sulfate, filtered, and concentrated to yield 5.1 g **125** as a sticky oil (45% yield from methanesulfonyl chloride). R_f = 0.20 (100% EtOAc); ^{1}H-NMR(400 MHz, $CDCl_3$) δ: 3.77 (t, J = 5.8 Hz, 2H), 3.72 – 3.66 (m, 6H), 3.64 (t, J = 5.8 Hz, 2H), 3.39 (t, J = 5.0 Hz, 2H), 1.57 (s, 1H). Analytical data in agreement with literature.[117]

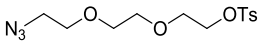

2-(2-(2-azidoethoxy)ethoxy)ethyl 4-methylbenzenesulfonate (126) 5.0 g (28.5 mmol) **125** was dissolved in 50 mL DCM and 50 mL pyridine and 6.0 g (31.5 mmol) 4-toluenesulfonyl chloride was added. The RM was stirred overnight at RT. The RM was evaporated to dryness and the residue was taken up in DCM and washed with sat. NaCl solution. The DCM was evaporated to dryness and the residue taken up in DCM. After washing the organic layer with sat. NaCl solution, the solvent was removed by evaporation. The product was purified by SiO_2 column chromatography, eluted with EtOAc (100%) to obtain 6.2 g of **126** (66% yield from **125**). R_f = 0.20 (100% EtOAc); ^{1}H-NMR(400 MHz, $CDCl_3$) δ: 7.80 (d, J = 8.3 Hz, 2H), 7.34 (d, J = 8.0 Hz, 2H), 4.19 – 4.15 (m, 2H), 3.79 – 3.61 (m, 8H), 3.41 – 3.33 (m, 2H), 2.45 (s, 3H). Analytical data in agreement with literature.[117]

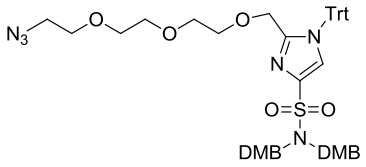

2-((2-(2-(2-azidoethoxy)ethoxy)ethoxy)methyl)-N,N-bis(2,4-dimethoxybenzyl)-1-trityl-1H-imidazole-4-sulfonamide (127) 50 mg (0.07 mmol) **58** was dissolved in 0.5 mL dry DMF and 3.0 mg (0.08 mmol) NaH 60 % dispersion in mineral oil was added and the mixture was stirred for 30 min. 33 mg (0.10 mmol) **126** dissolved in 0.5 mL DMF was added dropwise and the RM was stirred overnight at RT. The RM was concentrated and diluted with DCM and washed with sat $NaHCO_3$. The DCM was dried over Na_2SO_4(s) and evaporated. The product was purified by SiO_2 column chromatography, eluted with cyclohexane/EtOAc (7:3 to 1:1) to obtain 25 mg **127** (41% yield from **58**). R_f = 0.20 (toluene/EtOAc 1:3); ^{1}H-NMR(400 MHz, $CDCl_3$) δ: 7.35-7.30 (m, 9H), 7.24 (d, J=8.2Hz, 1H), 7.17 (s, 1H), 7.06-7.02 (m, 6H), 6.36 (dd, J=2.6Hz, J=8.2Hz, 2H), 6.31 (d, J=2.6Hz, 2H), 4.5 (s, 4H), 3.75 (s, 6H), 3.74 (s, 2H), 3.65 (s, 6H), 3.64-3.53 (m, 6H), 3.44 (t, J=4.8Hz, 2H), 3.36-3.32 (m, 4H); ^{13}C-NMR(101 MHz, $CDCl_3$) δ: 160.2, 158.4, 148.3, 141.7, 138.5, 130.6, 129.9, 128.52, 128.49, 124.9, 117.9, 104.2, 98.0, 76.4, 71.4, 70.8, 70.71, 70.66, 70.56, 70.2, 70.1, 66.2, 55.5, 55.3, 50.9, 46.1, 42.9; ESI HRMS calculated for $C_{47}H_{53}O_9N_6S$ $[M+H]^+$ = 877.35892. Mass found $[M+H]^+$ = 877.35963.

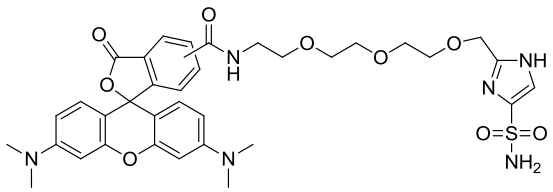

3',6'-bis(dimethylamino)-3-oxo-N-(2-(2-(2-((4-sulfamoyl-1H-imidazol-2-yl)methoxy)ethoxy)ethoxy)ethyl)-3H-spiro[isobenzofuran-1,9'-xanthene]-5/6-carboxamide (123) 25 mg (0.028 mmol) **127** was dissolved in 0.5 mL THF and 9.0 mg (0.034 mmol) PPh_3 was added and stirred for 6 hours. 10 uL water was added and the RM was stirred overnight. The solvent was evaporated and the residue was dissolved in 1 mL DMF and 14.8 mg (0.028 mmol) TAMRA-OSu was added and after addition of 4.0 µL (0.029 mmol) TEA stirred overnight at RT in a dark vial. The RM was diluted with 2 mL EtOAc and was washed with sat. $NaHCO_3$(aq) and evaporated to dryness.The residue was suspended in 2 mL TFA with 50 µL TiPS and 50 µL water and stirred at RT for 2 hours. The solvent was evaporated and the residue taken up in MeOH and purified using prep HPLC yielding 2.0 mg **123** (10% yield from **127**). ESI HRMS calculated for $C_{35}H_{41}O_9N_6S$ $[M+H]^+$ = 721.26502. Mass found $[M+H]^+$ = 721.26491.

9.13 Synthesis of Histone H4 Peptide Probes

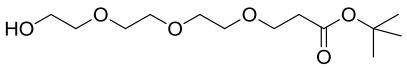

tert-butyl 3-(2-(2-(2-hydroxyethoxy)ethoxy)ethoxy)propanoate (135) 51.2 mL (376 mmol) triethyleneglycol **124** was dissolved in 200 mL dry THF and 80 mg (1.8 mmol) sodium was added under argon. The sodium was allowed to dissolve before adding 19.2 mL (132 mmol) tertbutylacrylate and stirring overnight at RT. 3.0 mL 1M HCl(aq) was added to the RM before removing the solvent. The oily residu was taken up in 150 mL saturated NaCl(aq) solution and extracted with EtOAc 3x. The combined EtOAc was washed with saturated NaCl(aq), dried over anhydrous Na_2SO_4(s), evaporated and extensively dried under high vacuum, yielding 30.0 g **135** (29% yield from **124**). ^{1}H-NMR(400 MHz, $CDCl_3$) δ: 3.76 – 3.56 (m, 14H), 2.50 (t, J = 6.6 Hz, 2H), 2.40 (s, 1H), 1.44 (s, 9H). Analytical data in agreement with literature.[118]

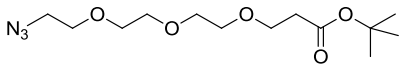

tert-butyl 3-(2-(2-(2-azidoethoxy)ethoxy)ethoxy)propanoate (136) 29.0 g (104 mmol) **135** was dissolved in 40 mL dry DCM before adding 35 mL (251 mmol) TEA. The RM was cooled with an icebath before adding 16.4 mL (214 mmol) mesyl chloride dropwise. The icebath was removed and the RM was stirred for 4 hours. The RM was filtered over celite before washing the DCM with icecold water (2x). The DCM was washed with sat. NaCl(aq) solution and dried over anhydrous $MgSO_4$(s) before removing the solvent through evaporation. The resulting oil was taken up in 40 mL DMF and 40.0 g (615 mmol) NaN_3 was added. The suspension was stirred overnight at 60 ºC. The DMF was removed by vacuum and the resulting solid material was dissolved in water and extracted with diethylether (2x). De combined organic layers were washed with sat. NaCl(s) solution, dried over anhydrous $MgSO_4$(s) and evaporated. The product was purified by SiO_2 column chromatography, eluted with petroleum ether/ethyl ether (3:1) to obtain 27.6 g **136** (87% yield from **135**). ^{1}H-NMR(400 MHz, $CDCl_3$) δ: 3.76 – 3.56 (m, 12H), 3.39 (t, J = 5.1 Hz, 2H), 2.50 (t, J = 6.6 Hz, 2H), 1.45 (s, 9H). Analytical data in agreement with literature.[119]

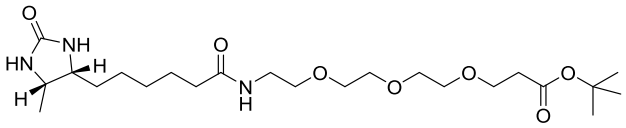

tert-butyl 19-((4R,5S)-5-methyl-2-oxoimidazolidin-4-yl)-14-oxo-4,7,10-trioxa-13-azanonadecan-1-oate (137) 334 mg (1.1 mmol) **136** was dissolved in 4 mL dioxane/water (9:1) and 317 mg (1.2 mmol) triphenylphosphine was added and the RM was stirred overnight. The RM was evaoprated to dryness and coevaporated with toluene (3x). The residue was dissolved in 1 mL DMF and a solution of 250 mg (1.16mmol) desthiobiotin, 232 mg (1.2 mmol) EDC.HCl and 28 mg (0.23 mmol) DMAP in 4 mL DMF was added. The RM was stirred overnight at RT and the DMF was evaporated. The residue was purified by SiO_2 column chromatography (DCM/MeOH 98:2 - 9:1) yielding 225 mg **137** (43% yield from **136**). R_f = 0.60 (DCM/MeOH 1:9); ^{1}H-NMR(400 MHz, $CDCl_3$) δ: 6.62 (bs, 1H), 5.86 (bs, 1H), 5.05 (bs, 1H), 3.77 (m, 1H), 3.68 (m, 3H), 3.59 (s, 10H), 3.53 (t, J = 5.9 Hz, 2H), 3.39 (m, 2H), 2.47 (t, J = 6.0 Hz, 2H), 2.16 (t, J = 6.0 Hz, 2H), 1.63 (m, 2H), 1.52 – 1.20 (m, 13H), 1.08 (d, J = 8.0 Hz, 3H). ESI HRMS calculated for $C_{23}H_{44}O_7N_3$ $[M+H]^+$ = 474.3174. Mass found $[M+H]^+$ = 474.3166.

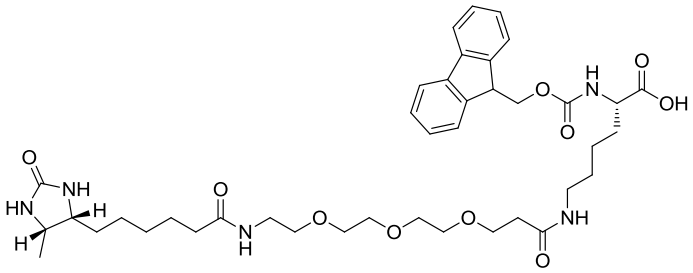

(S)-25-((((9H-fluoren-9-yl)methoxy)carbonyl)amino)-1-((4R,5S)-5-methyl-2-oxoimidazolidin-4-yl)-6,19-dioxo-10,13,16-trioxa-7,20-diazahexacosan-26-oic acid (134) 140 mg (0.30 mmol) **137** was dissolved in 3 mL DCE. 1 mL TFA was added dropwise and the RM was stirred for 30 min. The solvent was evaporated and the residue was taken up in DCE and evaporated to dryness. The residue was coevaporated with toluene (2x) and dried overnight under vacuum yielding 120 mg **138**. The oily material was redissolved in 2 mL DCM and 101 mg (0.88 mmol) N-Hydroxysuccinimide was added. After cooling the RM to 0 ºC, 191 mg (1.0 mmol) EDC.HCl was added under an argon atmosphere. The icebath was removed and the RM was stirred overnight. The RM was evaporated to dryness and redissolved in a ice cooled solution of 5 mL dioxane/$NaHCO_3$ (sat.) 1:1. 648 mg (1.6 mmol) Fmoc-Lys-OH was added (suspended in 10 mL dioxane/$NaHCO_3$ (sat.) 1:1) and the RM was stirred under argon atmosphere for 3 hours at RT. The RM was made acidic (pH 3) with $KHSO_4$(s) before evaporation to dryness. The solid was suspended in $CHCl_3$ with 10% ethanol added and stirred for 2 hours before decanting of the liquid (done twice). The combined liquid was evaporated and the oily material was purified using prep HPLC yielding 71 mg **134** (31% yield from **137**). R_f = 0.24 (DCM/MeOH 8:2); ^{1}H-NMR(400 MHz, CD_3OD) δ: 12.50 (s, 1H), 7.87 (d, J = 7.5 Hz, 2H), 7.83 – 7.75 (m, 2H), 7.71 (d, J = 7.4 Hz, 2H), 7.57 (d, J = 7.9 Hz, 1H), 7.40 (t, J = 7.4 Hz, 2H), 7.31 (t, J = 7.2 Hz, 2H), 6.26 (s, 1H), 6.08 (s, 1H), 4.31 – 4.15 (m, 3H), 3.89 (td, J = 9.1, 4.6 Hz, 1H), 3.57 (q, J = 6.6 Hz, 3H), 3.46 (d, J = 5.0 Hz, 9H), 3.36 (t, J = 5.9 Hz, 2H), 3.15 (q, J = 5.8 Hz, 2H), 3.06 – 2.95 (m, 2H), 2.27 (t, J = 6.5 Hz, 2H), 2.03 (t, J = 7.4 Hz, 2H), 1.75 – 1.51 (m, 2H), 1.32 (tdd, J = 50.4, 19.8, 13.0 Hz, 13H), 0.93 (d, J = 6.4 Hz, 3H); ESI HRMS calculated for $C_{40}H_{58}O_{10}N_5$ $[M+H]^+$ = 768.41782. Mass found $[M+H]^+$ = 768.41760

Peptides 131, 132 and 133 Synthesized like was described for peptides **37** and **38** but with an automated peptide synthesizer on Tentagel Rink-amide (0.24 mmol/g) resin. Before cleavage of the peptides from the resin, the alloc on the lysine was removed using 50 mol% $Pd(PPh_3)_4$ in piperidine/DMF (performed 2x) and **138** was coupled using standard HOAt/HATU conditions (performed 2x). Cleavage from the resin and global deprotecting was performed as described for peptides **37** and **38**. After preparative reverse phase HPLC purification (C18) and subsequent lyophilization the peptides **131**, **132** and **133** were isolated as white solids.

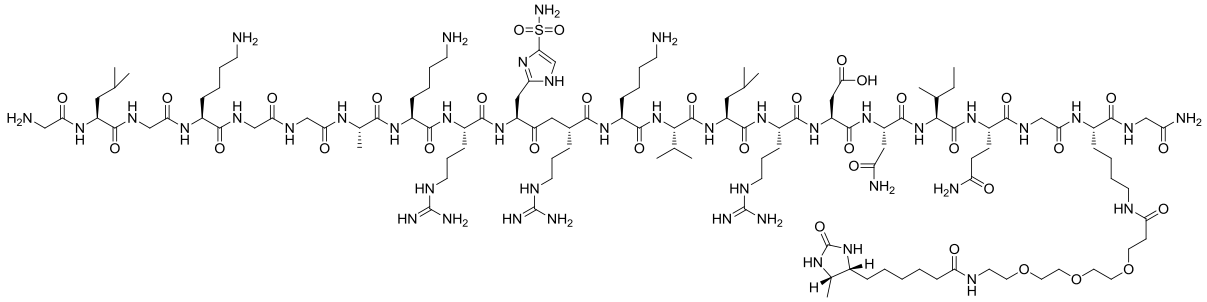

Peptide 131; Isolated was 47 mg (22 % yield from 0.25 g resin). ESI HRMS calculated for $C_{118}H_{214}O_{35}N_{43}P$ $[M+2H]^{2+}$ = 1412.30071. Mass found $[M+2H]^{2+}$ = 1412.29920.

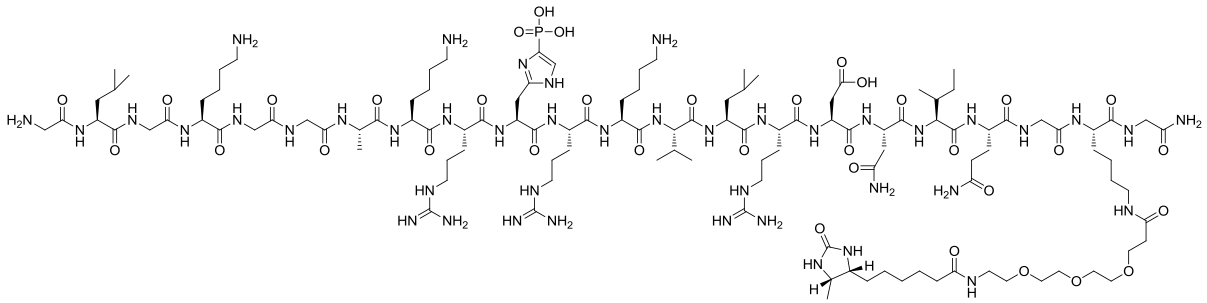

Peptide 132; Isolated was 42 mg (20 % yield from 0.25 g resin). ESI HRMS calculated for $C_{118}H_{216}O_{32}N_{43}$ $[M+5H]^{5+}$ = 549.53138. Mass found $[M+5H]^{5+}$ = 549.53107.

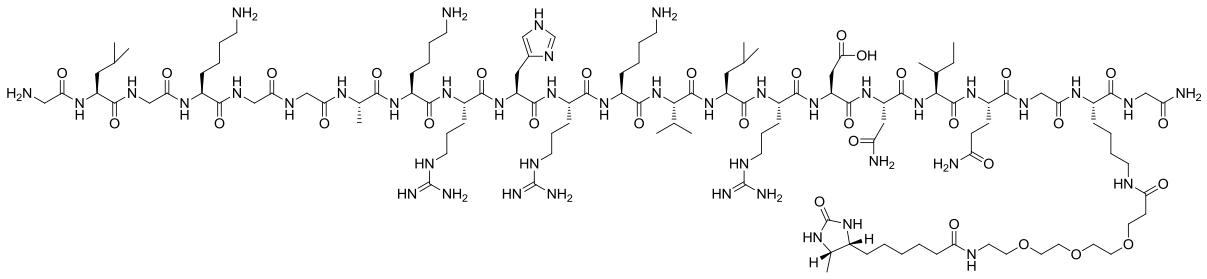

Peptide 133; Isolated was 37 mg (17 % yield from 0.25 g resin). ESI HRMS calculated for $C_{118}H_{217}O_{34}N_{44}S$ $[M+5H]^{5+}$ = 565.32594. Mass found $[M+5H]^{5+}$ = 565.32579

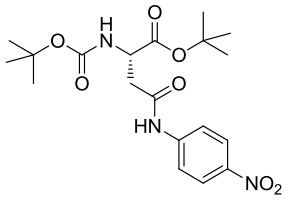

(S)-tert-butyl 2-((tert-butoxycarbonyl)amino)-4-((4-nitrophenyl)amino)-4-oxobutanoate (147) 1.0 g (3.5 mmol) **146** was dissolved in 10 mL DCM at 0 ^{0}C. 0.61 g (4.5 mmol) HOAt and 1.0 g (5.24 mmol) EDC.HCl were added. The RM was allowed to reach RT and was stirred overnight. The RM was washed with 5% citric acid solution, saturated NaCl(aq) solution and dried over anhydrous Na_2SO_4(s) and evaporated to dryness. The residue was dissolved in 20 mL dry DCM. The RM was cooled to 0 ^{0}C and 370 mg (2.68 mmol) 4-nitroaniline and 73 µL (0.49 mmol) DBU were added and the RM was stirred overnight at 35 ^{0}C. The RM was washed with a saturated $NaHCO_3$(aq) solution, dried over anhydrous Na_2SO_4(s) and evaporated to dryness. The product was purified by SiO_2 column chromatography (hexane/EtOAc 8:2 to 100%) to obtain 440 mg **147** (44% yield from **146**). R_f = 0.65 (EtOAc); ^{1}H-NMR(400 MHz, $CDCl_3$) δ: 8.48 (bs, 1H), 8.28 – 8.14 (m, 2H), 7.82 – 7.65 (m, 2H), 7.26 (s, 2H), 5.60 (s, 1H), 4.49 (dt, J = 7.7, 5.3 Hz, 1H), 3.11 – 2.84 (m, 2H), 1.48 (s, 9H), 1.45 (s, 10H).

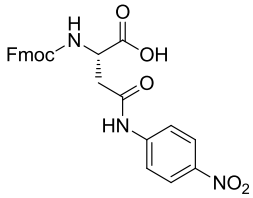

(S)-2-((((9H-fluoren-9-yl)methoxy)carbonyl)amino)-4-((4-nitrophenyl)amino)-4-oxobutanoic acid (145) 400 mg (0.98 mmol) **147** was dissolved in 10 mL DCM. 10 mL TFA and 2 mL H_2O were added and the RM was stirred for 4 hours. The solvent was removed by vacuum and the residue was redissolved in 10 mL dioxane and 10 mL water. 300 mg (2.0 mmol) $NaHCO_3$(s) was added and the RM was cooled to 0 ^{0}C. 600 mg (1.1 mmol) Fmoc-OSu was added and the RM was stirred at RT overnight. The RM was poured into EtOAc and washed with a 5% citric acid solution and with a sat. NaCl(aq) solution. The EtOAc was dried over anhydrous Na_2SO_4(s) and evaporated. The product was purified by SiO_2 column chromatography (DCM/MeOH 99:1 to 9:1) to obtain 256 mg **145** (57% yield from **147**). R_f = 0.38 (DCM/MeOH 8:2); ^{1}H-NMR(400 MHz, DMSO-d_6) δ: 11.03 (s, 1H), 8.12 (d, J = 8.9 Hz, 2H), 7.82 (dd, J = 13.5, 8.4 Hz, 4H), 7.65 (d, J = 7.2 Hz, 2H), 7.36 (m, 3H), 7.27 (q, J = 8.3, 7.3 Hz, 2H), 4.42 – 4.29 (m, 1H), 4.21 (m, 3H), 3.16 (s, 1H), 3.00 – 2.88 (m, 1H), 2.87 (s, 1H), 2.79 – 2.67 (m, 3H), 2.48 (dt, J = 3.6, 1.8 Hz, 1H); ^{13}C-NMR(101 MHz, DMSO-d_6) δ: 170.74, 162.99, 156.38, 146.22, 144.51, 142.57, 141.35, 128.25, 127.72, 125.91, 125.50, 120.74, 119.33, 66.30, 47.33, 36.46, 31.46; ESI HRMS calculated for $C_{25}H_{22}O_7N_3S$ $[M+H]^+$ = 476.14523. Mass found $[M+H]^+$ = 476.14465.

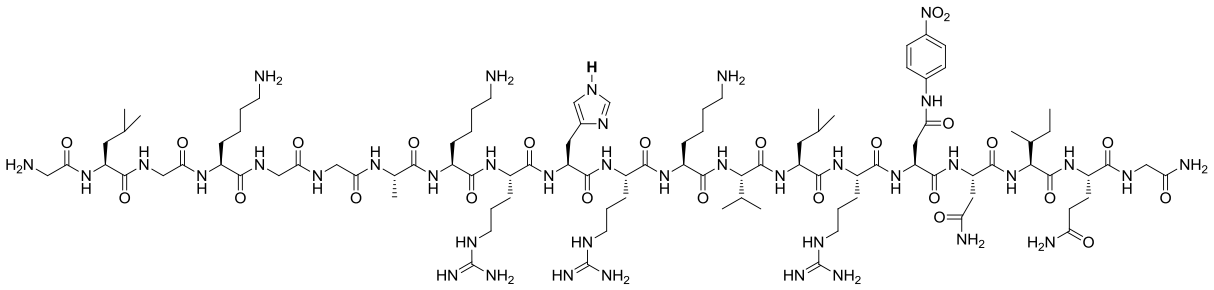

Peptides 143 Synthesized like was described for peptides **37** and **38** but with an automated peptide synthesizer on Tentagel Rink-amide resin (0.24 mmol/g). Cleavage from the resin and global deprotecting was performed as described for peptides **37** and **38**. After preparative reverse phase HPLC purification (C18) and subsequent lyophilization, 240 mg peptide **143** was isolated as a white solid (31 % yield from 1.0 g resin). ESI HRMS calculated for $C_{97}H_{167}O_{25}N_{39}$ $[M+2H]^{2+}$ = 1140.15759. Mass found $[M+2H]^{2+}$ = 1140.15741.

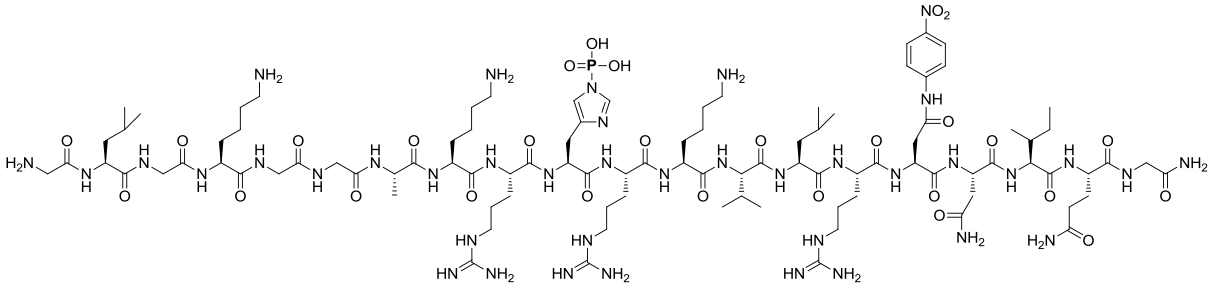

Peptide 144 10 mg (0.0044 mmol) **143** was dissolved in 2 ml H_2O. 5.9 mg (0.044 mmol) potassium phosphoramidate and 4.2 mg (0.053 mmol) NH_4HCO_3(s) were added. The mixture was stirred for 7 days at RT. The RM was purified by Source 15S cation exchange column chromatography using a gradient of NH_4HCO_3 salt solution 50 to 1500 mM). The fractions containing product were run a second type to obtain 5.0 mg of chemically pure material (….% yield from 143). ^{31}P-NMR(161 MHz, $CDCl_3$) δ: -3.73; MALDI-TOF calculated for $C_{97}H_{167}O_{28}N_{39}P$ $[M-1H]^-$ = 2357.25804. Mass found $[M-1H]^-$ = 2357.6.

Literature

[1] Consortium, I. H. G. S., Finishing the euchromatic sequence of the human genome. *Nature* **2004,** *431* (7011), 931-945.
[2] (a) Black, D. L., Mechanisms of alternative pre-messenger RNA splicing. *Annu. Rev. Biochem.* **2003,** *72*, 291-336; (b) Maniatis, T.; Tasic, B., Alternative pre-mRNA splicing and proteome expansion in metazoans. *Nature* **2002,** *418* (6894), 236-243.
[3] Su, A. A. H.; Randau, L., A-to-I and C-to-U editing within transfer RNAs. *Biochemistry* **2011,** *76* (8), 932-937.
[4] Walsh, C., Posttranslational modification of proteins : Expanding nature's inventory. *Roberts and Co. Publishers* **2006**, 490 p. p.
[5] Information extracted from webpage http://www.piercenet.com/browse.cfm?fldID =7CE3FCF5-0DA0-4378-A513-2E35E5E3B49B.
[6] (a) Srahl, B. O.; Allis, C. D., The language of covalent histone modifications. *Nature* **2000,** *403* (6765), 41-45; (b) Latham, J. A.; Dent, S. Y. R., Cross-regulation of histone modifications. *Nature Structural & Molecular Biology* **2007,** *14* (11), 1017-1024.
[7] (a) Martin, D. D. O.; Beauchamp, E.; Berthiaume, L. G., Post-translational myristoylation: Fat matters in cellular life and death. *Biochimie* **2011,** *93* (1), 18-31; (b) Tom, C. T. M. B.; Martin, B. R., Fat Chance! Getting a Grip on a Slippery Modification. *ACS Chem. Biol.* **2013,** *8* (1), 46-57.
[8] Varki, A.; Esko, J. D.; Colley, K. J., Cellular organization of glycosylation. *Essent. Glycobiol* **2009**, 37-46.
[9] (a) Reddie, K. G.; Carroll, K. S., Expanding the functional diversity of proteins through cysteine oxidation. *Curr. Opin. Chem. Biol.* **2008,** *12* (6), 746-754; (b) Hoshi, T.; Heinemann, S. H., Regulation of cell function by methionine oxidation and reduction. *J. Physio.* **2001,** *531* (1), 1-11.
[10] Cohen, P., The regulation of protein function by multisite phosphorylation - a 25 year update. *Trends in Biochemical Sciences* **2000,** *25* (12), 596-601.
[11] Steen, H.; Fernandez, M.; Ghaffari, S.; Pandey, A.; Mann, M., Phosphotyrosine mapping in Bcr/Abl oncoprotein using phosphotyrosine-specific immonium ion scanning. *Mol. Cell. Proteomics* **2003,** *2* (3), 138-145.
[12] Marks, F.; Editor, *Protein Phosphorylation*. 1996; p 366 pp.
[13] (a) Krebs, E. G., Protein phosphorylation and cell regulation. I (Nobel lecture). *Angew. Chem.* **1993,** *105* (8), 1173-80 (See also Angew Chem , Int Ed Engl , 1993, 32(8), 1122-9); (b) Fischer, E. H., Protein phosphorylation and cell regulation. II (Nobel lecture). *Angew. Chem.* **1993,** *105* (8), 1181-8 (See also Angew Chem , Int Ed Engl , 1993, 32(8), 1130-7).
[14] Johnson, G. L.; Lapadat, R., Mitogen-activated protein kinase pathways mediated by ERK, JNK, and p38 protein kinases. *Science* **2002,** *298* (5600), 1911-1912.
[15] Manning, G., Genomic overview of protein kinases. *WormBook* **2005**, 1-19.
[16] Endicott, J. A.; Noble, M. E. M.; Johnson, L. N., The structural basis for control of eukaryotic protein kinases. *Annu. Rev. Biochem.* **2012,** *81*, 587-613.
[17] Lindberg, R. A.; Quinn, A. M.; Hunter, T., Dual-specificity protein kinases: will any hydroxyl do? *Trends in Biochemical Sciences* **1992,** *17* (3), 114-19.
[18] Sukawa, Y.; Yamamoto, H.; Shinomura, Y., PI3K-Akt pathway. *G.I. Res.* **2012,** *20* (4), 346-348.
[19] Alonso, A.; Sasin, J.; Bottini, N.; Friedberg, I.; Friedberg, I.; Osterman, A.; Godzik, A.; Hunter, T.; Dixon, J.; Mustelin, T., Protein tyrosine phosphatases in the human genome. *Cell* **2004,** *117* (6), 699-711.

[20] Patterson, K. I.; Brummer, T.; O'Brien, P. M.; Daly, R. J., Dual-specificity phosphatases: critical regulators with diverse cellular targets. *Biochem. J.* **2009,** *418* (3), 475-489.
[21] (a) Patarca, R., Protein phosphorylation and dephosphorylation in physiologic and oncologic processes. *Crit. Rev. Oncog.* **1996,** *7* (5 & 6), 343-432; (b) Hardy, S.; Julien, S. G.; Tremblay, M. L., Impact of oncogenic protein tyrosine phosphatases in cancer. *Anti-Cancer Agents in Medicinal Chemistry* **2012,** *12* (1), 4-18; (c) Creus, M.; Zoller, H., Phosphatases as promising targets for cancer therapy. *Signaling Mol. Targets Cancer Ther.* **2007**, 69-85; (d) Supuran, C. T.; Scozzafava, A., Protein tyrosine kinase inhibitors as anticancer agents. *Expert Opin. Ther. Pat.* **2004,** *14* (1), 35-53.
[22] Liu, B. A.; Nash, P. D., Evolution of SH2 domains and phosphotyrosine signalling networks. *Philos. Trans. R. Soc., B* **2012,** *367* (1602), 2556-2573.
[23] Klumpp, S.; Krieglstein, J., Phosphorylation and dephosphorylation of histidine residues in proteins. *Eur. J. Biochem.* **2002,** *269* (4), 1067-1071.
[24] Stock, J. B.; Stock, A. M.; Mottonen, J. M., Signal transduction in bacteria. *Nature (London, United Kingdom)* **1990,** *344* (6265), 395-400.
[25] Kee, J.-M.; Villani, B.; Carpenter, L. R.; Muir, T. W., Development of Stable Phosphohistidine Analogues. *J. Am. Chem. Soc.* **2010,** *132* (41), 14327-14329.
[26] Klumpp, S.; Krieglstein, J., Reversible phosphorylation of histidine residues in vertebrate proteins. *Biochimica et Biophysica Acta, Proteins and Proteomics* **2005,** *1754* (1-2), 291-295.
[27] Wuichet, K.; Cantwell, B. J.; Zhulin, I. B., Evolution and phyletic distribution of two-component signal transduction systems. *Curr. Opin. Microbiol.* **2010,** *13* (2), 219-225.
[28] http://www.kraemerlab.uni-koeln.de/osmosensing.php.
[29] (a) Swanson, R. V.; Alex, L. A.; Simon, M. I., Histidine and aspartate phosphorylation: two-component systems and the limits of homology. *Trends in Biochemical Sciences* **1994,** *19* (11), 485-90; (b) Kennelly, P. J.; Potts, M., Fancy meeting you here! A fresh look at "prokaryotic" protein phosphorylation. *J. Bacteriol.* **1996,** *178* (16), 4759-4764; (c) Kennelly, P. J., Protein kinases and protein phosphatases in prokaryotes: a genomic perspective. *FEMS Microbiol. Lett.* **2002,** *206* (1), 1-8; (d) Loomis, W. F.; Kuspa, A.; Shaulsky, G., Two-component signal transduction systems in eukaryotic microorganisms. *Curr. Opin. Microbiol.* **1998,** *1* (6), 643-648; (e) Thomason, P.; Kay, R., Eukaryotic signal transduction via histidine-aspartate phosphorelay. *J. Cell Sci.* **2000,** *113* (18), 3141-3150.
[30] Besant, P. G.; Attwood, P. V., Mammalian histidine kinases. *Biochimica et Biophysica Acta, Proteins and Proteomics* **2005,** *1754* (1-2), 281-290.
[31] Besant, P. G.; Attwood, P. V., Histone H4 histidine phosphorylation: kinases, phosphatases, liver regeneration and cancer. *Biochem. Soc. Trans.* **2012,** *40* (1), 290-293.
[32] Besant, P. G.; Tan, E.; Attwood, P. V., Mammalian protein histidine kinases. *Int. J. Biochem. Cell Biol.* **2003,** *35* (3), 297-309.
[33] Klumpp, S.; Bechmann, G.; Maurer, A.; Selke, D.; Krieglstein, J., ATP-citrate lyase as a substrate of protein histidine phosphatase in vertebrates. *Biochem. Biophys. Res. Commun.* **2003,** *306* (1), 110-115.
[34] Klumpp, S.; Faber, D.; Fischer, D.; Litterscheid, S.; Krieglstein, J., Role of protein histidine phosphatase for viability of neuronal cells. *Brain Res.* **2009,** *1264*, 7-12.

[35] (a) Srivastava, S.; Li, Z.; Ko, K.; Choudhury, P.; Albaqumi, M.; Johnson, A. K.; Yan, Y.; Backer, J. M.; Unutmaz, D.; Coetzee, W. A.; Skolnik, E. Y., Histidine phosphorylation of the potassium channel KCa3.1 by nucleoside diphosphate kinase B is required for activation of KCa3.1 and CD4 T cells. *Molecular Cell* **2006,** *24* (5), 665-675; (b) Srivastava, S.; Zhdanova, O.; Di, L.; Li, Z.; Albaqumi, M.; Wulff, H.; Skolnik, E. Y., Protein histidine phosphatase 1 negatively regulates CD4 T cells by inhibiting the K+ channel KCa3.1. *Proceedings of the National Academy of Sciences of the United States of America* **2008,** *105* (38), 14442-14446.

[36] Kunst, F.; Ogasawara, N.; Moszer, I.; Albertini, A. M.; Alloni, G.; Azevedo, V.; Bertero, M. G.; Bessieres, P.; Bolotin, A.; Borchert, S.; Borriss, R.; Boursier, L.; Brans, A.; Braun, M.; Brignell, S. C.; Bron, S.; Brouillet, S.; Bruschi, C. V.; Caldwell, B.; Capuano, V.; Carter, N. M.; Choi, S. K.; Codani, J. J.; Connerton, I. F.; Cummings, N. J.; Daniel, R. A.; Denizot, F.; Devine, K. M.; Dusterhoft, A.; Ehrlich, S. D.; Emmerson, P. T.; Entian, K. D.; Errington, J.; Fabret, C.; Ferrari, E.; Foulger, D.; Fritz, C.; Fujita, M.; Fujita, Y.; Fuma, S.; Galizzi, A.; Galleron, N.; Ghim, S. Y.; Glaser, P.; Goffeau, A.; Golightly, E. J.; Grandi, G.; Guiseppi, G.; Guy, B. J.; Haga, K.; et al., The complete genome sequence of the gram-positive bacterium Bacillus subtilis. *Nature* **1997,** *390* (6657), 249-256.

[37] Matsubara, M.; Mizuno, T., The SixA phospho-histidine phosphatase modulates the ArcB phosphorelay signal transduction in Escherichia coli. *FEBS Letters* **2000,** *470* (2), 118-124.

[38] Klumpp, S.; Krieglstein, J., Reversible phosphorylation of histidine residues in proteins from vertebrates. *Sci. Signaling* **2009,** *2* (61), pe13.

[39] Klumpp, S.; Hermesmeier, J.; Selke, D.; Baumeister, R.; Kellner, R.; Krieglstein, J., Protein Histidine Phosphatase: A Novel Enzyme With Potency for Neuronal Signaling. *J. Cereb. Blood Flow Metab.* **2002,** *22* (12), 1420-1424.

[40] Ek, P.; Pettersson, G.; Ek, B.; Gong, F.; Li, J.-P.; Zetterqvist, O., Identification and characterization of a mammalian 14-kDa phosphohistidine phosphatase. *Eur. J. Biochem.* **2002,** *269* (20), 5016-5023.

[41] Zhang, X.-Q.; Sundh Ulla, B.; Jansson, L.; Zetterqvist, O.; Ek, P., Immunohistochemical localization of phosphohistidine phosphatase PHPT1 in mouse and human tissues. *Ups J Med Sci* **2009,** *114* (2), 65-72.

[42] Krieglstein, J.; Lehmann, M.; Maeurer, A.; Gudermann, T.; Pinkenburg, O.; Wieland, T.; Litterscheid, S.; Klumpp, S., Reduced viability of neuronal cells after overexpression of protein histidine phosphatase. *Neurochem. Int.* **2008,** *53* (5), 132-136.

[43] Seeger, A.; Rose, K.; Ma, N. T.; Kremmer, E.; Klumpp, S.; Krieglstein, J., Influence of protein histidine phosphatase overexpression and down-regulation on human umbilical-vein endothelial cell viability. *Cell Biol. Int.* **2012,** *36* (3), 245-249.

[44] Steeg, P. S.; Palmieri, D.; Ouatas, T.; Salerno, M., Histidine kinases and histidine phosphorylated proteins in mammalian cell biology, signal transduction and cancer. *Cancer Lett.* **2003,** *190* (1), 1-12.

[45] Xu, A.; Hao, J.; Zhang, Z.; Tian, T.; Jiang, S.; Hao, J.; Liu, C.; Huang, L.; Xiao, X.; He, D., 14-kDa phosphohistidine phosphatase and its role in human lung cancer cell migration and invasion. *Lung Cancer* **2010,** *67* (1), 48-56.

[46] Han, S.-X.; Wang, L.-J.; Zhao, J.; Zhang, Y.; Li, M.; Zhou, X.; Wang, J.; Zhu, Q., 14-kDa phosphohistidine phosphatase plays an important role in hepatocellular carcinoma cell proliferation. *Oncol. Lett.* **2012,** *4* (4), 658-664.

[47] Ma, R.; Kanders, E.; Sundh, U. B.; Geng, M.; Ek, P.; Zetterqvist, O.; Li, J.-P., Mutational study of human phosphohistidine phosphatase: Effect on enzymatic activity. *Biochem. Biophys. Res. Commun.* **2005,** *337* (3), 887-891.
[48] Busam, R. D.; Thorsell, A.-G.; Flores, A.; Hammarstroem, M.; Persson, C.; Hallberg, B. M., First structure of a eukaryotic phosphohistidine phosphatase. *Journal of Biological Chemistry* **2006,** *281* (45), 33830-33834.
[49] Gong, W.; Li, Y.; Cui, G.; Hu, J.; Fang, H.; Jin, C.; Xia, B., Solution structure and catalytic mechanism of human protein histidine phosphatase 1. *Biochem. J.* **2009,** *418* (2), 337-344.
[50] Klumpp, S.; Ma, N. T.; Baeumer, N.; Bechmann, G.; Krieglstein, J., Relevance of glycine and cysteine residues as well as N- and C-terminals for the activity of protein histidine phosphatase. *Biochimica et Biophysica Acta, Proteins and Proteomics* **2010,** *1804* (1), 206-211.
[51] Heibeck, T. H.; Ding, S.-J.; Opresko, L. K.; Zhao, R.; Schepmoes, A. A.; Yang, F.; Tolmachev, A. V.; Monroe, M. E.; Camp, D. G., II; Smith, R. D.; Wiley, H. S.; Qian, W.-J., An Extensive Survey of Tyrosine Phosphorylation Revealing New Sites in Human Mammary Epithelial Cells. *J. Proteome Res.* **2009,** *8* (8), 3852-3861.
[52] Hosfield, D. J.; Mol, C. D., Targeting inactive kinases: structure as a foundation for cancer drug discovery. *Cancer Drug Des. Discovery* **2008**, 229-252.
[53] (a) Vintonyak, V. V.; Antonchick, A. P.; Rauh, D.; Waldmann, H., The therapeutic potential of phosphatase inhibitors. *Curr. Opin. Chem. Biol.* **2009,** *13* (3), 272-283; (b) Vintonyak, V. V.; Waldmann, H.; Rauh, D., Using small molecules to target protein phosphatases. *Bioorg. Med. Chem.* **2011,** *19* (7), 2145-2155.
[54] Ventura, J.-J.; Nebreda, A. R., Protein kinases and phosphatases as therapeutic targets in cancer. *Clin. Transl. Oncol.* **2006,** *8* (3), 153-160.
[55] Attwood, P. V.; Piggott, M. J.; Zu, X. L.; Besant, P. G., Focus on phosphohistidine. *Amino Acids* **2007,** *32* (1), 145-156.
[56] Vliet, B. v., Design, Synthesis and Applications of an Imidazole-Phosphonate-Based Mimic of 3-Phosphohistidine. *Dissertation Technische Universität Dortmund* **2012**.
[57] Lau, K. H.; Farley, J. R.; Baylink, D. J., Phosphotyrosyl protein phosphatases. *Biochem J* **1989,** *257* (1), 23-36.
[58] Montalibet, J.; Skorey, K. I.; Kennedy, B. P., Protein tyrosine phosphatase: enzymatic assays. *Methods* **2005,** *35* (1), 2-8.
[59] Xue, F.; Seto, C. T., Fluorogenic Peptide Substrates for Serine and Threonine Phosphatases. *Organic Letters* **2010,** *12* (9), 1936-1939.
[60] Information extracted from webpage http://homepage.univie.ac.at/ nikos.pinotsis/webPP/genetoprotein/ clo_vector/frame_our_Ec_vectors.html.
[61] Sun, W.-C.; Gee, K. R.; Haugland, R. P., Synthesis of novel fluorinated coumarins: excellent UV-light excitable fluorescent dyes. *Bioorg. Med. Chem. Lett.* **1998,** *8* (22), 3107-3110.
[62] Walther, T., Synthese und Struktur-Wirkungs-Beziehung von Brunsvicamid-Analoga. *Dissertation Technische Universität Dortmund* **2009**.
[63] (a) Schnell, S., Validity of the Michaelis-Menten equation - steady-state or reactant stationary assumption: that is the question. *FEBS Journal* **2014,** *281* (2), 464-472; (b) Cardenas, M. L., Michaelis and Menten and the long road to the discovery of cooperativity. *FEBS Letters* **2013,** *587* (17), 2767-2771; (c) Cornish-Bowden, A., The origins of enzyme kinetics. *FEBS Letters* **2013,** *587* (17), 2725-2730.

[64] Stroppolo, M. E.; Falconi, M.; Caccuri, A. M.; Desideri, A., Superefficient enzymes. *Cell. Mol. Life Sci.* **2001,** *58* (10), 1451-1460.
[65] (a) Webb, M. R., A continuous spectrophotometric assay for inorganic phosphate and for measuring phosphate release kinetics in biological systems. *Proceedings of the National Academy of Sciences of the United States of America* **1992,** *89* (11), 4884-7; (b) Drueckes, P.; Schinzel, R.; Palm, D., Photometric microtiter assay of inorganic phosphate in the presence of acid-labile organic phosphates. *Anal. Biochem.* **1995,** *230* (1), 173-7; (c) Wedler, F. C.; Ley, B. W.; Moyer, M. L., A continuous visible spectrophotometric assay for aspartate transcarbamylase. *Anal. Biochem.* **1994,** *218* (2), 449-53; (d) Gibson, K. J.; Lorimer, G. H.; Rendina, A. R.; Taylor, W. S.; Cohen, G.; Gatenby, A. A.; Payne, W. G.; Roe, D. C.; Lockett, B. A.; Nudelman, A.; et al., Dethiobiotin synthetase: the carbonylation of 7,8-diaminononanoic acid proceeds regiospecifically via the N7-carbamate. *Biochemistry* **1995,** *34* (35), 10976-84; (e) Nixon, A. E.; Brune, M.; Lowe, P. N.; Webb, M. R., Kinetics of Inorganic Phosphate Release during the Interaction of p21ras with the GTPase-Activating Proteins, p120-GAP and Neurofibromin. *Biochemistry* **1995,** *34* (47), 15592-8; (f) Webb, M. R.; Hunter, J. L., Interaction of GTPase-activating protein with p21ras, measured using a continuous assay for inorganic phosphate release. *Biochem. J.* **1992,** *287* (2), 555-9.
[66] Wei, Y. F.; Matthews, H. R., Identification of phosphohistidine in proteins and purification of protein-histidine kinases. *Methods in Enzymology* **1991,** *200* (Protein Phosphorylation, Pt. A), 388-414.
[67] Broom, A. D.; Milne, G. H., Synthesis and PMR studies of some methylated 6-thiopurine nucleosides. *J. Heterocycl. Chem.* **1975,** *12* (1), 171-4.
[68] Rudolph, F. B.; Baugher, B. W.; Beissner, R. S., Techniques in coupled enzyme assays. *Methods in Enzymology* **1979,** *63* (Enzyme Kinet. Mech., Part A), 22-42.
[69] (a) Jerabek-Willemsen, M.; Duhr, S.; Baaske, P., Biomolecular interactions by microscale thermophoresis. *BIOspektrum* **2012,** *18* (1), 30-32; (b) Jerabek-Willemsen, M.; Wienken, C. J.; Braun, D.; Baaske, P.; Duhr, S., Molecular Interaction Studies Using Microscale Thermophoresis. *Assay Drug Dev. Technol.* **2011,** *9* (4), 342-353.
[70] Seidel, S. A. I.; Wienken, C. J.; Geissler, S.; Jerabek-Willemsen, M.; Duhr, S.; Reiter, A.; Trauner, D.; Braun, D.; Baaske, P., Label-Free Microscale Thermophoresis Discriminates Sites and Affinity of Protein-Ligand Binding. *Angewandte Chemie, International Edition* **2012,** *51* (42), 10656-10659.
[71] Seidel, S. A. I.; Dijkman, P. M.; Lea, W. A.; van den Bogaart, G.; Jerabek-Willemsen, M.; Lazic, A.; Joseph, J. S.; Srinivasan, P.; Baaske, P.; Simeonov, A.; Katritch, I.; Melo, F. A.; Ladbury, J. E.; Schreiber, G.; Watts, A.; Braun, D.; Duhr, S., Microscale thermophoresis quantifies biomolecular interactions under previously challenging conditions. *Methods*, Ahead of Print.
[72] Wienken, C. J.; Baaske, P.; Rothbauer, U.; Braun, D.; Duhr, S., Protein-binding assays in biological liquids using microscale thermophoresis. *Nat. Commun.* **2010,** *1* (Oct.),
[73] (a) Burke, T. R., Jr.; Kole, H. K.; Roller, P. P., Potent inhibition of insulin receptor dephosphorylation by a hexamer peptide containing the phosphotyrosyl mimetic F2Pmp. *Biochem. Biophys. Res. Commun.* **1994,** *204* (1), 129-34; (b) Shen, K.; Keng, Y.-F.; Wu, L.; Guo, X.-L.; Lawrence, D. S.; Zhang, Z.-Y., Acquisition of a specific and potent PTP1B inhibitor from a novel combinatorial library and screening procedure. *Journal of Biological Chemistry* **2001,** *276* (50), 47311-47319.

[74] Yue Eddy, W.; Wayland, B.; Douty, B.; Crawley Matthew, L.; McLaughlin, E.; Takvorian, A.; Wasserman, Z.; Bower Michael, J.; Wei, M.; Li, Y.; Ala Paul, J.; Gonneville, L.; Wynn, R.; Burn Timothy, C.; Liu Phillip, C. C.; Combs Andrew, P., Isothiazolidinone heterocycles as inhibitors of protein tyrosine phosphatases: synthesis and structure-activity relationships of a peptide scaffold. *Bioorg Med Chem* **2006,** *14* (17), 5833-49.

[75] Elliott, T. S.; Slowey, A.; Ye, Y.; Conway, S. J., The use of phosphate bioisosteres in medicinal chemistry and chemical biology. *MedChemComm* **2012,** *3* (7), 735-751.

[76] Chen Yen, T.; Xie, J.; Seto Christopher, T., Peptidic alpha-ketocarboxylic acids and sulfonamides as inhibitors of protein tyrosine phosphatases. *J Org Chem* **2003,** *68* (10), 4123-5.

[77] Hill, B.; Liu, Y.; Taylor, S. D., Synthesis of α-Fluorosulfonamides by Electrophilic Fluorination. *Organic Letters* **2004,** *6* (23), 4285-4288.

[78] Ma, J.-A., Recent developments in the catalytic asymmetric synthesis of α- and β-amino acids. *Angewandte Chemie, International Edition* **2003,** *42* (36), 4290-4299.

[79] Lennon, I. C.; Moran, P. H., Asymmetric hydrogenation of pharmaceutically interesting substrates. *Curr. Opin. Drug Discovery Dev.* **2003,** *6* (6), 855-875.

[80] Panella, L.; Aleixandre, A. M.; Kruidhof, G. J.; Robertus, J.; Feringa, B. L.; De Vries, J. G.; Minnaard, A. J., Enantioselective Rh-Catalyzed Hydrogenation of N-Formyl Dehydroamino Esters with Monodentate Phosphoramidite Ligands. *Journal of Organic Chemistry* **2006,** *71* (5), 2026-2036.

[81] Baker, G. P.; Bourne, I. A.; Ford, M. J.; Foster, R. W. G.; Jackson, T. H.; Pannell, R. W.; Whitmore, M. W., Studies toward an Improved Process for N4,N4-Disubstituted-2-cyano-N1,N1-dimethyl-1H-imidazole-1,4-disulfonamides. *Org. Process Res. Dev.* **1999,** *3* (2), 104-108.

[82] (a) Jackson, R. F. W.; Moore, R. J.; Dexter, C. S.; Elliott, J.; Mowbray, C. E., Concise Synthesis of Enantiomerically Pure Phenylalanine, Homophenylalanine, and Bishomophenylalanine Derivatives Using Organozinc Chemistry: NMR Studies of Amino Acid-Derived Organozinc Reagents. *Journal of Organic Chemistry* **1998,** *63* (22), 7875-7884; (b) Jackson, R. F. W.; Wishart, N.; Wood, A.; James, K.; Wythes, M. J., Preparation of enantiomerically pure protected 4-oxo α-amino acids and 3-aryl α-amino acids from serine. *Journal of Organic Chemistry* **1992,** *57* (12), 3397-404; (c) Oswald, C. L.; Carrillo-Marquez, T.; Caggiano, L.; Jackson, R. F. W., Negishi cross-coupling reactions of α-amino acid-derived organozinc reagents and aromatic bromides. *Tetrahedron* **2007,** *64* (4), 681-687.

[83] Nicolaou, K. C.; Estrada, A. A.; Zak, M.; Lee, S. H.; Safina, B. S., A mild and selective method for the hydrolysis of esters with trimethyltin hydroxide. *Angewandte Chemie, International Edition* **2005,** *44* (9), 1378-1382.

[84] Ross, A. J.; Lang, H. L.; Jackson, R. F. W., Much Improved Conditions for the Negishi Cross-Coupling of Iodoalanine Derived Zinc Reagents with Aryl Halides. *Journal of Organic Chemistry* **2010,** *75* (1), 245-248.

[85] Han, C.; Buchwald, S. L., Negishi Coupling of Secondary Alkylzinc Halides with Aryl Bromides and Chlorides. *J. Am. Chem. Soc.* **2009,** *131* (22), 7532-7533.

[86] Milne, J. E.; Buchwald, S. L., An Extremely Active Catalyst for the Negishi Cross-Coupling Reaction. *J. Am. Chem. Soc.* **2004,** *126* (40), 13028-13032.

[87] Supuran, C. T., Carbonic anhydrase inhibitors and activators for novel therapeutic applications. *Future Med. Chem.* **2011,** *3* (9), 1165-1180.

[88] Alterio, V.; Di Fiore, A.; D'Ambrosio, K.; Supuran, C. T.; De Simone, G., Multiple Binding Modes of Inhibitors to Carbonic Anhydrases: How to Design Specific Drugs Targeting 15 Different Isoforms? *Chem. Rev.* **2012,** *112* (8), 4421-4468.
[89] King, J. F.; Beatson, R. P., Sulfene by the "abnormal" route. *Journal of the Chemical Society [Section] D: Chemical Communications* **1970,** (11), 663-4.
[90] (a) Takeuchi, Y.; Kirk, K. L.; Cohen, L. A., Acid-catalyzed isotope exchange of ring hydrogens in fluoroimidazoles. *Journal of Organic Chemistry* **1979,** *44* (24), 4240-2; (b) Jain, R.; Avramovitch, B.; Cohen, L. A., Synthesis of ring-halogenated histidines and histamines. *Tetrahedron* **1998,** *54* (13), 3235-3242.
[91] (a) Gregoret, L. M.; Rader, S. D.; Fletterick, R. J.; Cohen, F. E., Hydrogen bonds involving sulfur atoms in proteins. *Proteins* **1991,** *9* (2), 99-107; (b) Wennmohs, F.; Schindler, M., Development of a multipoint model for sulfur in proteins: A new parametrization scheme to reproduce high-level ab initio interaction energies. *Journal of Computational Chemistry* **2004,** *26* (3), 283-293; (c) Tian, F.; Yang, L.; Lv, F.; Yang, Q.; Zhou, P., In silico quantitative prediction of peptides binding affinity to human MHC molecule: an intuitive quantitative structure-activity relationship approach. *Amino Acids* **2009,** *36* (3), 535-554.
[92] Gros, P.; Fort, Y.; Caubere, P., Aggregative activation in heterocyclic chemistry. Part 5. Lithiation of pyridine and quinoline with the complex base BuLi·Me2N(CH2)2OLi (BuLi·LiDMAE). *J. Chem. Soc., Perkin Trans. 1* **1997,** (24), 3597-3600.
[93] Corbett, J. W.; Guzman-Perez, A.; Pfefferkorn, J. A.; Tu, M. M. Preparation of substituted indazole amides as glucokinase activators. 2010-IB509442010103438, 20100304., 2010.
[94] (a) Lee, J.; Zhong, Y.-L.; Reamer, R. A.; Askin, D., Practical Synthesis of Sultams via Sulfonamide Dianion Alkylation: Application to the Synthesis of Chiral Sultams. *Organic Letters* **2003,** *5* (22), 4175-4177; (b) Yu, C.-B.; Wang, D.-W.; Zhou, Y.-G., Highly Enantioselective Synthesis of Sultams via Pd-Catalyzed Hydrogenation. *Journal of Organic Chemistry* **2009,** *74* (15), 5633-5635.
[95] Kansy, M.; Senner, F.; Gubernator, K., Physicochemical High Throughput Screening: Parallel Artificial Membrane Permeation Assay in the Description of Passive Absorption Processes. *Journal of Medicinal Chemistry* **1998,** *41* (7), 1007-1010.
[96] (a) Lampugnani, M. G., Cell migration into a wounded area in vitro. *Methods in molecular biology (Clifton, N.J.)* **1999,** *96*, 177-82; (b) Yarrow, J. C.; Perlman, Z. E.; Westwood, N. J.; Mitchison, T. J., A high-throughput cell migration assay using scratch wound healing, a comparison of image-based readout methods. *BMC Biotechnology* **2004,** *4*, No pp given.
[97] Winum, J.-Y.; Scozzafava, A.; Montero, J.-L.; Supuran, C. T., Inhibition of carbonic anhydrase IX: a new strategy against cancer. *Anti-Cancer Agents in Medicinal Chemistry* **2009,** *9* (6), 693-702.
[98] Kallio, H.; Martinez, A. R.; Hilvo, M.; Hyrskyluoto, A.; Parkkila, S., Cancer-associated carbonic anhydrases IX and XII: Effect of growth factors on gene expression in human cancer cell lines. *Journal of Cancer Molecules* **2010,** *5* (3), 73-78.
[99] Pollok, B. A.; Heim, R., Using GFP in FRET-based applications. *Trends in Cell Biology* **1999,** *9* (2), 57-60.
[100] Sekar, R. B.; Periasamy, A., Fluorescence resonance energy transfer (FRET) microscopy imaging of live cell protein localizations. *Journal of Cell Biology* **2003,** *160* (5), 629-633.

[101] (a) Didier, P.; Sharma, K. K.; Mely, Y., Fluorescence techniques to characterise ligand binding to proteins. *RSC Biomolecular Sciences* **2011,** *22* (Biophysical Approaches Determining Ligand Binding to Biomolecular Targets), 156-199; (b) Lakowicz, J. R., *Principles of Fluorescence Spectroscopy*. 1983; p 496 pp.
[102] Wallrabe, H.; Periasamy, A., Imaging protein molecules using FRET and FLIM microscopy. *Current Opinion in Biotechnology* **2005,** *16* (1), 19-27.
[103] Chen, Y.; Periasamy, A., Characterization of two-photon excitation fluorescence lifetime imaging microscopy for protein localization. *Microscopy Research and Technique* **2003,** *63* (1), 72-80.
[104] Chen, Y.; Mills, J. D.; Periasamy, A., Protein localization in living cells and tissues using FRET and FLIM. *Differentiation* **2003,** *71* (9-10), 528-541.
[105] Cook, R. M. Fluorescence energy transfer probes with stabilized conformations. 2006-52015220070059752, 20060913., 2007.
[106] http://dpf.mpi-dortmund.mpg.de.
[107] Attwood, P. V.; Ludwig, K.; Bergander, K.; Besant, P. G.; Adina-Zada, A.; Krieglstein, J.; Klumpp, S., Chemical phosphorylation of histidine-containing peptides based on the sequence of histone H4 and their dephosphorylation by protein histidine phosphatase. *Biochimica et Biophysica Acta, Proteins and Proteomics* **2010,** *1804* (1), 199-205.
[108] Rossetto, D.; Avvakumov, N.; Cote, J., Histone phosphorylation: a chromatin modification involved in diverse nuclear events. *Epigenetics* **2012,** *7* (10), 1098-1108.
[109] (a) Lo, W.-S.; Trievel, R. C.; Rojas, J. R.; Duggan, L.; Hsu, J.-Y.; Allis, C. D.; Marmorstein, R.; Berger, S. L., Phosphorylation of serine 10 in histone H3 is functionally linked in vitro and in vivo to Gcn5-mediated acetylation at lysine 14. *Molecular Cell* **2000,** *5* (6), 917-926; (b) Cheung, P.; Tanner, K. G.; Cheung, W. L.; Sassone-Corsi, P.; Denu, J. M.; Allis, C. D., Synergistic coupling of histone H3 phosphorylation and acetylation in response to epidermal growth factor stimulation. *Molecular Cell* **2000,** *5* (6), 905-915.
[110] (a) Taverna, S. D.; Li, H.; Ruthenburg, A. J.; Allis, C. D.; Patel, D. J., How chromatin-binding modules interpret histone modifications: lessons from professional pocket pickers. *Nature Structural & Molecular Biology* **2007,** *14* (11), 1025-1040; (b) Yun, M.; Wu, J.; Workman, J. L.; Li, B., Readers of histone modifications. *Cell Research* **2011,** *21* (4), 564-578.
[111] Ziegler, S.; Pries, V.; Hedberg, C.; Waldmann, H., Target Identification for Small Bioactive Molecules: Finding the Needle in the Haystack. *Angewandte Chemie, International Edition* **2013,** *52* (10), 2744-2792.
[112] Sarg, B.; Helliger, W.; Talasz, H.; Koutzamani, E.; Lindner, H. H., Histone H4 Hyperacetylation Precludes Histone H4 Lysine 20 Trimethylation. *Journal of Biological Chemistry* **2004,** *279* (51), 53458-53464.
[113] (a) Barford, D., Molecular mechanisms of the protein serine/threonine phosphatases. *Trends in Biochemical Sciences* **1996,** *21* (11), 407-412; (b) Zhang, Z.-Y., Protein tyrosine phosphatases: structure and function, substrate specificity, and inhibitor development. *Annual Review of Pharmacology and Toxicology* **2002,** *42*, 209-234; (c) Mumby, M. C.; Walter, G., Protein serine/threonine phosphatases: Structure, regulation, and functions in cell growth. *Physiological Reviews* **1993,** *4* (73), 673-99.
[114] Drews, J., Drug discovery: A historical perspective. *Science* **2000,** *287* (5460), 1960-1963.

[115] Graeve, R.; Okyayuz-Baklouti, I.; Seiffge, D. Preparation of imidazolesulfonamides as antithrombotic agents. 1990-40040614004061, 19900210., 1991.
[116] Bendale, P.; Olepu, S.; Suryadevara, P. K.; Bulbule, V.; Rivas, K.; Nallan, L.; Smart, B.; Yokoyama, K.; Ankala, S.; Pendyala, P. R.; Floyd, D.; Lombardo, L. J.; Williams, D. K.; Buckner, F. S.; Chakrabarti, D.; Verlinde, C. L. M. J.; Van Voorhis, W. C.; Gelb, M. H., Second Generation Tetrahydroquinoline-Based Protein Farnesyltransferase Inhibitors as Antimalarials. *Journal of Medicinal Chemistry* **2007,** *50* (19), 4585-4605.
[117] Fernandez-Megia, E.; Correa, J.; Rodriguez-Meizoso, I.; Riguera, R., A Click Approach to Unprotected Glycodendrimers. *Macromolecules* **2006,** *39* (6), 2113-2120.
[118] Lewis, J. G.; Jacobs, J. W.; Reich, N.; Leadbetter, M. R.; Bell, N.; Chang, H.-T.; Chen, T.; Navre, M.; Charmot, D.; Carreras, C.; Labonte, E. Benzamide compounds as inhibitors of phosphate transport and their preparation. 2011-US432672012054110, 20110707., 2012.
[119] Wong, L. S.; Janusz, S. J.; Sun, S.; Leggett, G. J.; Micklefield, J., Nanoscale Biomolecular Structures on Self-Assembled Monolayers Generated from Modular Pegylated Disulfides. *Chemistry - A European Journal* **2010,** *16* (40), 12234-12243, S12234/1-S12234/2.

Acknowledgements

First I would like to thank Prof. Waldmann for receiving me beginning 2008 when I was looking for an academic group where I could do my promotion and stimulating my enthusiasm for joining his group in Dortmund. The Waldmann group at the MPI Dortmund is a great mix of German and foreign bright minds and forms a stimulating environment for science. Without your encouragement to come to Dortmund I would not have met Christian nor Nancy.

Christian, thank you for taking me on in your group and giving me the right amount of stimulation and freedom to develop my own project. It was always a pleasant feeling that in case of complete failure your supervision and advice would not be far away. I also enjoyed de many discussion we had about all possible subjects, usually under the influence of nice beer or wine and good food.

Additionally, I would like to thank the third committee member Dr. Andreas Brunschweiger for taking the time to be part of my thesis committee.

Nancy, thank you for always being there for me when I needed support. You opened up my eyes to many things in live. I love you very much and the thought that we will spent our lives together makes me very happy.

Bart, Cornelis, Michael, Philip and Samy thank you for creating a great working environment in the lab. I really enjoyed working together while listening to loud music or making jokes together. Additionally, I worked together with many people from outside the department being Marcel, Julia and Sascha. I really enjoyed working together with you and learning a lot of things beyond the scope of organic synthesis. I especially thank Arthur Porfetye and Dr. Ingrid Vetter for learning me all about protein crystallography. I also thank Prof. Robert Schneider and the people in his group for the experiments performed with the phospho-histidine peptides described in this thesis. I also thank Prof. Dr. Hengstler at IfaDo and especially Dr. Rosemarie Marchan for performing the scratch assay experiments.

Finally, I say thank you to all the members of the Waldmann department, especially Frau Rose, Bjoern, Sascha, Daniel, Francisca, Gemma, Gloria, Kristina, Melanie, Bahar, Patrick, Tobias, Uschi, Sebastian en Robin. I had a great time in Dortmund.

I would like to thank my Dutch friends Arnout and Maurice for support and exploring with me the bowling alleys well beyond the Dutch-German border. I also thank Ruud and Helen, and Rob and Kristina for their support and showing interest in my progress and development.

I also thank my family for support and especially my mother and myrdith. Hartelijk dank voor jullie onvoorwaardelijke steun.

Declaration

Hiermit versichere ich an Eides statt, dass ich die vorliegende Arbeit selbständig und nur mit den angegeben Hilfsmitteln angefertigt habe.

I hereby declare that I performed the work presented independently and did not use any other but the indicated aids.

Goch, Juni 2015

Martijn Eerland